Isobutanol-Methanol Mixtures from Synthesis Gas

Final Technical Report

Contractor

University of California-Berkeley
Berkeley, California 94720

Enrique Iglesia - Program Manager

September 1998

Prepared for the United States Department of Energy *
Under Contract Number DE-AC22-94PC94066
Contract Period 1 October 1994 - 30 September 1998

TABLE OF CONTENTS

4. PARTICIPATING PROJECT PERSONNEL

Brandy L. Stephens
Graduate Student

Anne-Mette Hilmen
Postdoctoral Fellow

Marcelo J.L. Gines
Postdoctoral Fellow

Mingting Xu
Postdoctoral Fellow

Hyung-Seuk Oh
Postdoctoral Fellow

Anwu Li
Postdoctoral Fellow

Mai Tu
Postdoctoral Fellow

Enrique Iglesia
Principal Investigator

1. CONTRACT OBJECTIVES

The objectives of the research contract are:

1. To design a catalytic material for the synthesis of isobutanol with a productivity of 200 g isoalcohols/g-cat.·h and a molar isobutanol/methanol ratio near unity

2. To develop structure-function rules for the design of catalysts for the selective conversion of synthesis gas to isoalcohols

The research program has been grouped into four specific tasks and a set of project management and reporting activities. The remaining of the reports is structured to reflect this breakdown of activities:

- Reporting Activities and Project Management

- Catalyst synthesis and primary structural and surface catalyst characterization of catalytic materials (***Task 1***)

- Catalyst evaluation and mechanistic studies of reaction pathways and rate-determining steps in laboratory microreactors (***Task 2***).

- Identification and surface density measurements of reaction intermediates by in-situ infrared spectroscopy and by temperature programmed surface reaction studies (***Task 3***)

- Air Products and Chemicals (APCI) Subcontract: Catalyst evaluation in the laboratories of APCI using bench scale reactors at conditions similar to those of industrial practice. Economic evaluations to determine the most promising catalysts and technical guidance in the design and operation of laboratory microreactors (***Task 4***; APCI Subcontract).

2. EXECUTIVE SUMMARY

Isobutanol is potential as a fuel additive or precursor to methyl tert-butyl ether (MTBE). Alkali-promoted $Cu/ZnO/Al_2O_3$ and $Cu/MgO/CeO_2$ materials have been found to catalyze the formation of isobutanol from CO and H_2 at temperatures (573-623 K) that allow their use in slurry reactors. Our studies focus on the mechanism and structural requirements for selective isobutanol synthesis on these types of catalysts.

Alkali promoted $Cu/MgO/CeO_2$, Cu/MgO/ZnO, and $CuZnAlO_x$ materials and their individual components Cu/MgO, MgO/CeO_2, MgO and CeO_2 have been prepared for the use in kinetic studies of alcohol coupling reactions, in identification of reaction intermediates, and in isobutanol synthesis at high pressures. These samples were prepared by coprecipitation of mixed nitrate solutions with an aqueous solution of KOH (2M) and K_2CO_3 (1M) at 338 K at a constant pH of 9, except for $Cs-Cu/ZnO/Al_2O_3$ at a pH of 7, in a well-stirred thermostated container. The precipitate was filtered, washed thoroughly with dioinized water at 303 K in order to remove residual K ions, and dried at 353 K overnight. Dried samples were calcined at 723 K, except for $Cs-Cu/ZnO/Al_2O_3$ at 623 K, for 4 h in order to form the corresponding mixed oxides. Alkali addition (K or Cs) was performed by incipient wetness using K_2CO_3 (0.25 M) and CH_3COOCs (0.25 M) aqueous solutions. The crystallinity and phase structures of resulting materials were analyzed by powered X-ray diffraction.

The compositions were determined by atomic adsorption spectroscopy (AAS) and BET surface area was measured by N_2 adsorption. The number of Cu surface atoms was measured by N_2O titration methods. CeO_2 is a structural promoter increasing both surface area and Cu dispersion. The addition of K to $CuMgCeO_x$ samples decreases Cu surface area. A new $^{13}CO_2/^{12}CO_2$ isotopic switch method was developed to probe directly the density of basic sites on solid basic catalysts at temperatures typical of base-catalytic reactors. This method measures the dynamics of adsorption-desorption processes at equilibrium and the density of sites that interact reversibly with CO_2 at rates comparable to turnover rates for useful catalytic reactions. The addition of K to MgO and $Cu_{0.5}Mg_5CeO_x$ increases the number of such kinetically available adsorption sites. The number of sites determined by the $^{13}CO_2/^{12}CO_2$ isotopic switch method correlates well with the catalytic activity for base-catalyzed ethanol self condensation reactions. The exchange rate constant, corrected for readsorption, also provides an indirect measure of the basic strength distribution on non-uniform oxide surfaces.

$K-Cu_yMg_5CeO_x$ and $Cs-Cu/ZnO/Al_2O_3$ are selective catalysts for the synthesis of alcohols from H_2/CO mixtures at relatively low pressures and temperatures. CO_2 produced in higher alcohol synthesis steps and in water-gas shift reactions reversibly inhibits the formation of methanol and higher alcohols by increasing oxygen coverages on Cu surfaces and by titrating basic sites required for aldol-type chain growth steps. Inhibition effects are weaker on catalysts with high Cu site densities because the large abundance of Cu sites allows reactants to reach methanol synthesis equilibrium, even when catalysts are inhibited by CO_2. The addition of Pd to $K-Cu_{0.5}Mg_5CeO_x$ weakens CO_2 inhibition effects, because Pd remains metallic and retains its hydrogenation activity during CO hydrogenation. Basic sites on Mg_5CeO_x are stronger than on ZnO/Al_2O_3 and they are more efficiently covered by CO_2 during alcohol synthesis. K and Cs decreases

the number of acidic sites leading to dimethylether and hydrocarbons. Alcohol addition studies show that chain growth occurs predominantly by aldol-type addition of a methanol-derived C_1 species to ethanol and higher alcohols, following the rules of base-catalyzed aldol condensation, but the formation of ethanol proceeds via a different mechanism, at least on K-$Cu_{0.5}Mg_5CeO_x$. A detailed kinetic analysis shows that chain growth probabilities are very similar on both types of catalytic solids. Growth of C_1 chains to ethanol and of iso-C_4 chains to higher alcohols occurs with much lower probability than that of the rest of the chain growth steps.

Isotopic tracer studies of alcohol synthesis pathways carried out on K-$Cu_yMg_5CeO_x$ using a mixture of $^{13}CO/H_2$ and $^{12}CH_3OH$ have shown that ethanol is formed predominantly by direct reactions of ^{13}CO at short residence time, without significant involvement of the $^{12}CH_3OH$ present in the feed. The observed decrease in ^{13}C content in ethanol with increasing residence time is caused by reverse aldol reactions of higher alcohols, which contain lower ^{13}C contents because of the significant involvement of $^{12}CH_3OH$ in their formation. The effect of residence time on ^{13}C -distribution and on the rates of formation of ethanol, methyl formate, and methyl acetate are consistent with the intermediate role of methyl formate and methyl acetate in the formation of ethanol.

Ethanol reactions on K-$Cu_yMg_5CeO_x$ carried out in a recirculating reactor unit (RRU) show that both Cu and basic sites participate in alcohol dehydrogenation and aldol condensation steps to form n-butyraldehyde and acetone. Chain growth occurs by condensation reactions involving a metal-base bifunctional aldol-type coupling of alcohols. Reactions of $^{12}C_2H_5OH$-$^{13}C_2H_4O$ mixtures show that direct condensation reactions of ethanol may also occur without the intermediate formation of gas phase acetaldehyde. Reactions of C_2H_4O, deuterium incorporation reactions of C_2H_4O in the presence of D_2 on K-$Cu_yMg_5CeO_x$ show that Cu sites increase the rate of aldol condensation and the communication rate between surface and gas phase hydrogen pools. Cross exchange reactions between C_2H_4O and C_2D_4O suggests that C-H bond activation is quasi-equilibriated and is not the rate-limiting step. Therefore, from these results, it is elucidated that Cu sites increase the rate of aldol condensation by introducing recombinative desorption sites that remove hydrogen atoms formed in C-H activation steps leading to unsaturated aldol-type species required for chain growth. Reactions of acetaldehyde and ^{13}C-labeled methanol lead predominantly to 1-^{13}C-propionaldehyde and 2-^{13}C-isobutyraldehyde, precursors to isobutanol. Propionaldehyde and ^{13}C-labeled methanol mixtures lead to 1-^{13}C-isobutyraldehyde. Retro-aldol reactions after a hydride transfer account for the formation of acetone from ethanol reactants. Isobutyraldehyde is a preferred product end of alcohol chain growth reactions because it lacks the two α-hydrogens required for facile chain growth via aldol condensation pathways.

Temperature programmed surface reaction (TPSR) studies of ethanol and acetaldehyde pre-adsorbed on K-$CuMgCeO_x$ and its individual components show the formation of dehydrogenation, aldol-condensation, and decarboxylation products. K and Cu enhance the formation of acetone, a condensation product of ethanol and Cu sites increase the rate of hydrogen desorption and the fraction of the adsorbed ethanol that leads to condensation products. The effects of H_2 and CO on surface reactions of

adsorbed ethanol have also been examined concurrently with the in-situ infrared detection of surface species present during surface reactions of ethanol.

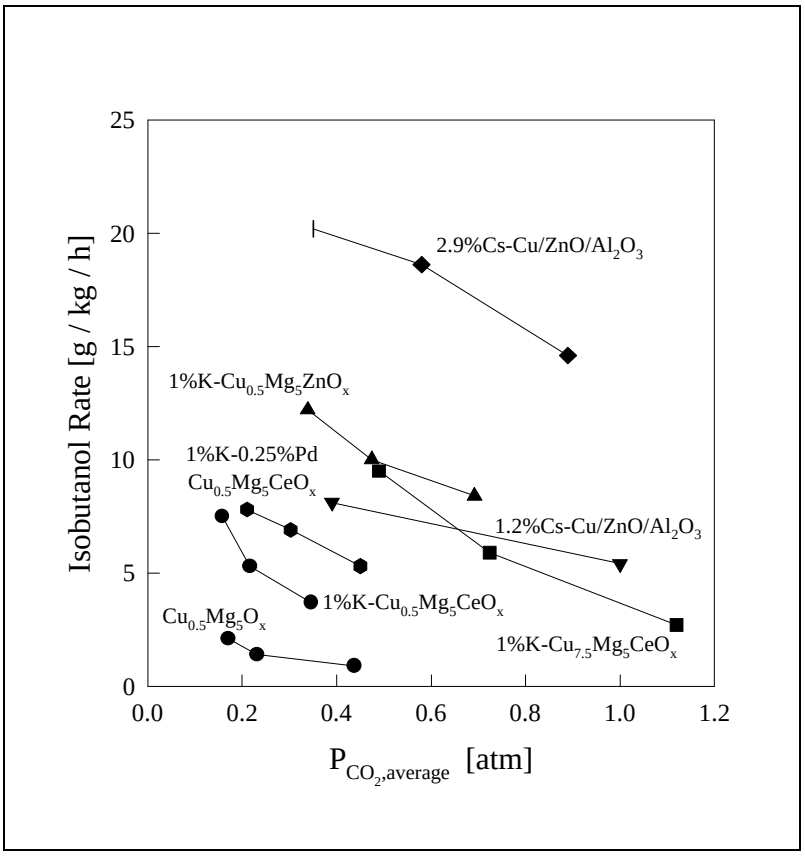

Figure 1.1. Effect of CO_2 on the formation rate of isobutanol on various bifunctional metal oxides.

3. EXPERIMENTAL, RESULTS, AND DISCUSSION

Task 1: Catalyst Synthesis

A controlled pH precipitation unit (CPPU) has been used for the synthesis of mixed-metal oxide precursors under constant pH and temperature conditions. A schematic diagram of the CPPU is shown in Figure 1.1. These materials prepared were tested for high alcohol synthesis from CO/H_2. These materials have been precipitated as metal hydroxides from nitrate precursors. We have focused the initial synthesis studies on three types of materials: methanol synthesis catalysts, isobutanol synthesis catalysts, and alcohol coupling catalysts based on high surface area metal oxide catalysts.

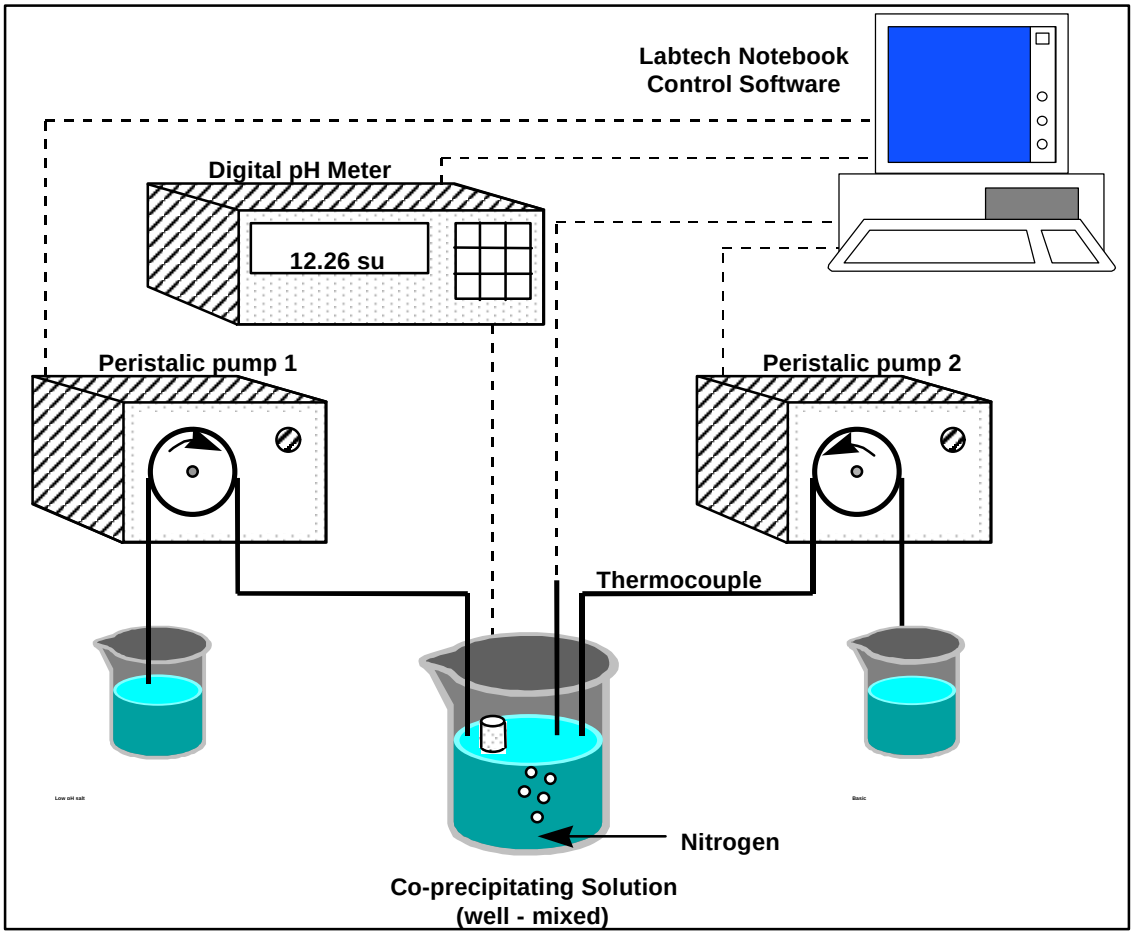

Figure 1.1. Schematic Diagram of Controlled pH Precipitation Unit (CPPU).

1.1. Methanol Synthesis Catalysts

Copper-based methanol synthesis catalysts have been prepared and used as the hydrogenation-dehydrogenation components in physical mixtures of basic oxides/ hydrogenation catalysts. The synthesis procedures follow those reported in the literature [1]. The following binary catalysts have been initially prepared.

Cu/Zn (65:35 atomic ratio) - prepared by co-precipitation of a solution of Cu and Zn nitrates with ammonium hydroxide at a constant pH of 9.0.

Cu/Zn (65:35 atomic ratio) - prepared by co-precipitation of a solution of Cu and Zn nitrates by the controlled addition of a sodium carbonate-sodium hydroxide solution to maintain a constant pH of 9.0. The resulting solid was subsequently washed in hot water to remove soluble Na cations.

Cu / Zn catalyst (30:70 atomic ratio) - prepared by coprecipitation from a solution of Cu and Zn nitrates by the controlled addition of potassium hydroxide-potassium carbonate mixture to maintain a constant pH of 9. The resulting material was washed in hot water to remove any residual potassium cations.

As will be discussed later, the synthesis of higher alcohols from methanol and ethanol requires at least two functions (hydrogenation/dehydrogenation and condensation) provided by metal and basic sites. The hydrogenation component is required to hydrogenate CO and to form aldehydic species. Basic sites are then used to form higher aldehydes and alcohols via aldol-type condensation reactions of aldehydic intermediates. The required level of intimacy between these functions remains one of the fundamental issues preventing the development of isobutanol synthesis catalysts from physical mixtures of independently optimized functions. The catalysts described in Table 1.1 have been prepared in order to examine these intimacy requirements. These materials have also been used in alcohol coupling studies (Task 3) in order to examine their properties for the aldol coupling steps involved in the isobutanol reaction sequence.

Table 1.1. Composition and Surface Areas of Modified Methanol Synthesis Catalysts

Sample	**Composition** (at. %)			**BET Surface Area**
	Cu	**Zn**	**Cs**	(m^2/g)
Cu-Zn-9-1	30	70	0	58.0
Cs-Cu-Zn-9-1	30	70	0.4	38.0
Cs-Zn-9-1	0	99.6	0.4	3.5
Zn-9-1	0	100	0	1.8
Zn-9-1*	0	100	0	4.1

All the samples were prepared by the controlled pH co-precipitation method. The controlled precipitation was carried out at a constant pH of 9 using copper and zinc nitrates solutions. The beaker in which the precipitation was carried out contained 1000 ml of deionized water before the addition or either the acidic or basic component. The precipitation was carried out using 1 M KOH + 1 M K_2CO_3 equimolar mixtures as precipitants. The acid pump flow and the base pump flow were monitored so that the pH was maintained at 9.0. The precipitation period was about an hour and the suspension was aged for an additional 30 min before filtration. After filtration, the filter cake was washed in two 250 ml aliquots of hot deionized water. These catalysts were subjected to a treatment procedure previously reported by Klier et al. [2]. The catalysts were first heated to 623 K in air at the rate of 5 K/min and then maintained at 623 K for 3 h.

Sample Zn-9-1* was prepared in an attempt to improve the surface area of sample Zn-9-1, which used NH_4OH instead of K_2CO_3 as the precipitant. Precipitation with K_2CO_3 leads to the formation of hydroxycarbonate species that may have been responsible for the higher surface area of the Cu/ZnO samples (Table 1.1). This procedure, however, did not increase the surface area of pure ZnO.

We have been unable to prepare ZnO samples with high surface areas using simple precipitation techniques. The presence of Cu appears to stabilize intermediate hydroxycarbonate precursors that cannot form during precipitation of pure Zn hydroxycarbonates, and which appear to be required to maintain high-surface area ZnO species during subsequent calcination and catalytic use.

1.2. Alcohol Coupling Catalysts

Aldehyde/alcohol coupling is an important step in the synthesis of the isobutanol from synthesis gas. The coupling between two aldehydes containing β–hydrogens to form a branched aldehydes (aldol condensation) requires basic catalysts or acid catalysts. The alcohol coupling reaction of interest in isobutanol synthesis would then require dehydrogenation of alcohols to the corresponding aldehyde followed by aldol condensation of the latter on basic metal oxides.

MgO is known to catalyze the condensation of alcohols to form higher alcohols, even without the presence of a separate dehydrogenation function [3]. However, MgO sinters readily in the presence of water at envisioned isobutanol synthesis temperatures leading a rapid and marked decrease in surface area from initial values above 200 m^2/g to less than 100 m^2/g. The presence of Al oxides appears to stabilize high surface area MgO under hydrothermal conditions. Segregation of a separate alumina phase in these metal oxides, however, would be detrimental because the resulting acid sites catalyze dehydration of required alcohol intermediates to ethers. The atomic mixing between magnesium and aluminum oxides in materials prepared from hydrotalcite precursors should introduce stabilizing effects of Al oxide species without the deleterious formation of a separate alumina phase.

Hydroxycarbonate precursors with hydrotalcite structures and general composition have general formulas of the type: $(A^{+2})_6(B^{+3})_2(OH^-)_{16}(CO_3)^{2-}4H_2O$, where, A can be Mg, Mn, Co, Zn , Cr and B can be Al, Fe, Cr etc. Metal oxides prepared by

calcination of hydrotalcite precursors have been used as catalysts for base-catalyzed reactions. These hydrotalcites materials offer compositional flexibility and form high surface area mixed-metal oxides after calcination at 573-773 K [4]. Calcined Mg-Al hydrotalcites have been shown to be selective for the formation of propanone from 2-propanol, a base-catalyzed reaction [5].

The usual atomic composition (Mg:Al) in hydrotalcites is 3:1. Hydrotalcite structures, however, can accommodate Mg:Al ratios from 2:1 to 10:1 under controlled synthesis conditions [6]. Samples with the following Mg:Al ratios: 1:0, 1.5:1, 2.5:1, 5:1, 10:1 have been prepared from hydrotalcite precursors. The Mg:Al (1.5:1) sample consists of a mixture of Mg aluminate and hydrotalcite phases, while the other compositions form pure hydrotalcites. These materials have been calcined at a temperature of 773 K for 12 h to form the mixed-metal oxides. Surface areas are being determined by N_2 physisorption and the density of basic sites will be measured by CO_2 chemisorption. The compositional range of these samples will allow the study of Al effects on the basicity and surface area stability of Mg oxides.

Hydrotalcites are aluminum-stabilized magnesium hydroxycarbonates that form layered structures and which decompose to high surface basic mixed Mg-Al oxides upon treatment in air at 773 K. They exhibit a potentially advantageous compositional flexibility. In our work, hydrotalcite materials have been synthesized in two different batches, A and B, using identical procedures while varying the Mg:Al atomic ratio in the synthesis mixture. Samples of batch A with atomic composition 10:1 MgAl-A and 5:1 MgAl-A showed BET surface areas (N_2 physisorption at 77 K) of 130 m^2/g and 230 m^2/g, respectively, after calcination. These samples had been precipitated at a pH of 8.5. The increase in surface area with increasing Al content is consistent with the sintering stability imparted by the Al component to MgO.

Samples in batch-B contained Mg:Al atomic ratios of 10:1, 5:1 and 3:1. X-ray diffraction analysis shows the formation of hydrotalcites, characterized by diffraction lines at low angles caused by the repeating hydrotalcite layered structure. X-ray diffraction patterns after calcination are consistent with the formation of mixed Mg-Al oxides. Line breadth analysis shows that the presence of Al decreases the crystallite size of the metal oxides, consistent with the higher surface area obtained when Al oxide is present in MgO samples. Transmission electron microscopy studies of the 10:1 MgAl-B sample after drying shows the characteristic layered structure of the undecomposed hydrotalcite. Also, this technique revealed pure MgO particles in regions devoid of Al ions, suggesting that the Mg:Al limiting ratio was met locally during precipitation and that the excess Mg ions precipitated as a segregated MgO phase.

1.3. Isobutanol and Methanol Synthesis Catalysts

Our target is the development of good isobutanol and methanol synthesis catalysts from CO/H_2 mixtures operating at relatively low temperature (~573 K) and pressures (~5 MPa). We chose two catalyst formulations among the best catalysts reported in the literature: the bifunctional Cu catalysts supported on modified MgO [7] and the modified methanol synthesis catalysts [1, 2].

1.4. Copper Catalysts Supported on Modified MgO

Alkali promoted $Cu/MgO/CeO_2$ materials and its individual components Cu/MgO, MgO/CeO_2, MgO, and CeO_2 were prepared for use in kinetic studies of alcohol coupling reactions, in identification of reaction intermediates, and in isobutanol synthesis from CO/H_2 mixtures at high pressures.

A first set of samples was prepared by coprecipitation of 1.2 M mixed metal nitrate solutions with potassium carbonate at 338 K and a constant pH of 9 under vigorous agitation in a stirred thermostated batch reactor. The precipitates were filtered, washed with deionized water at 333 K, and then dried at 353-363 K for 9 h. The resulting materials were calcined at 723 K for 4 h. The bulk compositions of the catalysts are shown in Table 1.2. The atomic ratios of Ce/Cu and Ce/Me(II) were determined by atomic absorption (AA) spectroscopy. Here, Me(II) represents Group IIA alkaline earth elements. Only the surface area of $Cu_{0.5}Ce_2MgO_x$ (34 m^2/g) was measured by dinitrogen physisorption BET methods.

Table 1.2. Composition of $Cu_{0.5}Ce_2MeO_x$ Samples

Sample	Formula	Ce/Cu	Ce/Me(II)
MG 1 - 1 O	$Cu_{0.5}Ce_2MgO_x$	3.76	1.70
MG 1 - 2 O	$Cu_{0.5}Ce_2CaO_x$	3.86	1.52
MG 1 - 3 O	$Cu_{0.5}Ce_2SrO_x$	3.58	1.44
MG 1 - 4 O	$Cu_{0.5}Ce_2BaO_x$	3.79	1.50

A second set of Cu-Mg-CeO_x catalysts was prepared in order to reproduce the catalysts reported by Apesteguia et al. [7, 8]. Cu-Mg-CeO_x samples were prepared by coprecipitation of mixed nitrate solutions with an aqueous solution of 2 M KOH and 1 M K_2CO_3 at 338 K and a constant pH of 9 in a well-stirred thermostated container. The solids formed were filtered, washed thoroughly with 300-500 cm^3 of deionized water at 343 K, and dried at 353-363 K overnight. Dried samples were treated in flowing air at 723 K for 4 h in order to form the corresponding mixed metal oxides. The controlled pH coprecipitation technique produces uniform precipitates that lead, after thermal treatment, to mixed metal oxides with high surface area and intimate contact between components [9]. K and Cs were introduced by incipient wetness of the oxidized samples using K_2CO_3 (0.25 M) and CH_3COOCs (0.25 M) aqueous solutions (K_2CO_3: Fisher Scientific, A.C.S. certified; CH_3COOCs: Stream Chemicals, 99.9%). Powder X-ray diffraction (XRD) patterns were collected using a D5000 Siemens Diffractometer and monochromatic Cu-K_α radiation. Total surface areas were determined using the single point BET method by measuring N_2 physisorption at 77 K using a continuous flow Quantasorb Surface Area Analyzer (Quantachrome Corp.). Bulk catalyst compositions were measured by atomic absorption spectroscopy (AAS). The propeties of alkali promoted $Cu/MgO/CeO_2$ and its individual components Cu/MgO, MgO/CeO_2, MgO and CeO_2 are summarized in Table 1.3.

A typical X-ray diffraction pattern of a dried precipitate Cu-Mg-Ce sample shows the presence of $Mg(OH)_2$ and $Ce(OH)_4/CeO_2$ phases (Figure 1.2a). The poor sample

crystallinity and the coincidence of diffraction lines for Ce oxide and hydroxide phases make it difficult to determine conclusively the form of Ce in dried samples. Precipitates did not show any diffraction lines corresponding to layered hydrotalcite-type structures.

Separate MgO and CeO_2 phases were detected by X-ray diffraction after air treatment at 723 K (Figure 1.2b). Diffraction lines occurred at the positions expected for the pure monometallic oxides and provided no evidence for $MgCeO_x$ mixed oxides. CuO crystallites were not detected, suggesting that the Cu component is well dispersed, either as small crystallites or as a solid solution within the CeO_2 lattice. Mixed Cu/Ce oxide solid solutions can form during co-precipitation and remain after high temperature oxidative treatment [10, 11, 12, 13].

The atomic ratios of Mg/Cu and Mg/Ce are in good agreement with the theoretical values. Irreproducible residual K-loadings (0.4 - 3.5 wt %) in $Cu/MgO/CeO_2$ and Cu/MgO initially occurred even though the samples have been thoroughly washed. The amount of potassium left on MgO/CeO_2 is even greater. The unusually low surface area of MG3-1O/K (K-$Cu/MgO/CeO_2$) was attributed to the presence of large amount of potassium on the catalyst.

Table 1.3. Composition and Surface Area of the Catalytic Oxides

Sample	**Mg/Cu** AAS	**Mg/Ce** AAS	**K** (wt %) nominal	**K** (wt %) AAS	**BET Surface Area** (m^2/g)
MG3 - 1 O	9.4	3.9	< 0.01	4.1	62
MG3 - 1 O/K	10.4	5.7	3.0	6.5	32
MG3 - 1b O			< 0.01	0.4	108
MG3 - 1b O/K	8.6	4.7	1.0	1.5	88
MG3 - 10 O	9.6	4.7	< 0.01		96
MG3 - 10 O/K			1.0		190
MG3 - 10 O/Cs			3.4		143
MG3 - 10 bO/K	11.1	4.8	1.0	1.0	162
MG3 - 11 O	9.6	4.7	< 0.01	2.6	93
MG3 - 11 O/K	9.6	4.7	1.0	3.5	61
MG3 - 11 Ow	9.6	4.7	<0.01	01	167
MG3 - 11 Ow/K	9.6	4.7	1.0	0.9	147
MG3 - 2 O (Mg-Ce)	---	4.6	<0.01	5.3	53
MG3 - 3 O (Ce)		---			0.2
MG3 - 4 O (Mg)	---	---			1.5
MG3 - 5 O (Cu-Mg)	8.0	---	<0.01	0.2	118
MG3 - 5 O/K (Cu-Mg)	8.0	---	1.0	1.1	112
MG3 - 6 O	0.7	4.9	<0.01	1.9	65
MG3 - 6 Ow	0.7	4.9	<0.01	0.03	117
MG3 - 6 Ow/K	0.7	4.9	1.0	1.2	92

For catalysts with similar compositions, the surface areas shown in Table 1.3 vary from sample to sample. This is a result of different amount of potassium left in the catalyst after precipitation. The presence of potassium causes sintering of the $MgCeO_x$ support. It is noteworthy that the surface area of MG3-10 O/K is twice as much as that of MG3-10 O, even though the amount of potassium is expected to be larger in the former. This reflects the fact that MG3-10 O/K was prepared via incipient wetness of MG3-10 O using K_2CO_3 solution. During this process, MG3-10 O was re-exposed to water and MgO was converted back to hydroxide, resulting in a higher surface area after calcination. It has been well established that the commercial, low surface area MgO (15-30 m^2/g) can be readily transformed to high surface area MgO (100-300 m^2/g) by hydrating MgO in boiling water and then calcining at temperatures > 673 K (10-12). Neither MgO (MG3-4 O) nor CeO_2 (MG3-3 O) gave a surface area greater than 1 m^2/g. The low surface area could be attributed to the presence of residual potassium ions left during catalyst preparation. As reported by Lunsford and co-workers [14, 15], the addition of Li to MgO resulted in a marked decrease in MgO surface area because of enhanced sintering rates.

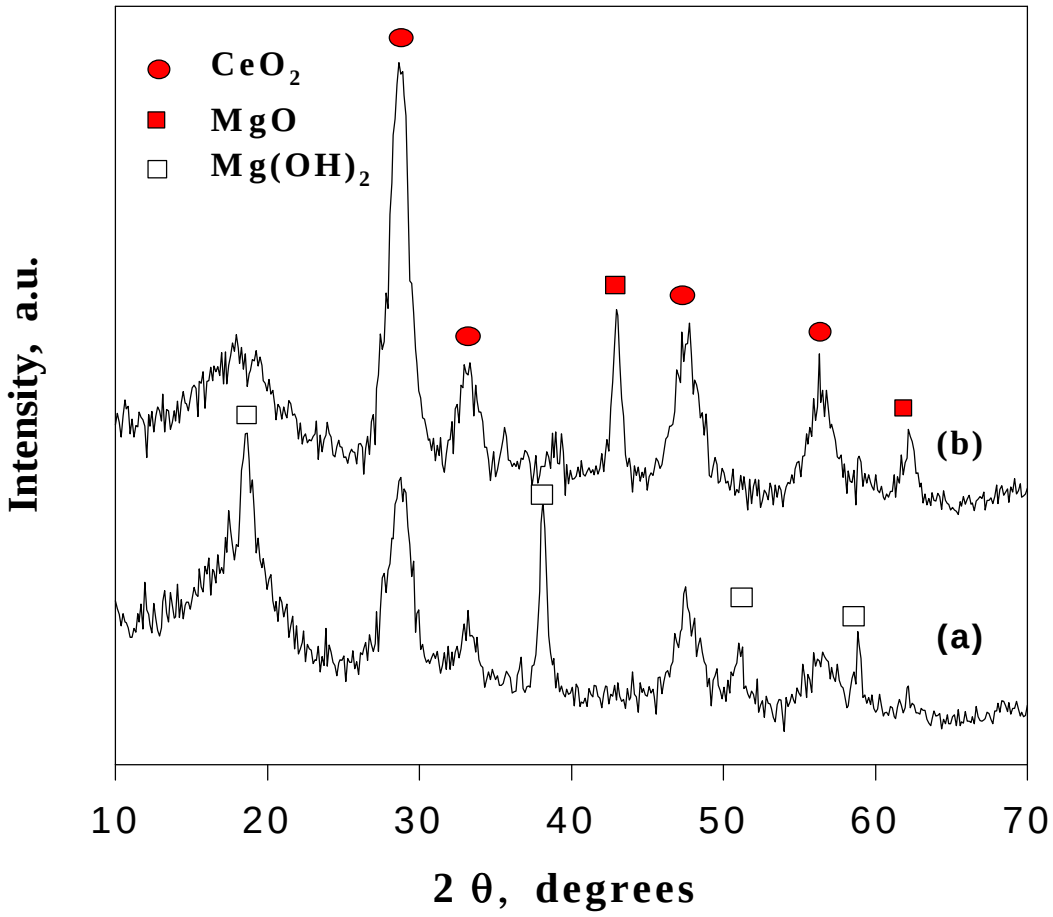

Figure 1.2. Powder X-ray diffraction patterns of Cu/Mg/Ce = 0.5/5.0/1.0 (atomic ratio) samples: (a) uncalcined and (b) treated in air at 723 K.

MG3-6 O ($Cu_{7.5}Mg_5CeO_x$) and MG3-11 O ($Cu_{0.5}Mg_5CeO_x$) contained large amounts of K, left behind during co-precipitation (Table 1.3). The MG3-6 and MG3-11 O precursor materials were re-washed in 1000 mL deionized water at 65 °C for 30 min in a stirred-batch reactor. The resultant precipitates were filtered, washed with 600 ml deionized water and calcined to give the mixed oxides MG3-6 Ow and MG3-11 Ow, respectively. MG3-6 Ow and MG3-11 Ow were impregnated with potassium by incipient wetness using a K_2CO_3 solution to give the corresponding MG3-6 Ow/K and MG3-11 Ow/K catalysts. The nominal potassium addition was 1 wt %. The samples were re-calcined at 723 K for 4 h. Their properties are summarized in Table 1.3. The difference between the nominal and the actual K concentrations on $Cu/MgO/CeO_2$, MgO/CeO_2 and MgO are due to the inability of removing K during the washing step. The surface area was found to decrease with increasing K-loading.

Both MG3-10 O/K and MG3-10 b O/K were prepared from MG3-10 O, but via different pathways. In the case of MG3-10 O/K, the precursor was calcined at 723 K prior to potassium impregnation. After impregnation, the sample was recalcined at 723 K for 4 h, and the resulting material was designated as MG-10 O/K. MG3-10 b O/K was prepared by impregnating the precursor with potassium carbonate before subject to calcination at 723 K.

Due to the high concentrations of residual potassium left behind during co-precipitation on MG3-2 O (Mg_5CeO_x), MG3-3 O (CeO_2), and MG3-4 O (MgO) (Table 3), a new batch of each material was synthesized. They were designated as MG3-7 O, MG3-9 O and MG3-8 O, respectively. Atomic analysis results showed less residual K on these samples because of improved washing procedures. The total surface area increased dramatically upon the removal of K (Table 1.4). Samples MG3-7 O and MG3-8 O were impregnated with K.

Table 1.4. Composition and Surface Areas of Catalytic Oxides

Sample	**Mg/Cu**	**Mg/Ce**	**K** (wt %) nominal	**K** (wt %) AAS	**BET Surface Area** (m^2 / g)
MG 3 - 2 O	---	4.6	<0.01	5.3	53
MG 3 - 3 O	---	---	<0.01		0.2
MG 3 - 4 O	---	---	<0.01		1.5
MG 3 - 7 O	---	5.2	<0.01	0.03	188
MG 3 - 7 O/K	---	5.2	1.0	0.8	155
MG 3 - 8 O	---	---	<0.01	0.2	194
MG 3 - 8 O/K	---	---	1.0	1.0	129
MG 3 - 9 O	---	---	<0.01	0.2	194

New batches of Mg_5CeO_x (MG3-12 O) and $Cu_{0.5}Mg_5CeO_x$ (MG3-13 O) were synthesized in order to verify the reproducibility in catalyst preparation and to provide large amounts of sample for testing in CMRU. The properties are given in Table 1.5.

Table 1.5. Composition and Surface Areas of Catalytic Oxides

Sample	Mg/Cu	Mg/Ce	K (wt %) nominal	K (wt %) AAS	BET Surface Area (m^2 / g)
MG 3 - 12 O	---	4.8	<0.01	0.01	183
MG 3 - 13 O	---	---	<0.01	<0.01	160
MG 3 - 13 O/K	---	---	1.0	1.0	150

Several new catalytic materials have also been prepared in order to improve the chain growth by incorporating a chain growth component (Co) into the best $CuMgMeO_x$ material (Me=Ce, Al). Some of these materials have been prepared in collaboration with Professor Carlos Apesteguia's research group in the Department of Chemical Engineering at Universidad Nacional del Litoral in Santa Fe (Argentina). $Cu_{0.5}Mg_5Al_{10}O_x$ (MG3-15 P) and $Cu_{0.5}Co_{0.1}Mg_5Al_{10}O_x$ (MG3-16 P) samples were provided by Apesteguia's research group without calcination (precursor samples). These samples were prepared by co-precipitation of 1.5 M mixed metal nitrate solutions with a mixture of KOH (2M) and K_2CO_3 (1M) at 333 K and a constant pH of 10 in a stirred-batch reactor following the procedures described by Apesteguia et al. [15]. The precipitates were filtered, washed with 600 ml of distilled water at 333 K and dried at 348 K overnight. Then, the precursors were crushed and suspended in 300 cm^3 of hot water, washed again with 600 cm^3 of hot water, filtered and dried at 348 K. The resulting precursors were calcined at 723 K for 4 h in order to obtain the mixed oxides. The amount of residual potassium, determined by atomic analysis, was less than 0.05 wt %. K- and Cs-promoted $CuMgAlO_x$ catalysts were prepared by incipient wetness of the oxidized samples using K_2CO_3 (0.25 M) and CH_3COOCs (0.25 M) aqueous solutions. Catalyst properties are summarized in Table 1.6.

Table 1.6. Compositions and Surface Area of Cu-Mg-Al-O_x

Sample	Nominal composition	Experimental composition			S.A. (m^2 / g)
		Cu/Mg	Al/Mg	alkali	
MG 3 - 15 O	$Cu_{0.5}Mg_5Al_{10}O_x$	0.12	2.3	---	327
MG 3 - 15 O/K	1.0 wt % K-$Cu_{0.5}Mg_5Al_{10}O_x$	0.12	2.3	1.2	264
MG 3 - 15 O/Cs	3.4 wt % Cs-$Cu_{0.5}Mg_5Al_{10}O_x$	0.12	2.3	2.9	258

As reported by Keim [16] and more recently by Dombeck [17], Pd has a promoting effect on higher alcohol production from synthesis gas. In our study, Pd-promoted $CuMgCeO_x$ samples were prepared in order to test the effect of Pd on total alcohol selectivity, isobutanol productivity, and isobutanol/methanol ratio. These catalysts were prepared by incorporating Pd into the modified MgO catalysts (K-$Cu_{0.5}Mg_5CeO_x$ and K(Cs)-Mg_5CeO_x). The precursor [$Cu_{0.5}Mg_5CeO_x$ (MG3-17 P)] was synthesized and washed with deionized water. No residual K was found by atomic absorption analysis. This sample was calcined at 723 K for 4 h in order to obtain the mixed oxides (MG3-17 O). Pd-promoted (0.25 wt %) $Cu_{0.5}Mg_5CeO_x$ samples were

prepared by incipient wetness impregnation of the mixed oxides with Pd solution, followed by dryness. The resulting material was calcined at 723 K for 4 h by using a heating rate of 0.5 K/min in order to decompose the Pd precursor. Finally, potassium was added by incipient wetness impregnation followed by drying and air treatment at 723 K (MG3-17 O/K/Pd). The sample properties are summarized in Table 1.7.

Table 1.7. Composition and Surface Area of the K-Pd-$Cu_{0.5}Mg_5CeO_x$ Oxide

Sample	**Mg/Cu** AAS	**Mg/Ce** AAS	**Pd** (wt %) nominal	**Pd** (wt %) AAS	**K** (wt %) nominal	**K** (wt %) AAS	**Sg** (m^2/g)
MG3-17 O/K/Pd	9.5	5.0	0.25	0.24	1.0	0.8	139

It is possible that acidic sites can be created during the reduction of K-$CuMgCeO_x$ catalysts, as shown below schematically:

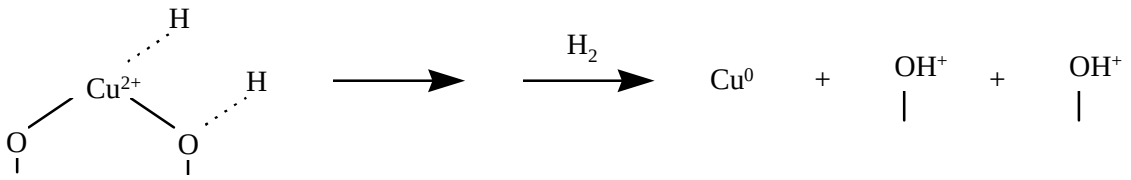

In order to investigate this possibility, the 0.25 wt % Pd-1 wt % K-$Cu_{0.5}Mg_5CeO_x$ catalyst was reduced in pure H_2 flow at 583 K, and passivated (10% air in He, i.e., ~2 % O_2, at 296-317 K) in CMRU. The catalyst was removed from the reactor and impregnated with an aqueous solution of KCO_3 by incipient wetness to add an additional 0.5 wt % of K and thus exchange K^+ ions for any H^+ species. The impregnated catalyst was then dried over night in He at 353-373 K. After drying the catalyst was heated in He to 673 K for 4 h (0.5 K/min) in order to decompose the K-precursor in the CMRU-unit. After reduction, its catalytic activity for methanol/isobutanol synthesis was tested.

1.5. Modified Methanol Synthesis Catalysts

Cs-$CuO/ZnO/Al_2O_3$ catalysts were also prepared. These types of catalysts are the most studied catalysts for low-temperature higher alcohol synthesis. Especially, Klier and co-workers have carried out significant studies on such catalysts [1, 2]. Samples were prepared by co-precipitation of 1 M mixed metal nitrate solutions with Na_2CO_3 (1 M) at 338 K and with a pH of 7 in a well stirred-batch reactor. The precipitates were filtered, *washed thoroughly* with deionized water at 338 K to remove sodium, and dried at 353-363 K overnight. The resulting precursors were calcined at 623 K for 4 h in order to obtain the mixed metal oxides. Catalyst compositions and surface areas of the oxides are given in Table 1.8.

Table 1.8. Composition and Surface Areas of Cu/Zn/Al Catalytic Oxides

Sample	M_xO_y (wt%), AAS				BET Surface Area (m^2 / g)	Identified compound (XRD)
	Cu	Zn	Al	Na		
MG 4 - 1 O	26.7	56.9	15.1	0.3	99	CuO, ZnO
MG 4 - 2 O	55.1	31.0	9.7	0.1	76	CuO, ZnO
MG 4 - 3 O	---	91.2	7.8	0.1	146	ZnO

The MG 4-2 O sample was subsequently impregnated with Cs by incipient wetness impregnation using CH_3COOCs (0.25 M) solution (CH_3COOCs: Stream Chemicals, 99.9%). Based on the results of higher pressure isobutanol synthesis from CO/H_2 obtained on 1.3 wt % Cs-$CuZnAlO_x$ catalysts in CMRU, a new $CuZnAlO_x$ catalyst with twice the amount of Cs was prepared in order to increase the ratio of basic to acid sites, which appears to favor isobutanol synthesis and to inhibit DME production. The catalyst properties are summarized in Table 1.9.

Table 1.9. Composition and Surface Areas of Cs-Cu/Zn/Al Catalytic Oxides

Sample	Cs (wt %) Nominal composition	Cs (wt %) AAS	BET Surface Area (m^2 / g)
MG 4 - 2 O/Cs	1.2	1.3	74
MG 4 - 2 O/Cs*	2.6	2.9	62

Based on the results obtained on K-$Cu_yMg_5CeO_x$ and Cs-$CuZnAlO_x$, in CMRU we synthesized a new catalytic material in order to test the effect of Zn on total alcohol selectivity, isobutanol productivity, hydrocarbons and DME selectivity, and CO_2 effects on basic sites by incorporating Zn into the modified MgO catalysts. These catalysts (1.0 wt % K-$Cu_{0.5}Mg_5ZnO_x$) were prepared by incorporating Zn instead of Ce into the modified MgO catalysts. The catalyst properties are given in Table 1.10.

Table 1.10. Composition and Surface Area of the 1.0 wt % K-$Cu_{0.5}Mg_5ZnO_x$ Oxide

Sample	Mg/Cu AAS	Mg/Zn AAS	K (wt %) nominal	K (wt %) AAS	BET Surface Area (m^2/g)
MG3-18 O	11.5	4.5	-	0.0026	108
MG3-18 O/K	11.5	4.5	1.0	1.3	69
MG3-19 O/K	---	5.0	1.0		
MG3-20 O/K	0.7	5.0	1.0		

Task 2: Catalyst Evaluation in Laboratory Scale Reactors

2.1. Background

The selective synthesis of methanol and isobutanol is attractive for the subsequent manufacture of methyl-tert-butyl-ether (MTBE) after dehydration to form isobutene. An equimolar molar ratio of methanol to isobutanol would be preferred for MTBE synthesis. Methanol and higher alcohols can also be used for direct blending with hydrocarbon fuels. A mixture of higher alcohols and methanol is preferred over pure methanol because of its higher water tolerance, reduced fuel volatility and lower vapor lock tendency, and also because of their higher volumetric heating values than pure methanol [18].

The addition of alkali to methanol synthesis catalysts leads to the formation of higher alcohols from H_2/CO mixtures [18], [19]. Cs appears to be the best promoter for higher alcohol synthesis, but Rb and K also increase the selectivity to higher alcohols [2], [20], [21]. Potassium is often used because of its availability and low cost. The most studied catalysts for low-temperature higher alcohol synthesis are based on Cu and ZnO, often with Al_2O_3 or Cr_2O_3 as structural promoters that increase the surface area and prevent sintering [2], [20]- [22]. Other Cu-based catalysts, such as K-$Cu_xMg_yCeO_z$ [7], [8], have recently been shown to catalyze the synthesis of isobutanol at low temperatures. Li-Pd/ZrO_2-MnO_2-ZnO catalysts show very high isobutanol synthesis productivity at high temperatures (>673 K) and pressures (>10 MPa) [16].

The development of isobutanol synthesis catalysts that can be used at relatively low temperatures (~573 K) and pressures (~5 MPa) may lower production costs and allow the use of slurry reactors. Slurry reactors are well-suited for highly exothermic reactions because of their excellent heat removal properties. At low temperatures, however, catalysts show high selectivity to methanol because methanol equilibrium, which is often approached during higher alcohol synthesis [23], [24], is favored at low temperatures. At the same time, the kinetically-limited synthesis of higher alcohols becomes slower at low temperatures. As a result, the molar ratio of methanol to isobutanol is far from unity at low temperatures.

The synthesis of methanol proceeds via reactions of CO_2 when using CO/CO_2/H_2 reactant mixtures and it is catalyzed by Cu surface atoms [25], [26]. When CO_2-free feeds are used, the rate of methanol formation is not proportional to the Cu surface area [25], and basic sites appears to be involved along with Cu sites in methanol synthesis from H_2/CO mixtures [25]. Isobutanol synthesis requires the initial formation of methanol and higher linear alcohols and subsequent chain growth reactions leading to 2-methyl alcohols. The formation of ethanol is the least understood step in this reaction sequence. Recent results suggest that ethanol is formed directly from CO on K-$Cu_{0.5}Mg_5CeO_x$ catalysts, but via methanol condensation steps on Cs-Cu/ZnO/Al_2O_3 [27], [28]. Although methanol is not involved in the formation of ethanol on K-$Cu_{0.5}Mg_5CeO_x$, it acts as a C_1 precursor in the synthesis of 1-propanol and isobutanol from ethanol [29], [30]. 2-Methyl-branched alcohols are formed by aldol-type condensation reactions; our recent

studies have shown that these reactions require both Cu and basic sites [30]. These findings are discussed in detail later on in this report (section 2.3). Condensation steps occur on basic sites, but Cu sites appear to be required in order to remove hydrogen from the surface and allow the initial C-H bond activation step. The addition of C_1 species to isobutanol (2-methyl-1-propanol) is slow because of steric effects and because isobutanol lacks two α-hydrogens required for aldol condensation reactions.

Small amounts of CO_2 (<2 %) promote methanol formation, but larger concentrations inhibit methanol synthesis [21], [31]. The sensitivity to CO_2 depends on catalyst composition. For example, Vedage et al. [21] showed that methanol synthesis rates on Cu/ZnO increased when 2-6% CO_2 was added to H_2/CO mixtures, but a much smaller effect was observed on Cs-Cu/ZnO. Steady-state oxygen coverages during methanol synthesis on Cu surfaces depend on the relative rates of addition and removal of oxygen during CO hydrogenation reactions [32]. At high CO_2 concentrations, the rate of surface oxidation increases relative to reduction, leading to higher steady-state oxygen coverages and to a (reversible) decrease in the number of surface Cu metal atoms available for methanol synthesis steps. Similar trends have been reported for higher alcohol synthesis [33].

2.2. Isobutanol Synthesis at High Pressure in a Catalytic Microreactor Unit (CMRU)

Our study focuses on high pressure microreactor studies of catalysts consisting of Cu metal crystallites and basic oxides for low temperature methanol-isobutanol synthesis. The study includes space velocity studies and CO_2 and alcohol addition experiments designed to probe reaction pathways required for isobutanol synthesis and detailed characterization studies of K-$Cu_yMg_5CeO_x$ and Cs-Cu/ZnO/Al_2O_3 catalytic materials.

High-pressure isobutanol synthesis studies were performed in a 1.27 cm i.d. stainless steel fixed-bed reactor held within a three-zone heated furnace in order to ensure uniform axial temperatures (Figure 2.1). The catalyst sample (2 g) was reduced in pure hydrogen (Matheson, 99.99 %) at 573-593 K and atmospheric pressure for 12 h before catalytic experiments were carried out at 4.5 MPa using synthesis gas (H_2/CO/Ar 0.45/0.45/0.1 at.; Matheson: 99.99% CO, 99.99 % Ar). Metal carbonyls were removed from synthesis gas streams using activated carbon (Sorb-Tech RL-13). H_2 was purified by passing through a catalytic purifier (Matheson, Model 64-1008). Traces of water were removed from H_2 and H_2/CO using molecular sieves (Matheson, Model 452:4A).

On-line GC samples were taken at regular intervals using a HP5890 II Plus gas chromatograph equipped with a thermal conductivity detector (TCD) and a flame ionization detector (FID). Products and reactants were separated using a 5% phenyl-methyl-silicone capillary column (HP-5, 50 m, 0.32 mm diameter, 1.05 μm film thickness) and a packed column (Porapak Q, 1.8 m length, 0.32 cm diameter). The concentration of Ar, N_2, CO, and CO_2 in the effluent from the packed column was analyzed on the TCD. FID was used to measure the concentrations of all organic compounds eluting from the capillary column.

CO_2 was added to the synthesis gas in order to examine the inhibiting effect of CO_2 on methanol and isobutanol synthesis rates. CO_2 was introduced together with an internal standard (N_2) in a 1:1 ratio. The gas mixture was passed through molecular sieves (Matheson, Model 452:4A) in order to remove trace amounts of water.

1-Propanol or ethanol were added using an ISCO 500 D liquid syringe pump. Propanol and ethanol were degassed with He for ~10 hours before charging it to the pump. The catalyst was isolated in the reactor in hydrogen at 1 atm and the alcohol-containing feed gas was analyzed while bypassing the reactor. After feed analysis, the alcohol-containing feed gas was switched through the reactor. After the alcohol addition study, the alcohol feed was stopped and the synthesis gas was kept flowing through the reactor in order to ensure recovery of activity and selectivity to the corresponding values measured before alcohol addition.

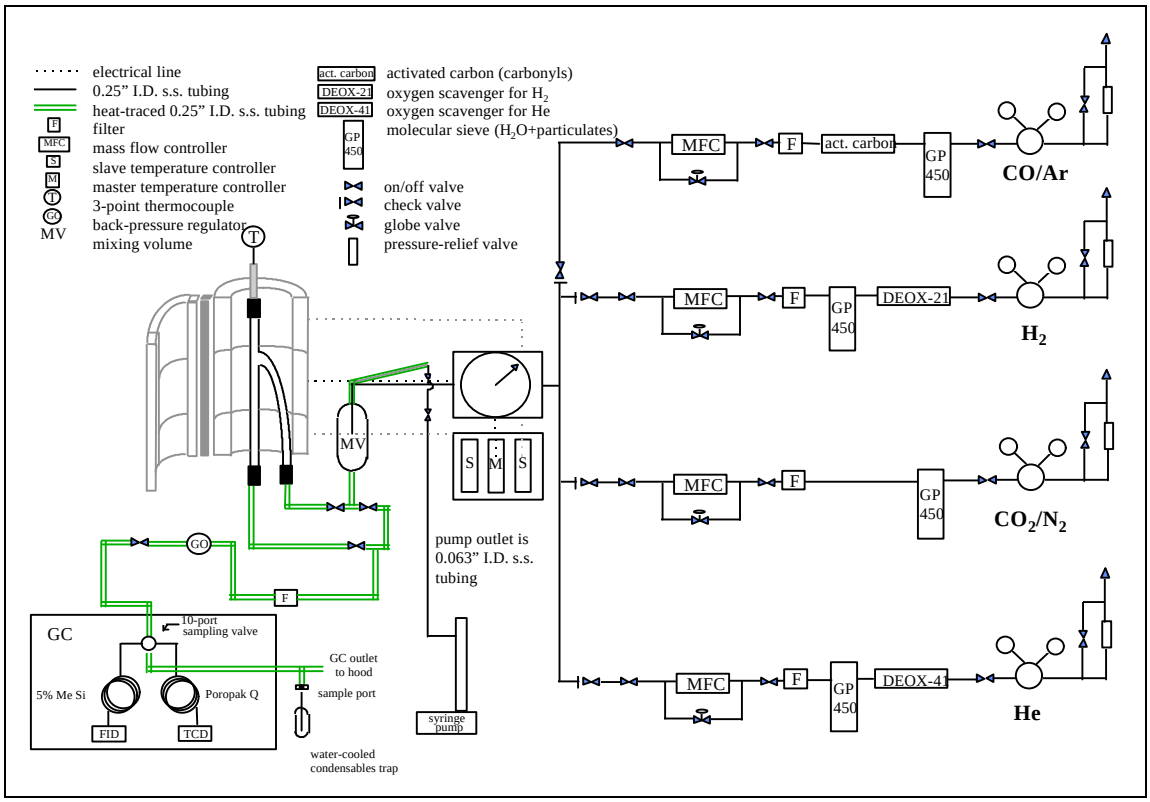

Figure 2.1: Catalytic Microreactor Unit.

2.2.1. Effects of Catalyst Physical Properties on Activity - K-$Cu_xMg_yCeO_z$.

Higher BET surface area K-$Cu_xMg_yCeO_z$ materials led to in more active catalysts for both methanol and isobutanol formation (Figure 2.2). Conversely, materials with surface areas lower than 100 m^2/g gave conversions of less than 4%. The positive correlation between surface area and activity led us to examine more closely at the K-loading on these catalysts, because higher K-loadings (> 1.5 wt. %) typically lead to low surface area materials.

Unpromoted catalysts contained residual amounts of K because coprecipitation was performed with KOH and K_2CO_3. Atomic absorption spectroscopy (AAS) of the mixed oxide solids after calcination showed a range of 0.4-3.5 wt. % K, resulting from variation in the residual amount of K left on the catalyst during coprecipitation.

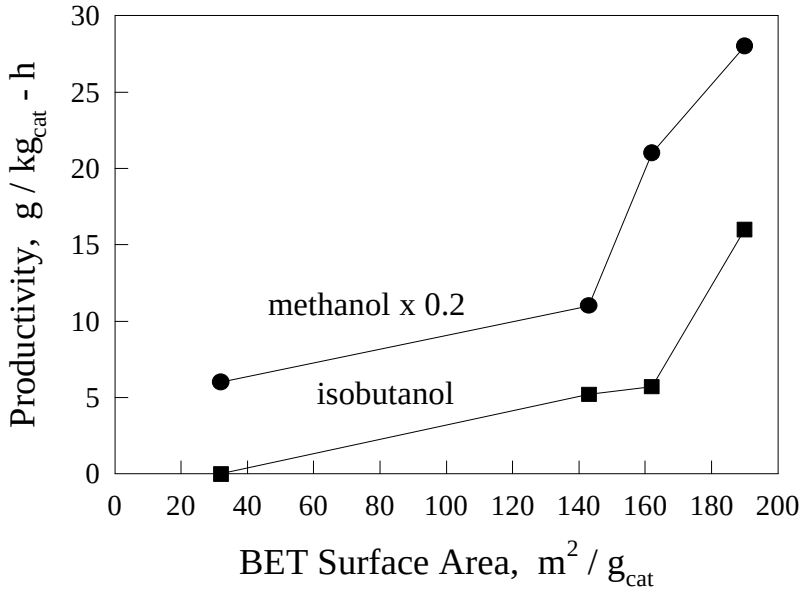

Figure 2.2. Alcohol Productivity vs. Surface Area on M-$Cu_{0.5}Mg_5CeO_{7.5}$ (M=K,Cs). [T=593 K, P=4.5-5.1 MPa, GHSV=1800 cm^3/g-cat·h, H_2/CO=1.]

Surface area measurements taken prior to K-impregnation showed that the addition of K usually decreased the surface area. Lunsford and co-workers [18], [19] showed that the addition of Li to MgO results in markedly decreased surface areas due to the sintering of MgO. Also, the surface area of M-Cu/MgO/CeO_2 (M=K,Cs) materials was found to decrease linearly with increasing alkali-loading (Figure 2.2).

The observed differences in total surface area and K-content the K-Cu/MgO/CeO_2, with the same nominal composition were attributed to irreproducible precursor washing and K-addition steps. MG3-11 O/K (K-$Cu_{0.5}Mg_5CeO_x$) contained 3.5 wt. % K and had a very low surface area (56 m^2/g). MG3-11 O/K was re-washed and re-impregnated to give MG3-11 Ow/K (0.9 wt% K-$Cu_{0.5}Mg_5CeO_x$); the latter gave a surface area of 145 m^2/g, suggesting that the efficiency of K removal during synthesis is the cause of the observed variation in BET surface area and Cu dispersion.

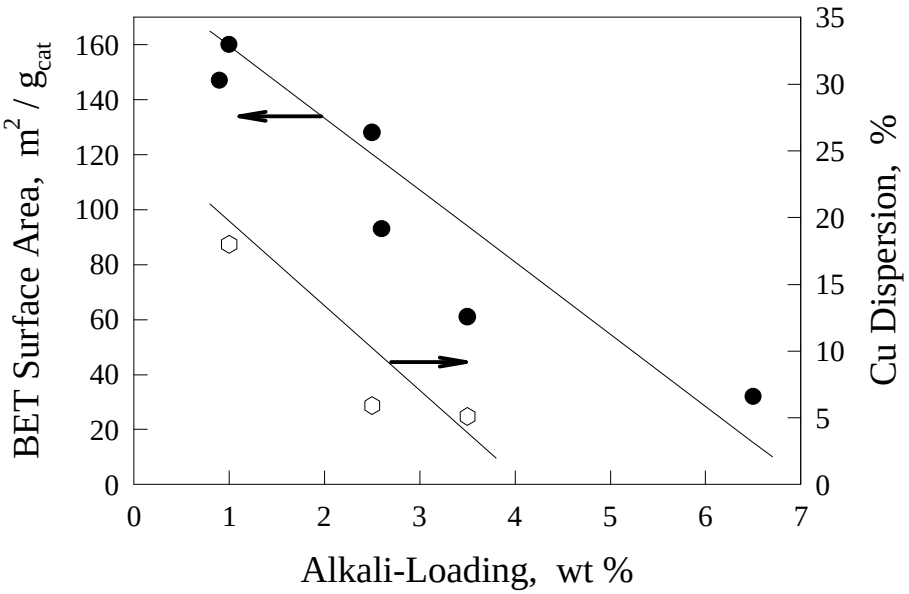

Figure 2.3. Cu Dispersion and Total Surface Area vs. Alkali-Loading on M-$Cu_{0.5}Mg_5CeO_x$ (M = K, Cs).

While unpromoted catalysts, Cu-Mg-Ce system (Catalysts MG3-1bO, MG3-11O, and MG3-10 O) showed similar surface areas (108, 93, and 96 m^2/g), the K-impregnated oxides (Catalysts MG3-1bO/K, MG3-11 O/K, and MG3-10 O/K) showed significantly different surface areas (89, 56, and 190 m^2/g). It suggests that K-impregnation is critical in the control of surface area (Table 1.3). The large increase in surface area of MG3-10 O after K-addition to give MG3-10 O/K was attributed to a transformation of the MgO phase to MgOH in the presence of water during K-impregnation [34].

High K materials also lead to low Cu dispersions, suggesting that K either enhances Cu sintering or covers surface Cu atoms (Figure 2.3) rendering them inactive for both N_2O decomposition. An optimum level of K on these catalysts is required so that basic and Cu sites are balanced to produce a sufficient number of methanol species (Cu, K-Cu) for the subsequent condensation (as surface formaldehyde) with another C_1 surface species to form ethanol (K, MgO). A basic function is also required to form 1-propanol (surface aldehydic derivatives of methanol and ethanol) and isobutanol (surface aldehydic derivatives of methanol and 1-propanol). MG3-11 O/K (3.5 wt.% K) gave a low CO conversion of 2.3 % at 593 K, 4.5 MPa, and 2500 cm^3/g-cat·h; however, the initial isobutanol selectivity was very high at 14.2, suggesting it contains a high density of basic sites but a low density of Cu sites. MG3-11 Ow/K (0.9 wt.% K) gave a CO conversion of 7.1% and an isobutanol selectivity of 5.2% at similar reaction conditions, suggesting that lower K-loadings give more active materials while higher K-loadings result in more basic catalysts. The higher activity obtained on low K materials, however, is more directly a result of their higher total surface areas.

2.2.2. Effect of Alkali Identity on Cu/MgO/CeO_2: K vs. Cs

Vedage et al. [21] studied methanol and higher alcohol synthesis on Cu/ZnO and on 0.4 at.% MOH-Cu/ZnO (M=Li,K,Rb,Cs,Ba), and reported that CsOH was the most effective alkali additive, based on a higher methanol synthesis rate and higher C_{2+} alcohol selectivities compared with the other alkali hydroxides. MG3-10 O/Cs (2.5 wt. % Cs-$Cu_{0.5}Mg_5CeO_x$) was studied at reaction conditions similar to those used with MG3-10 O/K (K-$Cu_{0.5}Mg_5CeO_x$) in order to explore the role of alkali identity on Cu/MgO/CeO_2 catalysts in the synthesis of higher alcohols. Mg3-10 O/Cs differs from MG3-10 O/K only in the alkali dopant ion and alkali loading, because both materials were derived from the identical mixed-metal oxide precursors. These catalysts are compared at high space velocities in order to circumvent artifacts, such as CO_2 inhibition and catalyst deactivation, both of tend to be more prevalent at low space velocities. At the space velocity given in Table 2.1, MG3-11 Ow/K had been on stream for ~ 100 h while MG3-10 O/Cs had been on stream for only ~10 h.

The low CO conversion (Table 2.1) on MG3-10 O/Cs compared with MG3-10 O/K at the same space velocity by the higher alkali-loading (2.1 wt. % Cs + 0.4 wt. % K) on the former. The alkali-content of MG3-10 O/K was never determined, however, the high activity of MG3-10 O/K suggests that the K-loading on this material was less than 1.5 wt. %. The surface area of MG3-10 O/Cs was 143 m^2/g compared to the value of 190 m^2/g of MG3-10 O/K, further suggesting a higher alkali-loading on MG3-10 O/K.

Comparison of product selectivities for these catalysts shows that MG3-10 O/K was much more selective in the formation of methanol and isobutanol than MG3-10 O/Cs (Table 2.1). The higher rates to isopropanol, dimethylether, and hydrocarbons on MG3-10 O/Cs are responsible for the high selectivity to CO_2. On an areal basis, MG3-10 O/Cs was exposed to ~ 30% more CO_2 than MG3-10 O/K due to the high formation rates of these products. CO_2 has been shown to decrease the rates for both methanol and isobutanol synthesis on these materials. The high CO_2 production on MG3-10 O/Cs was also shown to result in CO conversion and product selectivities that did not change with decreasing space velocity.

Ethanol formation appears to be the rate-limiting step in higher alcohol formation on alkali-modified Cu/ZnO/Al_2O_3 catalysts. Ethanol production was much higher on MG3-10 O/Cs (2.0 g/kg-cat·h) than on MG3-10 O/K (0.4 g/kg-cat·h) suggesting that Cs is more effective than K in catalyzing this rate-limiting step. Selectivities to ethanol and 1-propanol were high on MG3-10 O/Cs, however, the rate of their subsequent condensation reactions were lower on this catalyst (Table 2.1). The 1-propanol/ethanol and isobutanol/1-propanol ratios were 12.2 and 6.3 on MG3-10 O/K compared with values of 4.2 and 1.6 on MG3-10 O/Cs, indicating that 1) both the C_2 to C_3 and C_3 to i-C_4 growth steps were slower on MG3-10 O/Cs compared with MG3-10 O/K, and 2) the C_3 to i-C_4 growth step decrease more than the C_2 to C_3 growth step on MG3-10 O/Cs. These results are attributed to both CO_2 oxidation of Cu and CO_2-inhibition of basic sites on MG3-10 O/Cs.

Table 2.1. MG3-10 O/K (K-$Cu_{0.5}Mg_5CeO_x$) and MG3-10 O/Cs (2.5 wt. % Cs-$Cu_{0.5}Mg_5CeO_x$) results at 593 K and 5.1 MPa

	CMRU-13	**CMRU-14**
Catalyst	A	C
	K-$Cu_{0.5}Mg_5CeO_{7.5}$	2.1 % Cs-$Cu_{0.5}Mg_5CeO_{7.5}$
BET S.A. (m^2/g)	190	143
Mg/Ce atomic ratio	5	5
Charge (g)	4.32	3.21
T (K)	594	593
P (MPa)	5.1	5.1
GHSV (cm^3(STP) /g-cat·h)	3626	3600
H2/CO feed ratio	1	1
CO Conversion	14.0%	10.0%
Rate (mmol CO coverted/g-cat·h)	9.3	6.6
Rate (mmol CO converted/m^2·h)	0.21	0.15
Product Selectivities[a] (mol% C)		
methanol	**75.5**	**66.1**
ethanol	0.2	1.3
1-propanol	2.0	5.3
isopropanol	0.1	3.4
2-butanol	0.1	0.2
isobutanol	**12.9**	**8.5**
1-butanol	0.1	0.2
1-pentanol	0.2	0.4
2-methyl-1-butanol	1.1	0.8
dimethylether	1.0	2.4
CH_4	2.3	3.3
C_{2+} paraffins	0.4	0.5
CO_2	12.7	22.9
MeOH/i-BuOH	5.9	7.8
Alc/HCs	41.2	25.5

[a]Selectivities are normalized on a CO_2-free basis (except CO_2).

The observation that neither the CO conversion nor product selectivities changed appreciably over a wide range of space velocities on both MG3-10 O/K and MG3-10 O/Cs, the lack of space velocity effects being more pronounced on MG3-10 O/Cs, was explained by a shortened active catalyst bed . The differences in the product distributions obtained on MG3-10 O/K and MG3-10 O/Cs at a high space velocity (Table 2.1) suggests that the shorter active catalyst bed on MG3-10 O/Cs results from the following sequence of events (Figure 2.4): at high space velocities (at the start of the run) and high ethanol, isopropanol, and 1-propanol productivities accompanied by H_2O (with ethanol and 1-propanol) and CO_2 formation (with isopropanol), result in CO_2 oxidation of Cu and

CO_2 inhibition of basic sites at reactor outlet regions. The number of available Cu and basic sites decreased down the length of the bed, because the number of condensation reaction events increased with bed length due to the sequential scheme required to grow higher alcohols. The progression of site-blocking by CO_2 rendered the end of the bed, where isobutanol forms, inactive. Meanwhile, the number of available acid sites was unchanged. At the end of the bed, which contained a large number of active acid sites compared to active basic sites, surface carbon species were converted to dimethylether and hydrocarbons. As the reactor residence time was increased (by lowering the space velocity), site-blocking by CO_2 progressed upwards in the bed because the longer residence times enabled C_{2+} alcohol formation at earlier regions in the bed.

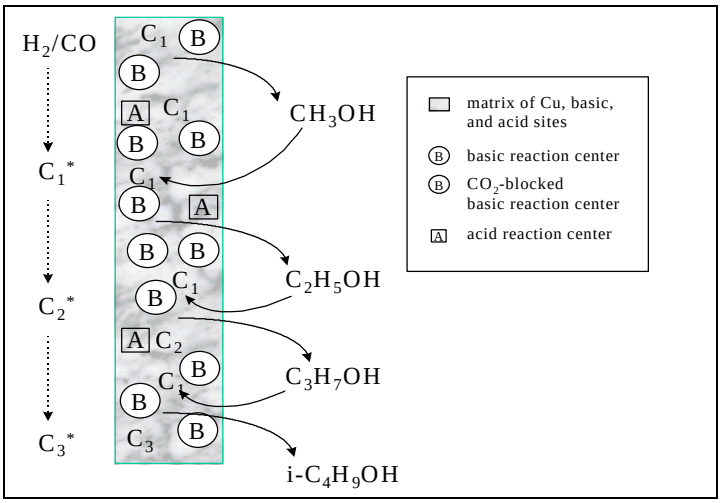

Figure 2.4. Progression of Cu and basic site inhibition by CO_2. As residence time increases, the number of available Cu and basic sites decreases while the number of available acid sites remains unchanged. At very long residence times, there are no available basic sites at the reactor outlet where isobutanol forms.

At the lowest space velocity, only the basic sites at the reactor inlet were active for C_{2+} alcohol formation, however, the residence time in this region of the bed is short and the probability that ethanol will re-adsorb onto the catalyst to grow to 1-propanol is small. The probability that 1-propanol will re-adsorb onto the catalyst and grow to isobutanol then becomes.

The observation that MG3-10 O/K gave a higher CO conversion and selective formation of isobutanol was attributed a longer active catalyst bed. The apparent differences in CO_2 inhibition of basic sites on MG3-10 O/K and MG3-10 O/Cs were attributed to the alkali dopant ion. The observation that Cs is more effective than K for C_{2+} alcohol formation has been explained by the higher basicity of Cs [21]. Cs, therefore, probably has a higher binding energy for CO_2 than K and therefore interacts more strongly with the inhibiting CO_2 products of higher alcohol synthesis reactions.

2.2.3. Reproducibility of CMRU-unit

Two samples of the same catalyst MG3-13 O/K (1.0 wt % K-$Cu_{0.5}Mg_5CeO_x$) was tested at the same conditions in order to check reproducibility of the CMRU. Figure 2.5 shows the conversion and selectivities for the two comparable runs (CMRU-23 and -24) and Table 2.2 shows comparison of the two runs at 6000 cm^3/g-cat·h. The reproducibility is excellent, but a somewhat lower isobutanol (3.2 % vs. 4.3 % at 10 % conversion) and higher hydrocarbon selectivity (5.9 vs. 4.7 %) were observed in CMRU-24 most likely due to inhomogeneity within the catalyst bed.

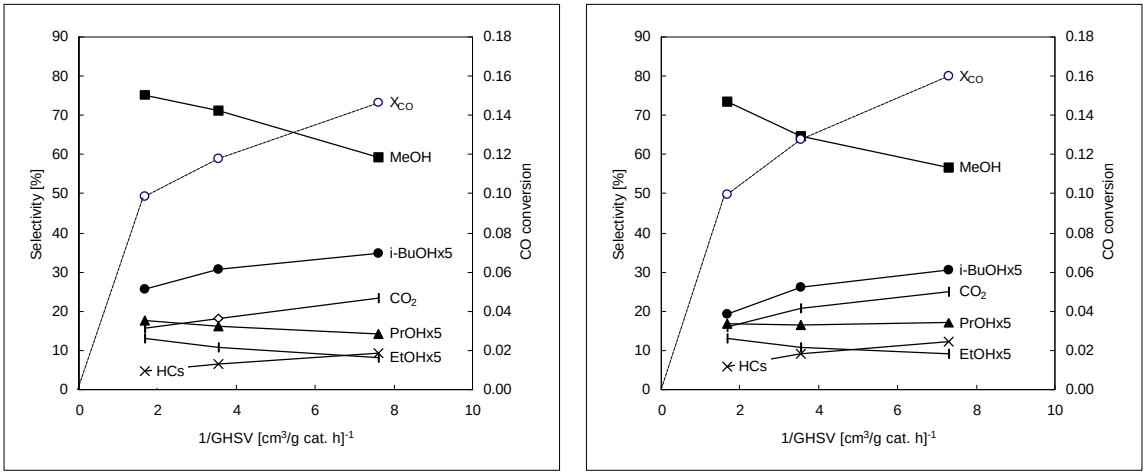

Figure 2.5. CO conversion and product selectivities for CMRU-23 and -24. [Catalyst: 1%K-$Cu_{0.5}Mg_5CeO_x$, 2.06 g, 4.5 MPa, 593 K, H_2/CO=1, 1500-6000 cm^3/g-cat·h.]

Table 2.2. Comparison of CMRU-23 and –24 [Catalyst: 1wt % K-$Cu_{0.5}Mg_5CeO_x$, 2.06 g, 4.5 MPa, 593 K, H_2/CO=1, 6000 cm^3/g-cat·h]

RUN	CMRU-23	CMRU-24
Catalyst	MG3-13O/K	MG3-13O/K
Amount [g]	2.06	2.06
GHSV [cm^3/g cat. h]$^{-1}$	6000	6000
CO conversion [%]	9.9	10.0
Rate of Reaction (mmol CO converted/g. cat.*hr.)	10.9	11.1
Methanol Productivity (g/kg*hr)	227.8	224.2
Isobutanol Productivity (g/kg*hr)	7.5	5.6
Selectivities (CO_2-free)		
CO_2 (%C)	15.6	16.1
Methanol	75.2	73.5
Ethanol	2.6	2.6
1-Propanol	3.6	3.4
Isopropanol	1.0	1.3
2-butanol	0.07	0.15
Isobutanol	4.3	3.2
1-butanol	0.00	0.27
1-pentanol	0.18	0.11
2-methyl-1-butanol	0.49	0.48
2-methyl-2-butanol	0.12	0.18
2-methyl-1-pentanol	0.14	0.14
1-hexanol	0.00	0.00
2-methyl-1-hexanol	0.02	0.00
Methane	3.6	4.4
C_{2+} Paraffins	1.1	1.5
Alcohols Selectivity	88.9	86.6
Paraffins Selectivity	4.7	5.9

2.2.4. Methanol Synthesis

Methanol can be formed from synthesis gas following reaction (1). However, methanol synthesis catalysts also catalyze water-gas-shift reaction (2). The stoichiometry of methanol synthesis from CO_2 is described by reaction (3).

$$CO + 2H_2 = CH_3OH \quad (1)$$
$$CO + H_2O = CO_2 + H_2 \quad (2)$$
$$CO_2 + 3H_2 = CH_3OH + H_2O \quad (3)$$

The H_2/CO consumption ratio for methanol produced from CO is 2:1. Based on the stoichiometry of higher alcohol synthesis (reaction (4)), the H_2/CO consumption ratio for this reaction should also be 2:1. However, simultaneous water-gas shift reactions modify this ratio as illustrated by the combination of reaction (2) and (4) resulting in (5).

$$n\text{CO} + 2n\text{H}_2 \rightarrow \text{C}_n\text{H}_{2n+1}\text{OH} + (n\text{-}1)\text{H}_2\text{O} \quad (4)$$
$$(2n\text{-}1)\text{CO} + (n\text{+}1)\text{H}_2 \rightarrow \text{C}_n\text{H}_{2n+1}\text{OH} + (n\text{-}1)\text{CO}_2 \quad (5)$$

Thus, the H_2/CO usage ratio tends to decrease with increasing alcohol chain length, because of the larger number of water molecules formed and subsequently converted to CO_2 and H_2 in reaction (2).

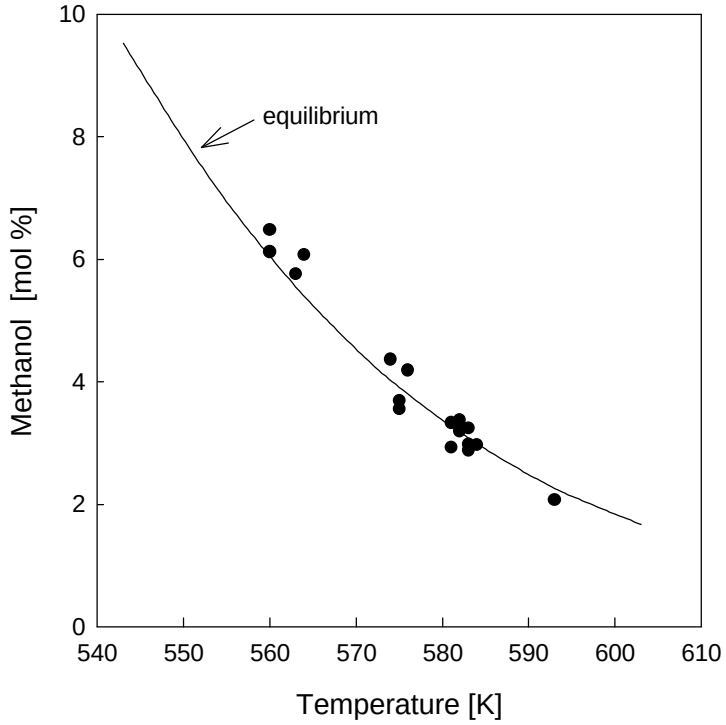

Figure 2.6. Methanol mole fraction as a function of reaction temperature for Cs-Cu/ZnO/Al_2O_3 and K-$Cu_yMg_5CeO_x$. [4.5 MPa, 1500-6000 cm^3/g/h, H_2/CO = 1.0 Solid line: equilibrium methanol mole fraction.].

Figure 2.6 shows how the measured mole fraction of methanol in the effluent stream varies with temperature. Equilibrium methanol mole fractions, assuming methanol is produced by reaction (1), are also plotted in Figure 2.6. The equilibrium mole fraction was calculated using temperature and pressure correlations for the equilibrium constant reported by Klier et al. [31], which account for non-ideal gas behavior. The excellent agreement between measured and thermodynamic methanol concentrations shows that methanol synthesis reactions are at equilibrium at the reaction conditions of this study. As a result, the effect of changing process variables such as temperature, pressure and CO/H_2 feed composition on methanol synthesis rates can be predicted from thermodynamics. When methanol yields are limited by equilibrium, synthesis rates become proportional to space velocity, because CO conversion to methanol remains constant with increasing bed residence time, as illustrated for two catalysts in Figure 2.7. The formation of higher alcohols are favored by higher temperatures and by low space velocities. However, these conditions also favor the rapid equilibration of methanol synthesis reactions.

Methanol synthesis catalysts also catalyze water-gas-shift (WGS) reactions and the latter reaction is also expected to approach equilibrium. During higher alcohol synthesis, WGS reactions convert the water formed in the synthesis of higher alcohols, hydrocarbons, and dimethylether (DME), to CO_2 and H_2, while consuming carbon monoxide, because thermodynamics favors the formation of CO_2 at our reaction conditions (K_{eq}=30). Water can inhibit higher alcohol synthesis [35] therefore its conversion to CO_2 may be desirable. Rapid WGS equilibration, however, makes it difficult to determine independently the inhibitory effect of CO_2 and H_2O on alcohol synthesis reactions because any addition of CO_2 leads to an increase in both H_2O and CO_2 concentrations.

2.2.5. Bed Residence Time Effects

The effects of space velocity (bed residence time) on alcohol synthesis rates and selectivities are shown in Figure 2.7 for 2.9 wt. % Cs-Cu/Zn/Al_2O_3 and 1.0 wt. % K-$Cu_{0.5}Mg_5CeO_x$ catalysts. CO conversion should increase linearly with increasing bed residence time at the low CO conversion levels of our study, unless the predominant methanol synthesis steps approach thermodynamic equilibrium. The observed decrease in the slope for the CO conversion curve with increasing bed residence time in Figure 2.6 reflects mainly the rapid approach to methanol synthesis equilibrium, as discussed above. It may also be influenced by an inhibition effect of CO_2 and H_2O on methanol synthesis, which becomes stronger as CO_2 and H_2O concentrations increase with increasing CO conversion. Isobutanol and higher alcohols form in secondary chain growth reactions, such as methanol carbonylation and aldol coupling reactions, and therefore their concentrations increase with increasing bed residence. C_2-C_3 alcohols are intermediate products that undergo further chain growth; therefore, their selectivity reaches a maximum value at intermediate residence times.

Isobutanol is a kinetic end product of aldol condensation chain growth processes, because it lacks the two α-hydrogens required for facile chain growth via aldol condensation pathways. Therefore, isobutanol selectivity increases monotonically with increasing residence time. This increase, however, is less marked on K-$Cu_{0.5}Mg_5CeO_x$ than on Cs-Cu/ZnO/Al_2O_3, because chain growth reactions are inhibited by CO_2 reaction products more strongly on K-$Cu_{0.5}Mg_5CeO_x$ than on Cs-Cu/ZnO/Al_2O_3. These effects are discussed in detail below. CO_2 appears to inhibit aldol coupling reactions during isobutanol synthesis reactions on K-promoted $Cu_{0.5}Mg_5CeO_x$ catalysts. Weaker basic sites on Cs-Cu/ZnO/Al_2O_3 [36] appear to be less sensitive to CO_2 poisoning; as a result, isobutanol selectivities reach higher values than on K-$Cu_{0.5}Mg_5CeO_x$ as bed residence time and CO conversion increase (Figures 2.7a and 2.7b).

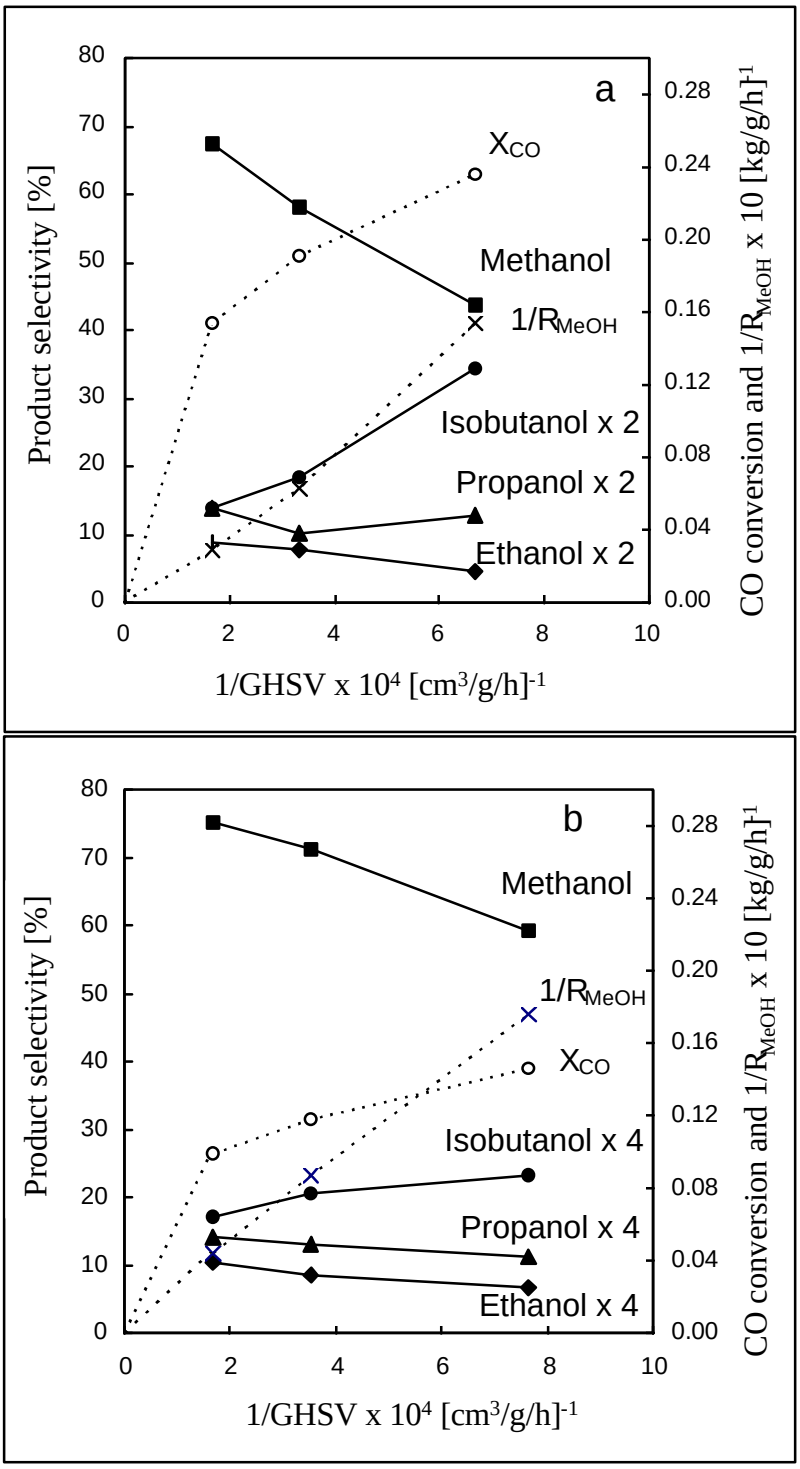

Figure 2.7. CO conversion and product selectivities vs. space velocity on: a) Cs-Cu/ZnO/Al_2O_3; b) K-$Cu_{0.5}Mg_5CeO_x$. [583 K, 4.5 MPa, CO/H_2 = 1, product selectivities are on CO_2-free basis.]

2.2.6. CO_2-Addition Effects

The presence of CO_2 in modest concentrations (1-2 % mol) increases methanol synthesis rates on typical methanol synthesis catalysts (e.g., $Cu/ZnO/Al_2O_3$) [31]. High CO_2 concentrations (>10 % mol), lead to surface oxidation and inhibit methanol synthesis on these catalysts [31]. Cs-modified methanol synthesis catalysts reach maximum rates at very low CO_2 concentrations (~2 % mol) [20]. Relative rates of oxidation and reduction of Cu surface atoms determine the steady-state coverage of oxygen reaction intermediates during methanol synthesis. High concentrations of an oxidant, such as CO_2 or H_2O, will increase the rate of oxidation relative to reduction and lead to higher steady-state oxygen coverages and to fewer Cu surface atoms available for methanol synthesis. These Cu surface metal atoms catalyze methanol synthesis reactions of $CO/CO_2/H_2$ mixtures [25], [26].

The details of CO_2 inhibition effects on methanol and isobutanol synthesis were examined by adding CO_2 to the H_2/CO reactants. As already mentioned, the effect of CO_2 cannot be separated from the effect of H_2O, because of the rapid equilibration of WGS reactions. CO_2 addition results are shown in Figure 2.8 as the reciprocal of the methanol, ethanol, 1-propanol and isobutanol synthesis rates as a function of CO_2 concentration. Typical Langmuir-Hinshelwood rate expressions (Equation (6)) lead to straight lines when data are plotted in this form.

$$r = r_0/(1+KP_{CO_2}) \qquad (6)$$

Methanol synthesis rates on catalysts with high Cu contents decreased only slightly as CO_2 concentrations increased. Methanol synthesis rates on catalysts with lower Cu contents (1.0 wt. % $K\text{-}Cu_{0.5}Mg_5CeO_x$) were more strongly inhibited by CO_2. These results are consistent with the more complete approach to equilibrium on catalysts with higher Cu surface densities. Catalysts containing a higher density of Cu surface sites (e.g., on 1.0 wt. % $K\text{-}Cu_{7.5}Mg_5CeO_x$ and 2.9 wt. % $Cs\text{-}Cu/ZnO/Al_2O_3$) can maintain equilibrium methanol concentrations even after a significant fraction of such sites are covered with oxygen adatoms during steady-state catalysis; therefore, the effect of CO_2 on methanol productivity is observed only at higher CO_2 concentrations. Equilibrium methanol concentrations vary slightly with CO_2 concentration [24]; this may account for the slight decrease in methanol yield observed even on catalysts with high Cu content. As expected, catalysts containing fewer Cu sites (e.g., 1.0 wt. % $K\text{-}Cu_{0.5}Mg_5CeO_x$) become unable to maintain methanol synthesis equilibrium conversions at lower CO_2 concentrations than catalysts with higher density of Cu sites.

The effect of CO_2 on higher alcohol synthesis has not been as thoroughly studied as that on methanol synthesis. Tronconi *et al*. [35] observed decreased higher alcohol yields on $K\text{-}ZnCrO_x$ at 673 K when CO_2 (3-6%) was added to the H_2/CO feed. These authors proposed that water, formed from CO_2 in reverse water-gas-shift reactions, titrated alcohol synthesis sites. Elliot [37] showed that synthesis rates for higher alcohols on Cu/ZnO were increased by the addition of small amounts of CO_2 (6%). Calverley and Smith [33] observed that higher alcohol rates at 558 K reach a maximum at intermediate

CO_2 concentrations (~4 % CO_2) on $Cu/ZnO/Cr_2O_3$ (0-0.5 wt. % K_2CO_3). They also observed that CO_2 inhibition became stronger with increasing alkali concentrations (0.5-4.0 wt. % K_2CO_3) when 9 % CO_2 was added.

Figures 2.8b, c and d show reciprocal ethanol, 1-propanol, and isobutanol synthesis rates as a function of the average CO_2 partial pressure within the catalyst bed. The catalyst with low Cu content ($Cu_{0.5}Mg_5CeO_x$) was inhibited more strongly by the presence of CO_2 than catalysts with higher Cu content. This may be due to 1) the decrease in [33] methanol concentrations observed only on the low-Cu content catalysts, and 2) the loss of Cu and basic sites required for isobutanol synthesis. Although methanol is not involved in the initial formation of ethanol on K-$Cu_{0.5}Mg_5CeO_x$ [28], it acts as a C_1 precursor in the synthesis of 1-propanol and isobutanol from ethanol. Aldol coupling-type reactions of alcohols require both Cu and basic sites [29]; therefore any blocking of surface Cu atoms by oxygen can also lead to a decrease in isobutanol synthesis rates, even when such blocking does not influence the rate of equillibrated methanol synthesis steps.

CO_2 inhibition of isobutanol synthesis reactions may also reflect the reversible titration of basic sites on oxide surfaces by an acidic molecule, such as CO_2. The inhibiting effect of CO_2 on isobutanol synthesis rates is greater on 0.9 wt. % K-$Cu_{7.5}Mg_5CeO_x$ than on 2.9 wt. % Cs-$Cu/ZnO/Al_2O_3$, possibly because of the stronger basicity of the former (measured from the rate of CO_2 isotopic exchange [30]. On catalysts with low Cu content, chain growth reactions appear to be limited by the availability of minority Cu sites and thus CO_2 titration of such sites decreases chain growth rates. Higher Cu contents lead to chain growth rates limited by steps occurring on basic sites, which are blocked by CO_2 most effectively on the stronger basic sites present on the modified MgO materials. Basic sites on 0.9 wt. % Cu-$Mg_{7.5}Mg_5CeO_x$ appear to be more sensitive to CO_2 than corresponding sites on 2.9 wt. % Cs-$Cu/ZnO/Al_2O_3$, as previously shown from the faster CO_2 isotopic exchange rates on the latter catalysts [30] and discussed in detail later on in this report.

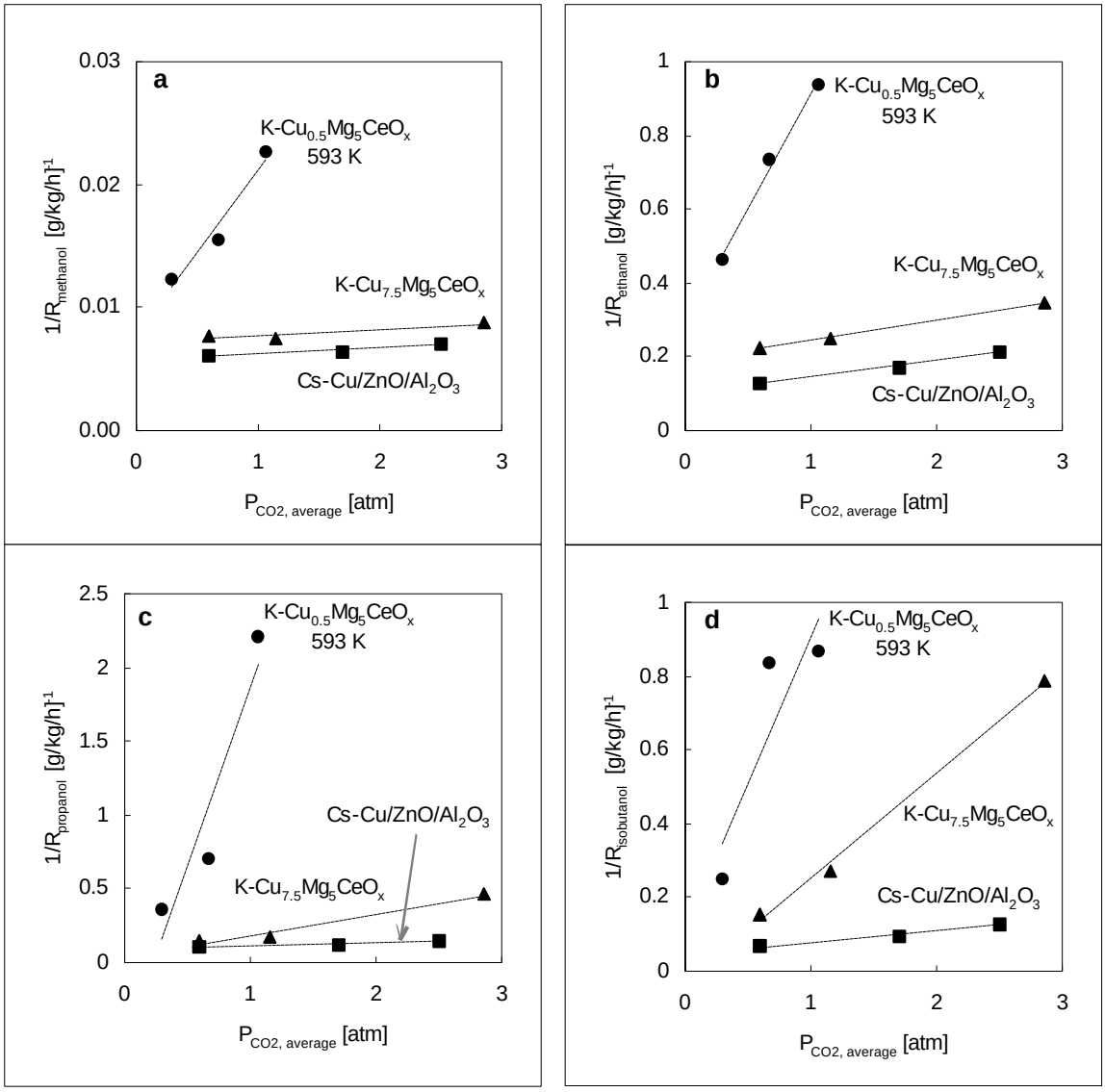

Figure 2.8. Reciprocal methanol (a), ethanol (b), propanol (c) and isobutanol (d) productivity vs. average CO_2 partial pressure on 1 wt. % K-$Cu_{0.5}Mg_5CeO_x$, 2.9 wt. % Cs-$CuZnAlO_x$ and 0.9 wt. % K-$Cu_{7.5}Mg_5CeO_x$. [583 K, 4.5 MPa, H_2/CO=1, 3000 $cm^3/g/h$.]

2.2.7. Cu Concentration Effects

As shown previously, alcohol synthesis on catalysts with higher Cu concentrations is more weakly inhibited by CO_2 than on catalysts with lower Cu contents. Therefore, high Cu concentrations should lead to higher alcohol synthesis rates and selectivities. Table 2.3 shows CO conversion and product selectivities for 0.9 wt. % K-$Cu_{7.5}Mg_5CeO_x$ and 1 wt. % K-$Cu_{0.5}Mg_5CeO_x$.

At similar CO conversions, isobutanol synthesis rates are higher on the catalyst with high Cu content. Isobutanol selectivity, however, is lower on this catalyst. Isobutanol selectivity does not increase with decreasing the space velocity on the catalyst with high Cu content because CO_2 (or H_2O) concentrations increase, leading to more severe inhibition, as CO conversion increases.

The 0.9 wt. % K-$Cu_{7.5}Mg_5CeO_x$ catalyst shows a higher selectivity to methyl acetate than the 1.0 wt. % K-$Cu_{0.5}Mg_5CeO_x$ catalyst. Methyl acetate and other esters can be formed by Canizzaro-type condensations of two aldehydes, by reactions of surface carboxylates with formyl or formaldehyde, or by Tishchenko-type reaction of aldehyde species with surface alkoxides [20]. The latter reaction seems to be the most plausible pathway, in view of the expected presence of both aldehydes and surface alkoxides on the surface o our catalytic materials. The high selectivity to methyl acetate on the 0.9 wt. % K-$Cu_{7.5}Mg_5CeO_x$ catalyst suggests that Cu sites promote the formation of methyl acetate, possibly by increasing aldehyde surface concentrations during higher alcohol synthesis.

The high Cu catalyst has a higher selectivity to hydrocarbons than the low Cu catalyst at similar CO conversions. Both hydrocarbons and dimethylether are formed on acidic sites, but the formation of hydrocarbons requires subsequent reactions of dimethylether. This suggests that the high Cu catalysts has a higher acid density than the low Cu catalyst. This may reflect the formation of acids during reduction of CuO, which is present in higher concentration on catalysts with high Cu content. Hydrocarbon selectivity increases rapidly with decreasing space velocity on both catalysts, apparently because basic sites are inhibited by CO_2, while acidic sites remain active throughout the catalyst bed.

Increasing the copper concentration leads to catalysts that are more resistant to CO_2 inhibition (Figure 2.8). High CO_2 concentrations titrate basic sites on both high and low-Cu catalysts, but high Cu catalysts retain a higher density of Cu sites required in condensation reactions. Higher isobutanol synthesis rates will then be obtained on high Cu catalysts at similar levels of CO conversion and CO_2 concentration.

Table 2.3. Alcohol synthesis rates and selectivities on 0.9 wt. % K-$Cu_{7.5}Mg_5CeO_x$ and 1 wt. % K-$Cu_{0.5}Mg_5CeO_x$ [583 K, 4.5 MPa, H_2/CO=1]

Catalyst	0.9 wt. % K $Cu_{7.5}Mg_5CeO_x$		1 wt. % K $Cu_{0.5}Mg_5CeO_x$
Gas Hourly Space Velocity [cm^3/g/h]	6000	1500	1500
CO conversion [%]	17.6	26.9	14.7
Rate of Reaction [mmol CO conv./g/h]	19.4	7.4	4.0
Methanol Synthesis Rate [g/kg/h]	289	58	65
Isobutanol Synthesis Rate [g/kg/h]	9.5	2.7	3.7
Methyl Acetate Productivity [g/kg/h]	19.3	9.3	1.3
Methanol Turnover Rate [mmol/mol Cu_s/s]	4.4	0.9	2.3
Isobutanol Turnover Rate [mmol/mol Cu_s/s]	0.06	0.02	0.06
CO_2 selectivity [% C]	27.5	40.5	23.4
Carbon Selectivities [%, CO_2-free]			
Methanol	57.4	35.5	63.1
Isopropanol	2.7	3.9	2.3
Ethanol	2.0	1.2	1.8
1-Propanol	3.1	1.7	3.0
Isobutanol	3.3	2.8	6.2
Paraffins	19.9	39.0	9.9
Methyl acetate	4.7	6.4	1.2
DME	0.7	1.0	6.8

2.2.8. Effect of replacing Ce with Al in K-$Cu_{0.5}Mg_5CeO_x$

A 1 wt% K-$Cu_{0.5}Mg_5Al_{10}O_x$ catalyst have been tested for isobutanol synthesis activity. $MgAlO_x$ materials have been reported to catalyze condensation reactions [38]. McKenzie et al. [8] have shown, however, that these catalysts are less basic than MgO. $^{13}CO_2/^{12}CO_2$ isotopic exchange studies performed in our laboratory indicate that these catalysts have a low density of basic sites exchangeable at 573 K and hence few basic sites that are likely to participate in the base-catalyzed formation of higher alcohols. Also, alcohol reaction studies on MgAlO materials in our recirculating reactor studies led to production of DME, indicating the presence of acid sites.

The catalyst was reduced at 623 K, a temperature that was chosen after studying the reduction of the catalyst by temperature-programmed reduction. It is reasonable to expect that the substitution of Al for Ce results in an decreased reducibility of Cu, because Ce promotes the reduction of Cu (probably by providing atomic hydrogen). Such an effect is not expected for Al, which generally results in slower reduction of metal oxides (for example Co- and Ni-oxides) and thus in a higher required reduction temperature.

CO conversion and productivities on 1 wt% K-$Cu_{0.5}Mg_5Al_{10}O_x$ are shown in Table 2.4. This catalyst produces a large amount of DME and the isobutanol productivity is very low. This suggests that the catalyst has high density of acid sites available. These results are not unexpected since high DME selectivity was also observed when MgAlO materials were tested in recirculating reactor studies of methanol-propanol coupling reactions.

The equilibrium constant for DME ($K = P_{DME}\ P_{H2O}/P_{MeOH}^2$) is of the order ~10 at our reaction conditions. The experimentally determined K's, assuming that the water-gas-shift reaction is equilibrated (in order to obtain P_{H2O}) are of the order 0.1, and the DME reaction has not reached equilibrium at our reaction conditions. Decreasing the space velocity led to a decrease in methanol productivity. DME is formed from two methanol molecules. As the space velocity is decreased more methanol can be consumed in secondary reactions. This effect is expected to be more pronounced on this catalyst because of the large amount of secondary products (i.e. DME).

After the initial space velocity study, the catalyst was tested at the initial reaction conditions again (i.e. 6000 $cm^3/g/h$, 583 K, 4.5 MPa), in order to check the stability of the catalyst (Table 2.5). The catalyst lost about 35% of its methanol productivity and 28% of its DME productivity.

The reaction temperature was decreased to 563 K at 6000 $cm^3/g/h$ in order to investigate the DME productivity of this catalyst at temperatures compatible use in slurry reactors. The results are presented in Table 2.5. Decreasing the temperature resulted in increased methanol productivity and decreased DME productivity. The DME productivity is decreased, because this reaction is kinetically-limited at higher temperatures and the increase in methanol productivity is a result of less methanol being converted to DME and not primarily a result of thermodynamic constraints on the methanol synthesis.

Table 2.4. Product selectivities and productivities on 1 wt. % K-$Cu_{0.5}Mg_5Al_{10}O_x$ [583 K, 4.5 MPa, H_2/CO=1]

CMRU-28, 1 wt. %K-$Cu_{0.5}Mg_5Al_{10}O_x$				
GHSV $cm^3/g/h$	6000	3000	1500	6000
CO conversion %	15.5	22.0	29.5	12.0
Rate mmol CO converted/g/h	17.0	12.1	8.2	13.4
Methanol productivity g/kg/h	104	52.0	22.0	68
Isobutanol productivity g/kg/h	0.9	0.7	0.7	1.1
Dimethyl ether productivity g/kg/h	207	155	102	149
CO_2 selectivity (%C)	22	24.2	27.5	23

Table 2.5. Product selectivities and productivities on 1 wt. %K-$Cu_{0.5}Mg_5Al_{10}O_x$ at 583 K and 563 K [4.5 MPa, H_2/CO=1, 6000 $cm^3/g/h$]

CMRU-28, 1 wt. % K-$Cu_{0.5}Mg_5Al_{10}O_x$		
Temperature [K]	583	553
CO conversion [%]	12.0	10.0
Rate [mmol CO conv./g/h]	13.4	10.8
Methanol productivity [g/kg/h]	68	79
Isobutanol productivity [g/kg/h]	1.1	-
Dimethyl ether productivity [g/kg/h]	149	83
CO_2 productivity [g/kg/h]	136	119

Based on the low isobutanol productivity obtained on 1 wt % K-$Cu_{0.5}Mg_5Al_{10}O_x$, we decided to omit further testing of Cs-$Cu_{0.5}Mg_5Al_{10}O_x$ and K/Cs-$Cu_{0.5}Mg_5CoAlO_x$ in CMRU.

2.2.9. Effect of substituting Ce with Zn in K-$Cu_{0.5}Mg_5CeO_x$

ZnO is a weak basic oxide which is used in methanol synthesis catalysts. In addition to its basic properties, it also has hydrogenating ability. We have substituted ZnO with CeO_2 component in the K-$Cu_{0.5}Mg_5CeO_x$ in order to explore potential improvements in catalyst performance. The results are shown in Figure 2.9 and Table 2.6.

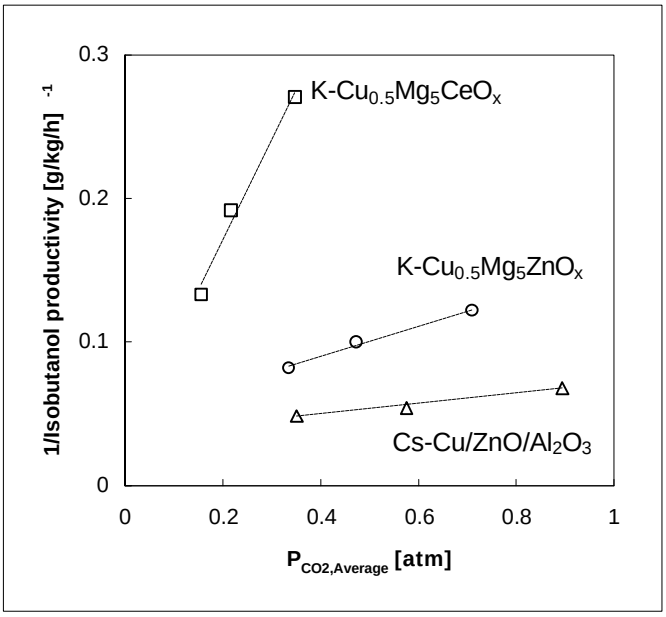

Figure 2.9. Reciprocal isobutanol synthesis rate vs. average CO_2 partial pressure on K-$Cu_{0.5}Mg_5ZnO_x$, 1 wt. % K-$Cu_{0.5}Mg_5CeO_x$ and 2.9 wt. % Cs-Cu/ZnO/Al_2O_3. [583 K, 4.5 MPa, H_2/CO=1, 1500-6000 cm^3/g/h].

The K-$Cu_{0.5}Mg_5ZnO_x$ catalyst shows improved isobutanol synthesis rates and is less inhibited by CO_2 than the K-$Cu_{0.5}Mg_5CeO_x$ catalyst. Isobutanol synthesis rate and CO_2 inhibition effects are between those of K-$Cu_{0.5}Mg_5CeO_x$ and Cs-Cu/ZnO/Al_2O_3 catalysts. The K-$Cu_{0.5}Mg_5ZnO_x$ catalyst also has lower DME and hydrocarbon selectivity than the K-$Cu_{0.5}Mg_5CeO_x$ catalyst when compared at similar CO conversions. This is not unexpected since both ZnO and MgO are basic oxides which should have low acid site densities. The composition of this catalyst has not been varied (i.e. alkali content, Cu/Mg/Zn ratio) and it is likely that optimization of the composition could lead to even more effective catalysts.

Table 2.6. Product selectivities and productivities on K-$Cu_{0.5}Mg_5ZnO_x$ and the K-$Cu_{0.5}Mg_5CeO_x$ [583 K, 4.5 MPa, H_2/CO=1]

Catalyst	1 wt % K $Cu_{0.5}Mg_5ZnO_x$			1 wt % K $Cu_{0.5}Mg_5CeO_x$		
GHSV [cm^3/g/h]	6000	3000	1500	6000	3000	1500
CO Conversion [%]	13.6	16.4	19.9	9.9	11.8	14.7
Rate [mmol CO conv./g/h]	15.0	9.1	5.5	10.9	6.5	4.0
Methanol Productivity [g/kg/h]	257.9	141.3	67.1	227.8	122.2	65.0
Isobutanol Productivity [g/kg/h]	12.2	10.0	8.4	7.5	5.2	3.7
CO_2-selectivity [% C]	24.3	28.6	35.1	15.6	18.1	23.4
Carbon selectivities [%, CO_2-free]						
Methanol	64.6	60.2	50.6	75.2	71.1	63.1
Ethanol	5.7	4.7	3.4	2.6	2.2	1.8
1-Propanol	6.4	6.3	6.1	3.6	3.3	3.0
Isobutanol	**5.3**	**7.4**	**10.9**	**4.3**	**5.1**	**6.2**
Dimethylether		-		4.0	4.5	6.8
Methyl acetate	0.8	1.2	1.8	1.1	1.0	1.2
Paraffins Selectivity		4.7	6.5	4.7	6.5	9.9

2.2.10. Effect of adding small amounts of Pd

Isobutanol synthesis on catalysts with low Cu content appears to be limited by the hydrogenation/dehydrogenation function on these catalyst, especially at high CO_2 concentrations when Cu surfaces become partially covered with oxygen atoms. Pd metal is an excellent hydrogenation/dehydrogenation catalyst, and its presence in small amounts may provide hydrogenation sites even at high CO_2 concentrations. Metal-oxygen bonds are weaker on PdO than on CuO, and thus Pd metal is less likely to oxidize than Cu metal ($\Delta G \approx$ -170 and -100 kJ/mol, respectively [39]). Pd has been used as catalyst for the synthesis of higher alcohols [16], but at much higher temperatures and pressures than in our study.

Table 2.7 shows the effect of adding small amounts of Pd (0.25 wt. %; Pd/Cu at.=0.02) to 1 wt. % K-$Cu_{0.5}Mg_5CeO_x$. CO conversions are similar on both 1 wt. % K-$Cu_{0.5}Mg_5CeO_x$ and 1 wt. % K-0.25 wt. % Pd-$Cu_{0.5}Mg_5CeO_x$ catalysts at all space velocities. Methanol synthesis rates are similar because methanol synthesis is near equilibrium on both catalysts. Isobutanol synthesis rates are similar on the two catalysts at high space velocities, at which CO conversions and CO_2 concentrations are low. Thus, Pd seems to have only a minor effect on the behavior of 1 wt. % K-$Cu_{0.5}Mg_5CeO_x$, at low these CO_2 concentrations.

At lower space velocities the Pd-promoted catalyst shows higher isobutanol synthesis selectivity and rates, suggesting that Pd indeed prevents the adverse effects of CO_2. Pd may remain metallic as CO_2 concentrations increase and continue to provide hydrogenating sites required for alcohol coupling reactions, even at higher CO_2 concentrations. A horizontal line in Figure 2.10 is expected for a differential reactor in the absence of product inhibition. The addition of Pd to the K-$Cu_{0.5}Mg_5CeO_x$ leads to a near horizontal line in Figure 2.10.

Table 2.7. Productivities and selectivities on 1 wt. % K - 0.25 wt. % Pd - $Cu_{0.5}Mg_5CeO_x$ and 1 wt % K-$Cu_{0.5}Mg_5CeO_x$ [583 K, 4.5 MPa, $H_2/CO=1$]

Catalyst	1 wt. % K 0.25 wt. % Pd $Cu_{0.5}Mg_5CeO_x$			1 wt. % K $Cu_{0.5}Mg_5CeO_x$		
Gas Hourly Space Velocity[$cm^3/g/h$]	6000	3000	1500	6000	3000	1500
CO Conversion [%]	10.6	13.1	15.8	9.9	11.8	14.7
Rate [mmol CO conv./g/h]	11.7	7.2	4.4	10.9	6.5	4.0
Methanol Synthesis Rate [g/kg/h]	236.2	130.4	64.5	227.8	122.2	65.0
Isobutanol Synthesis Rate [g/kg/h]	7.8	6.9	5.3	7.5	5.2	3.7
CO_2-selectivity [% C]	19.2	22.8	28.1	15.6	18.1	23.4
Carbon selectivities [%, CO_2-free]						
Methanol	74.3	68.4	59.3	75.2	71.1	63.1
Ethanol	3.6	3.0	2.6	2.6	2.2	1.8
1-Propanol	3.7	4.1	4.1	3.6	3.3	3.0
Isobutanol	4.3	6.2	8.4	4.3	5.1	6.2
Dimethylether	1.0	1.2	1.6	4.0	4.5	6.8
Methyl acetate	0.7	0.9	1.3	1.1	1.0	1.2
Paraffins Selectivity	6.3	8.7	13.3	4.7	6.5	9.9

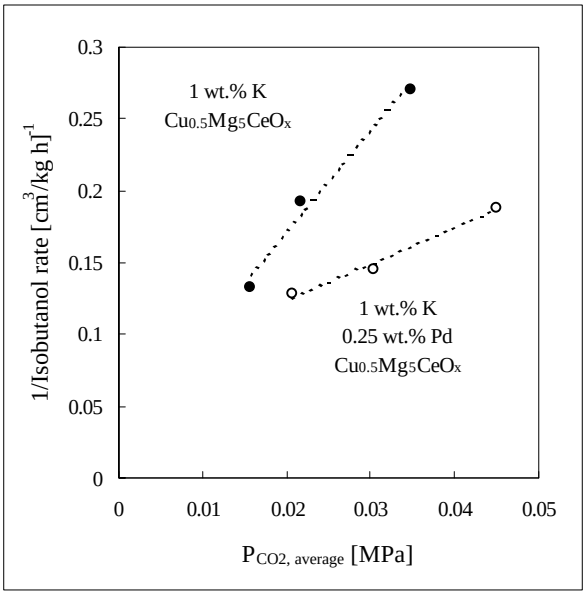

Figure 2.10 Reciprocal isobutanol synthesis rate as a function of average CO_2 partial pressure on 1 wt. % K-0.25 wt. % Pd-$Cu_{0.5}Mg_5CeO_x$ and 1 wt % K-$Cu_{0.5}Mg_5CeO_x$. [583 K, 4.5 MPa, $H_2/CO=1$.]

2.2.11. Effect of acid site titration after CuO reduction

It is possible that acidic sites can be created during reduction for the K-$Cu_xMg_5CeO_x$ catalysts.

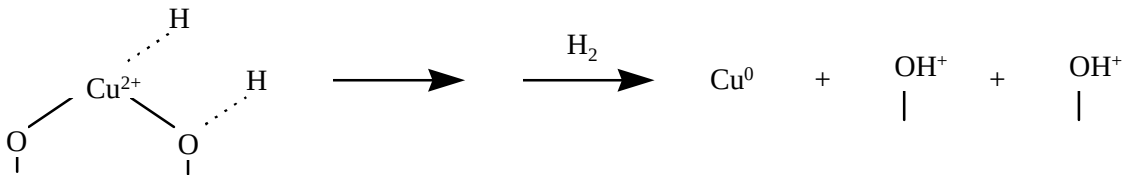

In order investigate this possibility, this catalyst was reduced and passivated and then a small additional amount of K was introduced in order to neutralize any new acidic sites formed during reduction. The catalyst was then tested in CMRU in order to study the effect of post-reduction acid site titration on methanol/isobutanol synthesis activity.

After reduction in pure H_2 at 583 K, the catalyst was cooled down to 300 K and flushed with He for 30 min.. The reduced catalyst was then treated in an air/He mixture (10 % air in He, i.e. 2 % O_2) at 300 K for 1 h in order to passivate the catalyst. The catalyst was removed from the reactor and impregnated with an aqueous solution of KCO_3 by incipient wetness, in order to add about an additional 0.5 wt % of K. The impregnated catalyst was then dried over night in He at 353-373 K. After drying the catalyst was heated in He to 673 K for 4 h (0.5 K/min) in order to decompose the K-precursor in the CMRU-unit. This procedure was followed by a normal reduction.

Table 2.8 shows the CMRU results of the reduced/passivated sample together with the results of the reduced only catalyst. This specially treated catalyst has lower methanol and isobutanol productivity than the reduced only catalyst. The decrease in methanol productivity suggests that the treated catalyst has a lower Cu surface area. This is further illustrated by plotting the methanol yield (i.e. selectivity times CO conversion) as a function of 1/GHSV (Figure 2.11). The yield increases significantly with decreasing space velocity as expected when equilibrium is not attained by the reactor exit. It is likely that the decrease in isobutanol productivity mainly is a result of decrease in Cu surface area. For these low Cu catalysts the dehydrogenation/hydrogenation function limits the isobutanol rate.

DME was not detected for the treated catalyst, while the selectivity to hydrocarbons remained essentially unchanged. The methyl acetate selectivity also remained essentially the same. The only effect of the treatment described above therefore seems to be decreasing the Cu surface area, which again results in lower methanol and isobutanol productivity. The Cu surface area or BET area were not measured, but it is expected to have decreased significantly for this higher K content. Nunan et al. [27] have tested Cu/ZnO catalysts in which Cs was added to either the calcined or the reduced catalyst and found no difference in methanol activity for these two catalysts.

Table 2.8. Productivities and selectivities for 0.25 wt % Pd - 1 wt % K-$Cu_{0.5}Mg_5CeO_x$ [583 K, 4.5 MPa, H_2/CO=1]

Catalyst	Reduced only		Reduced, passivated	
GHSV [cm^3/g h]	6000	3000	6000	3000
CO Conversion [%]	10.6	13.1	7.2	9.1
Rate (mmol CO conv./g h)	11.7	7.2	8.0	5.0
Methanol Productivity (g/kg h)	236.2	130.4	162.5	87.5
Isobutanol Productivity (g/kg h)	7.8	6.9	2.3	1.4
Selectivities (CO_2-free)				
CO_2 (% C)	19.2	22.8	19.1	24.4
Methanol	74.3	68.4	76.6	67.0
Ethanol	3.6	3.0	3.9	4.0
1-Propanol	3.7	4.1	2.6	2.7
Isobutanol	4.3	6.2	1.2	1.9
DME	1.0	1.2	-	-
Methyl acetate	0.7	0.9	0.7	0.9
Paraffins Selectivity	6.3	8.7	6.0	11.2

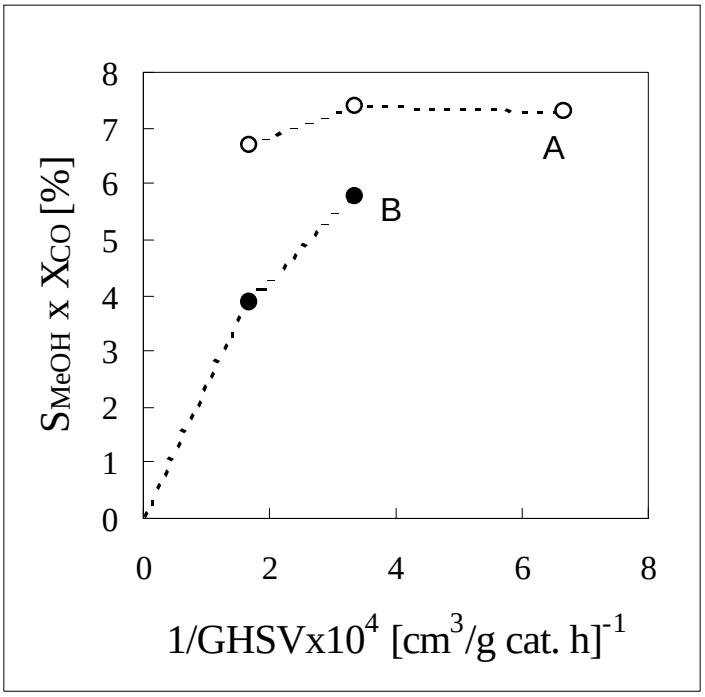

Figure 2.11. Methanol selectivity times CO conversion as a function of reciprocal space velocity. [H_2/CO = 1, 4.5 MPa, 583 K, 0.25 wt % Pd-1 wt % K-$Cu_{0.5}Mg_5CeO_x$. A-reduced only, B- reduced, passivated and more K added.]

2.2.12. Effect of Cs Concentration

The effect of increasing Cs concentration was studied on $Cu/ZnO/Al_2O_3$ catalysts. Methanol and higher alcohol synthesis rates were previously shown to reach a maximum with increasing alkali loading [20]- [40]. The amount required for optimum higher alcohol synthesis depends on the identity of the alkali added and also on the density of acid sites on the catalyst [41].

Table 2.9 shows alcohol synthesis rates on $Cu/ZnO/Al_2O_3$ catalysts promoted with Cs at two concentration levels (1.2 and 2.9 wt. %). Data reported by Klier *et al.* [41] on a similar $Cs\text{-}Cu/ZnO/Al_2O_3$ sample are also shown in Table 2.9. An increase in Cs concentration from 1.2 wt. % to 2.9 wt. % causes a significant increase in C_{2+}-alcohol synthesis rates and a decrease in dimethylether synthesis rate. Dimethylether is formed by condensation of methanol on acid sites. Alkali promoters, such as Cs, appear to titrate acid sites and increase the density of basic sites on these catalysts (Table 1.1). This leads to lower dimethylether selectivity and higher alcohol selectivity as increasing amounts of Cs are added. At very high Cs concentrations, alcohol synthesis rates may ultimately decrease, because Cu metal sites, required for chain growth, can also be titrated by Cs species.

Higher Cs concentrations also lead to lower methyl acetate synthesis rates, suggesting that Cs addition favors aldol condensation reactions over esterification reactions, in contrast with earlier reports [40], which found that ester selectivity follows trends similar to alcohol selectivity. Our results are consistent with similar intermediates being involved in both ester formation and aldol condensation; for example, surface acetaldehyde species are likely to participate both in methyl acetate formation and in 1-propanol formation. The decrease in methyl acetate synthesis rate and increased isobutanol synthesis rate at high Cs concentrations suggests that Cs selectively promotes aldol-forming reactions.

Table 2.9. Productivities for Cs-promoted $Cu/ZnO/Al_2O_3$ catalysts

	Klier et al. [22]	This study	This study
Cs [wt. %]	4.3[1]	1.2	2.9
Cu [wt. %]	35	44	44
Temperature [K]	583	583	580
Pressure [MPa]	7.6	4.5	4.5
H_2/CO ratio	0.45	1	1
Gas Hourly Space Velocity [cm^3/g cat. h]	5330	6000	6000
Synthesis Rate [g/kg cat. h]			
Methanol	405.0	269.6	342.3
Ethanol	12.6	12.0	16.1
1-Propanol	6.1	6.4	21.9
1-Butanol	5.5	0.8	0.3
2-Methyl-1-propanol	9.4	8.1	20.3
Methyl formate	10.4	1.3	0.4
Methyl acetate	3.4	13.8	4.2
Dimethylether	-	21.3	5.7
Hydrocarbons	13.9	12.9	6.2

[1]calculated using data from reference.

2.2.13. Alcohol Addition Studies

Ethanol and 1-propanol were added to the H_2/CO feed in order to probe chain growth pathways in higher alcohol synthesis. Isotopic tracer studies of ethanol reactions on K-$Cu_{0.5}Mg_5CeO_x$ [29], [30] have shown that ethanol self-condensation reactions produce n-butyraldehyde, acetone, methyl-ethyl-ketone and 2-pentanone, which form 1-butanol, isopropanol, 2-butanol and 2-pentanol, respectively, at conditions typical of CO hydrogenation reactions. Isotopic tracer studies of methanol-acetaldehyde reactions have shown that propionaldehyde and 1-propanol are formed by condensation of a methanol-derived C_1 species with acetaldehyde; isobutyraldehyde and isobutanol are formed by a similar C_1 addition to propionaldehyde [29], [30].

Table 2.10 shows product selectivities on 2.9 wt. % Cs-Cu/ZnO/Al_2O_3 when ethanol was added to H_2/CO reactants. The amount of ethanol added corresponds to about 25 mol % of the methanol leaving the reactor. The selectivity to 1-propanol increases when ethanol is added, as expected from its formation via C_1 addition to C_2 intermediates. 1-Propanol can be formed both by aldol coupling and by linear chain growth (carbonylation) pathways. The selectivity to isobutanol also increases when ethanol is added. Isobutanol is formed only by C_1 addition to 1-propanol (or propionaldehyde). 1-Butanol selectivity also increased; 1-butanol is formed both by linear chain growth pathways and by ethanol aldol self-condensation pathways. Ethanol self-condensation can also lead to 2-propanol (after retro-aldol reactions) and 2-butanol. Increased selectivity for 2-propanol shows that self-condensation does occur, and that 1-butanol is predominantly formed by ethanol self-condensation and not by linear chain growth pathways. The selectivity to 1-pentanol and 1-hexanol also increases. 1-Pentanol can be formed by condensation of ethanol and propanol or by linear chain growth of 1-butanol. 1-Hexanol is formed by condensation of ethanol and 1-butanol or by linear chain growth of 1-pentanol.

Table 2.10 also shows the effect of adding 1-propanol to the H_2/CO feed. The amount of propanol added corresponds to about 20 mol % of the methanol concentration leaving the reactor. The large increase in isobutanol selectivity during 1-propanol addition confirms that isobutanol is formed predominantly by aldol-type C_1 addition to C_3 species derived from 1-propanol. The small increase in 1-butanol selectivity during 1-propanol addition shows that linear chain growth also occurs on Cs-Cu/ZnO/Al_2O_3. The ratio of increase in isobutanol selectivity to the increase in 1-butanol selectivity when propanol is added shows that aldol condensation pathways are about 22 times faster that linear chain growth on 2.9 wt. % Cs-Cu/ZnO/Al_2O_3 at the conditions of our study. Table 2.11 shows the effect of adding 1-propanol to the H_2/CO feed on a 1.2 wt. % K-$Cu_{7.5}Mg_5CeO_x$ catalyst. The ratio of increase isobutanol selectivity to increase in 1-butanol selectivity on this catalyst is somewhat lower (~9) than for the 2.9 wt. % Cs-Cu/ZnO/Al_2O_3, but aldol-type C_1 addition is still the predominant chain growth pathway on K-$Cu_{7.5}Mg_5CeO_x$.

Table 2.10. Ethanol and 1-propanol addition on 2.9 wt. % Cs-Cu/ZnO/Al_2O_3 [583 K, 4.5 MPa, 6000 cm^3/g-cat-h, H_2/CO/Ar/C_2H_5OH = 44.5/44.5/0.1/0.02, H_2/CO/Ar/ C_3H_7OH = 44.5/44.5/0.1/0.01]

	None	Ethanol	None	Propanol	None
CO conversion [%]	15.4	14.8	14.8	14.2	14.3
Selectivities (CO_2-free) [%]					
Methanol	67.6	67.5	69.2	69.9	71.0
Ethanol	4.4	12.2	4.3	3.5	4.2
1-Propanol	6.9	21.6	7.2	24.3	7.0
2-Propanol	0.7	2.8	0.6	1.1	0.6
2-Methyl-1-propanol	6.9	14.8	6.3	28.6	5.9
1-Butanol	1.0	2.9	1.0	2.0	0.9
1-Pentanol	0.3	1.2	0.3	1.4	0.2
1-Hexanol	0.2	0.6	0.2	0.5	0.2
2-Methyl-1-butanol	1.2	2.3	1.1	1.4	1.0
2-Methyl-1-pentanol	0.9	1.6	0.8	1.5	0.8
2-Methyl-1-hexanol	0.5	0.8	0.4	0.5	0.4
Methyl acetate	1.1	1.6	1.0	0.6	0.7
Dimethylether	0.8	0.3	0.7	0.5	0.6

Table 2.11. 1-Propanol addition on 1.2 wt. % K-$Cu_{7.5}Mg_5CeO_x$ [583 K, 4.5 MPa, 1500 cm^3/g-cat - h, H_2/CO/Ar/C_3H_7OH = 44.5/44.5/0.1/0.5]

	None	Propanol
CO conversion [%]	16.0	15.4
Selectivities (CO_2-free) [%]		
Methanol	60.6	53.3
Ethanol	2.8	1.2
1-Propanol	4.3	-
2-Propanol	3.0	1.3
2-Methyl-1-propanol	4.1	15.5
1-Butanol	0.2	1.5
1-Pentanol	0.1	1.0
1-Hexanol	0.2	0.4
2-Methyl-1-butanol	0.5	1.3
2-Methyl-1-pentanol	0.2	1.3

Aldol-type addition of C_1 species to linear alcohols leads to 2-methyl alcohols. The increase in 2-methyl-1-butanol and 2-methyl-1-pentanol is caused by the higher 1-butanol and 1-pentanol selectivity, respectively, when 1-propanol is added, and/or by the condensation of ethanol with propanol (leading to 2-methyl-1-butanol) or two propanol molecules leading to 2-methyl-1-pentanol. A conservative estimate of the contribution of carbonylation reactions to chain growth can be obtained by assuming that all products that can form from 1-butanol (1-pentanol, 1-hexanol, 2-methyl-1-butanol, 2-methyl-1-pentanol, etc.), are actually formed only from 1-butanol. Even then, aldol condensation pathways are about eight times faster than linear chain growth on the 2.9 wt. % Cs-Cu/ZnO/Al_2O_3.

Reaction pathways for the formation of observed products are shown in Figure 2.12. Similar chain growth schemes were proposed by Smith and Anderson [20], Smith *et al.* [42] and Breman *et al.* [43], [44]. This scheme suggests the possibility of applying a chain growth analysis method similar to that proposed by Herington [45] for the Fischer-Tropsch synthesis. The analysis is more complicated for higher alcohol synthesis than for Fischer-Tropsch synthesis because several chain growth pathways occur simultaneously.

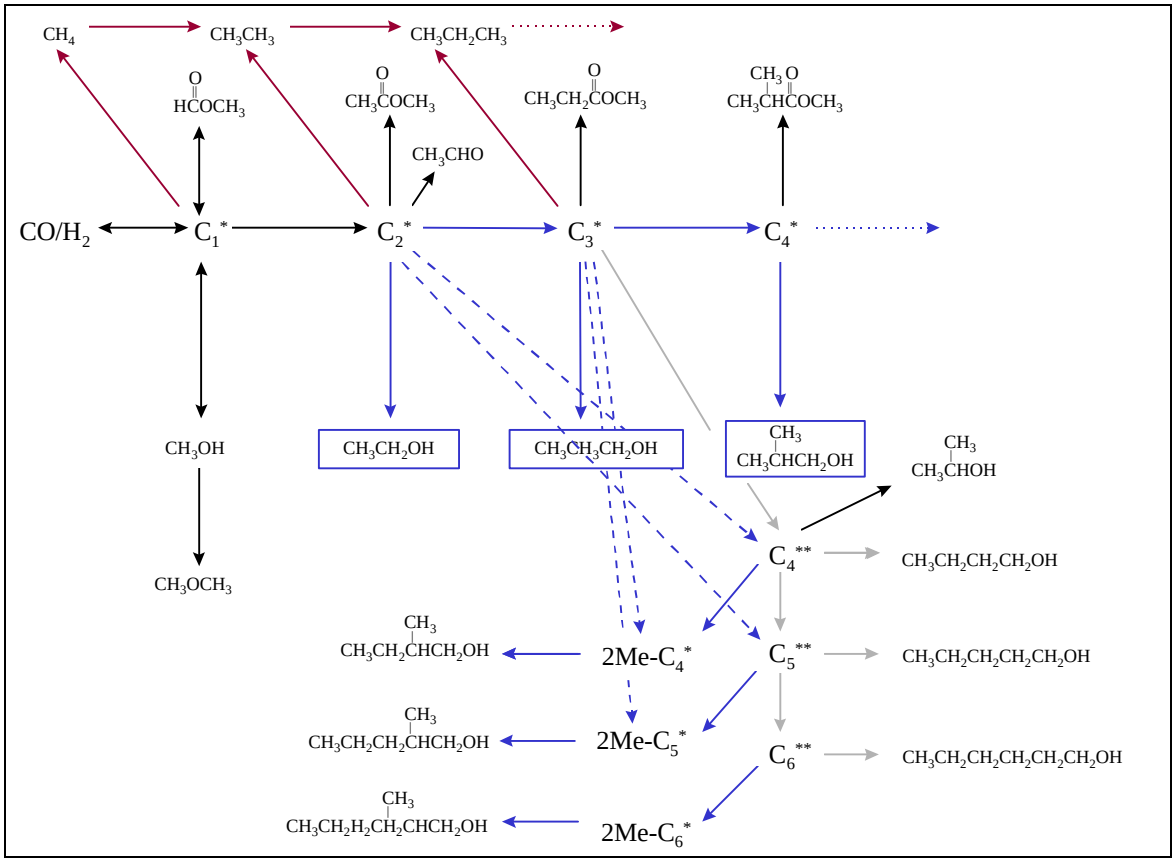

Figure 2.12. Reaction network for methanol and higher alcohol synthesis with simultaneous formation of hydrocarbons.

In this approach, individual chain termination probabilities for each chain size, β_n, are obtained using :

$$\beta_n = r_{t,n} / r_{p,n} = \phi_n / \sum_{n=n+1}^{\infty} \phi_i \quad , \qquad (7)$$

where ϕ_n is the mole fraction of chains of size n and $r_{t,n}$ and $r_{p,n}$ are their termination and propagation rates, respectively. The total termination probability $\beta_{T,n}$ becomes a linear combination of the values for the individual termination steps:

$$\beta_{T,n} = \beta_{x,n} + \beta_{y,n} + \beta_{z,n} \quad , \qquad (8)$$

where $\beta_{x,n}$ is the probability of termination as x and so on. It can be calculated from the mole fraction of each species in reaction products using equation (7).

Both linear and aldol condensation chain growth by C_1 can occur during higher alcohol synthesis. These pathways lead to different alcohols produced, except for the growth step from C_2 to C_3, in which both pathways lead to the same product (i.e. 1-propanol). Self-condensation reactions of C_{2+} oxygenates, however, also occur and they complicate the analysis.

As discussed above, linear chain growth is a minority pathway at the conditions of our study and can be ignored in our chain growth analysis, but self-condensation of ethanol and propanol, and ethanol with propanol cannot be neglected. In our treatment, we will examine only the condensation steps described in Figure 2.13. This analysis leads to the chain termination probabilities listed in Table 2.12 for Cs-Cu/ZnO/Al_2O_3, when 1-butanol and 2-methyl-1-pentanol are assumed to form only by self-condensation (of ethanol and propanol, respectively). 2-Methyl-1-butanol and 1-pentanol are assumed to form by condensation of C_2 whit C_3. The formation of other alcohols than primary alcohols (except for 2-propanol) was not included in this analysis. Hydrocarbons (mainly methane and ethane) are assumed to form from C_1 species.

Table 2.12. Chain growth probabilities for Cs-Cu/ZnO/Al_2O_3 [583 K, 4.5 MPa, H_2/CO=1]

Total chain growth probability by aldol condensation with C_1	1.2 wt. % Cs Cu/ZnO/Al_2O_3	2.9 wt. % Cs-Cu/ZnO/Al_2O_3	
Gas Hourly Space Velocity [cm^3/g cat. h]	6000	6000	1500
CO conversion [%}	15.0	15.4	23.6
C_1 (to C_2)	0.05	0.10	0.17
C_2 (to -C_3)	0.25	0.55	0.66
C_3 (to i-C_4)	0.23	0.38	0.56
i-C_4 (to neo-C_5)[1]	0	0	0

[1]neo-pentanol (2,2-dimethyl-1-propanol) was not detected.

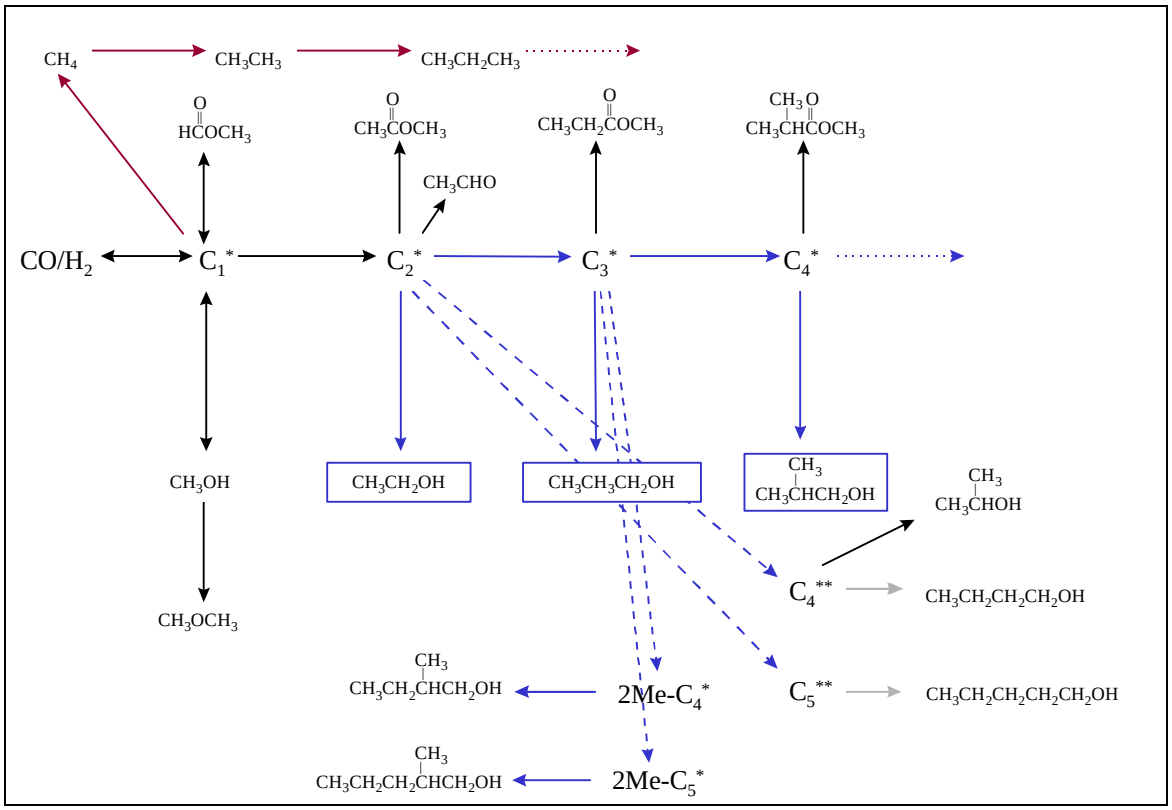

Figure 2.13. Reaction network for methanol and higher alcohol synthesis without including linear chain growth pathways.

All chain growth probabilities on 2.9 wt. % Cs-Cu/ZnO/Al_2O_3 increase with decreasing space velocity, because longer bed residence times and higher concentrations of intermediate products increase the probability for further chain growth reactions. Cs addition also leads to higher chain growth probabilities.

Table 2.13 shows chain growth probabilities on $Cu_{0.5}Mg_5CeO_x$ catalysts compared with Cs-Cu/ZnO/Al_2O_3 at similar CO conversions. These catalysts show higher (C_3-iC_4) chain growth values than the 2.9 wt. % Cs-Cu/ZnO/Al_2O_3 but chain growth values are otherwise very similar to those on Cs-Cu/ZnO/Al_2O_3 for C_1 and C_2 species. K-$Cu_{7.5}Mg_5CeO_x$ shows lower chain growth values than similar catalysts containing lower Cu concentrations.

Table 2.14 shows chain growth probabilities when ethanol or propanol are added to the H_2/CO feed. No significant change in chain growth probabilities was observe when alcohols were added, confirming the accurate and rigorous nature of the chain growth analysis described here.

Table 2.13. Chain growth probabilities for K-$Cu_{0.5}Mg_5CeO_x$ and Cs-$Cu/ZnO/Al_2O_3$ [583 K, 4.5 MPa, $H_2/CO=1$]

Total chain growth probability by aldol condensation with C_1	1 wt. % K $Cu_{0.5}Mg_5CeO_x$	0.25 wt. % Pd 1 wt. % K $Cu_{0.5}Mg_5CeO_x$	1 wt. % K $Cu_{7.5}Mg_5CeO_x$	2.9 wt. % Cs $Cu/ZnO/Al_2O_3$
Gas Hourly Space Velocity [cm^3/g cat h]	1500	1500	6000	6000
CO conversion [%]	14.7	15.8	17.6	15.4
C_1 (to C_2)	0.07	0.09	0.08	0.10
C_2 (to C_3)	0.47	0.53	0.35	0.55
C_3 (to i-C_4)	0.54	0.50	0.27	0.38
i-C_4 (to neo-C_5)[1]	0	0	0	0

[1]neo-pentanol (2,2-dimethyl-1-propanol) was not detected.

Table 2.14. Chain growth probabilities before and during alcohol addition on 2.9 wt. % Cs-CuZnAlO [583 K, 4.5 MPa, 6000 cm^3/g cat. h, $H_2/CO/Ar/C_2H_5OH$ = 44.5/44.5/ 0.1/0.02, $H_2/CO/Ar/ C_3H_7OH$ = 44.5/44.5/0.1/0.01]

Total chain growth probability By aldol condensation with C_1	Before Alcohol Addition	Ethanol Added	Propanol Added
C_1 (to C_2)	0.10	-	-
C_2 (to C_3)	0.55	0.55	-
C_3 (to i-C_4)	0.38	0.32	0.45

In summary, K-promoted $Cu_{0.5}Mg_5CeO_x$ catalysts are active and selective for isobutanol synthesis from CO/H_2 mixtures with high alcohol-to-hydrocarbon ratios at relatively low temperatures (583 K) and pressures (4.5 MPa), but Cs-promoted $Cu/ZnO/Al_2O_3$ catalysts show higher isobutanol synthesis rates at high conversion conditions. CO_2 strongly inhibits methanol and isobutanol synthesis rates on catalysts with low Cu concentration (K-$Cu_{0.5}Mg_5CeO_x$). Methanol production was not affected by CO_2 on catalysts with high Cu (K-$Cu_{7.5}Mg_5CeO_x$ and Cs-$Cu/ZnO/Al_2O_3$) because they typically operate at methanol synthesis equilibrium. Isobutanol synthesis was more severely inhibited by CO_2 on K-$Cu_{7.5}Mg_5CeO_x$ than on Cs-$Cu/ZnO/Al_2O_3$. The addition of small amounts of Pd to K-$Cu_{0.5}Mg_5CeO_x$ reduces the adverse effect of CO_2, probably because Pd resists oxidation and retains its hydrogenation activity at high CO_2 partial pressures. The addition of K (or Cs) to $Cu_xMg_5CeO_y$ (or $Cu/ZnO/Al_2O_3$) samples titrates residual acid sites, which lead to dimethylether and hydrocarbons. Ethanol and 1-propanol addition data show that predominant chain growth pathways are aldol-type C_1 addition to higher alcohols on both K-$Cu_yMg_5CeO_x$ and Cs-$Cu/ZnO/Al_2O_3$. A chain growth analysis showed only minor differences in chain growth probabilities between 1 wt. % K-$Cu_{0.5}Mg_5CeO_x$ and 2.9 wt. % Cs-$Cu/ZnO/Al_2O_3$.

2.3. Isotopic Tracer and Kinetic Studies of Alcohol Coupling Reactions

Alcohol coupling reactions were carried out in a gradientless recirculating reactor unit (RRU) operated in the batch mode (Figure 2.14). Catalyst samples were first reduced in H_2 (10 % H_2/He, 175 cm^3/min, 5 K/min) at 623 K for 0.5 h. After the desired reaction temperature was achieved, a reaction mixture was introduced along with a small amount of methane, used as an unreactive internal standard. The reaction was carried out at 101.3 kPa. H_2 was purified by passing through a catalytic purifier (Matheson, Model 64-1008). Traces of water were removed from H_2 and helium using molecular sieves (Matheson, Model 452:4A). CH_4 was used without further purification (CH_4: Matheson, ultra high purity). Reactants were purified by several freeze-pump-thaw cycles before catalytic experiments.

The reactant mixture was circulated continuously through the catalyst sample and reaction products were sampled by syringe extraction after various contact times. Reactants and products were analyzed using a dual detector gas chromatograph (Hewlett-Packard, Model 5890 II Plus; TCD/FID detectors). One sample was injected into a 5% phenyl-methyl-silicone capillary column (HP-1, 50 m, 0.32 mm diameter, 1.05 μm film thickness) and the other into a packed column (Porapak Q, 1.8 m length, 0.32 cm diameter). A thermal conductivity detector (TCD) was used to measure the concentration of CO and CO_2 and C_2H_5OH in the effluent from the packed column. A flame ionization detector (FID) was used to measure the concentrations of all organic compounds eluting from the capillary column. Products were also analyzed by mass spectrometry after capillary chromatography in order to confirm the identity of reaction products and the chemical composition and to measure the isotopic content in reactants and products (Hewlett-Packard, Model 5890 II Plus GC; Hewlett-Packard, Model 5972 Mass Selective Detector).

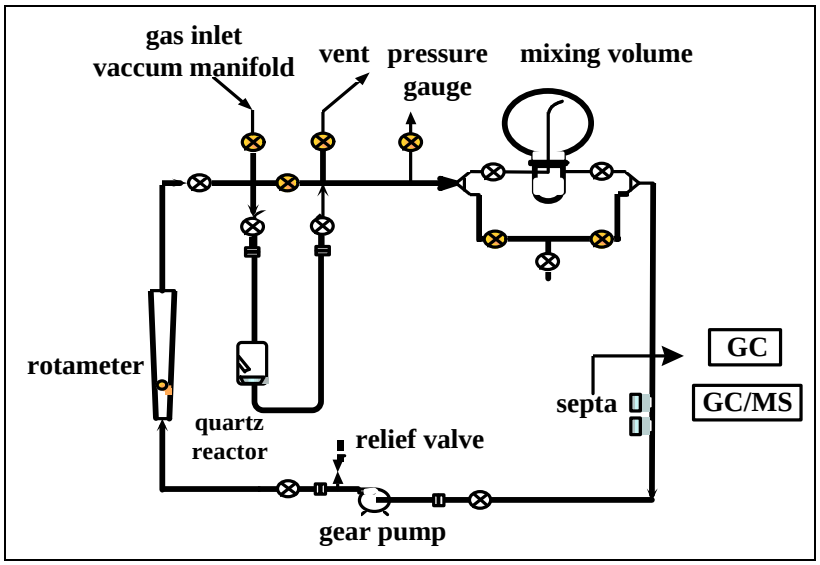

Figure 2.14. Schematic diagram of recirculating reactor unit (RRU).

2.3.1. $^{13}CH_3OH/C_2H_5OH$ Reactions on Cu/ZnO, Cs-Cu/ZnO and CuZnMnO Catalysts

A preliminary study of alcohol coupling reactions was carried out using the RRU. The literature on alcohol coupling reaction suggests that aldehydes formed by dehydrogenation steps are reactive intermediates in chain growth [21]. Studies on Cu/ZnO catalysts by Elliott et al. [46] have shown that primary alcohols containing n-carbon atoms condense at atmospheric pressure to form predominantly C_{2n} esters and C_{2n} and C_{2n-1} ketones. These authors report that the presence of CO influences product distributions; esters were formed preferentially in N_2 atmospheres but ketones were favored when CO was present. They have suggested a role for surface oxygen vacancies in the formation of ketones on the basis of the enhanced selectivity to ketones at high CO pressures (~ 65 bar). The role of CO (and H_2) in the formation of surface vacancies was confirmed by the appearance of CO_2 when Cu/ZnO catalysts were exposed to CO and then heated from 300 to 520 K. These surface reduction steps are likely to occur during isobutanol synthesis from CO/ H_2 mixtures, where they can also lead to the formation of CO_2.

Elliott and Penella's [46] mechanistic proposal can be summarized by the sequence of steps as illustrated below:
1) The initial formation of a C_n-aldehyde from a C_n-alcohol by dehydrogenation

2) The reaction of a C_n-aldehyde with a C_n-alcohol to form the C_{2n}-ester

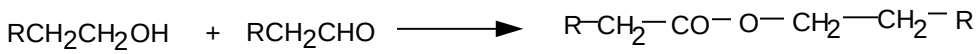

3) The self addition of the C_n-aldehyde by aldol-type condensation to yield C_{2n}-aldehydes or ketones

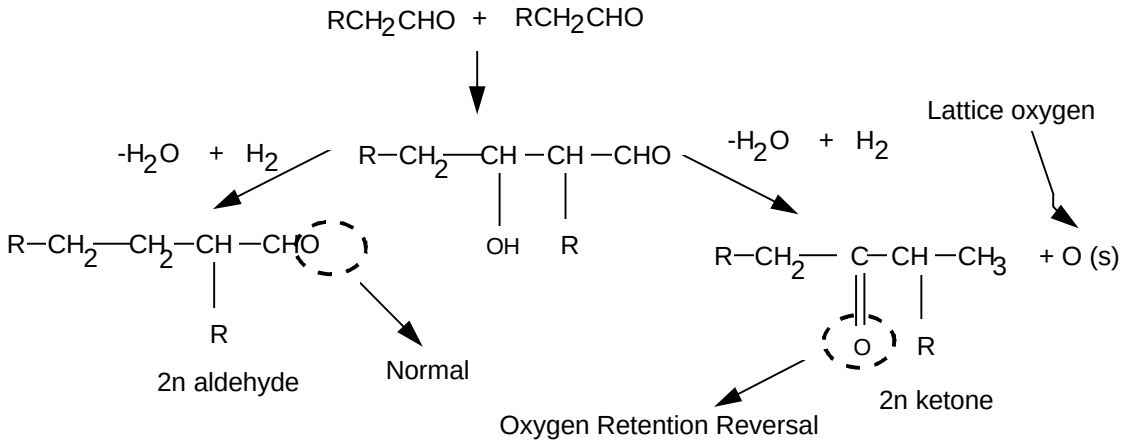

4) The condensation of the C_n-aldehyde to give C_{2n-1}-ketones using up a surface oxygen vacancy

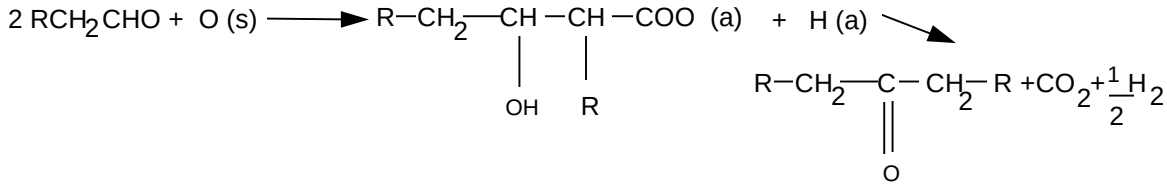

[(s) enclosed by parenthesis refers to surface species and a enclosed by parenthesis refers to adsorbed species]

This mechanism accounts for the formation of C_{2n}-aldehydes and ketones. Reactions between the C_n-alcohols and aldehydes account for C_{2n}-esters and the self-condensation reaction for C_{2n} aldehydes and ketones. This explanation is similar to the normal and oxygen retention reversal modes of the mechanism proposed by others [18],[47]. The mechanism proposed by Klier et al. for higher pressure isobutanol synthesis conditions from synthesis gas is shown in Figure 2.15.

Tronconi et al. [24] have suggested that under high pressure conditions ketones are thermodynamically less favorable (< 2% equilibrium yield at 7.6 MPa) because of an inverse cubic dependence of their equilibrium concentration on reaction pressure (under HAS conditions). These authors show that primary alcohols and ketones equilibrate rapidly; at high temperatures and contact time this equilibrium tends to favor alcohols over ketones.

The mechanism for the formation of C_{2n-1}-ketones is less clear. Some authors [48] suggest that acetone forms from ethanol via ethyl acetate intermediates. Acetone is not formed on basic MgO catalysts, suggesting that vacancies (not prevalent on MgO) may be required for ketone formation [3]. This redox mechanism for the formation of ketones intermediates may also account for the role of Mn in high-temperature isobutanol synthesis catalysts, as reported by Keim et al. [16] and Kotowski et al. [49], and referenced to in the review article by Sofianos [50]. MnO is a well known oxidation catalyst and it is expected to contain a high density of oxygen vacancies at the reducing conditions of alcohol reactions.

The addition of 2-propanol or acetone to CO/H_2 mixtures under higher alcohol synthesis conditions, not surprisingly, gave identical results on a Cs/Cu/ZnO type catalyst [21]. In both cases a significant increase in the yield of ethanol and acetaldehyde was observed under higher alcohol synthesis (HAS) conditions. These studies show that under higher alcohol synthesis conditions two reactions involving acetone attain thermodynamic equilibria: between ethanol and acetone and between 2-propanol and acetone.

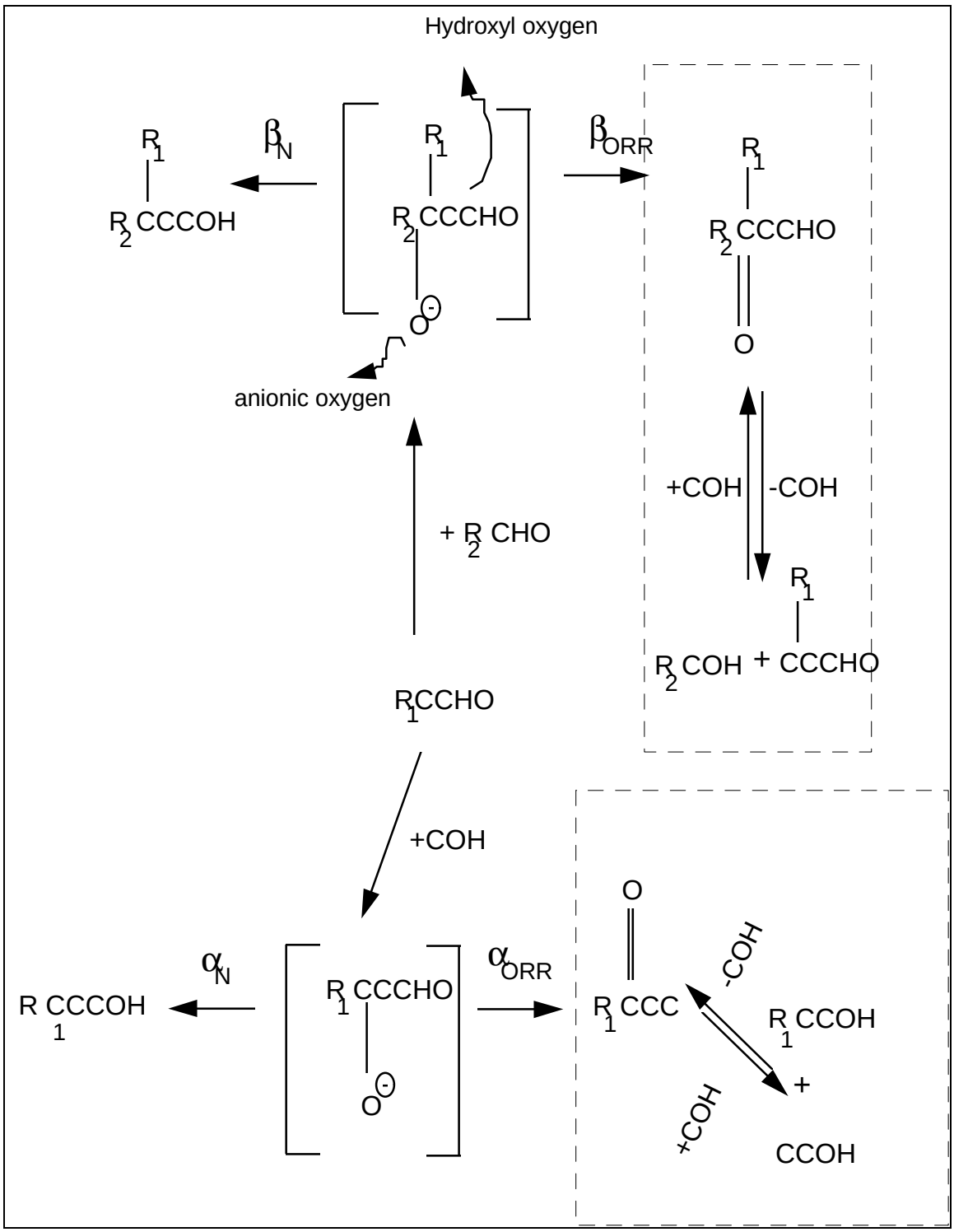

Figure 2.15. Mechanism for higher pressure isobutanol synthesis according to Klier et al. [47].

In our initial study of alcohol reactions, we have addressed the mechanism of the formation of aldehyde and ketone synthesis formed from ethanol-methanol mixtures and its relationship to higher pressure alcohol synthesis reactions. We have also explored the potential roles of Mn and Cs components, which are usually present as promoters in isobutanol synthesis catalysts. Also, in isobutanol synthesis from synthesis gas, methanol can be the initial alcohol from which higher alcohols and aldehydes are formed [51]. Therefore, we have chosen to study the coupling reaction between ^{13}C-methanol and unlabeled ethanol. Measurements of reaction rates and selectivity and of the rate of appearance and the location of ^{13}C atoms can reveal the details about the mechanism of alcohol coupling and provide a direct measure of the relative reactivities of methanol and ethanol in coupling reactions. These types of experiments are complicated by the usual presence of ^{18}O impurity (12% ^{18}O) in ^{13}C-methanol.

Alcohol coupling reactions were conducted at 523 K in the RRU at a total pressure of 101.3 kPa. The make-up of the feed was: 4.0 kPa ethanol, 8.0 kPa methanol, 2.0 kPa neon (internal standard) and the balance helium. Cu/ZnO [Cu:Zn at. 30:70], Cs/Cu/ZnO [Cs:Cu:Zn at. 0.4:30:70] and Cu/ZnO/MnO [Cu:Zn:Mn at. 4:3:1] catalysts were evaluated using 22 mg catalyst charges.

Methanol and ethanol conversions were calculated from thermal conductivity data using Ne as an internal standard. Ne was used because it was readily separated from CO and CO_2 using our chromatographic arrangement (6ft, 1/8" Porapak Q column; temperature program: 318 K for 4 min, heating to 473 K at 10 K/min). The remaining products were separated using a 5% phenyl-methyl silicone 60 m capillary column (HP-5) and analyzed by flame ionization (temperature program: 323 K for 2 min, heating up to 483 K at 20 K/min). CO formation rates were calculated by difference because extensive overlap between CO and the N_2/O_2 peaks (from air leak into the syringe) precluded direct chromatographic measurements of CO concentrations. Our product formation rates are reported as site (copper)-time yields, based on the total number of copper atoms. This is a convenient choice, as it can be easily converted to the correct site-time yields from independent copper dispersion measurements. Selectivities are reported on a carbon basis, as a fraction, in terms of the moles of carbon appearing within each product formed per mole of carbon in the ethanol and methanol converted.

The Cs/Cu/ZnO catalyst is a Cs-modified methanol synthesis catalyst and chosen in order to examine the effect of Cs. The conversion of methanol on this sample under our reaction conditions (523 K, 101.3 kPa total pressure) was very low (< 1%), while the ethanol conversion was higher and reached an asymptotic value about 60% (Figure 2.16(a)). The same behavior is observed when the methanol and ethanol turnovers are plotted as a function of time (Figure 2.16(b)).

On this sample, the acetaldehyde site-time yield increases initially, reaches a maximum, and then decreases (Figure 2.17a). When the selectivity for acetaldehyde formation is plotted as a function of ethanol conversion, there is also an initial increase in the selectivity, the attainment of a maximum, and then a decrease (Figure 2.17b). This behavior is expected of a reactive intermediate in a classical series reaction. Therefore, acetaldehyde appears to be a reactive intermediate product or an equilibrate side product of ethanol in methanol-ethanol coupling reactions.

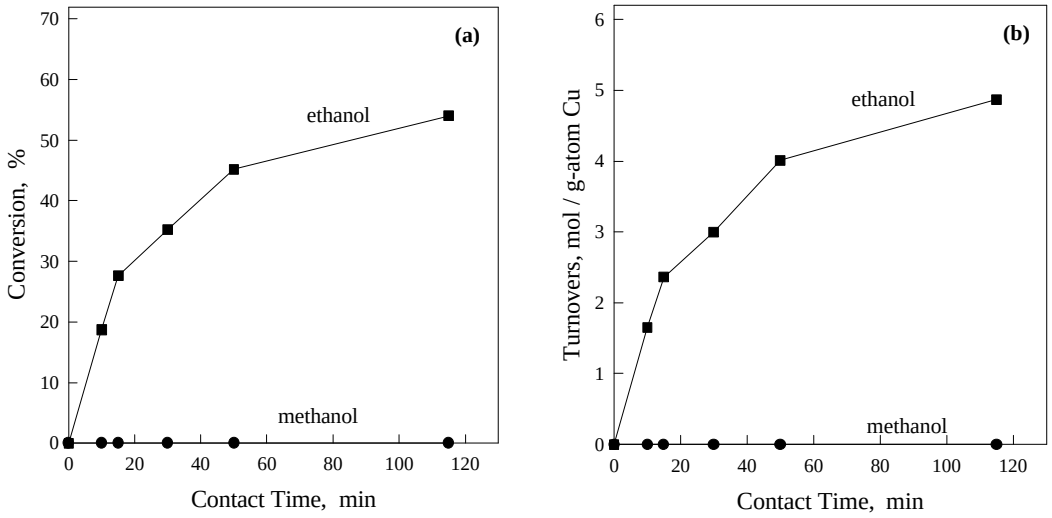

Figure 2.16. Methanol-ethanol reactions. (a) Conversion and (b) Turnovers as a function of contact time on Cs-CuZnO catalysts. [523 K, 101.3 kPa total pressure, 8.0 kPa methanol, 4.0 kPa ethanol, balance He].

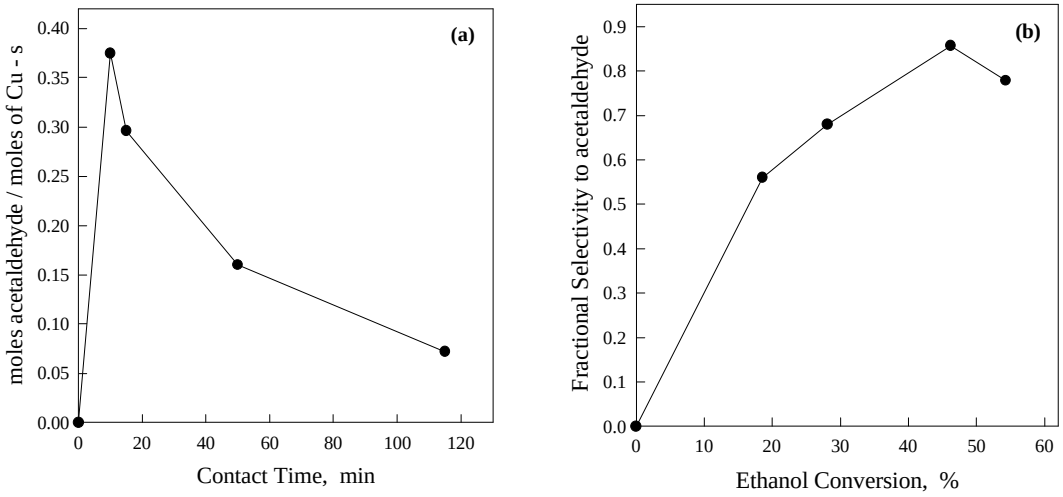

Figure 2.17 Methanol-ethanol reactions. (a) Acetaldehyde site-yields as a function of contact time; (b) Selectivity to acetaldehyde as a function of ethanol conversion, on Cs-CuZnO catalysts. [523 K, 101.3 kPa total pressure, 8.0 kPa methanol, 4.0 kPa ethanol, balance He].

Acetone site-time yields reach a maximum rapidly and then decline to a constant value (Figure 2.18a). Isobutyraldehyde site-time yields obtained on this catalyst are lower than for acetone, but its behavior with increasing contact time is similar. The acetone and isobutyraldehyde selectivities increase monotonically with ethanol conversion (Figure 2.18b). This behavior suggests they are unreactive (final) products under these conditions on Cs/Cu/ZnO.

The site-time yields of ethylacetate and n-butyraldehyde decline after an initial increase, while the site-time yields of methylethyl ketone and 2-pentanone continue to increase with contact time (Figure 2.19), suggesting that both ethylacetate and n-butyraldehyde are reactive. When the ethyl acetate and butyraldehyde selectivities are plotted as a function of conversion, they initially increase, attain maxima at intermediate conversion and decrease. This confirms that ethylacetate and n-butyraldehyde are intermediates. The selectivities towards methylethyl ketone and 2-pentanone increase monotonically as conversion increases, suggesting that are unreactive final products.

In contrast with Cs/Cu/ZnO, Cu/ZnO/MnO leads to significant methanol conversion levels (Figure 2.20a). Methanol conversion turnovers are lower than ethanol turnovers, even though the feed contains 4.0 kPa of ethanol and the 8.0 kPa of methanol (Figure 2.20b). Ethanol dehydrogenation is significantly more rapid than methanol dehydrogenation on this catalyst. Acetaldehyde site-time yields show an initial increase with increasing contact time, then a maximum value and ultimately, a decrease (Figure 2.21a).

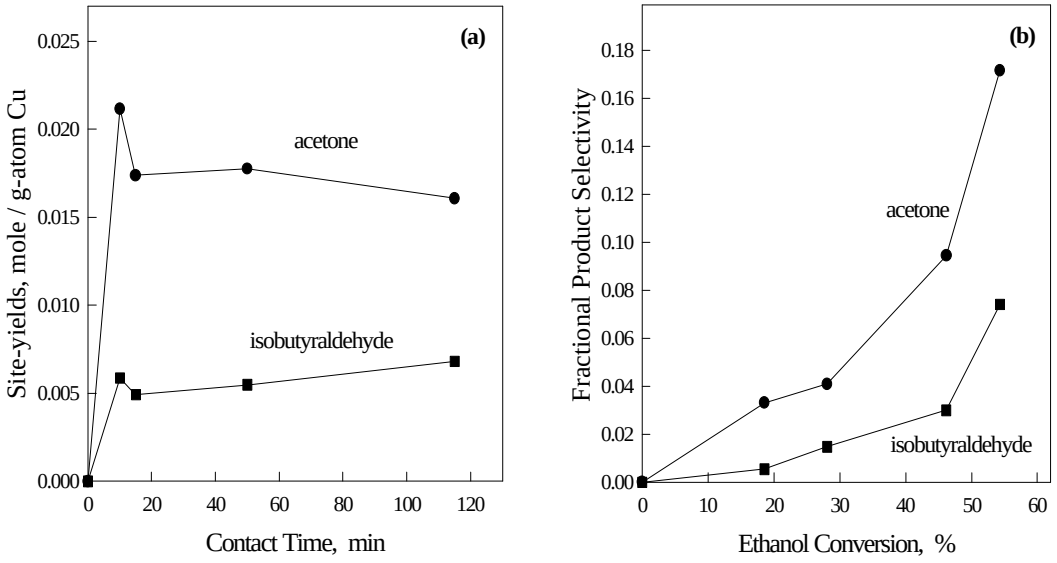

Figure 2.18. Methanol-ethanol reactions. (a) Acetone and isobutyraldehyde site-yields as a function of contact time; (b) Selectivity to acetone and to isobutyraldehyde as a function of ethanol conversion, on Cs-CuZnO catalysts. [523 K, 101.3 kPa total pressure, 8.0 kPa methanol, 4.0 kPa ethanol, balance He].

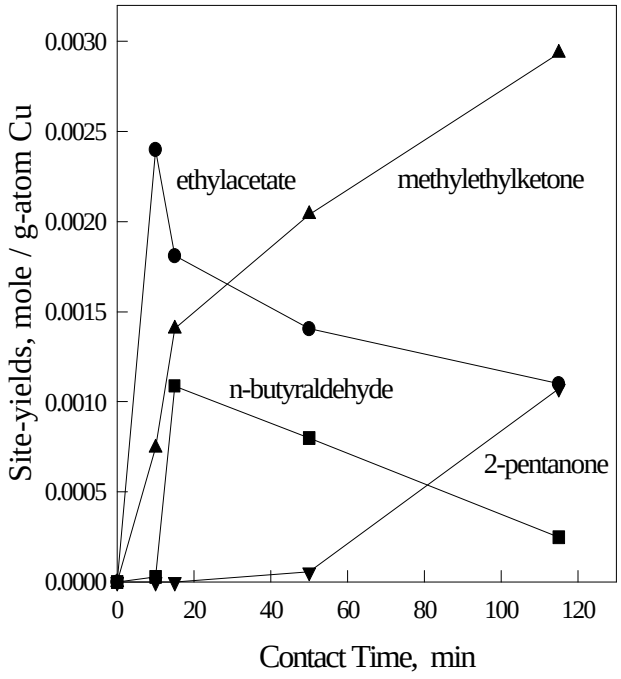

Figure 2.19. Methanol-ethanol reactions. Site-yields as a function of contact time on Cs-CuZnO catalysts. [523 K, 101.3 kPa total pressure, 8.0 kPa methanol, 4.0 kPa ethanol, balance He].

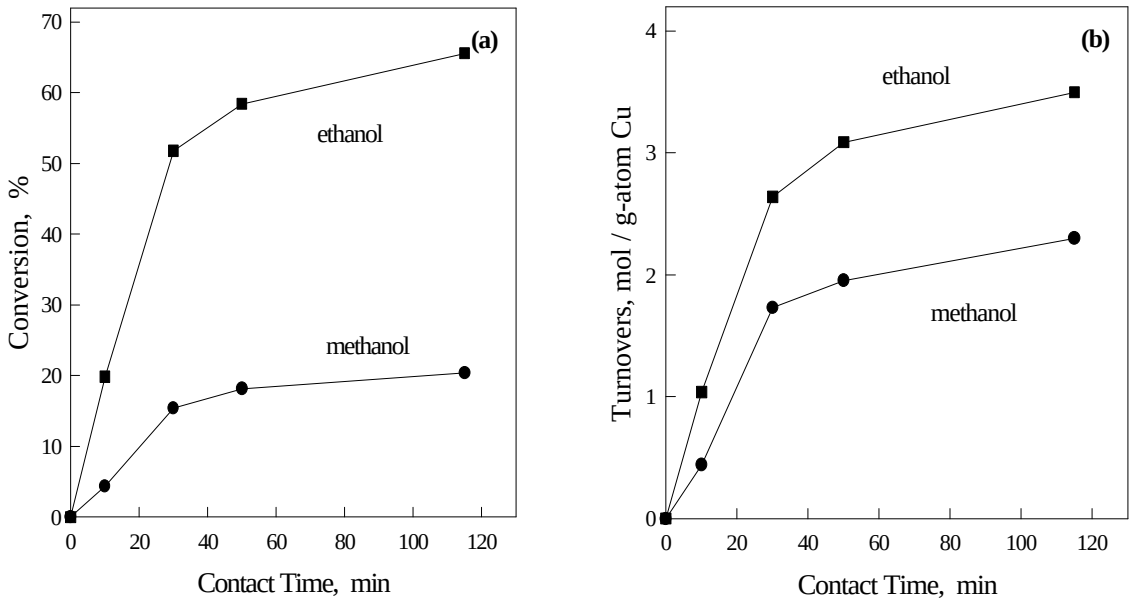

Figure 2.20. Methanol-ethanol reactions. (a) Conversion and (b) Turnovers as a function of contact time on CuZnMn catalysts. [523 K, 101.3 kPa total pressure, 8.0 kPa methanol, 4.0 kPa ethanol, balance He].

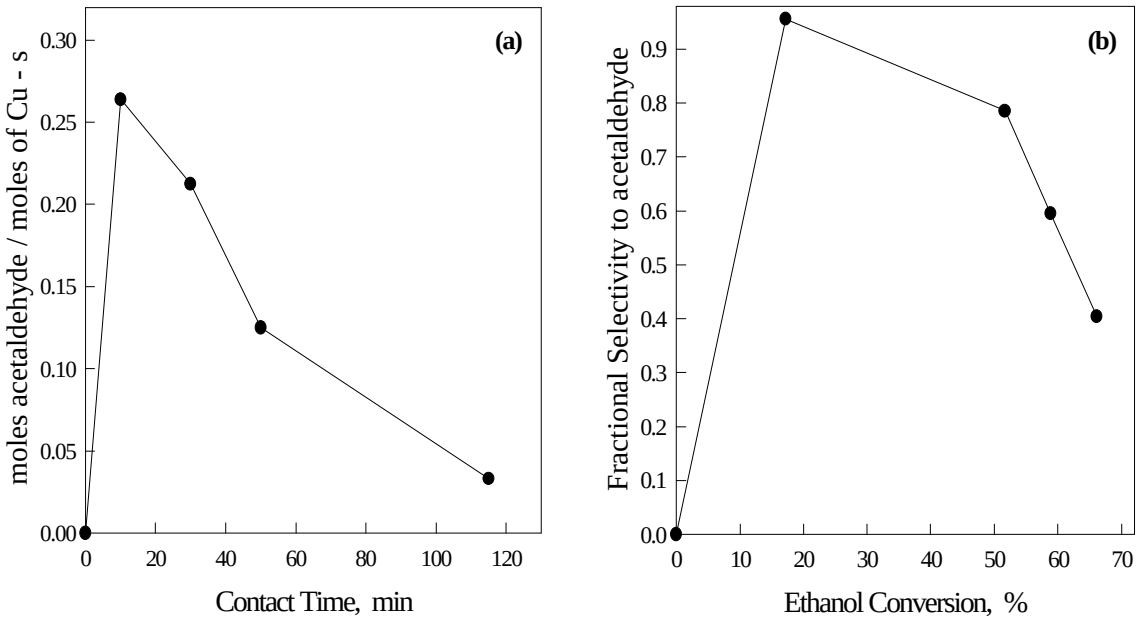

Figure 2.21. Methanol-ethanol reactions. (a) Acetaldehyde site-yields as a function of contact time; (b) Selectivity to acetaldehyde as a function of ethanol conversion, on CuZnMn catalysts. [523 K, 101.3 kPa total pressure, 8.0 kPa methanol, 4.0 kPa ethanol, balance He].

Acetone shows similar behavior on Cu/ZnO/MnO. It behaves as an intermediate on the Cu/ZnO/MnO with a maximum in acetone site-time yield at intermediate times (Figure 2.22). Among the condensation products, butyraldehyde and ethyl acetate appear to be reactive intermediates whereas isobutyraldehyde, methylethyl ketone, and 2-pentanone appear to be unreactive final products (Figure 2.22).

It is interesting to compare the activity of Cu/ZnO with the Cs-promoted Cu/ZnO methanol synthesis catalyst. Methanol shows a non-zero conversion on Cu/ZnO (Figure 2.23a), methanol turnover-time curves lie above the ethanol turnover-time curves (Figure 2.23b). As on Cs/Cu/ZnO and Cu/ZnO/MnO systems, it is found that acetaldehyde is an intermediate or is an equilibrated side product of ethanol dehydrogenation in methanol-ethanol coupling reactions (Figure 2.24a). Acetaldehyde site-time yields are similar in magnitude to those on the other two catalyst systems.

Among the condensation products, acetone and n-butyraldehyde are intermediates whereas isobutyraldehyde, methyl-ethyl ketone, and 2-pentanone are unreactive products. The magnitudes of the site-yields (Figure 2.24b) of these condensation products are much greater on the Cs/Cu/ZnO and Cu/ZnO/MnO catalysts.

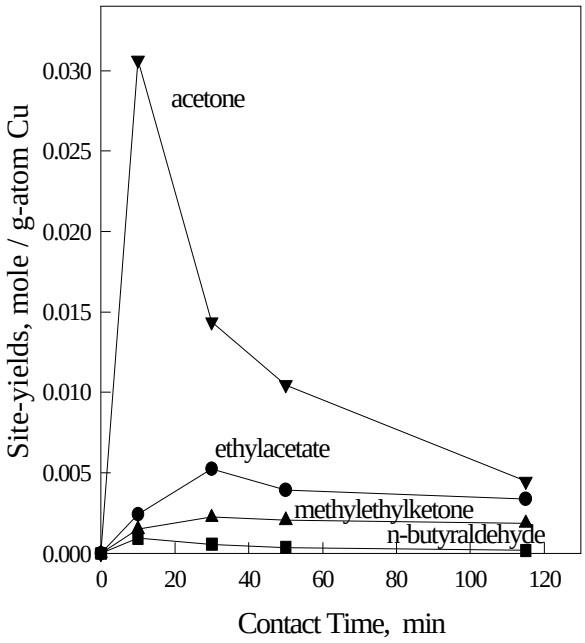

Figure 2.22. Methanol-ethanol reactions. Site-yields as a function of contact time on CuZnMn catalysts. [523 K, 101.3 kPa total pressure, 8.0 kPa methanol, 4.0 kPa ethanol, balance He].

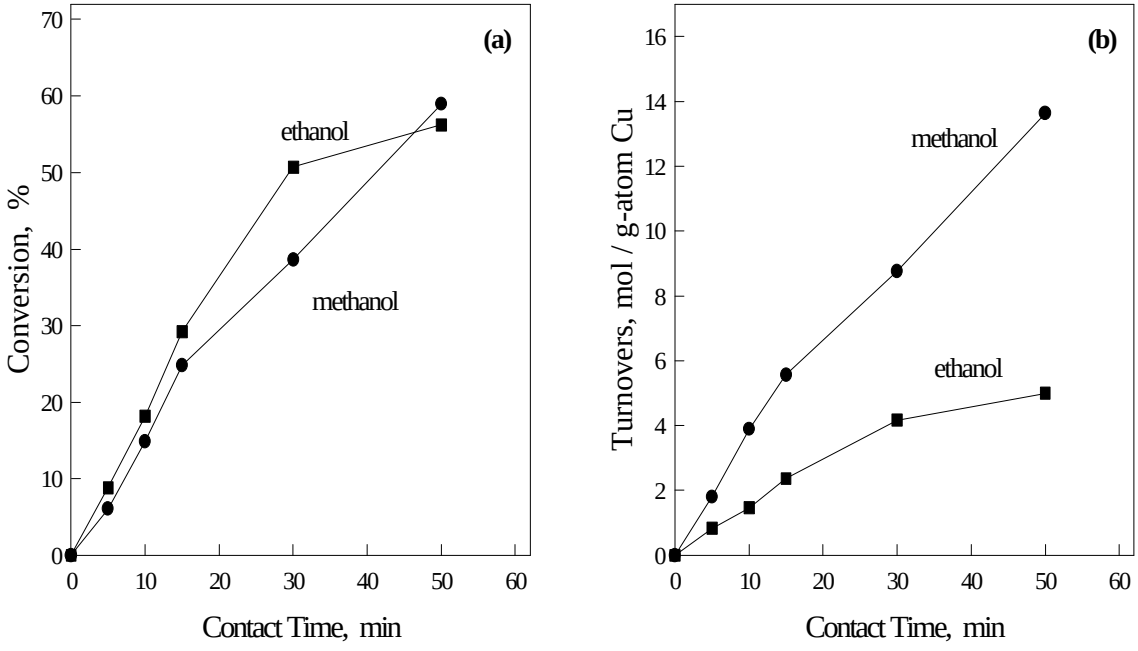

Figure 2.23. Methanol-ethanol reactions. (a) Conversion and (b) Turnovers as a function of contact time on CuZnO catalysts. [523 K, 101.3 kPa total pressure, 8.0 kPa methanol, 4.0 kPa ethanol, balance He].

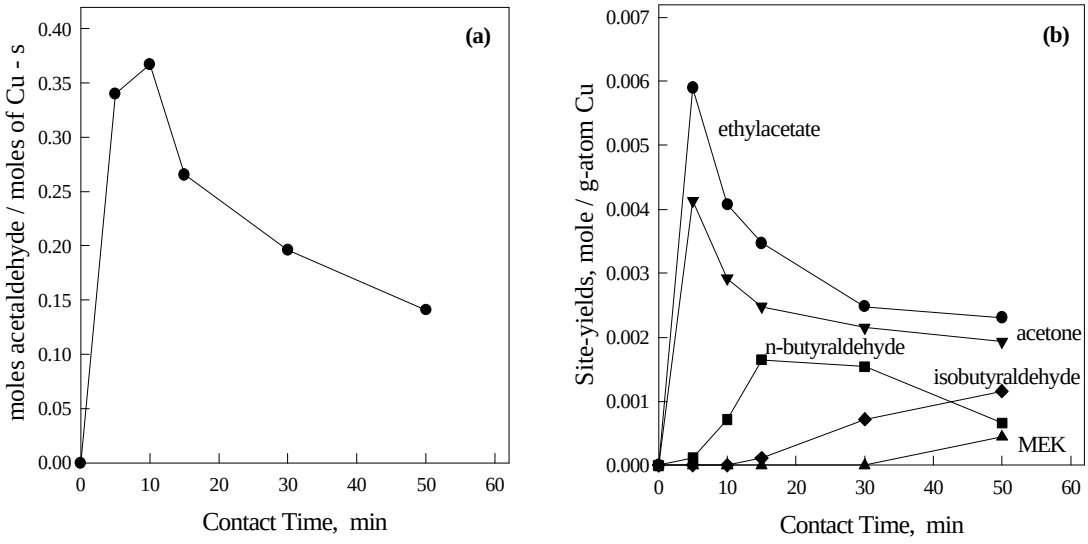

Figure 2.24. Methanol-ethanol reactions. (a) Acetaldehyde site-yields; and (b) Condensation product site-yields as a function of contact time on CuZnO catalysts. [523 K, 101.3 kPa total pressure, 8.0 kPa methanol, 4.0 kPa ethanol, balance He].

It appears that on modified methanol synthesis catalysts, ethanol dehydrogenation rates are higher than those of methanol reactions. On the Cs-modified Cu/ZnO, methanol did not react. On Cu/ZnO/MnO catalysts, the ethanol turnovers were higher than methanol turnovers at all times during the run. Only for the unmodified Cu/ZnO, ethanol turnovers were lower than those of methanol. On each catalyst, ethanol conversions reach a constant value (~ 60%) with increasing contact time. We conclude that ethanol conversion reaches the equilibrium for the predominant reaction of ethanol dehydrogenation to acetaldehyde.

The role of the alkali can be two-fold: 1) modification of methanol formation and decomposition sites and 2) stabilization of the intermediate necessary for the formation and decomposition of ethanol. Our experimental evidence suggests that Cs inhibits methanol decomposition to CO and H_2, because undoped Cu/ZnO is very active for methanol conversion to CO and H_2. It is possible that alkali decreases the size of Cu ensembles available for dehydrogenation or blocks surface Cu atom, rendering then unreactive for ethanol reactions.

On all three catalyst formulations acetaldehyde is the most abundant product, seems to be a reactive product that undergoes significant secondary reactions. The condensation steps are slower than the ethanol dehydrogenation step to form acetaldehyde or methanol dehydrogenation to form formaldehyde. The major secondary products that are formed on all of the catalyst formulations are: acetone, isobutyraldehyde, and methyl-ethyl ketone. Isobutyraldehyde is a final product and all ketones, except acetone, are also unreactive products. Acetone seems to be an intermediate species as well. The presence of acetone (the (2n-1) ketone) among reaction products is due to the presence of the CO product of methanol decomposition [46]. An earlier study [46] suggested that CO was necessary for the formation of oxygen vacancies.

The condensation products of the reaction can be grouped into two categories, those that can form directly from ethanol and those that require methanol-ethanol reactions. Acetone, ethyl acetate, methyl-ethyl ketone, n-butyraldehyde and 2-pentanone can form directly from ethanol as we shown later on, while propionaldehyde and isobutyraldehyde require formaldehyde reactants for their synthesis. The presence of the isobutyraldehyde and propionaldehyde as reaction products suggests that low concentrations of reactive formaldehyde species are available from methanol dehydrogenation.

As expected, the methanol synthesis component (Cu/ZnO) of the higher alcohol synthesis catalyst also acts as a dehydrogenation function. On Cu/ZnO, the condensation site-time yields are much lower than on the Cs/Cu/ZnO and Cu/ZnO/MnO catalysts. Therefore, Cs and Mn appear to be important functions for the condensation steps. Thus, in summary, the analysis of the recirculating batch reactor data on Cu/ZnO modified by Cs or Mn leads to the following conclusions:

1. The presence of Cs inhibits methanol decomposition to synthesis gas. On all catalysts, the ethanol conversion reaches a maximum asymptotic value of about 60% as contact time increases, suggesting that the predominant reaction, ethanol dehydrogenation to acetaldehyde, reaches thermodynamic equilibrium. Acetaldehyde is the most abundant product. Thus, conversion of acetaldehyde to higher molecular weight condensates is slow and rate-limiting at these reaction conditions.
2. The main products of the reaction are acetaldehyde and acetone (by acetaldehyde self-condensation and retro-aldol reactions), ethyl acetate (by acetaldehyde-ethanol condensation), methyl-ethyl ketone and 2-pentanone (from acetaldehyde condensation), propionaldehyde (from aldol-type condensation of acetaldehyde with formaldehyde), butyraldehyde (from condensation of acetaldehyde), and isobutyraldehyde (from condensation of formaldehyde and propionaldehyde).
3. Formaldehyde, though not observed experimentally, because of its low equilibrium concentrations at these reaction conditions, appears to be formed and involved in the synthesis of propionaldehyde and isobutyraldehyde. Also, formaldehyde species formed by methanol dehydrogenation decompose rapidly to CO and H_2, which are the predominant products of methanol reactions in $^{13}CH_3OH/C_2H_5OH$ mixtures. High CO selectivities are consistent with previous studies. In addition, the work of Elliott and Penella [46] shows that inert atmospheres favor the formation of ethyl acetate from ethanol. The presence of CO favors condensation reactions leading to acetone. Our observation of high selectivity to condensation products is consistent with the presence of significant CO partial pressures during reactions of $^{13}CH_3OH/C_2H_5OH$ mixtures.
4. Acetaldehyde and acetone site-time yields are significantly higher on the Cs/Cu/ZnO catalyst than on the other two catalysts. Site-time yields increase in the order of Cs/Cu/ZnO >CuZnMn>>Cu/ZnO for these products.
5. All aldehydes, except isobutyraldehyde, appear to be reactive intermediates at these reaction conditions. Their site-time yield-time curves show a maximum value at intermediate contact time. All ketones, except acetone, all ketones appear to be unreactive products and their site-time yields increase monotonically with contact time.

2.3.2. Ethanol Reactions on Cu/ZnO, Mg_5CeO_x, and $Cu_{0.5}Mg_5CeO_x$ Catalysts

The dehydrogenation and condensation reactions of ethanol were investigated on Cu/ZnO (30/70 at.%), Mg_5CeO_x, $Cu_{0.5}Mg_5CeO_s$ and 1 wt % K-$Cu_{0.5}Mg_5CeO_x$. In a typical experiment, 22 mg of catalyst was charged into the RRU. The ethanol partial pressure was 4.0 kPa with the balance helium.

The catalytic activity and product distribution obtained on Cu/ZnO at 523 K are shown in Figure 2.25 and summarized as follow:

a) The ethanol conversion reached an asymptotic value ~ 80%, indicating the reaction also approaches chemical equilibrium on this catalyst. Ethanol turnovers as a function of time is depicted in Figure 2.25a.
b) The main product was acetaldehyde, formed by dehydrogenation of ethanol (Figure 2.25b).
c) The condensation products, present in small quantities, were acetone, n-butyraldehyde and ethyl acetate.

Acetaldehyde is the most abundant product, and appears to be a reactive intermediate and undergoes significant secondary reactions. The selective production of aldehyde from alcohol on copper-based catalysts has been widely reported 1970 [52, 53]. These authors found that saturated aliphatic alcohols yield considerable amounts of aldehyde and ester on Cu metal catalysts. The ester was proposed to be formed by the reaction between an aldehyde and an alcohol. In our case, the formation of ethyl acetate is a result of ethanol-acetaldehyde condensation via a hemiacetal mechanism [53]. Recently, several authors [45 - 54] have reported that alcohol adsorbs dissociatively on copper to form ethoxy species, which then decompose to form aldehyde. On the other hand, several studies on ZnO [54, 55, 48] have showed that ethanol decomposed to form ethylene, acetaldehyde and/or ethylene oxide. The formation of ethylene is due to the presence of anionic vacancies on low-coordinated Zn^{2+} sites. These sites are produced during catalyst pretreatment under reducing conditions. In our reaction conditions, no ethylene was observed, perhaps because of the low reaction temperature employed in this study. Ethylene was reported to form readily only in large quantities at temperatures greater than 573 K [54].

Mg_5CeO_x was inactive in ethanol dehydrogenation. The ethanol conversion reached a low value of about 7% as shown in Figure 2.26a, even though the reaction was carried out at a temperature 50 K higher than on Cu/ZnO. It is surprising that the conversion leveled off at high contact time since the reaction was still far from equilibrium limitation. This might be due to CO_2 poisoning of basic sites or coordinately unsaturated cation sites. For a Cu-free Mg_5CeO_x sample, the basic sites in MgO are required for ethanol dehydrogenation. During the reaction, ethanol and its derivatives can react with the lattice oxygen from CeO_2 to form carbon oxides. The build-up of CO_2 during the reaction gradually decreased the number of basic sites available for dehydrogenation reaction. Thus, the activity decreased to zero. As shown in Figure 2.26b, the product distribution was similar to that obtained on Cu/ZnO.

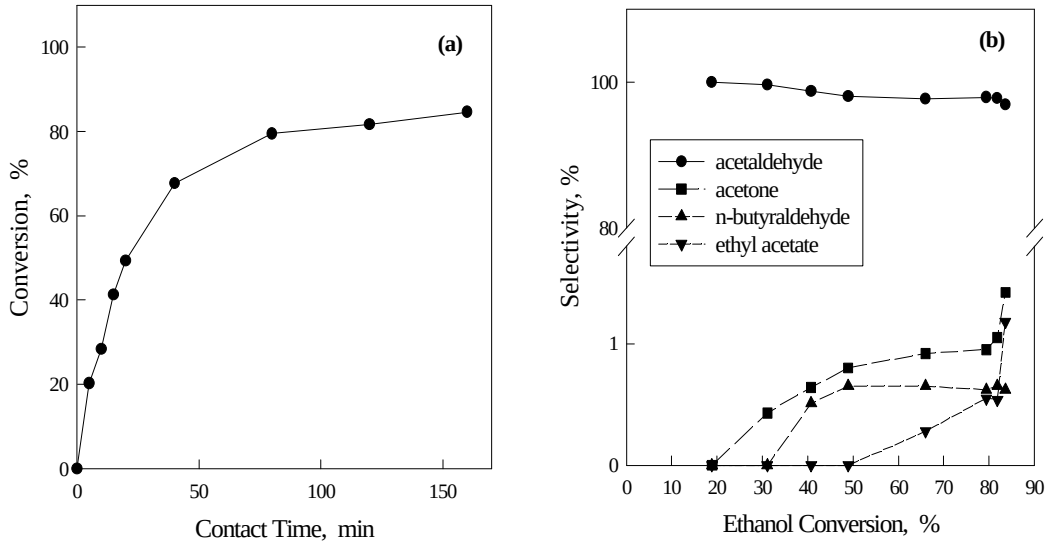

Figure 2.25. Ethanol reactions. (a) Ethanol conversion as a function of contact time. (b) Normalized selectivities as a function of ethanol conversion on CuZnO catalysts. [523 K, 101.3 kPa total pressure, 4.0 kPa ethanol, balance He].

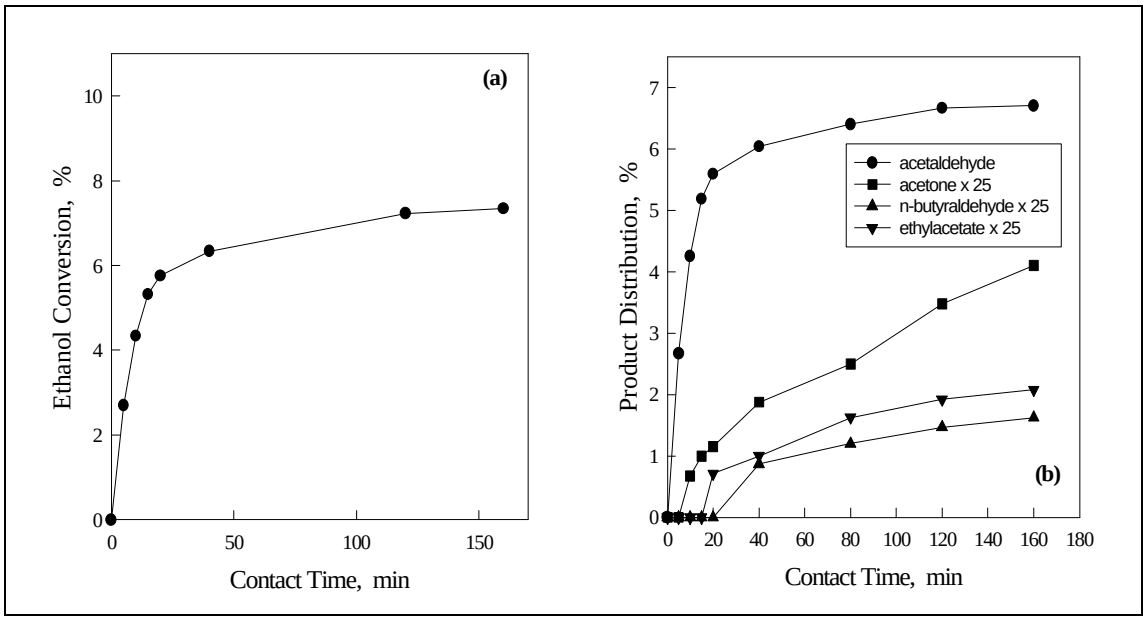

Figure 2.26. Ethanol reactions. (a) Ethanol conversion; and (b) Product distribution as a function of contact time on Mg_5CeO_x catalysts. [573 K, 101.3 kPa total pressure, 4.0 kPa ethanol, balance He].

Copper containing $Cu_{0.5}Mg_5CeO_x$ catalysts showed much higher activity than Mg_5CeO_x. The catalytic activities and product selectivities are illustrated in Figure 2.25. The ethanol conversion reached an asymptotic value ~ 80% (Figure 2.25a). This result indicates the importance of Cu in ethanol dehydrogenation. Moreover, CO_2 has a weaker effect on copper activity than on MgO activity [56]. Again, the main product was acetaldehyde, with small amounts of acetone, ethyl acetate, n-butyraldehyde, and β-keto-butanal (Figure 2.27b).

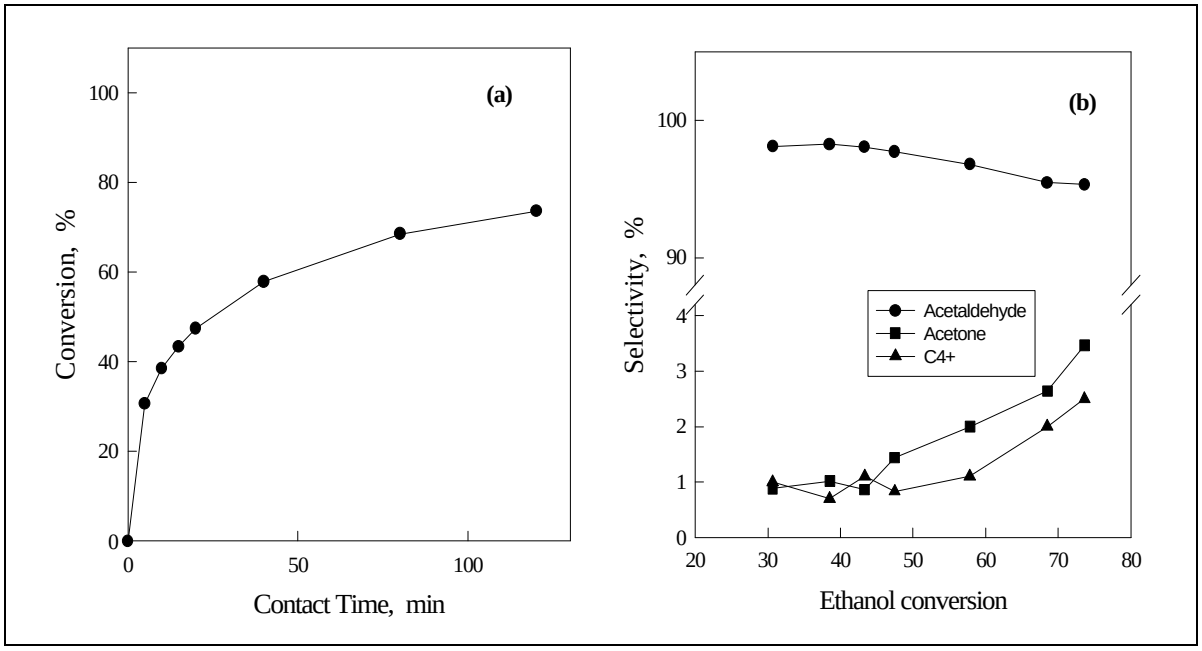

Figure 2.27. Ethanol reactions. (a) Ethanol conversion; and (b) Product distribution as a function of contact time on $Cu_{0.5}Mg_5CeO_x$ catalysts. [523 K, 101.3 kPa total pressure, 4.0 kPa ethanol, balance He].

2.3.3. Ethanol Reactions on Copper Catalysts Supported on Modified MgO

Ethanol dehydrogenation and coupling reactions were studied in order to probe reaction pathways involved in branched and linear higher alcohols synthesis from methanol, ethanol, and propanol intermediates formed initially during CO hydrogenation reactions at high pressures. These studies also address the roles of Cu, K, and Mg-Ce oxides in ethanol coupling reactions.

These experiments were carried out on MgO, Mg_5CeO_x, 0.8 wt % K-Mg_5CeO_x, $Cu_{0.5}Mg_5CeO_x$, 1.0 wt % K-$Cu_{0.5}Mg_5CeO_x$, 3.5 wt % K-$Cu_{0.5}Mg_5CeO_x$, and 1.2 wt % K-$Cu_{7.5}Mg_5CeO_x$ at atmospheric pressures. Catalyst samples (18.0 mg) were first reduced in H_2 (10 % H_2/He, 175 cm^3/min, 5 K/min) at 623 K for 0.5 h. The temperature was lowered to 573 K and ethanol was introduced along with a small amount of methane, used as an unreactive internal standard (C_2H_5OH/CH_4/He = 4.0/2.7/94.6 kPa; C_2H_5OH: Fisher Scientific, A.C.S. certified; CH_4: Matheson, ultra high purity).

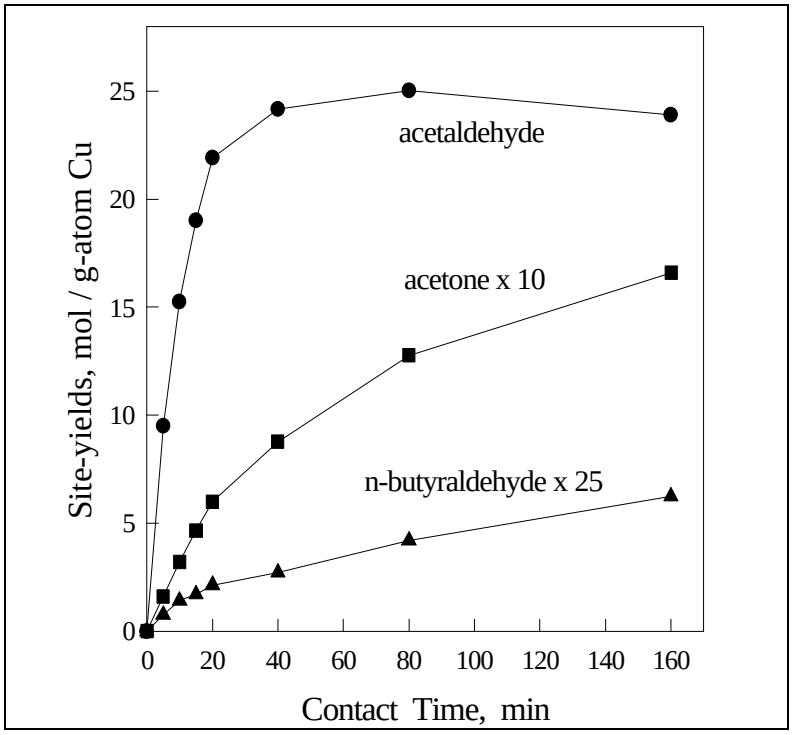

Figure 2.28. Site yields as a function of contact time on 1.0 wt % K-$Cu_{0.5}Mg_5CeO_x$ in ethanol reactions. [573 K, 101.3 kPa total pressure, 4.0 kPa ethanol, balance He].

Acetaldehyde was the predominant product of reactions of pure ethanol on 1.0 wt % K-$Cu_{0.5}Mg_5CeO_x$ (Figure 2.28). Dehydrogenation reactions occur much faster than chain growth reactions; the latter lead to the formation of acetone, n-butyraldehyde, and other oxygenates. Acetaldehyde reaches a maximum concentration at intermediate contact times during ethanol reactions and then decreases gradually. The acetaldehyde

concentration at this point corresponds to the acetaldehyde concentration calculated from thermodynamic equilibrium:

$$C_2H_5OH \rightleftharpoons C_2H_4O + H_2$$

The small decrease in acetaldehyde concentration at long contact times could be caused by further reaction of acetaldehyde to secondary products and/or because a reversal of the ethanol-acetaldehyde equilibrium due to the reaction of ethanol into chain growth products. Acetone and n-butyraldehyde were the predominant condensation products. The non-zero initial slopes on acetone and n-butyraldehyde curves are inconsistent with their formation only in sequential reactions of gas phase acetaldehyde intermediates (Figure 2.28), such as:

$$C_2H_5OH \rightleftharpoons C_2H_4O \longrightarrow \text{Condensation products}$$

Therefore, condensation products are either formed directly by ethanol self-condensation or directly from acetaldehyde but at reaction rates that do not depend on acetaldehyde concentration. Methyl-ethyl ketone (by acetaldehyde self-condensation with intramolecular hydride shift before dehydration) [1, 21], 2-pentanone (by acetaldehyde-acetone condensation), 2-propanol (by hydrogenation of acetone), 1-butanol (by hydrogenation of n-butyraldehyde), and ethyl acetate (by ethanol-acetaldehyde) were also detected in much smaller concentrations among reaction products.

The formation of all detected products of ethanol reactions on K-Cu-Mg_5CeO_x catalysts can be described by the reaction pathways shown in Figure 2.29. Acetaldehyde is formed via ethanol dehydrogenation (step I). Self-condensation of acetaldehyde (or surface acetaldehyde formed from dissociative adsorption of ethanol and further α-hydrogen abstraction) leads to the formation of n-butyraldehyde (steps II-IV) and methyl ethyl ketone (steps II-V) [46]. The aldol species converts to the keto form via H transfer (step VI); methyl-ethyl ketone is also formed by dehydration-dehydrogenation reactions of this keto form (step VII). Acetone can be formed via two pathways: (i) by reaction of aldol intermediates with surface lattice oxygen to form the β-keto acid followed by decarboxylation (steps VIII-IX) and/or (ii) by reverse aldol condensation of the keto form of reaction intermediates (step X). Formaldehyde formed in the latter reaction decomposes rapidly to CO and H_2. Surface lattice oxygen consumed by reaction (i) are replenished by the water and CO_2 formed in condensation reactions. 2-Pentanone is formed by condensation of aldol-type intermediates formed in acetone-acetaldehyde reactions (steps XI-XII). Diethyl ether was only detected in trace amounts on Mg_5CeO_x catalysts, and it appears to be formed on CeO_x acid sites by dehydration of ethanol. Ethyl acetate can form by the reaction of ethanol with acetaldehyde (step XIII) [46].

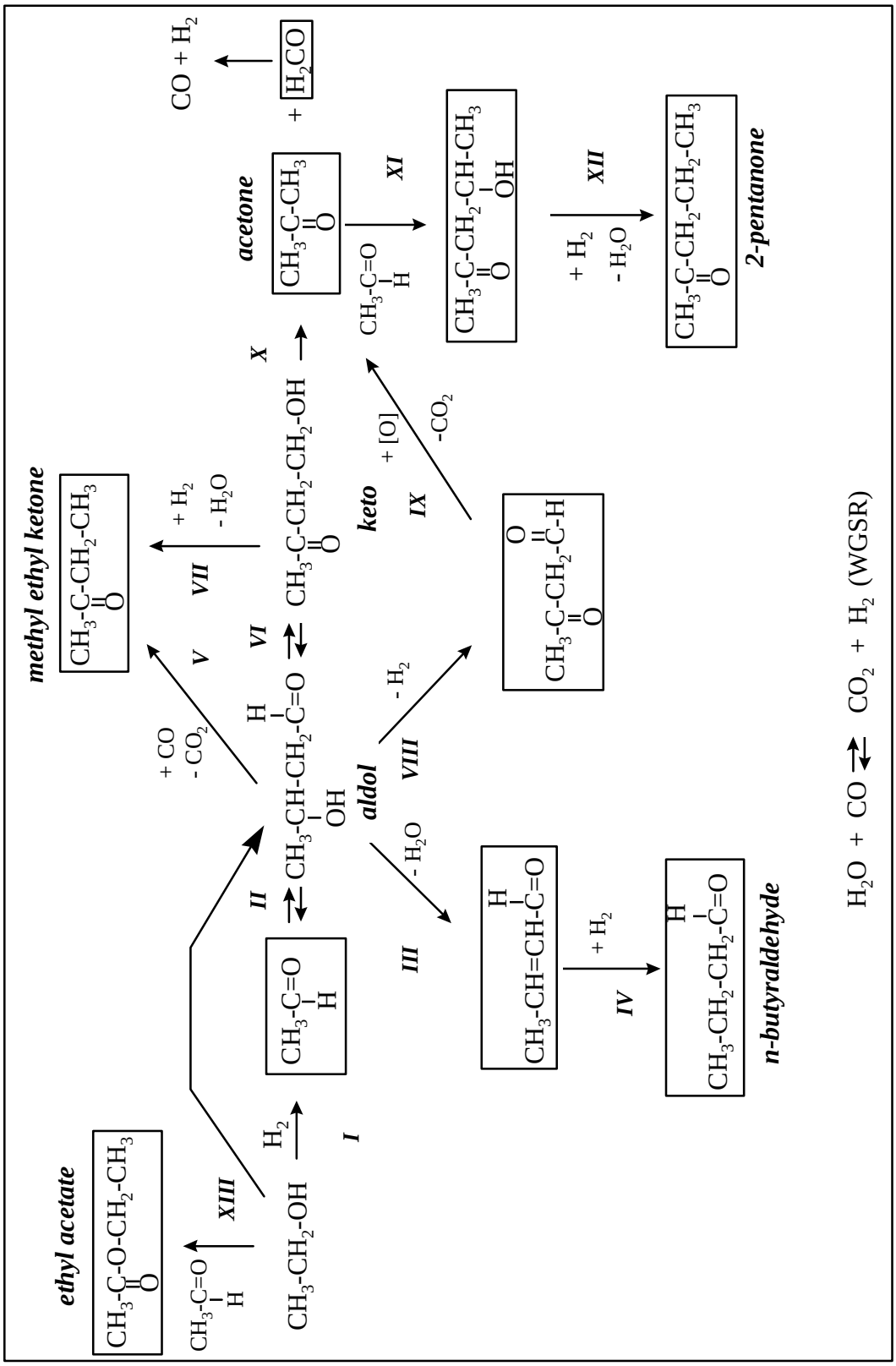

Figure 2.29. Reaction scheme for ethanol reactions on K-Cu-Mg_5CeO_x catalysts.

Ethanol reaction rates and selectivity to acetaldehyde, n-butyraldehyde, and acetone were measured on K-Cu-$MgCeO_x$ catalysts with a range of Cu and K contents in order to examine the role of Cu and basic sites on dehydrogenation and condensation reactions. The results are shown in Table 2.15. Initial reaction rates were obtained from the initial slopes of the site-yield plots at short contact times using the total surface area, the $MgCeO_x$ surface area (estimated from the difference between the total surface area and the copper surface area), the number of basic sites from CO_2 exchange, or the Cu metal surface area of each sample in order to normalize reaction rates.

Table 2.15. Effects of Cu- and K-loading on ethanol consumption and product formation on Mg_5CeO_x

Cu wt %	K wt %	Ethanol dehydrogenation		Rates of formation: Acetone+2-Propanol		Butyraldehyde+Butanol	
		areal rate $^{(1)}r_1$	turnover rate $^{(2)}r_1$	areal rate $^{(3)}r_2$	turnover rate $^{(4)}r_2$	areal rate $^{(3)}r_3$	turnover rate $^{(4)}r_3$
0	0	4.0×10^{-9}	-	7.5×10^{-11}	7.9×10^{-5}	2.8×10^{-11}	2.9×10^{-5}
0	0.8	3.4×10^{-9}	-	9.7×10^{-11}	5.6×10^{-5}	1.6×10^{-10}	9.4×10^{-5}
7	0.1	3.6×10^{-7}	0.24	3.0×10^{-9}	2.2×10^{-3}	4.5×10^{-10}	3.4×10^{-4}
7	1.0	2.4×10^{-7}	0.23	4.3×10^{-9}	1.8×10^{-3}	7.6×10^{-10}	3.2×10^{-4}
49	1.2	9.4×10^{-7}	0.24	4.4×10^{-8}	1.0×10^{-2}	1.2×10^{-9}	2.8×10^{-4}

(1) r_1 is the rate of ethanol consumption, in mol / m^2 total · s.
(2) Turnover rates per Cu surface atom, in s^{-1}.
(3) r_2 and r_3 are the rates of product formation, in mol / m^2 $MgCeO_x$ · s.
(4) Turnover rates per accessible site from $^{13}CO_2/^{12}CO_2$ in mol / mol basic site · s; basic sites measured by $^{13}CO_2/^{12}CO_2$ isotopic switch method [38, 51].

Initial dehydrogenation rates were very low on both Mg_5CeO_x and 0.8 wt % K-Mg_5CeO_x catalysts and ethanol conversion reached a limiting value of about 9 % after 0.33 h; this conversion value is much lower than the equilibrium conversion (90 %) under these reaction conditions. The decrease in ethanol conversion rates with increasing conversion may reflect 1) the formation of surface polymeric species from acetaldehyde and/or 2) an inhibition effect of CO_2 formed in ethanol condensation on base-catalyzed dehydrogenation reactions on Mg_5CeO_x. Dehydrogenation rates were much higher on $Cu_{0.5}Mg_5CeO_x$, 1.0 wt % K-$Cu_{0.5}Mg_5CeO_x$, and 1.2 wt % K-$Cu_{7.5}Mg_5CeO_x$ catalysts than on Mg_5CeO_x, suggesting that Cu sites catalyze ethanol dehydrogenation to acetaldehyde. The presence of K decreased areal ethanol dehydrogenation rates slightly, because K decreases Cu dispersion. Ethanol dehydrogenation turnover rates (normalized by exposed Cu atoms) on $Cu_{0.5}Mg_5CeO_x$, 1.0 wt % K-$Cu_{0.5}Mg_5CeO_x$, and 1.2 wt % K-$Cu_{7.5}Mg_5CeO_x$ catalysts were 0.24, 0.23 and 0.24 s^{-1}, respectively. Thus, ethanol dehydrogenation occurs predominantly on exposed Cu atoms, which become inactive for both N_2O decomposition and alcohol dehydrogenation when covered with K species and/or by alkali-promoted Cu sintering. Dehydrogenation turnover rates are not affected by Cu crystallite size or by the titration of some Cu surface atoms with KO_x species.

Aldol coupling chain growth rates are lower on Mg_5CeO_x than on $Cu_{0.5}Mg_5CeO_x$ because of lower acetaldehyde concentrations when Cu sites are not present. K increases the rate of base-catalyzed aldol coupling reactions to acetone and butyraldehyde (Table 2.15), even though steady-state acetaldehyde concentrations on $Cu_{0.5}Mg_5CeO_x$ and 1.0 wt % K-$Cu_{0.5}Mg_5CeO_x$ catalysts are identical. Thus, it appears that the higher basic site density determined by $^{13}CO_2/^{12}CO_2$ isotopic switch measurements indeed lead to higher rates of base-catalyzed aldol condensation reactions. The total rates of base-catalyzed aldol coupling reactions, when normalized by the number of accessible basic sites, are similar on $Cu_{0.5}Mg_5CeO_x$ (2.5×10^{-3} s^{-1}) and K- $Cu_{0.5}Mg_5CeO_x$ (2.2×10^{-3} s^{-1}). Aldol condensation rates on 1.2 wt % K-$Cu_{7.5}Mg_5CeO_x$ (49 wt % Cu, 0.047 Cu dispersion) are, however, much higher than on catalysts with lower Cu content, even though the density of basic sites is similar in these two samples. The difference in condensation rates suggests that Cu sites are involved in rate-determining steps required for condensation reactions, even though such Cu sites are present in sufficient number to ensure ethanol-acetaldehyde thermodynamic equilibrium. The lower aldol coupling chain growth reaction rates observed on Cu-free catalysts, which is caused not only by the low concentration of required acetaldehyde intermediates but also by the absence of Cu sites required in condensation steps, is consistent with this proposal.

A sequential reaction scheme, where ethanol dehydrogenates to form gas phase acetaldehyde, which then undergoes self-condensation reactions into products, is not considered, because it is not consistent with the sharp initial increase in product site-yield curves (Figure 2.28). On Cu containing catalysts, the steady-state acetaldehyde concentrations are similar. The effect of copper suggests a bifunctional mechanism for aldol condensation on metal-promoted basic oxides; this mechanistic proposal is discussed in detail below.

The proposed mechanism involves the initial dissociative adsorption of ethanol on MgO to form ethoxide and hydrogen species [57, 58]. Hydrogen species can then be removed by migration to Cu sites, recombination with another hydrogen adatom, and desorption as H_2:

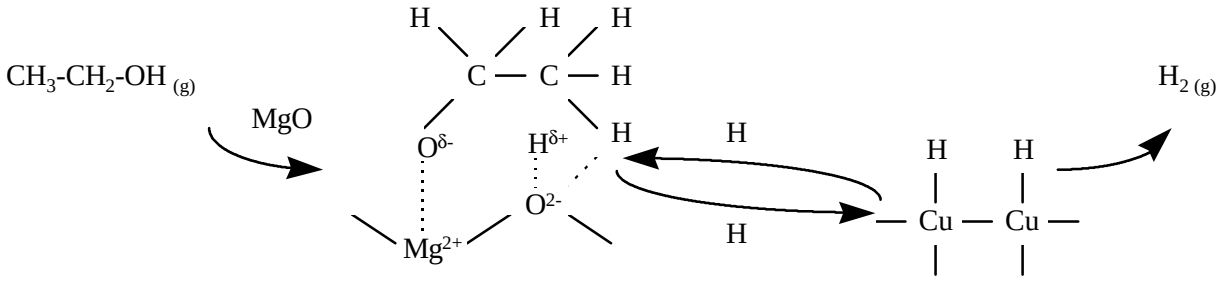

Additional C-H bond cleavage in ethoxide species then occurs and hydrogen atoms are transferred to oxygen ions and form surface acetaldehydic species:

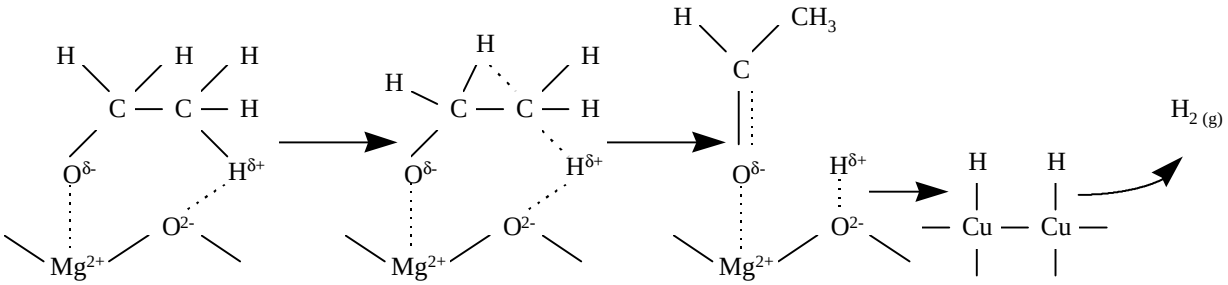

Hydrogen atoms thus migrate from basic to Cu sites and recombine on Cu sites to form H_2; as a result, basic oxygens become available for additional hydrogen abstraction step required for the formation of aldol surface species. H-H recombination rates increase with increasing ratio of surface Cu atoms to basic sites, which is 0.31 on K-$Cu_{7.5}Mg_5CeO_x$ and 0.07 on K-$Cu_{0.5}Mg_5CeO_x$ at similar basic site densities. The high ratio of Cu to basic oxide surface area on K-$Cu_{7.5}Mg_5CeO_x$ leads to higher aldol-condensation rates than on catalysts with lower ratios. Adsorbed acetaldehyde species can desorb as acetaldehyde, or react with other surface species to form aldol condensation products. The abstracted hydrogen atoms then diffuse from basic to Cu sites and again recombine on Cu sites to form H_2.

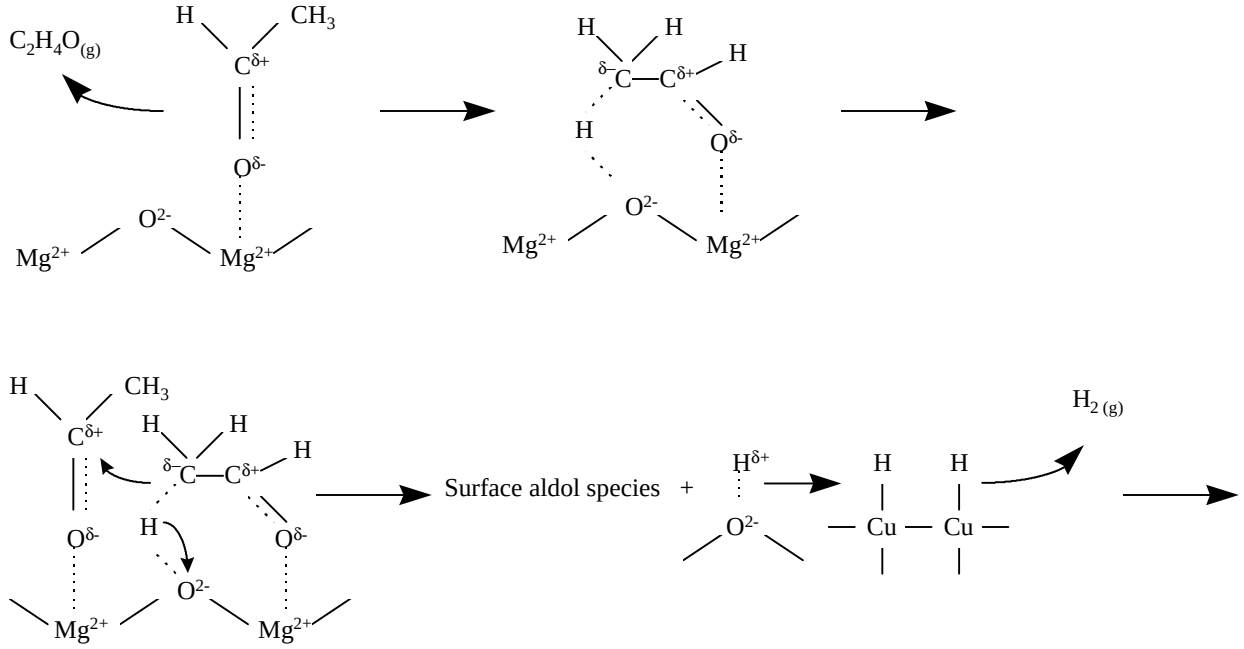

Surface aldol species can undergo condensation reactions via the pathways shown in Figure 2.29. In these reactions, the presence of copper sites increases the rate of hydrogen removal and reintroduction and provides hydrogen atoms required for the hydrogenation of the unsaturated aldehyde species (steps IV, VII, and XII, Figure 2.29). The non-zero initial slopes of acetone and n-butyraldehyde turnover-time plots (Figure

2.28) are consistent with direct condensation of ethanol reactants. These bifunctional condensation pathways are qualitatively similar in kinetic structure to those proposed for C-H activation of alkanes on cation-modified zeolites [59 - 60].

The ratio of C_3 to C_4 oxygenates measured on the various catalysts gives the selectivity for decomposition of surface keto-isomers to acetone (Figure 2.29, step X) compared to that for aldol dehydration-hydrogenation to n-butyraldehyde (Figure 2.29, steps III and IV). On Cu-free catalysts, this ratio is less than 3, and the total condensation rate is ~10^{-10} mol/m^2-s. At high Cu loadings, the selectivity C_3/C_4 increases to 36.7, while the total condensation rate increase to ~10^{-8} mol/m^2-s. Thus, in addition to increasing the surface concentration of aldol species via removal of adsorbed hydrogen atoms, Cu appears to enhance intramolecular hydrogen transfer (Figure 2.29, step VI), therefore increases keto isomer surface concentration and increases the rate of the step X (Figure 2.29).

2.3.3.a. Effects of CO_2 addition

The temperature-programmed surface reaction (TPSR) studies of preadsorbed ethanol showed that CO decreases the rate of base-catalyzed self-condensation reactions of ethanol to acetone, possibly due to the poisoning of basic and metal sites by the CO_2 formed from CO via water-gas shift, Boudouard reactions or oligomerization of CO on basic sites (MgO). Also, in the high-pressure methanol and isobutanol synthesis from CO/H_2 on K-promoted $CuMgCeO_x$ [30, 56]. In order to examine the effects of CO_2 on both ethanol dehydrogenation and coupling reactions, reaction rates were measured on 1.0 wt % K-$Cu_{0.5}Mg_5CeO_x$ and 1.2 wt % K-$Cu_{7.5}Mg_5CeO_x$ catalysts by adding CO_2 (3.5 kPa, 20 kPa) to ethanol/H_2 (4.0/29.3 kPa) reactant mixtures at 573 K.

Ethanol dehydrogenation rates were not affected by CO_2 addition (Table 2.16) on both catalysts, suggesting that Cu surface atoms are not blocked by CO_2 at the low concentrations of this study. CO_2 also did not affect n-butyraldehyde formation rate on either low or high-Cu catalysts and acetone formation rates on low-Cu catalysts. These data differ from the observed decrease in methanol and isobutanol synthesis rates as CO_2 is formed (or added) during high-pressure alcohol synthesis reactions from CO/H_2 [38, 61], suggesting that Cu sites are influenced by CO_2 only at the higher CO_2 pressures typical of isobutanol synthesis reactions. As discussed early, competitive adsorption between CO_2 and acetaldehyde on basic sites may account for the observed inhibition of CO_2 on condensation reactions on 1.0 wt % K-$Cu_{0.5}Mg_5CeO_x$ catalysts under high pressure isobutanol synthesis conditions. The ratio of CO_2 to aldehydic intermediates is much higher at these conditions than in low-pressure ethanol reaction experiments. Because of the lower CO_2/acetaldehyde ratio in ethanol dehydrogenation reactions, CO_2 competition for basic sites is not favorable and, therefore, the aldol coupling reactions are not influenced strongly by CO_2. The rate of acetone formation, however, decreased when CO_2 was present during ethanol reactions. CO_2 inhibition effects on acetone production may reflect: 1) the reversal of the reaction step that forms acetone and CO_2 (steps IX and X, Figure 2.29), or 2) different parallel reaction for acetone synthesis using stronger basic sites that are inhibited by CO_2.

Table 2.16. Effect of CO_2 on ethanol reaction on K-$Cu_yMg_5CeO_x$

Product	1.0 wt % K-$Cu_{0.5}Mg_5CeO_x$		1.2 wt % K-$Cu_{7.5}Mg_5CeO_x$	
	[a]Ethanol	[b]Ethanol/CO_2	[a]Ethanol	[b]Ethanol/CO_2
Acetaldehyde (r_1)	2.3×10^{-7}	2.1×10^{-7}	1.2×10^{-6}	9.1×10^{-7}
Acetone (r_2)	3.9×10^{-9}	1.6×10^{-9}	7.2×10^{-8}	1.1×10^{-8}
n-butyraldehyde (r_3)	8.0×10^{-10}	7.2×10^{-10}	1.7×10^{-9}	3.8×10^{-10}

r_j are the rate of ethanol consumption and products formation, and are expressed in mol/m^2 total · s.

[a] $C_2H_5OH/CO_2/H_2/CH_4/He$=4.0/0/26.7/2.7/67.9 kPa, 573 K).

[b] $C_2H_5OH/CO_2/H_2/CH_4/He$=4.0/5.3/26.7/2.7/62.6 kPa, 573 K).

Initially, we hypothesized that the highly dispersed Cu crystallites on K-$Cu_{0.5}Mg_5CeO_x$ are more likely to react with CO_2 resulting in a decrease in Cu sites. Owen and co-workers [62] have also reported that $CeCu_2$ materials are irreversibly deactivated by low concentrations (<1% CO_2) in H_2/CO feeds during high-pressure methanol synthesis reactions. This suggests that the strong metal-support interaction (SMSI) between Cu and Ce results in a loss of Cu sites in the presence of CO_2, possibly due to the stabilization of Cu^+ by CeO_2 via SMSI-type decoration of Cu surfaces with CeO_x. In order to address the latter proposal, ethanol reactions were conducted on $Cu_{0.1}Mg_5O_x$ catalyst (Ce-free), with and without CO_2 in the feed, respectively. The results are summarized as follows:

a) Ethanol conversion reached an asymptotic value of ~70% in both cases (Figures 2.30 and 2.31).

b) The main product was acetaldehyde, produced by ethanol dehydrogenation.

c) The condensation products were: acetone, ethyl acetate, n-butyraldehyde, and 2-pentanone.

d) CO_2 addition decreased the rates of condensation reactions (on basic sites), but had no apparent effect on dehydrogenation (on Cu sites) (Figures 2.30b and 2.31b).

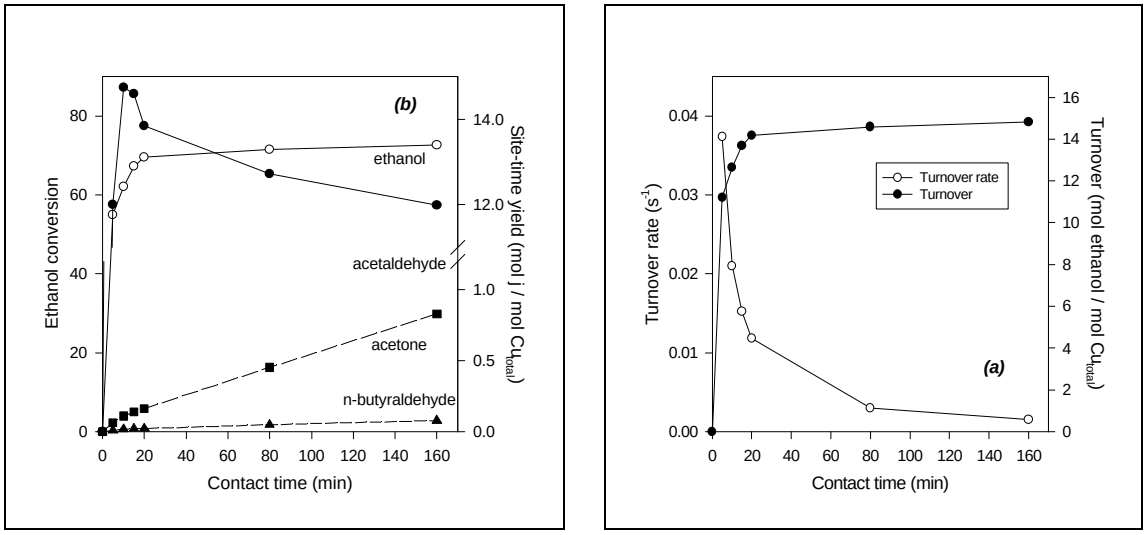

Figure 2.30. Ethanol reactions with CO_2-free feed gas. (a) Ethanol turnovers and turnover rates. (b) Site-time yields as a function of contact time on $Cu_{0.1}MgO_x$.

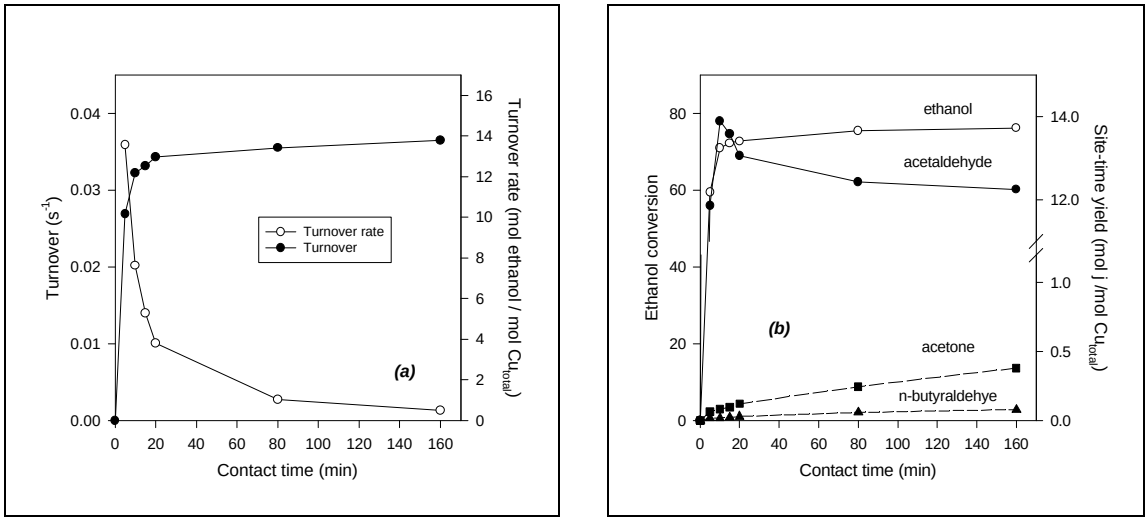

Figure 2.31. Ethanol reactions with CO_2-addition to feed gas. (a) Ethanol turnovers and turnover rates. (b) Site-time yields as a function of contact time on $Cu_{0.1}MgO_x$.

2.3.3.b. Effects of replacing Ce with Zn in K-$Cu_{0.5}Mg_5CeO_x$

These experiments were carried out in order to compare reaction pathways for the ethanol coupling reactions on K-$Cu_{0.5}Mg_5CeO_x$ with those on K-$Cu_{0.5}Mg_5ZnO_x$ catalysts. Substituting ZnO for CeO leaded to decrease the total surface area of catalyst. It shows that ZnO is not a structural promoter in the Cu-based catalysts, while CeO is a structural promoter that increases the total surface area of Cu-MgO catalyst. In both catalysts, however, the addition of K decreased the total surface area, suggesting that potassium promotes the sintering of $MgZnO_x$ and $MgCeO_x$.

The reaction pathways of the ethanol coupling were very similar on both catalysts. Acetaldehyde was the primary product of ethanol reactions and acetone and n-butyraldehyde were the predominant condensation products (Figure 2.32). However, the non-zero initial slopes on acetone and n-butyraldehyde curves indicates that the direct condensation of ethanol can occur without gas phase acetaldehyde as an intermediates, as also observed on K-Cu-Mg-CeOx catalysts.

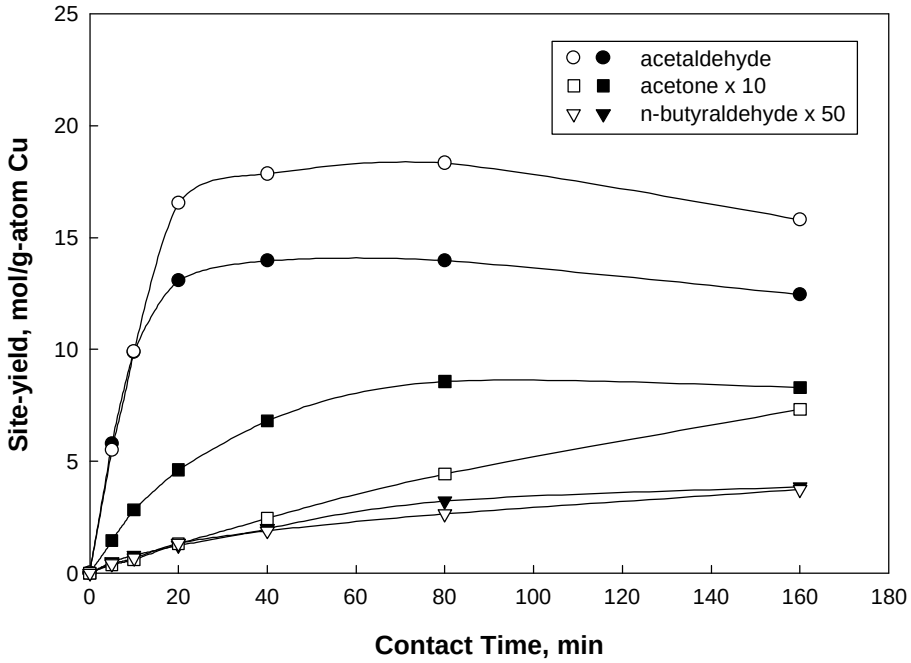

Figure 2.32. Site-yields as a function of contact time on K-Cu-Mg-Zn catalysts; open symbols: $Cu_{0.5}Mg_5ZnO_x$, closed symbols: K- $Cu_{0.5}Mg_5ZnO_x$. [T_r = 573 K, P_t = 101.3 kPa, $P_{ethanol}$ = 4.0 kPa].

Initial reaction rates were obtained from yield *vs.* contact time plots and normalized using the total surface area of each sample (Table 2.17). As the K is added to catalysts, the site-yield of acetaldehyde decreased and the site-yield of acetone and n-butyraldehyde increased. This indicates that the addition of K increases the basic

properties of catalysts and the rate of chain growth reactions. In the case of K-Cu-Mg-CeO_x catalysts, the areal ethanol dehydrogenation rates decreased with the addition of K because K decreases the dispersion of Cu. Also, the condensation reactions increased with addition of K because the density of basic sites increases. As compared with Cu-Mg-CeO_x, Cu-Mg-ZnO_x catalysts have higher dehydrogenation rates even after adding K because of the strong hydrogenating ability of the ZnO component.

ZnO is a typical basic oxide which is used in methanol synthesis catalyst and possesses the hydrogenation activity. Ueda et al. [3] reported that ZnO is less active compared with MgO for the condensation reaction of ethanol and mainly catalyzes the dehydrogenation reaction of ethanol to acetaldehyde. Adding K, however, increases the basicity by ZnO, and the condensation rate of acetaldehyde increases.

Table 2.17. Effects of Cu- and K-loading on ethanol consumption and product formation on Mg-ZnO_x

Sample	Ethanol Dehydrogenation rate $r_1 \times 10^{7}$ [1)]	Rates of formation rate Acetone + 2-Propanol $r_2 \times 10^{9}$ [2)]	Butyraldehyde + Butanol $r_3 \times 10^{9}$ [2)]
$Cu_{0.5}Mg_5ZnO_x$	2.2	1.5	0.31
1.3 wt % K-$Cu_{0.5}Mg_5ZnO_x$	3.9	9.2 [3)]	0.63 [3)]
$Cu_{0.5}Mg_5CeO_x$	3.6	3.0	0.45
1.0 wt % K-$Cu_{0.5}Mg_5CeO_x$	2.4	4.3	0.76

[1)] Rates of ethanol consumption, in mol/m^2-total·s.
[2)] Rates of product formation, in mol/m^2 $MgCeO_x$·s; $MgCeO_x$ surface area is estimated from the different between the total surface area and the copper surface area.
[3)] Rates of product formation, in mol/m^2-total·s.

2.3.3.c. Ethanol reactions on Cs-Cu/Zn/Al_2O_3

Ethanol dehydrogenation and coupling reactions on 2.9 wt% Cs-Cu/ZnO/Al_2O_3 catalysts were studied in order to determine the roles of Cu and of basic sites and to compare reaction pathways on Cs-Cu/ZnO/Al_2O_3 catalyst with those on K-$Cu_yMg_5CeO_x$ catalysts. The site-yields of acetaldehyde, acetone, and n-butyraldehyde on the Cs-Cu/ZnO/Al_2O_3 are shown in Figure 2.33 as a function of contact time. Their normalized selectivities are shown in Figure 2.34 as a function of ethanol conversion.

The reaction pathways on Cs-Cu/ZnO/Al_2O_3 are similar to those on K-$Cu_yMg_5CeO_x$ and K-$Cu_yMg_5ZnO_x$. Acetaldehyde is a primary product that can react further in secondary condensation reactions to give acetone, n-butyraldehyde, and other oxygenates. The non-zero initial slopes of acetone and n-butyraldehyde curves are consistent with an additional direct pathway for condensation reactions of ethanol without the requirement for gas phase acetaldehyde intermediates.

The roles of Cu and basic sites on dehydrogenation and condensation reactions can be probed by measuring each reaction rate on K-$Cu_yMg_5CeO_x$ and Cs-Cu/ZnO/Al_2O_3 catalysts (Table 2.18). Ethanol dehydrogenation rates are similar on all catalysts, suggesting that only Cu sites are required and that each Cu surface atom shows the same catalytic activity for this hydrogenation reactions. Aldol condensation rates (per surface area of the basic support) increase with increasing Cu content in the catalysts, even though ethanol dehydrogenation turnover rates are similar on these Cs-Cu/ZnO/Al_2O_3 and K-$Cu_yMg_5CeO_x$ catalysts and acetaldehyde concentrations reach thermodynamic equilibrium very quickly during ethanol condensation reactions. Cu sites provide ethanol dehydrogenation sites and also dispose of H-atoms abstracted by oxygen anions during C-H and O-H activation steps involved in ethanol conversion reactions [16, 2]. Reactions of C_2H_5OH/D_2 mixtures have shown that Cu sites increase the rate of hydrogen adsorption-desorption, which is an irreversible and rate-determining step in ethanol reactions on Cu-free K-Mg_5CeO_x catalysts.

Dehydrogenation rates were higher on high Cu-content catalysts than on low Cu-content catalysts, suggesting that Cu sites catalyze ethanol dehydrogenation steps leading to acetaldehyde. Ethanol dehydrogenation turnover rates (per Cu surface atom), however, are very similar on Cs-Cu/ZnO/Al_2O_3, K-$Cu_{0.5}Mg_5CeO_x$, and K-$Cu_{7.5}Mg_5CeO_x$ catalysts. Aldol condensation rates on catalysts with high Cu content are higher than on catalyst with low Cu content, suggesting that Cu sites are also involved in rate-determining steps required for ethanol condensation reactions. Cu sites provide ethanol dehydrogenation sites and they also dispose of H-atoms abstracted by oxygen anions during C-H and O-H activation reactions of ethanol [30, 29]. Reactions of C_2H_5OH/D_2 mixtures [29], [60] show that Cu sites increase the rate of hydrogen adsorption-desorption, a step that is effectively irreversible (rate-determining) in ethanol reactions on Cu-free K-Mg_5CeO_x catalysts.

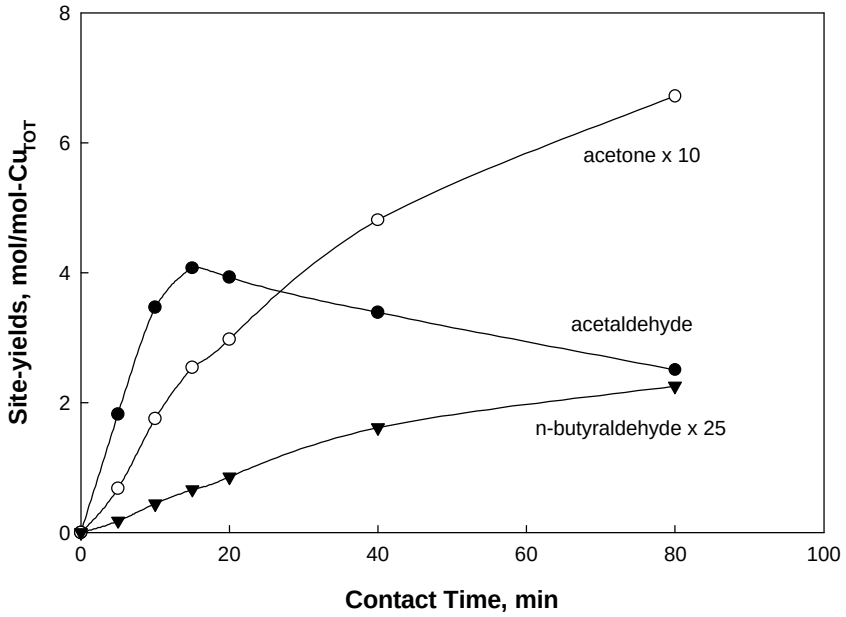

Figure 2.33. Site-yields as a function of contact time for the ethanol reaction on 2.9 wt% Cs-Cu/ZnO/Al_2O_3 catalyst. [T_r=573 K, P_t=101.3 kPa, $P_{ethanol}$ = 4.0 kPa].

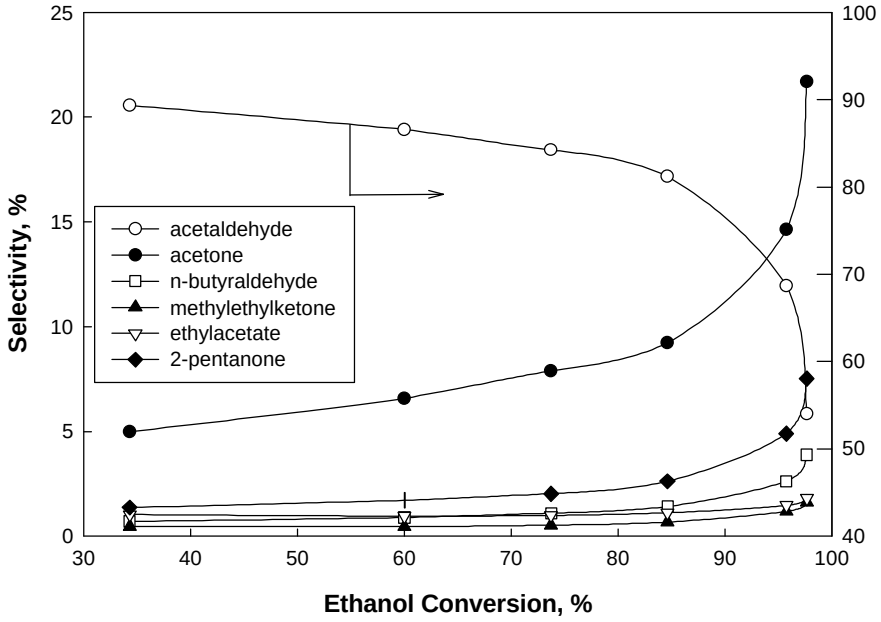

Figure 2.34. Normalized selectivites as a function of ethanol conversion for the ethanol reaction on 2.9 wt% Cs-Cu/ZnO/Al_2O_3 catalyst. [T_r=573 K, P_t=101.3 kPa, $P_{ethanol}$=4.0 kPa].

Table 2.18. Effects of Cu- and basic sites on Ethanol Conversion and Product Formation

	Initial Ethanol Dehydrogenation [a)]	Initial Condensation Rate [b)]
K-$Cu_{0.5}Mg_5CeO_X$	0.22	0.5
K-$Cu_{7.5}Mg_5CeO_X$	0.24	4.5
Cs-Cu/ZnO/Al_2O_3	0.14	4.2

[(a)] Turnover rates per Cu surface atom, in s^{-1}; [(b)] Product formation rates, in $x10^{-8}$ mol / m^2-support • s

The rapid establishment of ethanol-acetaldehyde equilibrium suggests the uses of this equlibrated pool as the "reactant pool" in calculating conversions and selectivites. The selectivities of reaction products obtained at similar conversion levels of is reactant pool are shown in Table 2.19. As compared with the initial turnover rates, the turnover rates of ethanol dehydrogenation reactions decrease because of the rapid formation of surface polymer species at the beginning of ethanol reaction and also because of the inhibiting effect of CO_2 and H_2O. In the case of Cs-Cu/ZnO/Al_2O_3 catalyst, small amounts of hydrocarbons (0.1%) such as propylene were observed.

Table 2.19. Activities, rates, and carbon pool selectivities for ethanol reactions on Cs-Cu/ZnO/Al_2O_3 and K-$Cu_yMg_5CeO_x$ catalysts

Catalyst	Cs-Cu/ZnO/Al_2O_3	K-$Cu_{7.5}Mg_5CeO_x$	K-$Cu_{0.5}Mg_5CeO_x$
Ethanol pool conversion, %	18.2	16.8	20.3
Contact time, min	20	10	80
Ethanol turnover rate per Cu surface atom, s-1	0.08	0.14	0.04
Rate, x 10^{-8} mol/m^2-support s			
Acetaldehyde	55.1	60.7	4.20
Acetone	4.17	3.48	0.21
n-butyraldehyde	0.48	0.11	0.03
Methyl ethyl ketone	0.23	0.05	0.00
Acetone/n-buryraldehyde [a)]	8.7	32.9	7.6
Carbon Pool Selectivities, %			
Hydrocarbons (< C_3)	0.1	0.0	0.0
Acetone	49.1	67.5	55.3
n-Butyraldehyde	7.5	2.7	9.7
Methyl ethyl ketone	3.6	1.3	0.0
Ethylacetate	5.9	1.8	0.0
Crotonaldehyde	1.0	0.0	0.0
2-Pentanone	13.9	4.3	12.6
CO_x	19.2	22.4	22.4
	100.2	100.0	100.0

2.3.4. Acetaldehyde Reactions on Isobutanol Synthesis Catalysts

Condensation and hydrogenation reactions of acetaldehyde were examined on 0.8 wt % K-Mg_5CeO_x, 1.0 wt % K-$Cu_{0.5}Mg_5CeO_x$, and 1.2 wt % K-$Cu_{7.5}Mg_5CeO_x$. The catalyst (33.0 mg) was first reduced in H_2 (10% H_2/He) at 623 K for 0.5 h. The reaction was carried out at 573 K. The reactant mixture was: $C_2H_4O/CH_4/He$ = 6.6/2.7/92.0 kPa (C_2H_4O: Fisher Scientific, Reagent Grade; CH_4: Matheson, ultra high purity). Products were sampled following the procedures described in the previous section.

In Section 2.2.3, we proposed that condensation reactions could proceed (i) via direct reactions of ethanol without the intermediate formation of gas phase acetaldehyde molecules or, (ii) the condensation reaction products are formed through consecutive reactions with the formation of gas-phase acetaldehyde and its condensation with zero order kinetics. Catalytic activity and product yields for acetaldehyde reactions on 1.0 wt % K-$Cu_{0.5}Mg_5CeO_x$ were measured at various acetaldehyde pressures in order to estimate kinetic reaction order respect acetaldehyde concentration.

Acetone and crotonaldehyde are the predominant products of acetaldehyde reactions (Figure 2.35). Carbon dioxide, n-butyraldehyde, methyl-propenyl ketone, and 2-pentanone were also detected in small concentrations among reaction products. Ethanol forms by acetaldehyde hydrogenation using H-adatoms formed in C-H activation steps or H_2 molecules desorbed by Cu sites. Aldol-type condensation of acetaldehyde forms crotonaldehyde, which can then hydrogenate to form n-butyraldehyde. Hydrogen is also produced by decomposition of the formaldehyde formed in retro-aldol reactions leading to acetone (Figure 2.29).

Solid basic catalysts are often deactivated either by the presence of acid molecules and water in gas phase or by in situ coke formation during reactions. At the early stage of the acetaldehyde reaction, the catalytic activity of K-$Cu_yMg_5CeO_x$ was sharply decreased (Figure 2.104). This decay of the catalytic activity can be caused by water or coke formed during the reaction, or by CO_2 formed by the water-gas shift reaction (WGSR). In these experiments, it appears that the coke formed on the basic sites mainly leads to initial deactivation of the catalysts because of the poor overall mass balance (carbon selectivity totals less than 45 %). Acetaldehyde can polymerize to give dimer and trimer compounds and/or by sequential aldol condensations leading to high molecular weight aldehydes (Figure 2.36) [63]. These polymeric species are likely to remain on the catalyst surface. Di Cosimo and Apestequia [64] proposed that non-cyclic trimers, such as phorone produced by aldol condensation of mesityl oxide with acetone, are the key intermediate species for coke formation in the aldol-condensation reaction on MgO and alkali-promoted catalysts.

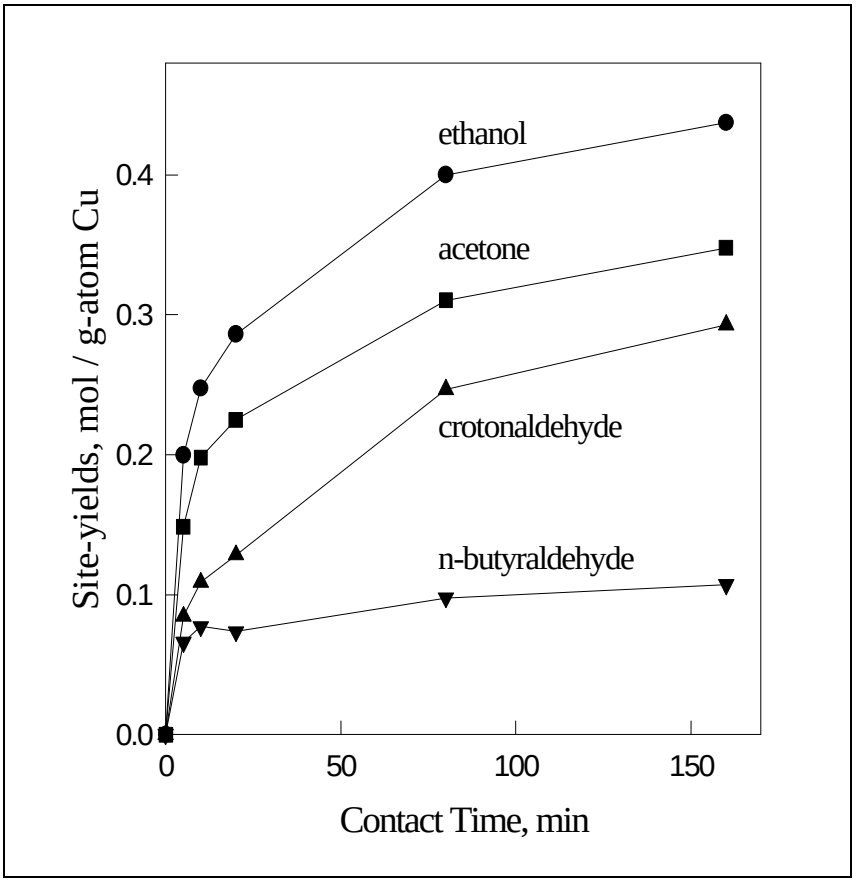

Figure 2.35. Acetaldehyde reactions. Site yields as a function of contact time on 1.0 wt. % K-$Cu_{0.5}Mg_5CeO_x$. [573 K, 101.3 kPa total pressure, 8.0 kPa acetaldehyde pressure, balance He].

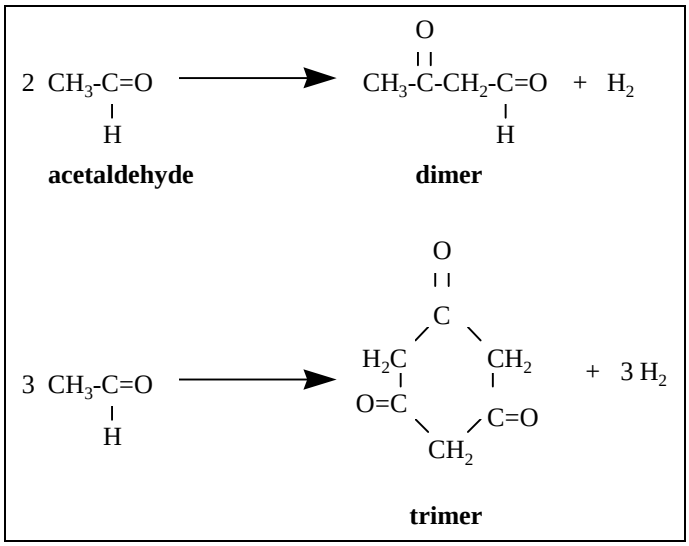

Figure 2.36. Formation of dimer and trimer compounds from acetaldehyde.

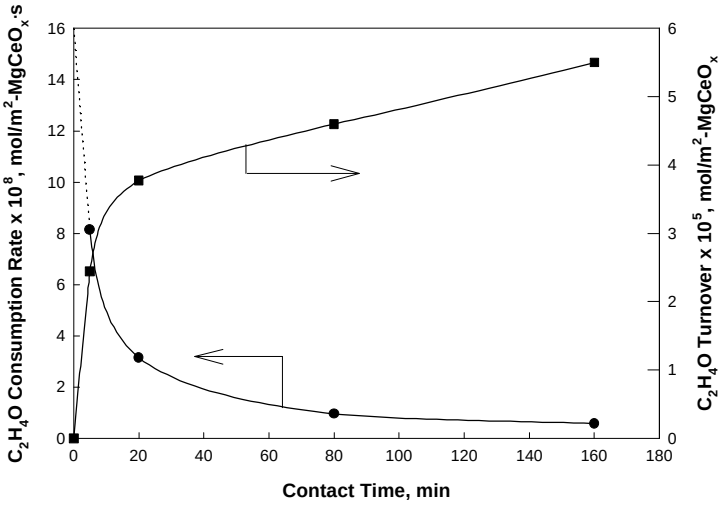

Figure 2.104. Acetaldehyde (C_2H_4O) reaction. Turnover and Turnover rate of acetaldehyde as a function of contact time on 1.0 wt % K-$Cu_{0.5}Mg_5CeO_x$. [573 K, 101.3 kPa total pressure, 6.4 kPa acetaldehyde pressure, balance He].

The initial reaction rates at different initial partial pressures of acetaldehyde are shown in Figure 2.37. Condensation, hydrogenation, and total conversion rates are approximately first order in acetaldehyde concentrations. These results show that the initial reaction non-zero slope for condensation products in ethanol reactions (Figure 2.26) cannot reflect a zero-order dependence of the aldehyde condensation (n=0) in equation (1):

$$r_j = k_j (P_{C2H4O})^n \qquad (1)$$

Instead, it suggest that direct reactions of ethanol account for a significant fraction of the condensation products formed from ethanol reactants.

Figure 2.38 shows the molar ratio of ethanol to acetone and of C_4 oxygenates (crotonaldehyde and n-butyraldehyde) to acetone among products of acetaldehyde reactions. Aldol coupling chain growth rates increse with increasing copper surface area. The increase, however, is less pronounced than on ethanol reactions. These results show that Cu sites also improve C-H bond activation when acetaldehyde is the reactant. Acetone is a condensation product, while ethanol is an hydrogenation product. The molar ratio between ethanol/acetone is a measurement of the catalyst ability to remove H-atoms from the surface by recombinative desorption compared to its ability to carry out condensation reactions. On Mg_5CeO_x catalyst ethanol is produced selectively over acetone. The catalyst surface is saturated with H-atoms provided by abstraction of one α-hydrogen from acetaldehyde over basic sites. Without Cu, it is more probable that the H-atoms are emplyed to hydrogenate acetaldehyde to ethanol. When Cu sites are presented, ethanol selectivity decreases markedly because H-atoms recombine H_2 instead of hydrogenating adsorbed acetaldehyde species. On the other hand, the ratio of C_4 oxygenates and acetone shows that the reverse aldol condensation step from aldol C_4 intermediates becomes less likely as Cu is introduced in the catalysts (Figure 2.38). Acetone is formed selectively over Cu-containing catalysts instead of n-butyraldehyde or crotonaldehyde.

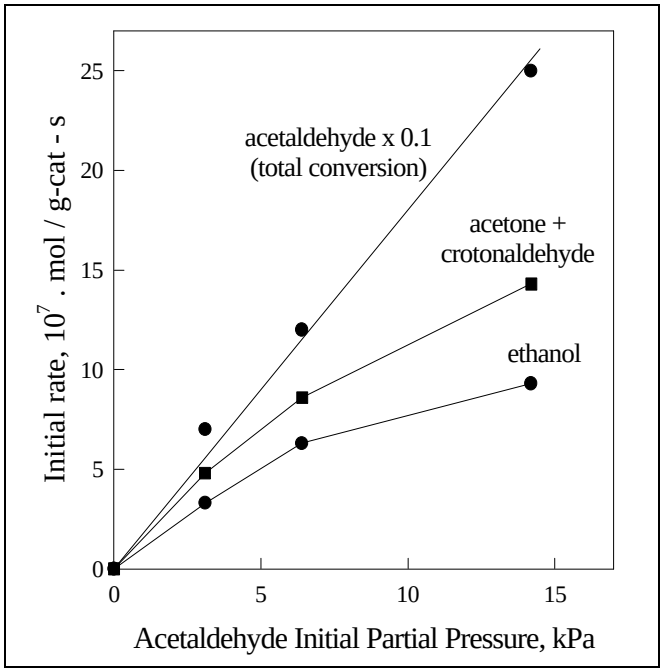

Figure 2.37. Acetaldehyde reactions. Effect of the acetaldehyde initial partial pressure over the initial rates. Acetaldehyde conversion as a function of contact time on 1.0 wt. % K-$Cu_{0.5}Mg_5CeO_x$. [573 K, 101.3 kPa total pressure, 3-15 kPa acetaldehyde pressures, balance He]

Figure 2.38 shows the molar ratio of ethanol to acetone and of C_4 oxygenates (crotonaldehyde and n-butyraldehyde) to acetone among products of acetaldehyde reactions. Aldol coupling chain growth rates increase with increasing copper surface area. The increase, however, is less pronounced than on ethanol reactions. These results show that Cu sites also improve C-H bond activation when acetaldehyde is the reactant. Acetone is a condensation product, while ethanol is an hydrogenation product. The molar ratio between ethanol/acetone is a measurement of the catalyst ability to remove H-atoms from the surface by recombinative desorption compared to its ability to carry out condensation reactions. On Mg_5CeO_x catalyst ethanol is produced selectively over acetone. The catalyst surface is saturated with H-atoms provided by abstraction of one α-hydrogen from acetaldehyde over basic sites. Without Cu, it is more probable that the H-atoms are employed to hydrogenate acetaldehyde to ethanol. When Cu sites are presented, ethanol selectivity decreases markedly because H-atoms recombine H_2 instead of hydrogenating adsorbed acetaldehyde species. On the other hand, the ratio of C_4 oxygenates and acetone shows that the reverse aldol condensation step from aldol C_4 intermediates becomes less likely as Cu is introduced in the catalysts (Figure 2.38). Acetone is formed selectively over Cu-containing catalysts instead of n-butyraldehyde or crotonaldehyde.

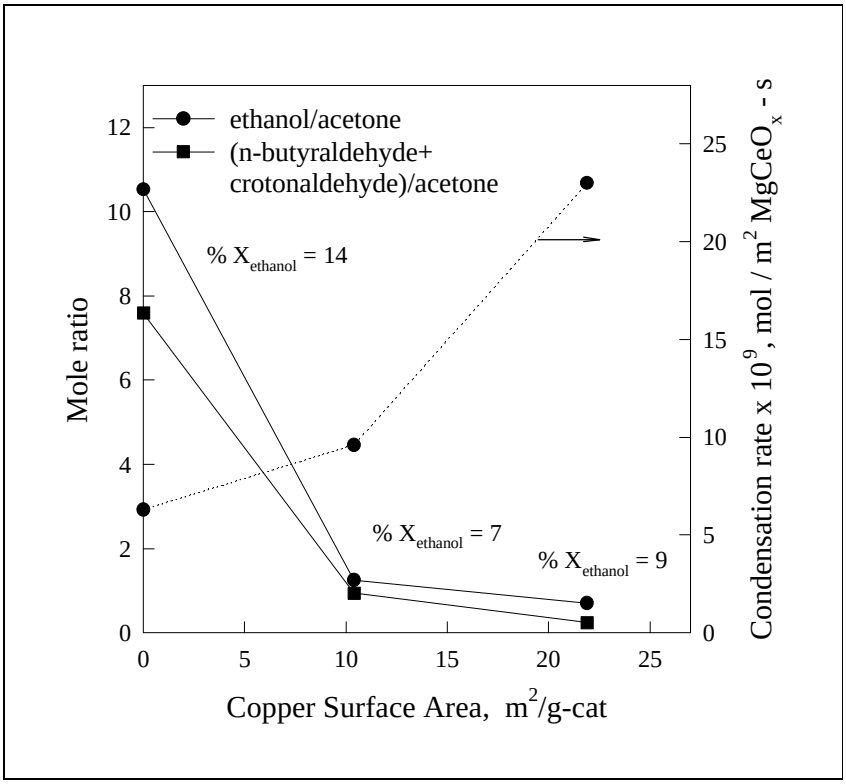

Figure 2.38. C_2 to C_3 and C_4 to C_3 molar ratios on acetaldehyde reactions as a function of Cu surface area on K-Cu_yMg_5CeOx catalysts. [573 K, 101.3 kPa total pressure, 6.6 kPa acetaldehyde, balance He].

2.3.5. $C_2H_5OH/^{13}C_2H_4O$ Reactions on Isobutanol Synthesis Catalysts

Competitive reactions between $^{12}C_2H_5OH$ and $^{13}C_2H_4O$ were examined on 0.8 wt % K-Mg_5CeO_x, 1.0 wt % K-$Cu_{0.5}Mg_5CeO_x$, and 1.2 wt % K-$Cu_{7.5}Mg_5CeO_x$ catalysts in order to probe the direct pathways from ethanol to condensation products. The catalyst (22.0 mg) was reduced in 10% H_2 (balance He) at 623 K for 0.5 h. Reactions were conducted at 523 K and 101.3 kPa in the RRU. The reactant mixture was introduced along with a small amount of methane (reaction mixture: $^{13}C_2H_4O/^{12}C_2H_5OH/H_2/CH_4/He$ = 2.9/1.1/2.9/2.4/92.0 kPa; $^{13}C_2H_4O$: Isotec Inc., 2 ^{13}C: 99 %; C_2H_5OH: Fisher Scientific, A.C.S. Certified; CH_4: Matheson, ultra high purity). ^{13}C content and isotopic distributions in reactants and products were analyzed by mass spectrometry using a matrix deconvolution method that accounts for the natural ^{13}C abundance and mass fragmentation pattern of each molecule [65].

As was discussed early (Section 2.2.3) it appears that ethanol undergoes condensation reactions directly, without requiring its intermediate conversion to gas phase acetaldehyde. Also, acetaldehyde conversion rates were shown to depend on acetaldehyde concentration (Section 2.2.4). On the other hand, Chung et al. [66], using $CH_3{}^{13}CH_2OH/C_2O_4H$ mixtures on Cu/ZnO catalysts found that acetone can be produced by the C-C bond cleavage in the C_4 species formed from two aldehydic species, and n-butyraldehyde can be produced by the C-O bond cleavage in the C_4 species formed from ethanolic and acetaldehydic species. In order to examine the role of ethanol and investigate the direct pathway from ethanol to condensation products competitive reactions between $^{12}C_2H_5OH$ and $^{13}C_2H_4O$ were performed on 0.8 wt % K-Mg_5CeO_x, 1.0 wt % K- $Cu_{0.5}Mg_5CeO_x$, and 1.2 wt % K-$Cu_{7.5}Mg_5CeO_x$ catalysts. The carbon-13 in reactants and in reaction products against contact time are shown in Figures 2.39, 2.40, and 2.41, respectively, on this three catalysts.

On all catalysts, the ^{13}C-content in both ethanol and acetaldehyde changes with contact time, as the products reach chemical and isotopic equilibrium at long contact time. The rate of ethanol-acetaldehyde equilibration is much higher on 1.2 wt % K-$Cu_{7.5}Mg_5CeO_x$ than on the other two catalysts. When copper is present, hydrogenation-dehydrogenation reactions occur more rapidly, in agreement with the results shown in section 3.2. On Cu-free catalysts (Figure 2.39), the ^{13}C-content in both ethanol (30%) and acetaldehyde (80%) reach values that differ markedly from the predicted isotopic equilibrium (70 %). This is consistent with the rapid deactivation observed during ethanol reactions on Cu-free catalysts (section 2.2.2.).

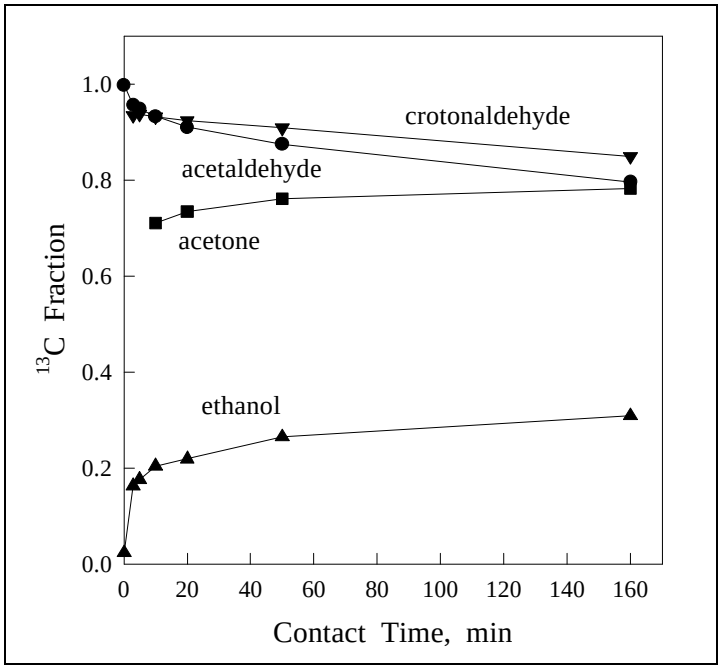

Figure 2.39. ^{13}C-content in reactants and reaction products ($^{13}C_2H_4O$-C_2H_5OH-H_2 reaction mixtures on 0.8 wt % K-Mg_5CeO_x). [523 K, 101.3 kPa total pressure, 2.9 kPa acetaldehyde pressure, 1.1 kPa ethanol pressure, 2.9 kPa hydrogen pressure, balance He].

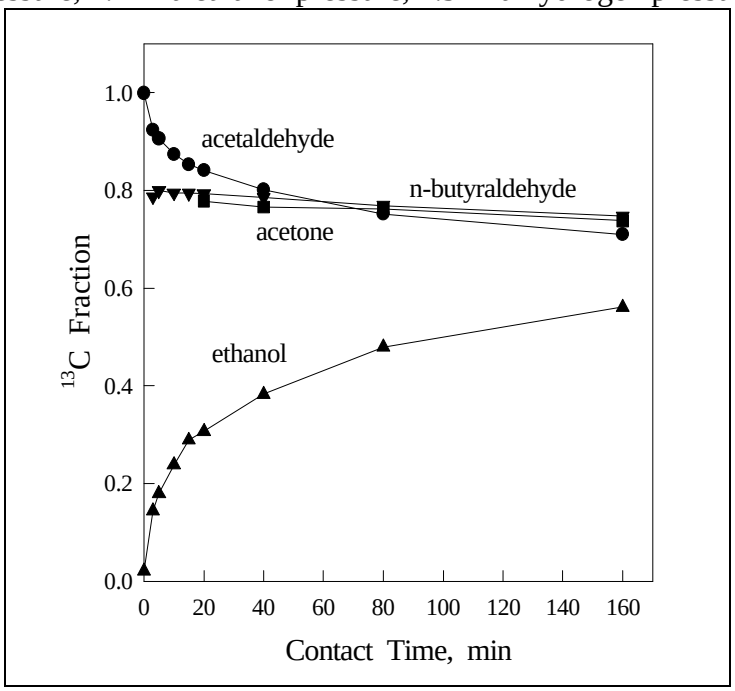

Figure 2.40. ^{13}C-content in reactants and reaction products ($^{13}C_2H_4O$-C_2H_5OH-H_2 reaction mixtures on 1.0 wt % K-$Cu_{0.5}Mg_5CeO_x$). [523 K, 101.3 kPa total pressure, 2.9 kPa acetaldehyde pressure, 1.1 kPa ethanol pressure, 2.9 kPa hydrogen pressure, balance He].

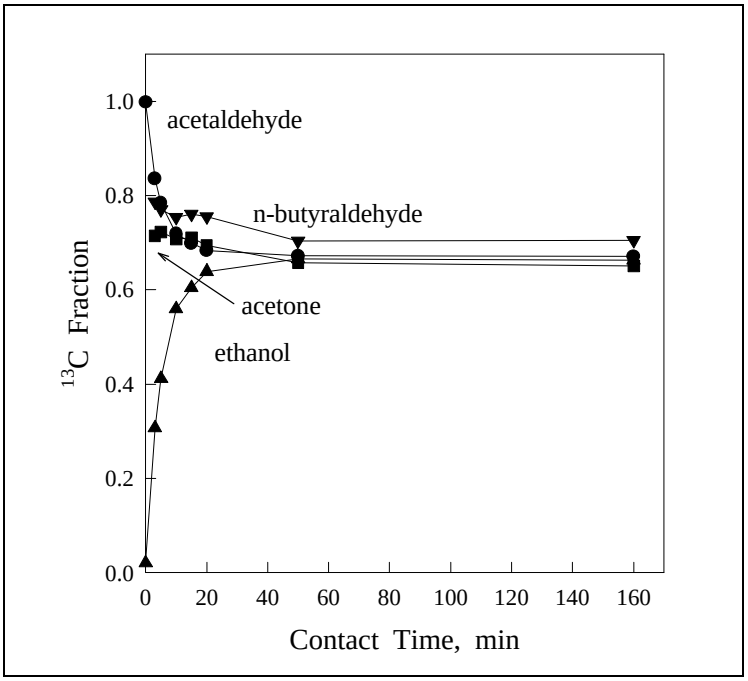

Figure 2.41. ^{13}C-content in reactants and reaction products ($^{13}C_2H_4O$-C_2H_5OH-H_2 reaction mixtures on 1.2 wt % K-$Cu_{7.5}Mg_5CeO_x$). [523 K, 101.3 kPa total pressure, 2.9 kPa acetaldehyde pressure, 1.1 kPa ethanol pressure, 2.9 kPa hydrogen pressure, balance He].

The ^{13}C-distributions of products formed on 1.0 wt % $Cu_{0.5}Mg_5CeO_x$ is shown in Figure 2.42. The ^{13}C-content in products changes slightly with contact time, but the carbon-13 distributions of reactants (Figure 2.42) change significantly. These data could reflect (i) reactants that lead initially to the formation of surface polymer species, which act as intermediates and decompose with time to give the observed product or (ii) ethanol and acetaldehyde reactants with the same reactivity. The first possibility is quite unlikely because the decomposition of surface polymer species should lead to C_1, C_2, C_3, etc. species and not only to C_4 species. The second possibility is more likely. On Cu-containing catalysts, hydrogenation-dehydrogenation steps (ethanol=acetaldehyde+H_2) are quite fast. The ^{13}C-content in acetone and n-butyraldehyde extrapolated to zero contact time is 80%. If these products come exclusively from acetaldehyde, the extrapolated value should be 100%, and if they come exclusively from ethanol the value should be 0 %. The 80% value reflects that the products are formed undistinguishly from ethanol and acetaldehyde (^{13}C composition of the initial reactant mixture was 73%). Also, a small decrease in ^{13}C contents in products and reactant mixture is observed. The product formation rates from acetaldehyde and from ethanol are almost the same, with that the product formation rates from acetaldehyde only slightly higher than from ethanol.

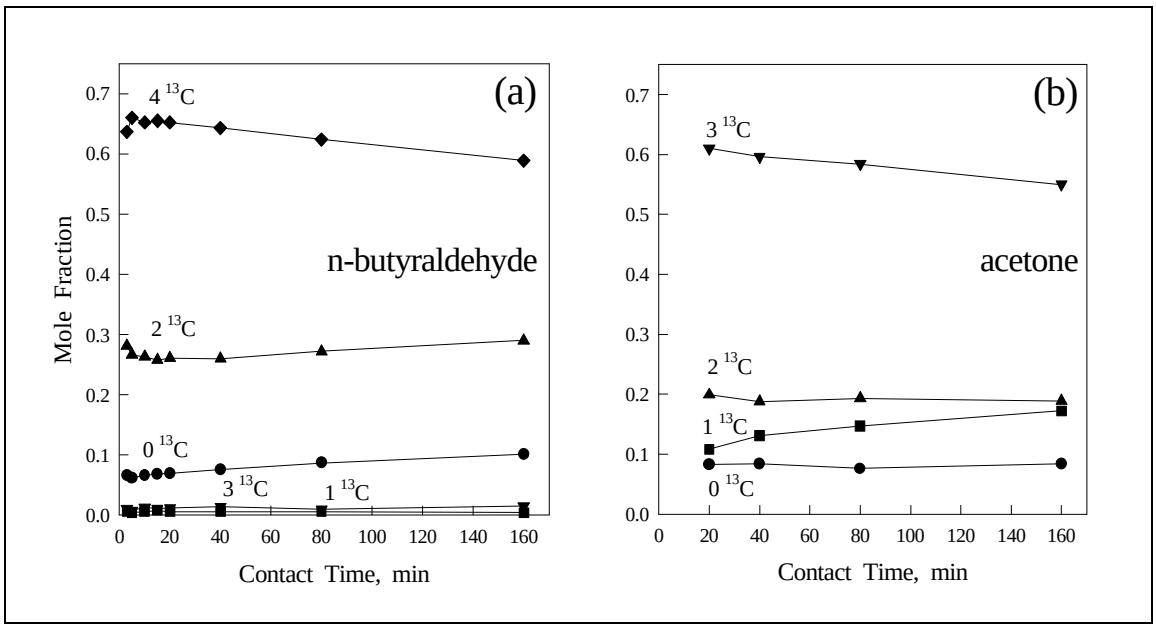

Figure 2.42. ^{13}C-distribution of products in $^{13}C_2H_4O$-C_2H_5OH-H_2 reactions on 1.0 wt % K-$Cu_{0.5}Mg_5CeO_x$ as a function of contact time. [523 K, 101.3 kPa total pressure, 2.9 kPa acetaldehyde pressure, 1.1 kPa ethanol pressure, 2.9 kPa hydrogen, balance He].

Table 2.20 shows the experimental ^{13}C-content in n-butyraldehyde on 1.0 wt % K-$Cu_{0.5}Mg_5CeO_x$ and crotonaldehyde on 0.8 wt % K-Mg_5CeO_x obtained by extrapolating to zero conversion, and also the binomial distributions of ^{13}C-atoms assuming that n-butyraldehyde comes from ethanol only, from acetaldehyde only, or from both ethanol and acetaldehyde with equal probability using the initial reactant composition. These data (Figure 2.42, Table 2.20) suggest that n-butyraldehyde and acetone are formed from both reactants (ethanol and acetaldehyde) and not exclusively from one of them.

Table 2.20. ^{13}C-distribution of Products (mole fraction) in $^{13}C_2H_4O$-C_2H_5OH-H_2 reactions on 1.0 wt % $Cu_{0.5}Mg_5CeO_x$ and 0.8 wt %K-Mg_5CeO_x

Number of ^{13}C	Ethanol	Acetaldehyde	Both	Experimental	
				1.0 wt % $Cu_{0.5}Mg_5CeO_x$	0.8 wt %K-Mg_5CeO_x
0	1.00	0	0.08	0.07	0.02
1	0	0	0	0	0
2	0	0	0.39	0.30	0.12
3	0	0	0	0	0
4	0	1.00	0.53	0.63	0.86

[523 K, 101.3 kPa total pressure, 2.9 kPa acetaldehyde pressure, 1.1 kPa ethanol pressure, 2.9 kPa hydrogen, balance He].

In contrast, the ^{13}C-content in crotonaldehyde formed in absence of Cu on 0.8 wt % K-Mg_5CeO_x at relatively low contact times (Table 2.20) shows that this condensation product is produced predominantly from acetaldehyde. It is known that ethanol adsorbed dissociatively on MgO to form surface ethoxide and hydrogen species (65, 66). In the absence of Cu, which provides the H-H recombination function, surface ethoxide and hydrogen recombine preferably and desorb as ethanol, instead of that ethoxide species remain on the surface, losing a β-H giving surface aldehydic species, and reacting with other surface species to form aldol condensation products as was proposed before (Section 2.2.3). Some of the H-atoms are used to hydrogenate the adsorbed aldehydic species, from acetaldehyde gas-phase, which leave the surface as labeled ethanol (Figure 2.43). In this situation is more likely that two adsorbed acetaldehyde molecules react each other leading to labeled aldol intermediates. It is important to pointed out that the ^{13}C-content in products is higher than in reactants at longer contact time (Figure 2.39). These results are consistent with the formation of surface intermediates that remain on the surface for a while and then decompose and/or desorb later to give the observed products.

Isotopic tracer studies using $^{12}C_2H_5OH$-$^{13}C_2H_4O$ reactant mixtures suggest that condensation reaction can proceed via direct reactions of ethanol without the intermediate formation of gas phase acetaldehyde molecules (Figure 2.43). These results show that "dehydrogenation" and condensation reactions occur after binding of ethanol to the same type of active site, such as an acid-base site pair on MgO. This proposal is consistent with i) the promoting effect of Cu on condensation rates (Table 2.15), and ii) the initial non-zero slopes of product turnovers formation observed in ethanol reactions (Figure 2.28).

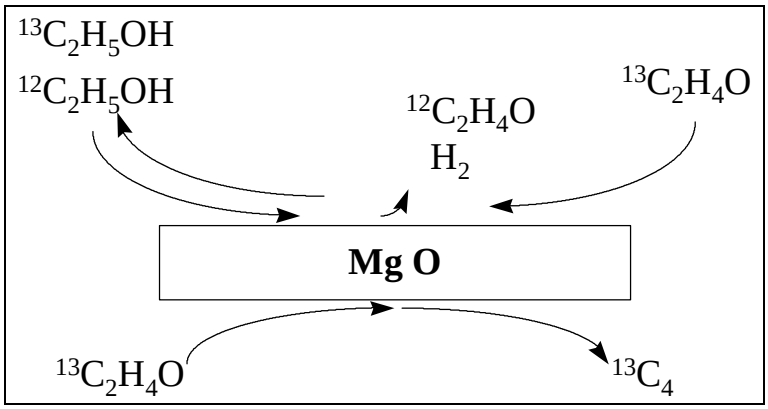

Figure 2.43. Competitive reactions of $^{13}C_2H_4O$-C_2H_5OH-H_2 mixtures.

2.3.6. C_2H_5OH/D_2 and C_2H_4O/D_2 Reactions on Copper Catalysts supported on MgO

2.3.6.a. C_2H_5OH/D_2 Reactions

Reactions of C_2H_5OH/D_2 mixtures were carried out in a gradientless recirculating batch reactor in order to probe the recombinative hydrogen disposal step during ethanol coupling reactions. Catalyst samples (20.0 mg) were treated in H_2 (10% H_2/He, 175 cm^3/min, 5 K/min) at 623 K for 0.5 h. The temperature was then decreased to 573 K and the reactant mixture was introduced along with a small amount of methane, as an internal standard (reaction mixture: $C_2H_5OH/CH_4/D_2/He$ = 3.6/2.4/27.0/68.3 kPa; C_2H_5OH: Fisher Scientific, A.C.S. certified; CH_4: Matheson, ultra high purity; D_2: C.P. Matheson). Products were sampled by syringe extraction from the recirculating stream at different contact times and analyzed as described previously. The deuterium content in reactants and products was measured by mass spectrometry.

As discussed previously, ethanol reactions on K-$Cu_yMg_5CeO_x$ lead to acetaldehyde, acetone, and n-butyraldehyde as predominant products. It was proposed that acetaldehyde and ethanol condensation reactions may occur on basic sites, but condensation rates also increase with increasing density of Cu surface atoms (Table 2.15). Hydrogen abstraction steps (involved in condensation reactions) appear be limited by the rate of hydrogen removal via recombinative desorption. The desorption process occurs rapidly on Cu surface atoms, but it is slow on metal-free MgO or $MgCeO_x$. Hydrogen migration and associative desorption on Cu sites would increase the rate of aldol condensation reaction by removing a surface bottleneck that tends to reverse the steps that form the initial unsaturated aldol-type species required for chain growth.

In order to probe the reversibility of hydrogen adsorption-desorption pathways (Figure 2.44), ethanol reactions were carried out in the presence of deuterium (D_2). The recombinative hydrogen disposal steps can be quasi-equilibrated or irreversible during ethanol coupling reactions. Quasi-equilibrated desorption steps would result in the formation of reaction products and reactants containing a statistical mixture of D-atoms from D_2 and H-atoms from ethanol. The deuterium content in reaction products, therefore, measures the rate of communication between the surface and gas phase hydrogen pools. In contrast, irreversible recombinative desorption step would lead to reaction products containing predominantly protium, because the slow communication between the gas phase (D_2) and surface hydrogen pools, leads to the predominant presence of protium atoms from C-H activation steps on the catalyst surface and to their selective use in hydrogen addition desorption steps of unsaturated intermediates.

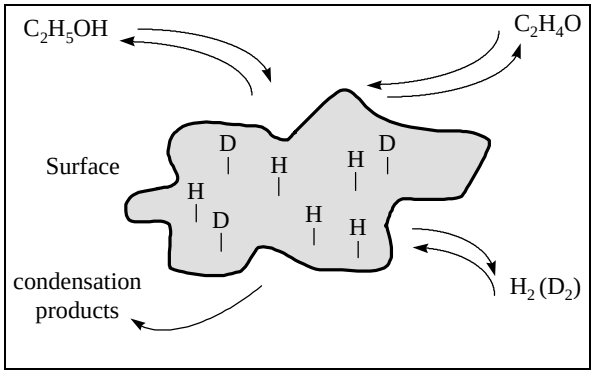

Figure 2.44. Ethanol reactions and hydrogen removal step.

The role of Cu sites in ethanol reactions was examined by measuring the initial rates of exchange and the deuterium distributions in the reactants and products. The deuterium content in reactants and products as a function of contact time on several samples is shown in Figure 2.45. The initial rates of incorporation of deuterium into ethanol, acetaldehyde, and acetone as a function of Cu surface area were calculated from the initial slopes in Figure 2.45 and the results on K-$Cu_yMg_5CeO_x$ (y = 0, 0.5, 7.5) catalysts are summarized in Table 2.21. The distribution of deuterium in unreacted ethanol, acetaldehyde, and acetone products of ethanol/D_2 mixtures at different contact times are shown in Figure 2.46.

Table 2.21. Ethanol/Deuterium reactions. Effect of Cu surface area on the initial rates of incorporation of deuterium into ethanol unreacted and products.

Catalyst	Cu Surface Area (m^2/g_{cat})	Ethanol		Acetaldehyde		Acetone	
		$^a\mathbf{r_D}$	$^b\mathbf{r_t}$	$^a\mathbf{r_D}$	$^b\mathbf{r_t}$	$^a\mathbf{r_D}$	$^b\mathbf{r_t}$
Mg_5CeO_x	0	5.4	78.2	1.4	57.9	0.02	0.38
$Cu_{0.5}Mg_5CeO_x$	10.4	150	514	200	469	6.7	5.6
$Cu_{7.5}Mg_5CeO_x$	21.9	930	683	601	585	78	27

$^a r_D$ is the rate of deuterium incorporation in unreacted ethanol and x 10^7, in mol D_2 / g-cat · s.
$^b r_t$ is the rate of ethanol consumption or product formation x 10^7, in mol / g-cat · s.\

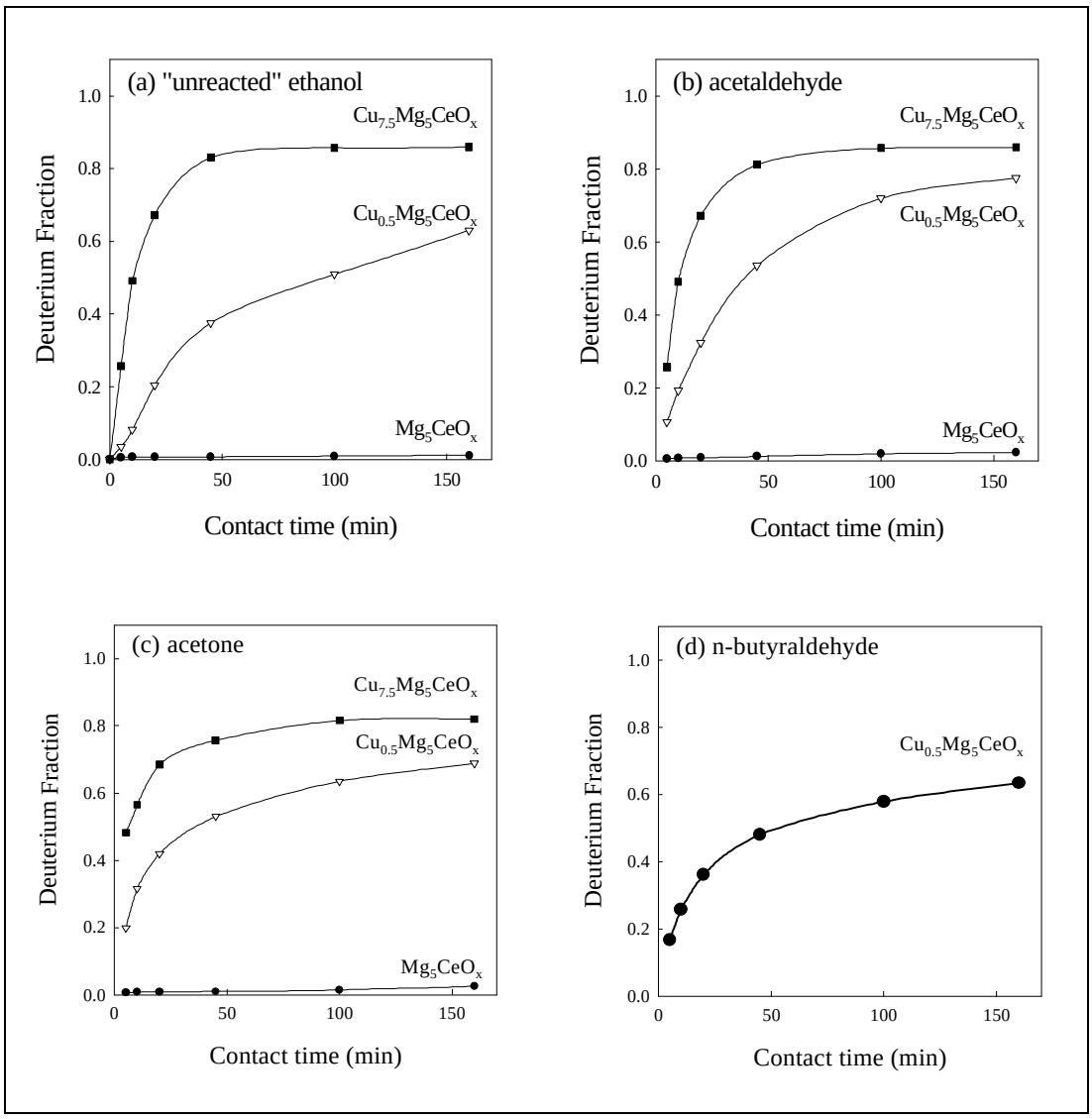

Figure 2.45. Deuterium fraction in unreacted ethanol (a) and in acetaldehyde (b), acetone (c) , and n-butyraldehyde (d) formed from ethanol/D_2 mixtures (~20 %H, ~80 %D) on K-$Cu_yMg_5CeO_x$ catalysts. [573 K, 101.3 kPa total pressure, 3.6 kPa ethanol pressure, 27 kPa D_2 pressure, balance He].

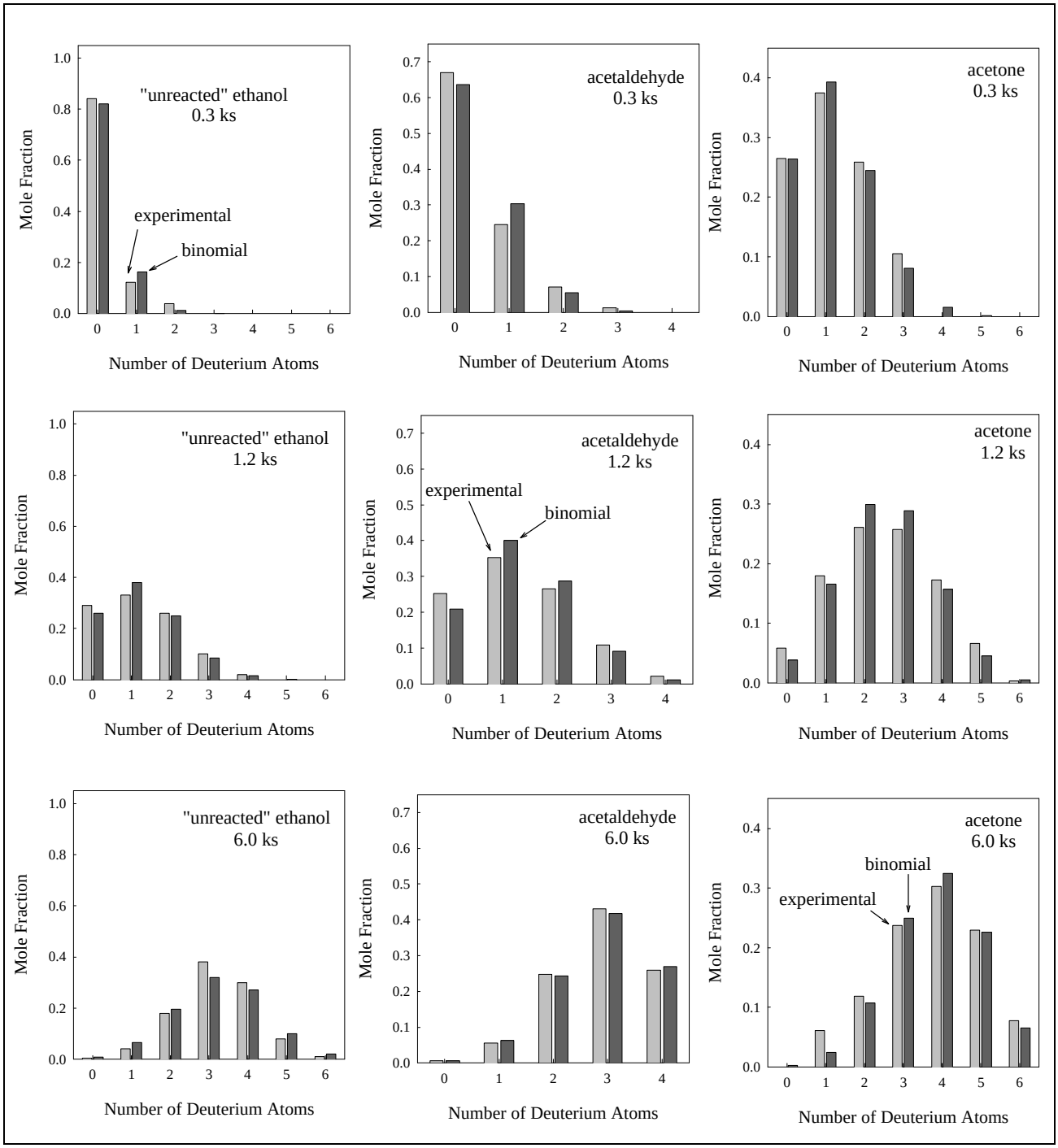

Figure 2.46. Reactions of C_2H_5OH/D_2 mixtures on 1.0 wt % K-$Cu_{0.5}Mg_5CeO_x$ catalyst. Deuterium distributions in unreacted ethanol and acetaldehyde and acetone products. [573 K, 101.3 kPa total pressure, 3.6 kPa ethanol pressure, 27 kPa D_2 pressure, balance He].

The rate of appearance of deuterium in unreacted ethanol and in reaction products (Figure 2.45 and Table 2.21) increases with increasing Cu content in $Cu_yMg_5CeO_x$ catalysts. The deuterium fraction is much lower on Mg_5CeO_x than on Cu-containing catalysts, suggesting that Cu sites increase the rates of communication between surface and gas phase hydrogen pools by providing a site for H_2 removal from the basic sites. Rate-limiting recombinative H_2 desorption steps become increasingly reversible as Cu sites increases.

At short contact times (Figure 2.46), gas phase molecules and any adsorbed species in equilibrium with them show relatively low deuterium contents and singly deuterated species are the most abundant, suggesting that gas phase D_2 contributes weakly to the surface hydrogen pool. This surface hydrogen pool contains predominantly H-atoms formed by ethanol dehydrogenation. The deuterium content in reactants and products increases with increasing contact time. All deuterium distributions are binomial, suggesting that every C-H (and O-H) bond is broken and reformed several times during the formation of one product molecule (in this case the formed molecule remains adsorbed on the surface) or that formed molecules visit the surface many times acquiring deuterium from the surface H-D pool. The latter is consistent with the increase in deuterium content with contact time. At relative high contact time, the surface contain higher amounts of deuterium than protium species, and product molecules sample the composition of surface H-D pool (Figure 2.45), which is near to H/D equilibrium composition for each experiment.

Initial rates of ethanol dehydrogenation and of deuterium incorporation into ethanol (in ethanol/D_2 mixtures) on K-$Cu_yMg_5CeO_x$ catalysts are shown in Figure 2.47 as a function of Cu surface area. The initial rate of ethanol dehydrogenation increases linearly with the Cu surface area (measured by N_2O decomposition methods), therefore, dehydrogenation turnover rates are not affected by Cu crystallite size. At similar steady-state acetaldehyde concentrations, condensation rates to form acetone and n-butyraldehyde increase markedly with increasing Cu surface area in $Cu_yMg_5CeO_x$ catalysts (Figure 2.47), even though basic site densities measured by CO_2 isotopic switch methods are very similar among these catalysts. Therefore, Cu metal sites participate in rate-determining steps required for condensation reactions. If hydrogen removal is rate-determining in ethanol dehydrogenation and condensation reaction, Cu may provide required site for the recombinative desorption of H-atoms formed in C-H bond activation reaction on MgO sites. The removal of H species from basic sites by Cu atoms freed the basic site for the next C-H bond activation. The increase of the rate of deuterium incorporation into unreacted ethanol with increasing Cu surface atoms is consistent with the removal of the surface bottleneck (the enhancement of hydrogen migration from basic sites to Cu sites and recombinative desorption on Cu) that tends to reverse the step that forms the unsaturated aldol-type species required for chain growth. As more Cu sites are introduced the surface becomes less H-rich and that favors α-H abstraction surface steps.

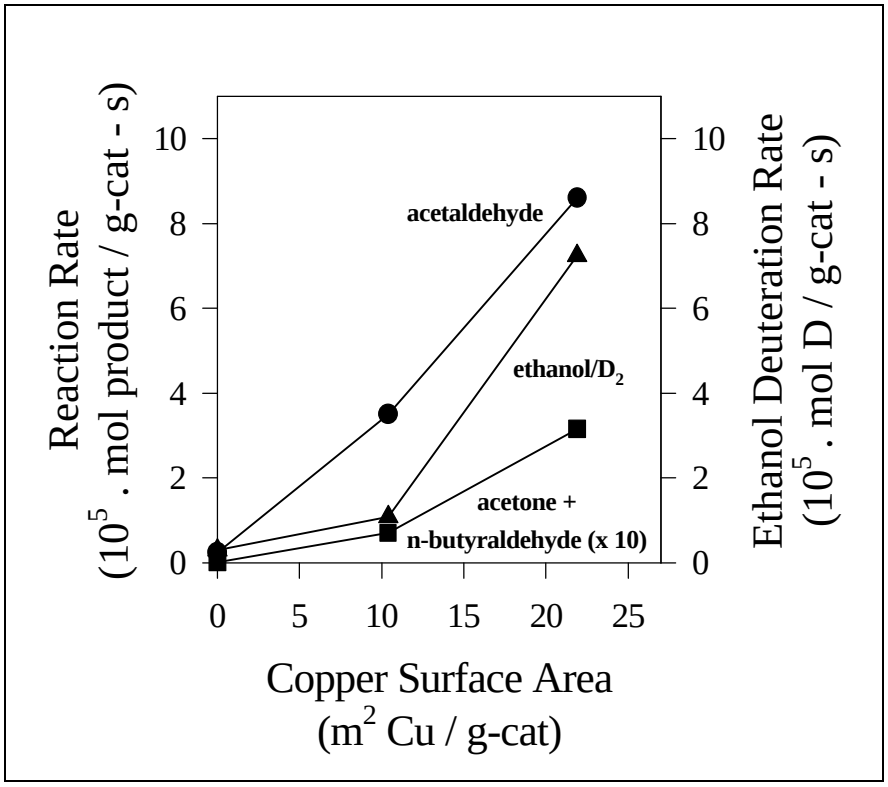

Figure 2.47. Initial rates of ethanol dehydrogenation and condensation reactions and of incorporation of deuterium into ethanol (in ethanol/D_2 mixtures) as a function of Cu surface area on K-Cu_yMg_5CeOx catalysts. [573 K, 101.3 kPa total pressure, 3.7 kPa ethanol (27 kPa D_2), balance He].

2.3.6.b. Reactions of C_2H_4O/D_2 Mixtures

Acetaldehyde condensation reaction occurs on basic sites and its rate increases with increasing density of Cu surface atoms. C-H bond activation steps on basic sites are limited by the rate of hydrogen removal. Migration and recombinative desorption can increase aldol condensation rates by removing a surface bottleneck that tends to reverse the steps that form the unsaturated aldol-type species required for chain growth. Acetaldehyde condensation reactions were carried out on $K\text{-}Cu_yMg_5CeO_x$ in the presence of gas phase D_2, in order to probe the reversibility of hydrogen adsorption-desorption pathways.

Recombinative hydrogen disposal steps can be quasi-equilibrated or irreversible. Quasi-equilibriated desorption steps would result in formation of reaction products and reactants containing a statistical mixture of D-atoms from D_2 and H-atoms from acetaldehyde. The deuterium content in unreacted acetaldehyde and in reaction products reflects the extent of communication between the surface and gas phase hydrogen pools. In contrast, irreversible recombinative desorption steps would lead to unreacted acetaldehyde and reaction products containing predominantly the protium atoms formed in C-H activation steps (Figure 2.48).

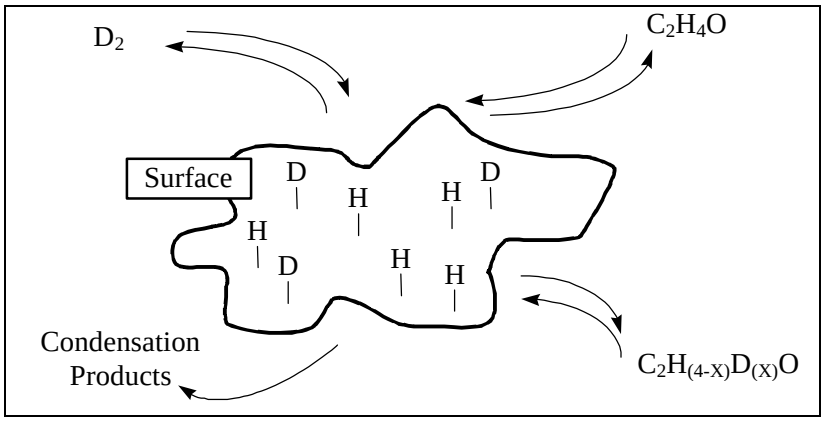

Figure 2.48. Acetaldehyde reaction and hydrogen removal steps.

The time evolution of the deuterium content in unreacted acetaldehyde, ethanol, acetone, and n-butyraldehyde products of C_2H_4O/D_2 reaction mixtures is shown in Figure 2.49 as a function of contact time, and the distribution of deuterium atoms at three different contact times are shown in Figure 2.50. The initial rates of incorporation of deuterium into acetaldehyde, ethanol, acetone, and n-butyraldehyde as a function of Cu surface area were calculated from the initial slopes in Figure 2.49 and they are summarized in Table 2.22.

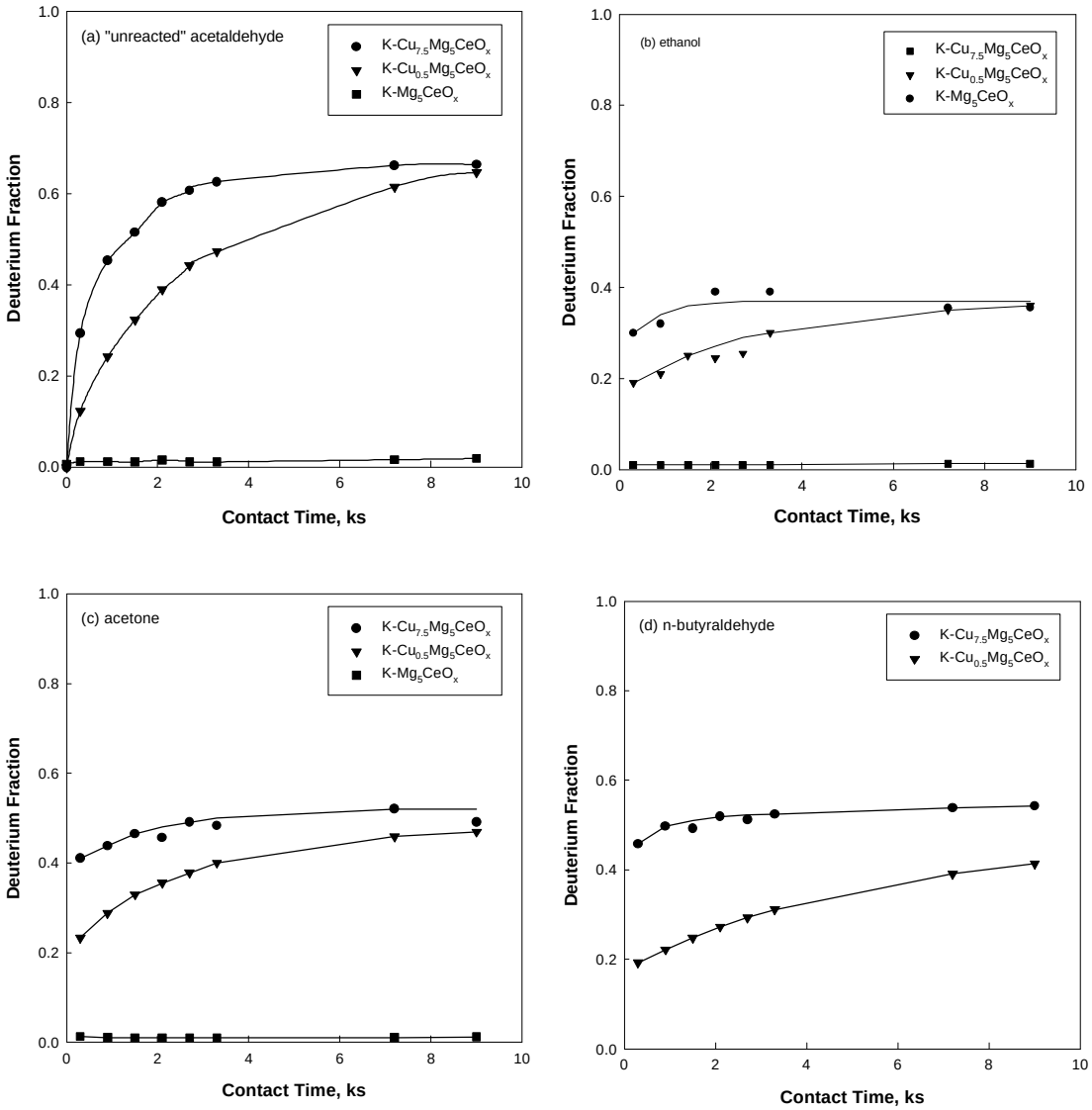

Figure 2.49. Reactions of C_2H_4O/D_2 mixtures on K-$Cu_yMg_5CeO_x$ catalyst. Deuterium fraction in (a) unreacted acetaldehyde, (b) ethanol, (c) acetone, and (d) n-butyraldehyde products as a function of contact time. [553 K, 101.3 kPa total pressure, 6.1 kPa acetaldehyde pressure, ca. 15 kPa D_2 pressure].

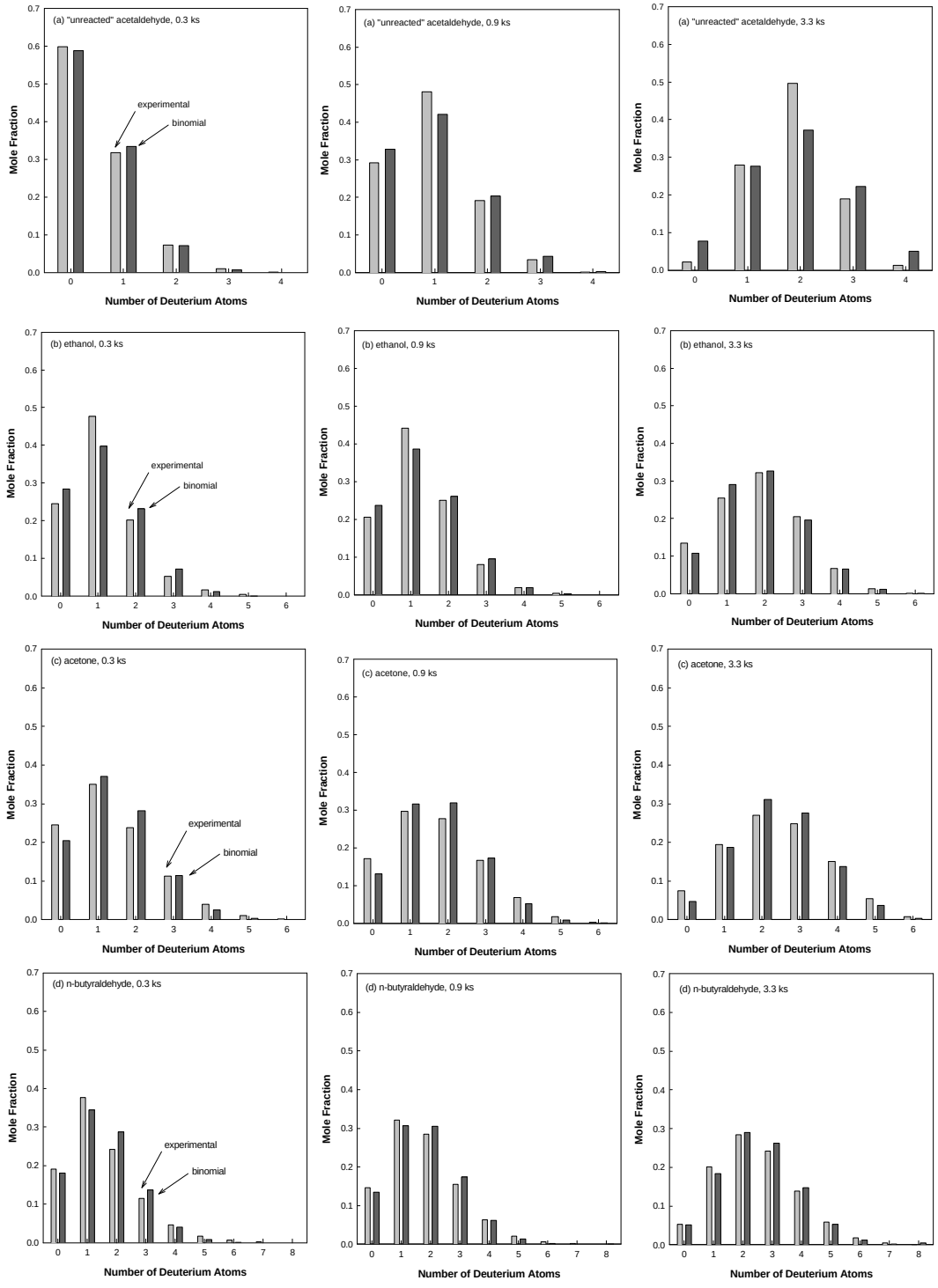

Figure 2.50. Reactions of C_2H_4O/D_2 mixtures on 1.0 wt % K-$Cu_{0.5}Mg_5CeO_x$ catalyst. Deuterium distributions in (a) unreacted acetaldehyde, (b) ethanol, (c) acetone, and (d) n-butyraldehyde products at various contact times (0.3 ks, 0.9 ks, 3.3 ks). [553 K, 101.3 kPa total pressure, 6.1 kPa acetaldehyde pressure, 16 kPa D_2 pressure].

Table 2.22. Reactions of C_2H_4O/D_2 mixtures. Effect of Cu surface area on the initial rates of incorporation of deuterium into unreacted acetaldehyde and products

Catalyst	Acetaldehyde		Ethanol		Acetone		n-Butyraldehyde	
	r_d [a]	r_t [b]	r_d	r_t	r_d	r_t	r_d	r_t
K- Mg_5CeO_x	9.1	12	0.05	5.9	0.007	0.52	0.09[c]	5.4[c]
K-$Cu_{0.5}Mg_5CeO_x$	86	35	4.0	21	0.5	2.1	0.4	2.1
K-$Cu_{7.5}Mg_5CeO_x$	349	438	101	333	14	34	2.1	4.5

[a] Rate of deuterium incorporation in unreacted acetaldehyde and products x 10^9, in mol D_2/Mg_5CeO_x·s.
[b] Rate of acetaldehyde consumption and products formation x 10^9, in mol D_2/Mg_5CeO_x·s.
[c] Rate of crotonaldehyde formation x 10^9, in mol D_2/Mg_5CeO_x·s.

The incorporation rate of deuterium and the deuterium fraction in unreacted acetaldehyde and in reaction products increase with Cu content on K-$Cu_yMg_5CeO_x$ catalysts. These data suggest that Cu sites increase the rate of communication between surface and gas phase hydrogen pools by providing a site for dissociative D_2 chemisorption and for their recombinative desorption of H-atoms formed in C-H bond activation steps occuring on basic sites.

2.3.7. C_2H_4O/C_2D_4O reactions on copper catalysts supported on K-Mg_5CeO_x

Aldol condensation reactions of ethanol or acetaldehyde on modified MgCeOx catalyst with Cu and K are influenced by the presence of Cu sites. In this section, the roles of Cu in C-H bond activation and C-C chain growth steps, and in hydrogen disposal during aldol-type condensation of acetaldehyde are investigated.

Kinetics and isotopic tracer studies were carried out in the RRU at 101.3 kPa total pressure. Catalyst samples (~ 30 mg) were first reduced in H_2 (10 % H_2/He, 175 cm^3/min, 5 K/min) at 623 K for 0.5 h, and then the temperature was lowered to 553K. Undeuterated acetaldehyde (C_2H_4O, Fisher Scientific, Reagent Grade) and perdeuterated acetaldehyde (C_2D_4O, Isotec Inc., chemical purity > 99.0 %, isotopic purity > 99.0 %) were used as reactants.

The deuterium content in reactants and products was determined from mass spectrometric data using matrix techniques that correct for ion fragmentation and natural ^{13}C abundance. Reaction rates are reported as turnover rates, defined as the molecules of reactant converted to products per unit time and per unit surface area of $MgCeO_x$. The local slope of turnover-time plots gives the turnover rate for the formation of each product. The surface area of $MgCeO_x$ was estimated from the difference between the total surface area and the copper surface area.

The aldol-condensation reaction of acetaldehyde involves α-hydrogen abstraction step, C-C chain growth step, and removal step of hydrogen adatoms. The rates of C-H activation and C-C chain growth condensation can influence the total condensation rates if these steps are not quasi-equilibriated. Therefore, in order to prove the revesibility of C-H bond activation step and to examine the C-H bond activation rate and the C-C bond condensation rates during acetaldehyde reaction, cross-exchange reactions between undeuterated and perdeuterated acetaldehydes (C_2H_4O and C_2D_4O) were carried out on K-$Cu_yMg_5CeO_x$ catalysts at 553 K (Figure 2.51).

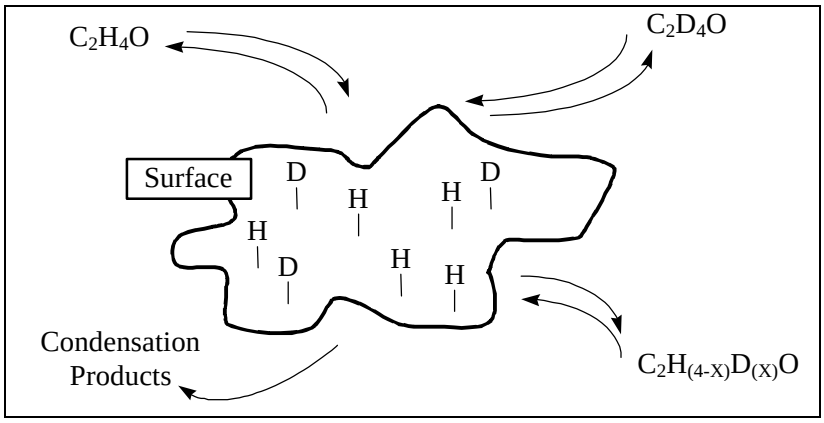

Figure 2.51. Acetaldehyde reaction and cross-exchange reaction of hydrogen and deuterium atoms.

If C-H bond activation steps are irreversible, cross-exchange reactions between H and D will occur and very slowly unreacted acetaldehydes would predominantly contain either protium or deuterium during acetaldehyde reactions. In contrast, quasi-equilibrated C-H activation steps would lead to rapid exchange and to the formation of unreacted acetaldehydes containing a statistical mixture of H-atoms and D-atoms. Therefore, the rate of C-H bond activation can be directly measured from the deuterium content in unreacted acetaldehyde.

Kinetic models

In order to analyze the data for the C-H bond activation rate measurements in C_2H_4O from C_2H_4O/C_2D_4O cross-exchange experiments, we consider the system to be a well-stirred batch reactor (because the bed height is about 2-3 particle diameters) with exchange occuring via stepwise exchange with a surface hydrogen (or deuterium) pool.

$$C_2H_4O + D^* \underset{k_{-1}}{\overset{4k_1}{\rightleftharpoons}} C_2H_3D_1O + H^*$$

$$C_2H_3D_1O + D^* \underset{2k_{-2}}{\overset{3k_2}{\rightleftharpoons}} C_2H_2D_2O + H^*$$

$$C_2H_2D_2O + D^* \underset{3k_{-3}}{\overset{2k_3}{\rightleftharpoons}} C_2H_1D_3O + H^*$$

$$C_2H_1D_3O + D^* \underset{4k_{-4}}{\overset{k_4}{\rightleftharpoons}} C_2D_4O + H^*$$

We note that the corresponding equations for the addition of H* to any $C_2H_{4-x}D_xO$ species are merely the microscopic reverse of those above.

The simplest kinetic model of the cross-exchange reaction neglects any kinetic isotope effects (KIE) either in the catalytic or mass spectrometric activation of C-H bonds. Then,

$$k_1 = k_2 = k_3 = k_4 = k_{-1} = k_{-2} = k_{-3} = k_{-4} = k$$

and the concentration of surface hydrogen (H*) and deuterium (D*) atoms depends only on the initial concentration of C_2H_4O and C_2D_4O:

$$\left.\frac{[C_2D_4O]}{[C_2H_4O]}\right|_{t=0} = \frac{[D^*]}{[H^*]} = \beta \quad \text{and} \quad [H^*]+[D^*] = (1+\beta)[H^*] = [L]$$

where [L] is the total number of sites that contain adsorbed hydrogen during acetaldehyde condensation reaction.

This problem can then be solved as an eigenvalue problem using matrix formalisms developed for networks of first order reaction:

$$\frac{d}{dt}\overline{C(t)} = \overline{\overline{A}}\,\overline{C(t)}$$

where

$$\overline{C(t)} = \begin{bmatrix} C_0(t) \\ C_1(t) \\ C_2(t) \\ C_3(t) \\ C_4(t) \end{bmatrix}$$

Subscripts are the number of deuterium atoms in each acetaldehyde isotopomer, *i.e.*, $C_0(t) = C_2H_4O$, $C_1(t) = C_2H_3DO$, $C_2(t) = C_2H_2D_2O$, $C_3(t) = C_2HD_3O$, and $C_4(t) = C_2D_4O$, and $\overline{\overline{A}}$ is the matrix (5 x 5) of rate coefficients:

$$\overline{\overline{A}} = \begin{bmatrix} -4k_1[D^*] & k_{-1}[H^*] & 0 & 0 & 0 \\ 4k_1[D^*] & -(k_{-1}[H^*]+3k_2[D^*]) & 2k_{-2}[H^*] & 0 & 0 \\ 0 & 3k_2[D^*] & -2(k_{-2}[H^*]+k_3[D^*]) & 3k_{-3}[H^*] & 0 \\ 0 & 0 & 2k_3[D^*] & -(3k_{-3}[H^*]+k_4[D^*]) & 4k_{-4}[H^*] \\ 0 & 0 & 0 & k_4[D^*] & -4k_{-4}[H^*] \end{bmatrix}$$

In the absence of KIE, this matrix reduces to:

$$\overline{\overline{A}} = k_{exch} \begin{bmatrix} -4\beta & 1 & 0 & 0 & 0 \\ 4\beta & -(1+3\beta) & 2 & 0 & 0 \\ 0 & 3\beta & -2(1+\beta) & 3 & 0 \\ 0 & 0 & 2\beta & -(3+\beta) & 4 \\ 0 & 0 & 0 & \beta & -4 \end{bmatrix}$$

where k_{exch} is an effective rate constant of the cross-exchange reaction:

$$k_{exch} = \frac{k\,[L]}{1+\beta}$$

This problem is then solved with the initial conditions, $C_0(t)$ and $C_4(t)$ at t = 0.

Solutions to the corresponding problems with KIE are not possible if the KIE depend on the composition and location of H-atoms not involved in the C-H bond activation step. When KIE depend only on the isotopic composition of the activated C-H bond, the rate constants become

$$k_1 = k_2 = k_3 = k_4 = k_+$$
$$k_{-1} = k_{-2} = k_{-3} = k_{-4} = k_-$$

and $[D^*] \neq \beta\,[H^*]$.

A pseudo-steady state analysis of H* and D* shows that then

$$[D^*] = \frac{k_-}{k_+}\beta\,[H^*],$$

and the corresponding matrix for rate coefficients becomes

$$\overline{\overline{A}} = k_-\,[H^*]\begin{bmatrix} -4\beta & 1 & 0 & 0 & 0 \\ 4\beta & -(1+3\beta) & 2 & 0 & 0 \\ 0 & 3\beta & -2(1+\beta) & 3 & 0 \\ 0 & 0 & 2\beta & -(3+\beta) & 4 \\ 0 & 0 & 0 & \beta & -4 \end{bmatrix}$$

with $[D^*] + [H^*] = [L]$ and so $[H^*] = \dfrac{[L]}{\left(1+\beta\dfrac{k_-}{k_+}\right)}$,

which can be simplified to $[H^*] = \dfrac{[L]}{(1+\beta)}$ for $k+ = k-$.

From these,

$$\overline{\overline{A}} = k_{exch}\begin{bmatrix} -4\beta & 1 & 0 & 0 & 0 \\ 4\beta & -(1+3\beta) & 2 & 0 & 0 \\ 0 & 3\beta & -2(1+\beta) & 3 & 0 \\ 0 & 0 & 2\beta & -(3+\beta) & 4 \\ 0 & 0 & 0 & \beta & -4 \end{bmatrix}$$

where

$$k'_{exch} = \frac{k_-\,[L]}{\left(1+\beta\dfrac{k_-}{k_+}\right)}$$

The general solution for both cases, with k_{exch} or k'_{exch} is given by

$$C_i(t) = A e^{\lambda_1 a t} + B e^{\lambda_2 a t} + C e^{\lambda_3 a t} + D e^{\lambda_4 a t} + E e^{\lambda_5 a t}$$

where A, B, C, D, and E are constants and λ_ι are eigenvalues of the matrix $\overline{\overline{B}}$. Also, in the absence of KIE,

$$\alpha = k_{exch} = \frac{k\,[L]}{1+\beta}$$

and, in the presence of KIE,

$$\alpha = k'_{exch} = \frac{k_{-}[L]}{\left(1+\beta\frac{k_{-}}{k_{+}}\right)}$$

The value of α in the absence of KIE is a lower limit for the exchange rate constant, because $k_{-}/k_{+} < 1$ for a normal KIE. The value of α can be obtained by non-linear regression using the experimental cross-exchange reaction data and the general solution of the kinetic model described above.

Therefore the problem with a KIE is identical to the one without a KIE within a multiplicative factor of:

$$\frac{k}{k'_{exch}} = \frac{1+\beta}{1+\beta\frac{k_{-}}{k_{+}}},$$

which affects only the value of the rate constant calculated from the analysis of isotopomer distribution but not the mathematical structure of the equations. The corresponding problem with secondary isotope effects

$$k_1 \neq k_2 \neq k_3 \neq k_4$$
$$k_{-1} \neq k_{-2} \neq k_{-3} \neq k_{-4}$$

contains too many adjustable constants and it is therefore of limited use.

Results and Discussions

The time evolution of the isotopomer distribution in unreacted acetaldehyde during reactions of C_2H_4O/C_2D_4O mixtures on K-Mg_5CeO_x catalyst is shown in Figure 2.52. Significant cross-exchange reaction between C_2H_4O and C_2D_4O on K-Mg_5CeO_x catalyst occurs even at low chemical conversion levels, suggesting that C-H activation is faster than acetaldehyde chemical conversion. The cross-exchange reaction occurs by stepwise transfer of single D or H-atoms, leading to statistical isotopomer distributions. Reaction products do not show a bimodal isotopic distribution consisting of mostly deuterated and mostly undeuterated acetaldehyde molecules, but show instead binomial deuterium distributions, consistent with statistical scrambling of the H and D atoms contributed by C_2H_4O and C_2D_4O reactants, respectively (Figure 2.53). These results confirm that a stepwise exchange reaction mechanism can be used to determine k_{exch} from the mathematical model described in this section.

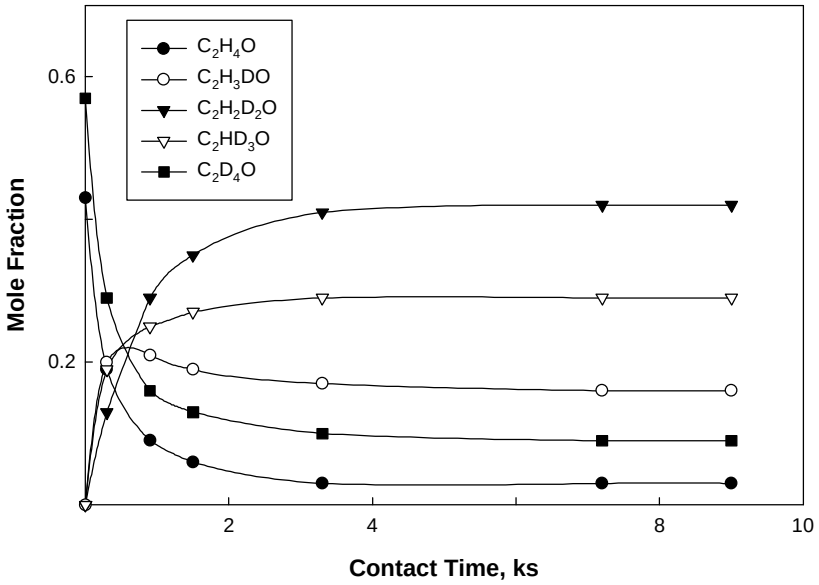

(a)

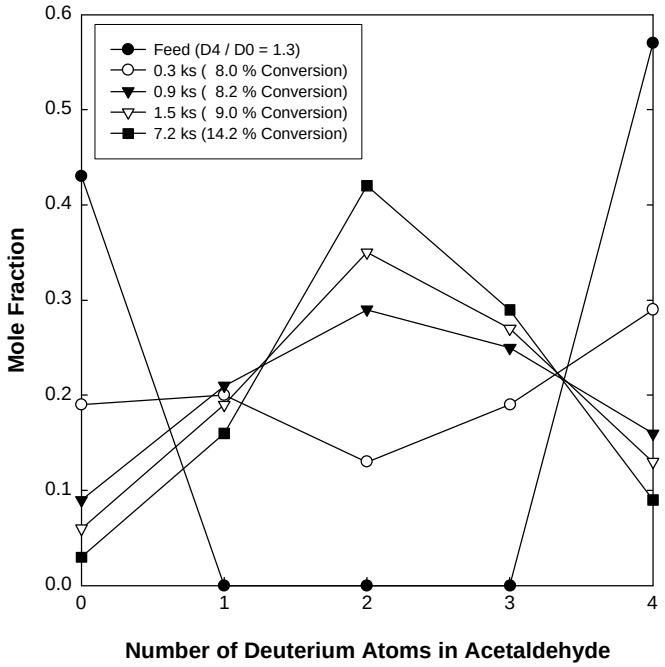

(b)

Figure 2.52. Cross-exchange reaction of C_2H_4O/C_2D_4O reactant mixture on K-Mg_5CeO_x: (a) Mole fraction of unreacted acetaldehyde as a function of contact time; (b) Deuterium distributions in unreacted acetaldehyde (contant times in ks, % acetaldehyde pool conversion within parentheses) [553 K, 6.4 kPa acetaldehyde, 3.0 kPa CH_4, balance He] .

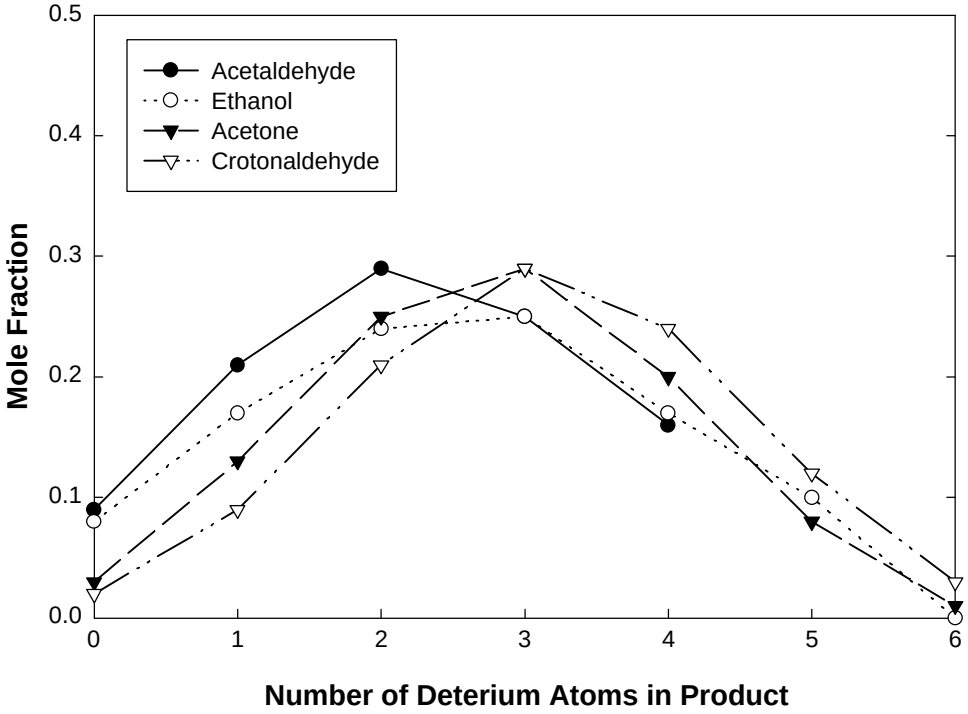

Figure 2.53. Cross-exchange reaction of C_2H_4O/C_2D_4O reactant mixture on K-Mg_5CeO_x: Deuterium distributions in reaction products (8.2 % acetaldehyde pool conversion, 0.9 ks contant time) [553 K, 6.4 kPa acetaldehyde, 3.0 kPa CH_4, balance He].

The deuterium content in the reaction products of C_2H_4O/C_2D_4O mixtures reflect the ratio of deuterium to hydrogen adsorbed on the catalyst surface (D*/H*) and therefore the relative rates of C-H bond activation and C-D bond activation, *i.e.*, the kinetic isotope effect for C-H bond activation. It can be evaluated from the deuterium content in reaction products and from the deuterium content in the unreacted C_2H_4O/C_2D_4O mixtures. Figure 2.54 shows the deuterium content normalized by the initial deuterium mole fraction in acetaldehyde reactants. The initial mole fraction of deuterium in ethanol, acetone, crotonaldehyde, n-butyraldehyde, and 2-pentanone were calculated from the initial slopes in Figure 2.54 and are summarized in Table 2.23. The isotopic composition of all cross-exchange reaction products except the deuterium content of ethanol produced on K-$Cu_{7.5}Mg_5CeO_x$ catalyst are less than the deuterium content in the initial reactant mixtures, suggesting a small H-D kinetic isotope effect in C-H bond activation steps (k_-/k_+ = 0.70-0.97) at these reaction conditions. Thus, the cross-exchange reaction constants predicted from α values by nonlinear regression are close to the real values, in view of this small KIE.

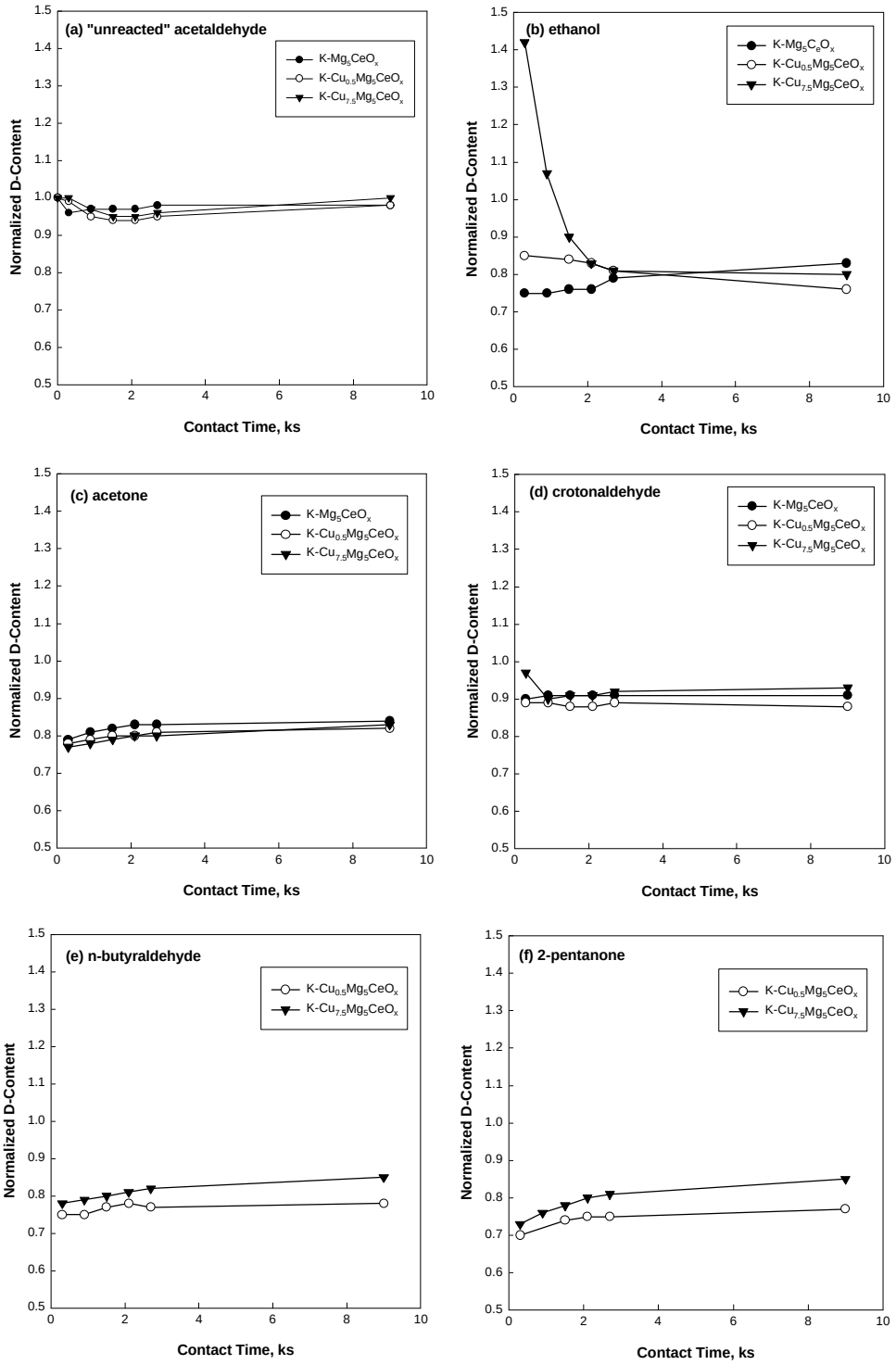

Figure 2.54. Deuterium content normalized by initial deuterium content in acetaldehyde for the cross-exchange reaction of C_2H_4O/C_2D_4O reactant mixture on K-$Cu_yMg_5CeO_x$: (a) unreacted acetaldehyde; (b) ethanol; (c) acetone; (d) crotonaldehyde; (e) n-butyraldehyde; (f) 2-pentanone [553 K, 6.4 kPa acetaldehyde, 3.0 kPa CH_4, balance He].

Table 2.23. Kinetic isotope effects from the cross-exchange reaction of C_2H_4O/C_2D_4O mixtures on K-$Cu_yMg_5CeO_x$

	K-Mg_5CeO_x		K-$Cu_{0.5}Mg_5CeO_x$		K-$Cu_{7.5}Mg_5CeO_x$	
	D content [a]	k_-/k_+ [b]	D content [a]	k_-/k_+ [b]	D content [a]	k_-/k_+ [b]
Acetaldehyde	0.57	-	0.58	-	0.60	-
EtOH	0.43	0.75	0.51	0.87	0.91	1.51
Acetone	0.45	0.78	0.45	0.77	0.46	0.76
Crotonaldehyde	0.52	0.90	0.52	0.89	0.58	0.97
n-Butyraldehyde	-	-	0.43	0.74	0.47	0.78
2-Pentanone	-	-	0.41	0.70	0.43	0.72

[a] Initial mole fraction of deuterium in reactants and products from C_2H_4O/C_2D_4O mixtures.
[b] The ratio of initial deuterium content in reaction products to that in initial unreacted reactant mixtures.
[553 K, 6.4 kPa acetaldehyde, 3.0 kPa CH_4, balance He].

Initial turnover rates of condensation and C-H bond activation are shown in Table 2.24 and the ratios of two rates are shown in Figure 2.55 as a function of Cu surface area. All rates are calculated from the slope in turnover vs. contact time plots at a contact time of 0.3 ks. C-H bond activation occurs much faster than C-C bond condensation reaction on K-$Cu_yMg_5CeO_x$ catalysts, suggesting that the C-H bond activation step is quasi-equilibrated and it does not limit the rate of the acetaldehyde conversion reaction to oxygenates. C-C bond condensation rate increase with the Cu content in K-Mg_5CeO_x catalysts. It implies that the Cu sites are involved in rate-determining steps required for acetaldehyde condensation reaction.

Table 2.24. Initial turnover rates of C-C condensation and C-H bond activation during the reactions of pure C_2H_4O and C_2H_4O/C_2D_4O mixture, respectively, on K-$Cu_yMg_5CeO_x$

Catalyst	Cu Surface Area (m^2/g-cat)	C-C condensation rate x 10^8 [a] (mol/m^2-basic oxide·s)	C-H bond activation rate x 10^8 [b] (mol/m^2-basic oxide·s)
K-Mg_5CeO_x	0	0.65	89.0
K-$Cu_{0.5}Mg_5CeO_x$	10.4	0.97	55.2
K-$Cu_{7.5}Mg_5CeO_x$	21.9	2.30	49.8

[a] Rates obtained from the reactions of pure C_2H_4O [573K, 6.6 kPa acetaldehyde, balance He].
[b] Rates obtained from the reactions of C_2H_4O/C_2D_4O mixture [553K, 6.4 kPa acetaldehyde, balance He].

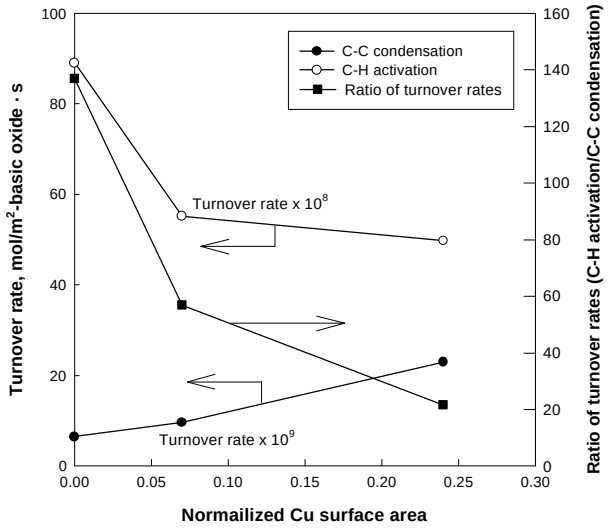

Figure 2.55. Initial rates of cross-exchange reaction of C_2H_4O/C_2D_4O mixture and C-C condensation reaction of pure C_2H_4O as a function of Cu surface area of K-$Cu_yMg_5CeO_x$ catalysts. [cross exchange reaction: 553K, 6.4 kPa acetaldehyde, balance He; acetaldehyde condensation reaction: 557K, 6.6 kPa acetaldehyde, balance He].

In Table 2.24 and Figure 2.55, the rate of C-H bond activation decrease with increasing Cu content in K-$Cu_yMg_5CeO_x$ catalysts. The same results were obtained by parameter estimation process for the stepwise cross-exchange reaction in the surface hydrogen (or deuterium) pool. In Table 2.25, The rate of C-H bond activation in K-Mg_5CeO_x catalyst is much higher than that of C-C bond condensation, suggesting that the rate of α-hydrogen abstraction on the surface of basic oxide is very fast. Hydrogen-deuterium scrambling (cross-exchange reaction) between C_2H_4O and C_2D_4O acetaldehyde occurs after α-hydrogen abstraction from acetaldehyde on the surface of basic oxide. The rate of cross-exchange reaction is related with the amount of hydrogen (or deuterium) on the surface of the basic oxide, *i.e.*, the concentration of hydrogen (or deuterium) on the surface of MgO_x after the α-hydrogen (or deuterium) abstraction. If hydrogen (or deuterium) atoms on the surface rapidly communicate with the gas phase by quasi-equilibrated adsorption-desorption steps, the rate of cross-exchange reaction between H and D in acetaldehyde decrease, even though the α-hydrogen abstraction step during the reaction of C_2H_4O/C_2D_4O mixture is very fast. In contrast, hydrogen (or deuterium) on the surface hydrogenate the adsorbed species on the surface or carry out the cross-exchange reaction.

Table 2.25. Effective rate constants for the cross-exchange reaction of C_2H_4O/C_2D_4O reactant mixture

Catalyst	Effective rate constant	
	x 10^4, k_{exch}, (1/s)	x 10^5, k_{exch}, (m^3/m^2-s) [a]
K-Mg_5CeO_x	6.1 ± 0.82	5.84
K-$Cu_{0.5}Mg_5CeO_x$	2.9 ± 0.59	3.11
K-$Cu_{7.5}Mg_5CeO_x$	1.4 ± 0.21	2.99

[a] Value multiplied by the ratio of reaction unit volume to basic oxide surface area. [553K, 6.4 kPa acetaldehyde, balance He].

2.3.8. Cross-Coupling Reactions of $^{13}CH_3OH/C_2H_4O$ and $^{13}CH_3OH/C_3H_6O$

Ethanol is a useful and simple probe molecule to test the role of individual components in metal-base bifunctional catalysts for isobutanol synthesis. Ethanol reactions, however, lead to acetone and n-butyraldehyde, which form only 2-propanol and 1-butanol by hydrogenation during CO/H_2 reactions. 2-Propanol and 1-butanol cannot, however, form isobutanol precursors (such as isobutyraldehyde and propionaldehyde) by condensation reactions during CO hydrogenation. ^{13}C-tracer studies of methanol-acetaldehyde or propionaldehyde cross-coupling reactions were carried out in order to examine reaction pathways leading to the formation of the C_3 and C_4 oxygenate precursors required for isobutanol formation.

Cross-coupling reactions of $^{13}CH_3OH$ (^{13}C: 99 %, ^{18}O: < 1 %; Icon Services Inc.) with acetaldehyde (Fisher Scientific, Reagent Grade) and propionaldehyde (Aldrich, 97%) were carried out using the following reactant mixture: $^{12}C_2H_4O(^{12}C_3H_6O)/$ $^{13}CH_3OH/CH_4/He$ = 7.3/4.0(4.0)/2.7/87.3 kPa. Reactions were conducted at 573 K and 101.3 kPa in the RRU. Mass spectrometry analysis after chromatographic separation was used to confirm the identity of each reaction product and to determine ^{13}C content, position, and distributions in reactants and products.

Cross-coupling site yields for $^{13}CH_3OH$-$^{12}C_2H_4O$ mixtures on K-$Cu_{0.5}Mg_5CeO_x$ are shown in Figure 2.56. The initial rates (site-time yields per total mole Cu) for methanol conversion were higher than that for the conversion of acetaldehyde to ethanol and to condensation products. Tables 2.26 and 2.27 show ^{13}C-distribution in products of $^{13}CH_3OH$-C_2H_4O reactions on K-$Cu_{0.5}Mg_5CeO_x$, K-$Cu_{7.5}Mg_5CeO_x$, and Cs-Cu/ZnO/ Al_2O_3. Although reaction pathways for ethanol formation from $^{13}CO/H_2/^{12}CH_3OH$ differ on these two catalysts (Section 3.7), reaction pathways for C_{2+} formation from $^{13}CH_3OH/^{12}C_2H_4O$ are similar on both catalysts.

The $^{13}CH_3OH$ component in the feed reacted predominantly to form ^{13}CO and H_2 (Tables 2.26 and 2.27); this reaction reverses methanol synthesis because of the unfavorable methanol synthesis thermodynamics at atmospheric pressures (but not during reactions CO hydrogenation at high pressures). The ethanol reaction product was predominantly unlabeled and it forms by hydrogenation of acetaldehyde using Cu sites and hydrogen produced by methanol decomposition. Propionaldehyde contains predominantly one ^{13}C atom, suggesting that it is formed by condensation of

acetaldehyde with reactive formyl or methoxy-type surface species or with gas phase formaldehyde derived from methanol. The analysis of the mass spectra pattern showed that the labeled carbon was either at the CH_3 or at the CHO fragment of propionaldehyde, suggesting that aldol condensation reactions occur with retention of either one of the two oxygen atoms in aldol-keto species as proposed by Nunan *et al.* [1], [40]. They used the term "oxygen retention reversal" to indicate the oxygen atom in formaldehyde remains in the final product, whereas the oxygen of the growing intermediate in the normal aldol condensation reaction remains in the final products. Both normal and oxygen retention reversal types of aldol condensation occur in our case. These types of reactions are caused by intraconversion of aldol (enol) and keto species via intramolecular H-transfer (Figure 2.57).

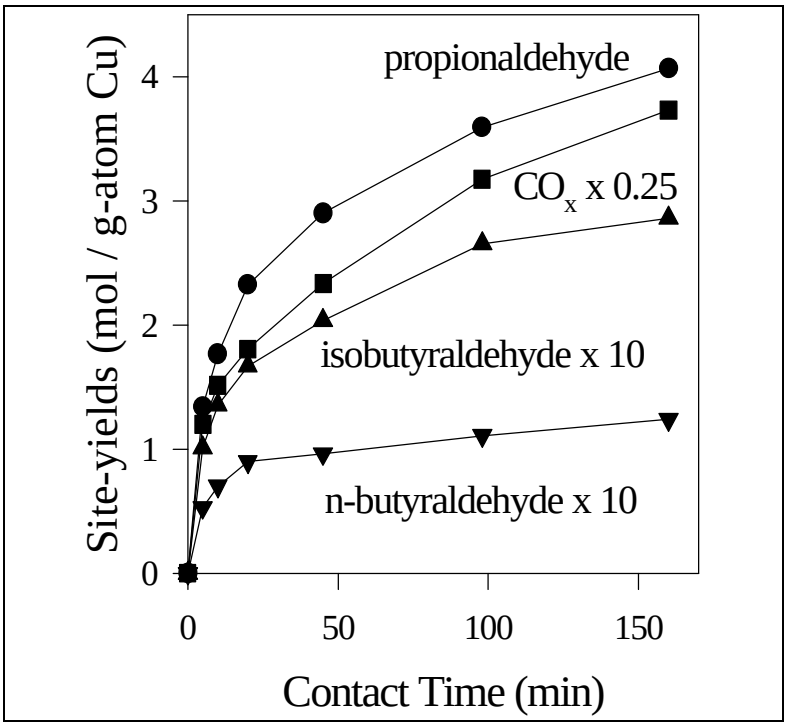

Figure 2.56. Methanol-acetaldehyde reactions. Site yields as a function of contact time on 1 wt % K-$Cu_{0.5}Mg_5CeO_x$. [573 K, 101.3 kPa total pressure, 8.0 kPa methanol, 4.0 kPa acetaldehyde, balance He].

Isobutyraldehyde contained predominantly two ^{13}C atoms, suggesting that it forms by condensation of propionaldehyde (with one ^{13}C) with a C_1 species formed from methanol. The CO_2 product of $^{13}CH_3OH$-$^{12}C_2H_4O$ mixtures on K-$Cu_yMg_5CeO_x$ and Cs-Cu/ZnO/Al_2O_3 was predominantly labeled and formed from the ^{13}CO (formed in methanol decomposition) via water-gas shift reactions. Acetone and n-butyraldehyde showed no significant ^{13}C-enrichment and they were formed exclusively via self-condensation reactions of acetaldehyde or ethanol, as also observed in reactions of pure ethanol (Figure 2.27). This also explains the presence of unlabeled CO_2. A small amount of labeled ethanol were detected among reaction products, suggesting that methanol coupling reactions, previously proposed as a route for C_1 to C_2 chain growth during

higher alcohol synthesis, do not readily occur at the low pressures on K-$Cu_yMg_5CeO_x$ catalysts. In contrast with high pressure CO hydrogenation conditions, our reaction conditions favor the decomposition of methanol and minimize its bimolecular chain-growth reactions.

These isotopic tracer studies are consistent with the sequence of steps shown in Figure 2.58. Reverse aldol condensation reactions of aldol and keto species (formed from $^{13}C_1$ aldehyde-type intermediate and acetaldehyde) form 1-^{13}C labeled acetaldehyde, which in turn lead to the observed propionaldehyde with 2-^{13}C atoms, isobutyraldehyde with 3-^{13}C atoms, and to the observed traces of labeled n-butyraldehyde.

Table. 2.26. ^{13}C-Distribution in products of $^{13}CH_3OH$-C_2H_4O reactions on 1.0 wt % K-$Cu_{0.5}Mg_5CeO_x$

	Number of Carbon-13				
	0 ^{13}C	1 ^{13}C	2 ^{13}C	3 ^{13}C	4 ^{13}C
Carbon dioxide	11.4	88.6	---	---	---
Acetaldehyde	99.4	0.6	0	---	---
Ethanol	100	0	0	---	---
Propionaldehyde	4.4	91.6	4.1	0	---
n-butyraldehyde	97.5	2.5	0	0	0
Isobutyraldehyde	0	10.1	70.3	20.6	0

[573 K, 101.3 kPa total pressure, 8.0 kPa methanol, 4.0 kPa acetaldehyde, balance He].

Table 2.27. ^{13}C-distribution in products of $^{13}CH_3OH$-C_2H_4O reactions on K-$Cu_yMg_5CeO_X$ and Cs-Cu/ZnO/Al_2O_3

Catalysts	K-$Cu_{7.5}Mg_5CeO_X$						Cs-Cu/ZnO/Al_2O_3					
Number of ^{13}C	0	1	2	3	4	%^{13}C	0	1	2	3	4	%^{13}C
Methanol	0.0	100	--	--	--	100	0.0	100	--	--	--	100
Acetaldehyde	99.1	0.9	0.0	--	--	0.5	99.3	0.7	0.0	--	--	0.4
CO_2	35.6	64.4	--	--	--	64	31.7	68.3	--	--	--	68
Ethanol	98.4	0.6	1.0	--	--	1.3	98.7	0.4	0.9	--	--	1.1
Propionaldehyde	16.8	73.4	9.8	0.0	--	31	6.7	82.6	10.7	0.0	--	35
i-Butyraldehyde	0.0	18.9	60.9	20.2	0.0	50	0.0	3.2	66.3	30.5	0.0	57
n-Butyraldehyde	83.5	16.5	0.0	0.0	0.0	4.1	82.0	18.0	0.0	0.0	0.0	4.5

[a] Values in parenthesis are %^{13}C in the products of $^{13}CH_3OH$-C_2H_4O reactions on K-$Cu_{7.5}Mg_5CeO_x$; [573 K, 101.3 kPa total pressure, 8.0 kPa methanol, 4.0 kPa acetaldehyde, balance He, 21 % Methanol conversion].

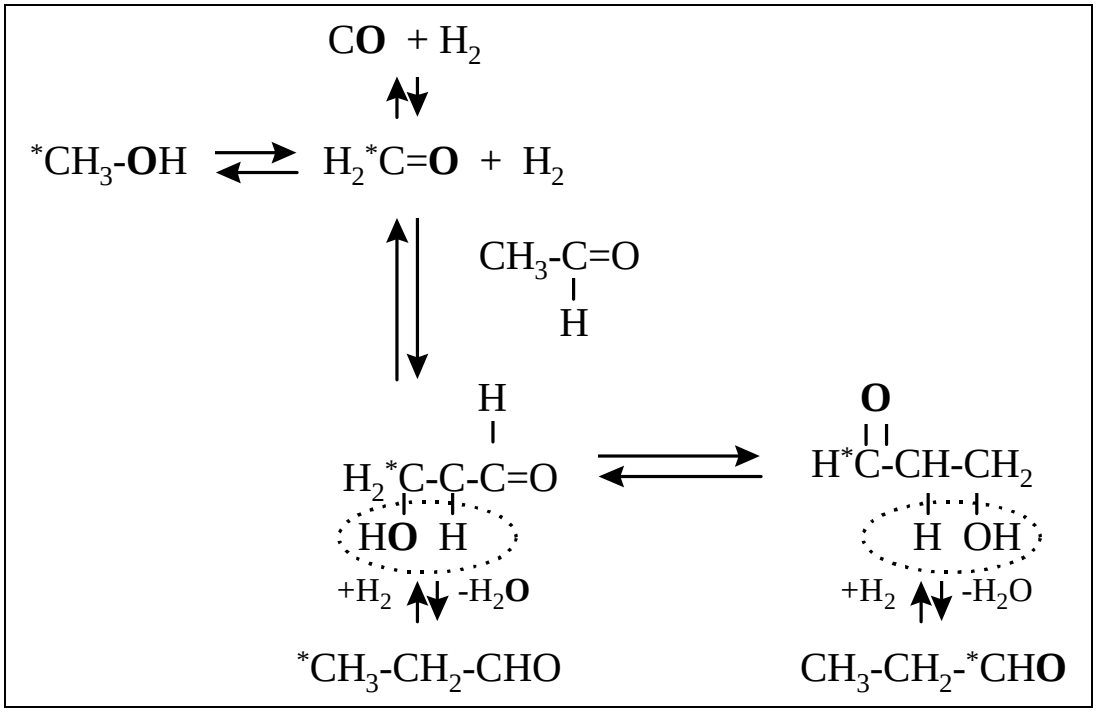

Figure 2.57. Reaction scheme of the interconversion of aldol and keto species.

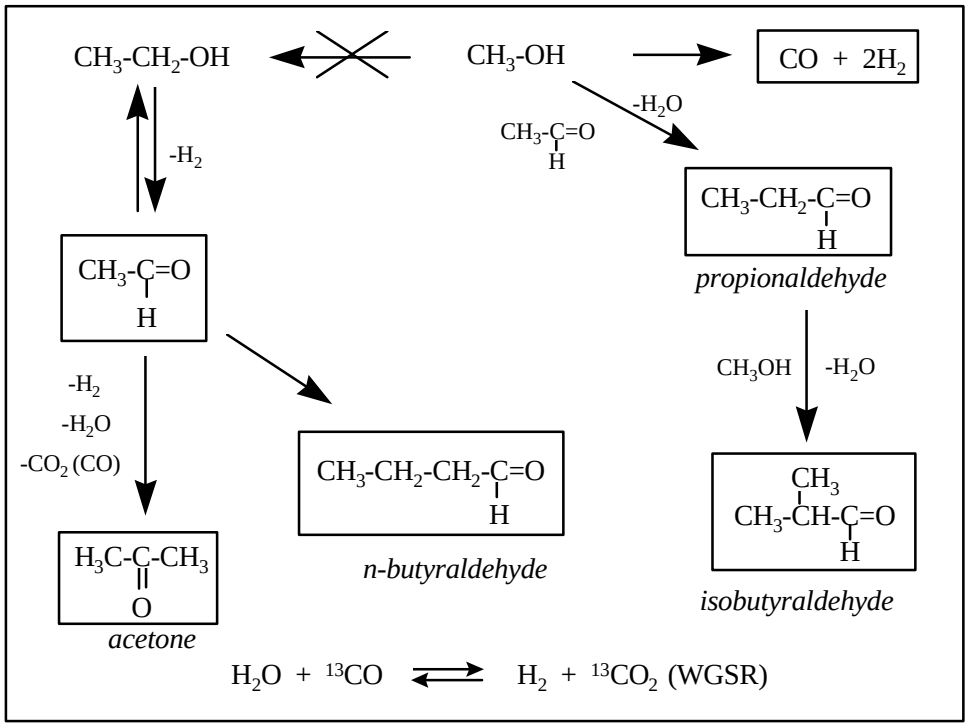

Figure 2.58. Reaction scheme for methanol-acetaldehyde reactions.

Additional studies of propionaldehyde-^{13}C-methanol coupling reactions confirm these isobutyraldehyde formation pathways. These studies also probe the reversibility of aldol formation and of dehydration-decarbonylation pathways. CO_x and H_2 (from methanol decomposition and water-gas shift reaction), isobutyraldehyde, 1-propanol and methyl propionate were the main reaction products. Other products included methyl formate, 3-pentanone (from propionaldehyde self-condensation followed by decarboxylation), and 2-methyl-pentaldehyde (from propionaldehyde self-condensation). 2,2-dimethyl butyraldehyde (from cross coupling of isobutyraldehyde with C_1 species) was not observed, indicating that isobutyraldehyde (precursor to isobutanol) is a preferred end-product of alcohol chain growth reactions. Neither ethanol nor acetaldehyde were detected, suggesting that coupling of methanol-derived C_1 species does not occur at our reaction conditions on K-$Cu_yMg_5CeO_x$ catalysts. Figure 2.59 shows a reaction scheme of propionaldehyde-^{13}C-methanol coupling reactions.

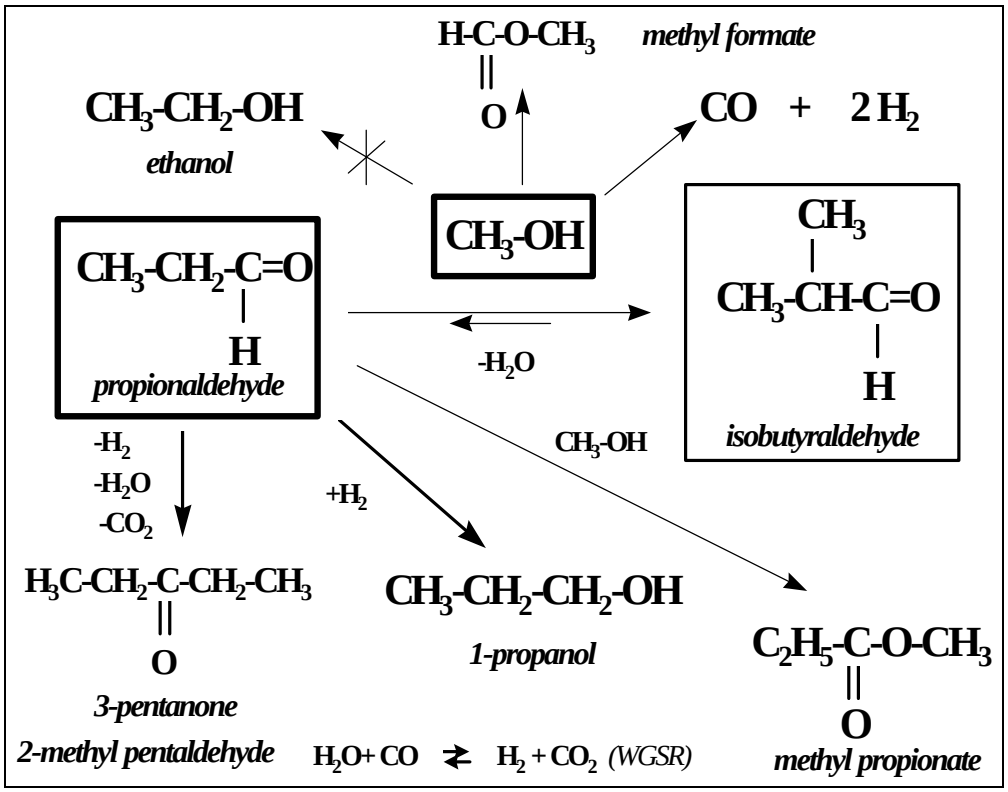

Figure 2.59. Reaction scheme for methanol-propionaldehyde reactions.

The results obtained from quantitative analysis of the isotopic content in propionaldehyde-^{13}C-methanol coupling reactions on K-$Cu_yMg_5CeO_x$ Cs-Cu/ZnO/Al_2O_3 and are shown in Table 2.28. CO_2 molecules were predominantly labeled and formed mainly from ^{13}CO via water-gas shift reaction. Unlabeled CO_2 was formed via decarboxylation reactions leading to 3-pentanone (Figure 2.59). Propionaldehyde acquired some ^{13}C during reaction. The increase in the ^{13}C content of propionaldehyde molecules as a function of contact time is consistent with the scheme shown in Figure 2.60. The proposed pathways includes: formation of surface aldol species (from

propionaldehyde and C_1 intermediates), keto-enol transformation (by intramolecular H-transfer), and reverse aldol condensation leading to propionaldehyde and C_1 species.

Isobutyraldehyde contains predominantly with one ^{13}C (Table 2.28), suggesting that it forms most frequently by cross coupling reactions between ^{13}C-labeled methanol-derived C_1 species and propionaldehyde. Isobutyraldehyde with two ^{13}C forms by aldol condensation reactions of labeled methanol ($^{13}C_1$ aldehyde-type intermediate) with singly-labeled propionaldehyde. Methyl propionate also has mainly one ^{13}C. Both carbon atoms of methyl formate were labeled, indicating that it is formed from two molecules of methanol.

Table 2.28. ^{13}C-Distribution in reactants and products of $^{13}CH_3OH$-C_3H_8O reactions on K-$Cu_yMg_5CeO_x$ and Cs-Cu/ZnO/Al_2O_3

Products	Catalysts	Number of Carbon-13				
		0	1	2	3	4
Propionaldehyde	K-$Cu_{0.5}Mg_5CeO_x$	97.7	2.3	0.0	0.0	
	K-$Cu_{7.5}Mg_5CeO_x$	94.9	5.1	0.0	0.0	
	Cs-Cu/ZnO/Al_2O_3	94.4	5.6	0.0	0.0	
Isobutyraldehyde	K-$Cu_{0.5}Mg_5CeO_x$	0.1	92.4	7.5	0.0	0.0
	K-$Cu_{7.5}Mg_5CeO_x$	5.4	68.6	26.0	0.0	0.0
	Cs-Cu/ZnO/Al_2O_3	4.6	56.4	39.0	0.0	0.0
Methyl propionate	K-$Cu_{0.5}Mg_5CeO_x$	9.3	85.3	5.4	0.0	0.0
	K-$Cu_{7.5}Mg_5CeO_x$	10.4	78.9	10.7	0.0	0.0
	Cs-Cu/ZnO/Al_2O_3	3.9	87.1	9.0	0.0	0.0

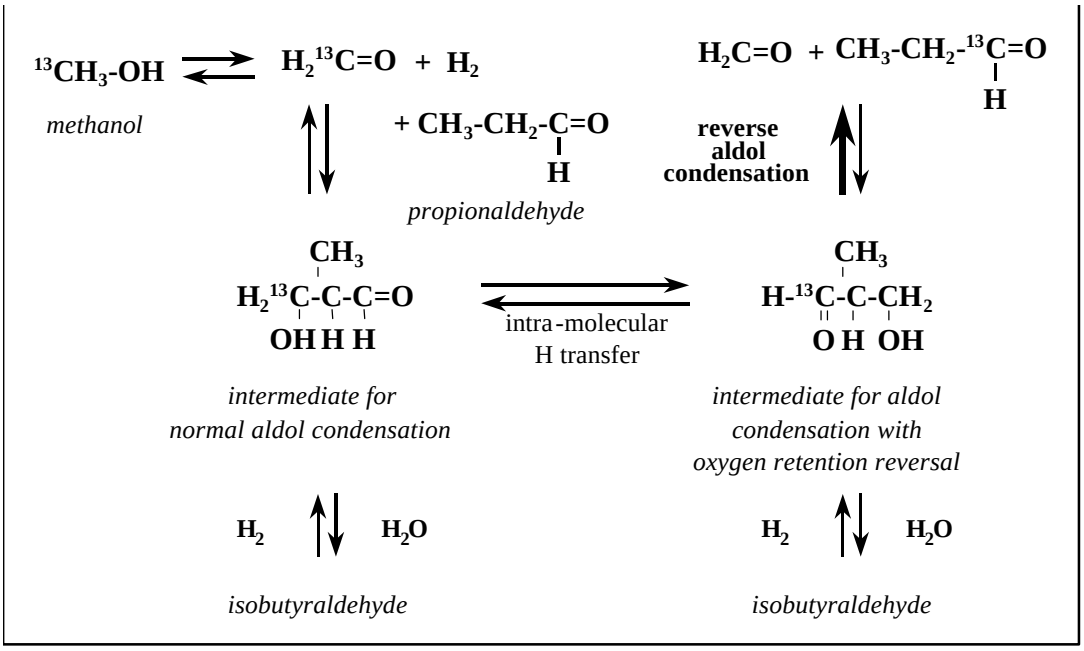

Figure 2.60. Reaction scheme of the labeled propionaldehyde production.

2.3.9. Methanol Reactions on Isobutanol Synthesis Catalysts and Their Individual Components

2.3.9.a. Methanol decomposition on K-$Cu_{0.5}MgCeO_x$ and MgO catalysts

CH_3OH reactions were carried out in order to explore chain growth pathways leading to higher alcohols on basic catalysts. In a typical experiment, the catalyst (18 mg) was charged into a gradientless batch reactor and reduced in 10 % H_2 (balance He) at 623 K for 30 min. In methanol decomposition reactions on K-$CuMgCeO_x$ and MgO catalysts, the feed gas composition was $CH_3OH/CH_4/He$ = 4.0/2.7/94.6. The reaction was carried out at 573 K and 101.3 kPa in the RRU.

Results of methanol decomposition reactions on K-$Cu_{0.5}Mg_5CeO_x$ and MgO can be summarized as follows:

a) CO and H_2 were the most abundant products on both catalysts. Methanol conversions as a function of contact time are shown in Figure 2.61a. Methanol turnovers (moles converted per gram of catalyst) as a function of contact time on both K-$Cu_{0.5}Mg_5CeO_x$) and MgO are shown in Figure 2.61b. The initial rate is higher on copper-containing catalysts (r_o = 7.6 x 10^{-5} mol / g_{cat}·s) than on pure MgO (r_o = 4.0 x 10^{-6} mol / g_{cat}·s).

b) In addition to CO and H_2, small amounts of methyl formate (formed from two methanol molecules) and CO_2 (Figure 2.62a) were produced. CO_2 can form via Boudouard reactions and/or methyl formate decomposition. It is unlikely that Boudouard reaction takes place at these reactions conditions. Aldol condensation of formaldehyde with acetaldehyde on various oxides supported on silica showed that the incorporation of CuO promotes the formation of CH_3OH and CO_2 [67]. These two products are believed to form from HCHO via the process showed in Figure 2.62. Also, it has been reported that the decomposition of formic acid to CO_2 and H_2 is very fast on basic oxides [68]. Methyl formate is an intermediate product that decomposes with increasing contact time. CO_2 can also be formed via methyl formate decomposition.

Methanol decomposition on Cu-based catalysts without using methane as internal standard was carried out in order to determined whether methane is produced from methanol under these conditions, thus corrupting conversion calculations using CH_4 as an inert internal standard. The amount of methane produced was low (< 0.5% selectivity) and it did not significantly corrupt methanol conversions reported here.

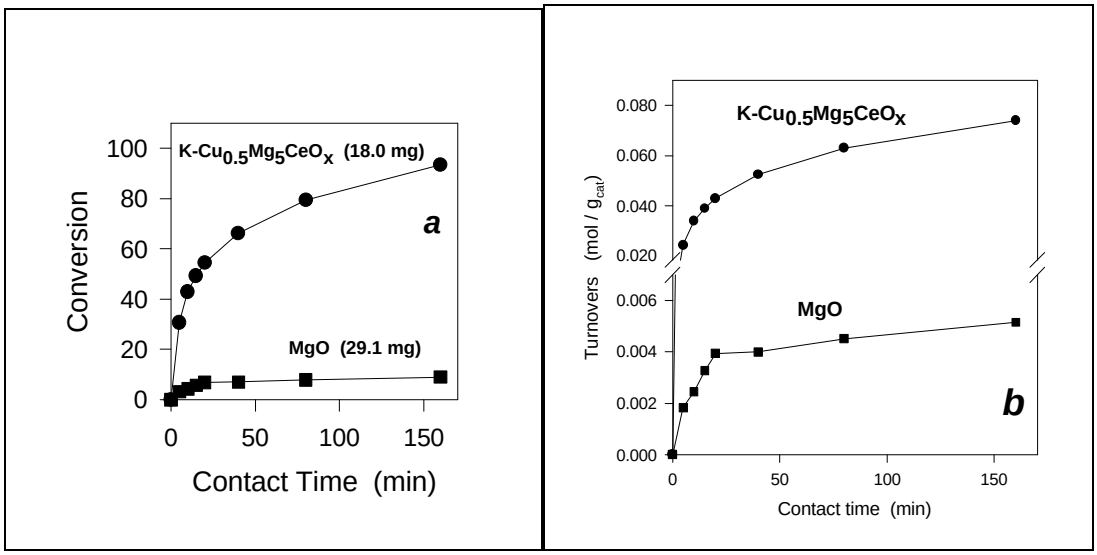

Figure 2.61. Methanol decomposition reaction on K-$Cu_{0.5}Mg_5CeO_x$ and MgO catalysts. (a) Methanol conversion. (b) Methanol turnovers.

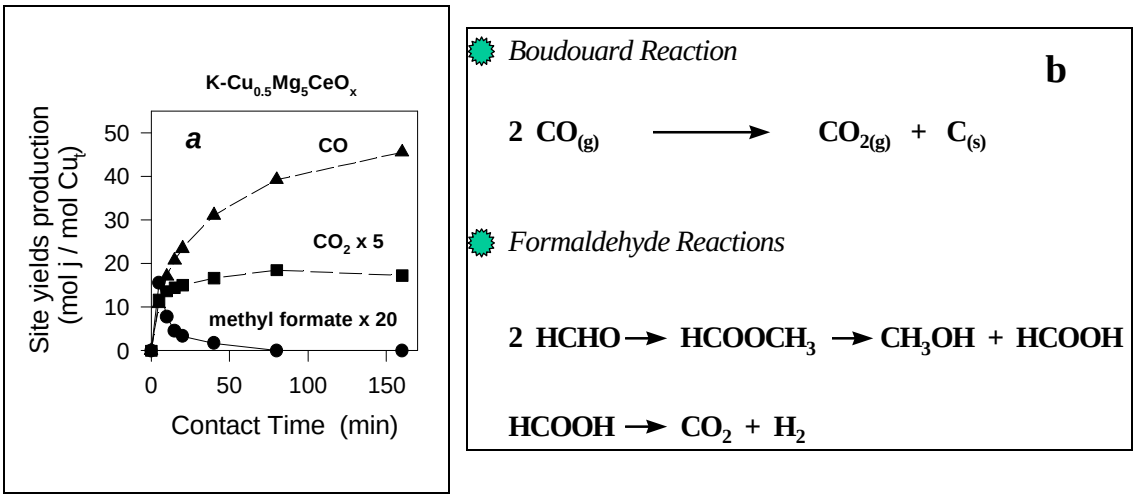

Figure 2.62. Methanol decomposition reaction on K-$Cu_{0.5}Mg_5CeO_x$. (a) Site-yields as a function of contact time; (b) Pathways of carbon dioxide production.

2.3.9.b. Methanol decomposition on MgO, Mg_5AlO_x and $MgAlO_x$ catalysts

Alcohol decomposition occurs primarily via dehydration or dehydrogenation on acidic or basic sites, respectively. In order to establish a correlation between the catalytic activity for methanol consumption and the surface acid-base properties in MgO, Mg_5AlO_x and $MgAlO_x$, methanol dehydrogenation and dehydration reactions were studied on these samples.

In a typical experiment, catalysts (30-40 mg) were charged into a gradientless batch reactor and pretreated in 10 % H_2 (balance He) at 623 K for 30 min. After the desired reaction temperature was reached, reactants were fed to the reactor. For the methanol decomposition reaction on $MgAlO_x$ and MgO catalysts, the feed gas composition was $CH_3OH/CH_4/He$ = 2.6/2.4/89.5 (methane was used as an internal standard). The reaction was carried out at 573 K and 101.3 kPa in the RRU.

Reaction rates, expressed as mol/g_{cat}-s, for each sample are shown in Figure 2.61. The initial rates of methanol consumption along with the catalyst properties are summarized in Table 2.29. CO_2, CO and H_2 were the only products, and dimethyl ether and hydrocarbons were not formed on pure MgO. CO_2 formed via methyl formate decomposition or from carbonaceous deposits (C_nH_x oxygen-deficient compounds) that remained on the surface. On Mg_5AlO_x and $MgAlO_x$ samples, dimethyl ether, CO_2, and CO were detected. Dimethyl ether was formed via dehydration of methanol on acid sites.

Table 2.29. Properties and rates of methanol conversion

Catalyst	Al/Mg	K wt. %	S.A. m^2 / g	$^{13}CO_2/^{12}CO_2$ exchange at 573 K x 10^{-6} μmol / m^2	r_0 mol / m^2-s
MgO	0	0.2	194	0.38	2.1 x 10^{-8}
Mg_5AlO_x	0.2	0.02	184	0.10	1.5 x 10^{-8}
$MgAlO_x$	1	0.08	230	0.21	2.0 x 10^{-8}

r_0 is the rate of methanol consumption, and is expressed in mol/g_{cat}.s or mol/m^2 total.s.

The ratio of the initial rates of DME and CO_x formation as a function of Mg/Al ratio on different Mg-Al samples is shown in Figure 2.64. The DME/CO_x ratio increases monotonically with increasing Al content. This ratio reflects the relative number of acid and basic sites in the catalyst. Acid sites lead to DME and basic sites are responsible for CO_x formation. For $MgAlO_x$, the amount of DME produced is higher than CO_2 and CO; whereas less DME and more CO_x formed on Mg_5AlO_x than on $MgAlO_x$, suggesting $MgAlO_x$ is less basic and more acidic than Mg_5AlO_x. DME was only observed on Al-containing MgO samples, suggesting that Al cations increase the acidity of MgO; as expected if a separate Al_2O_3 phase becomes more abundant as the Al content increases in mixed oxide samples.

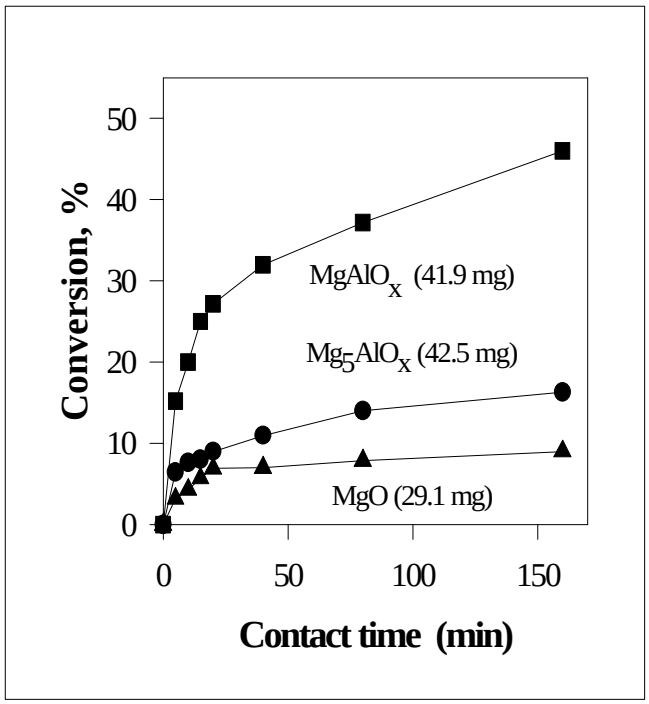

Figure 2.63. Methanol conversion as a function of contact time on different $MgAlO_x$ catalysts. [573 K, 2.6 kPa methanol pressure, 101.3 kPa total pressure].

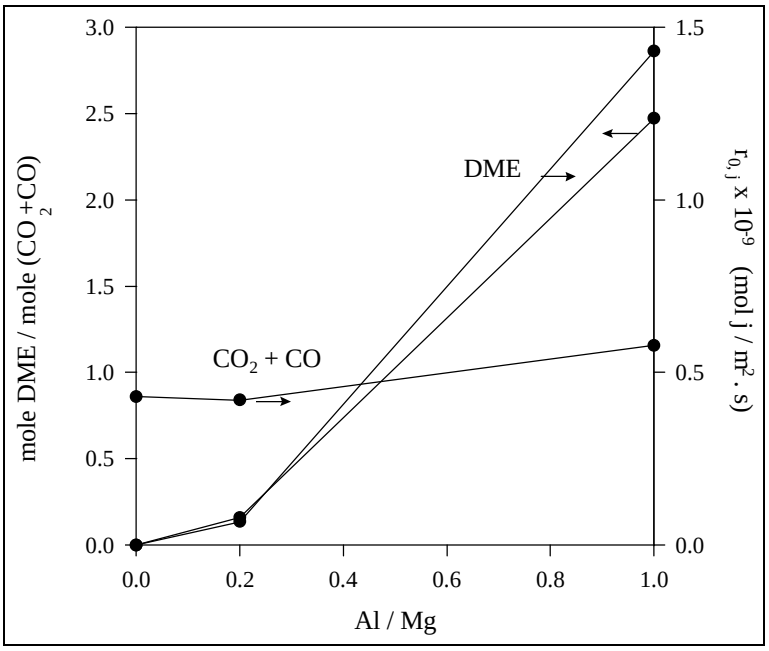

Figure 2.64. Methanol reaction on $MgAlO_x$ catalysts: Effect of Mg/Al ratio on product distribution. [573 K, 2.6 kPa methanol pressure, 101.3 kPa total pressure].

2.3.9.c. Methanol reaction with olefins on SAPO-34 and MgO hybrid catalysts

In recent patents [61, 69], reactions of methanol with olefins are reported to form higher alcohols on modified MgO catalysts:

$$C_2H_4 + CH_3OH \longrightarrow C_3H_7OH \xrightarrow{CH_3OH} \text{isobutanol}$$

It is known that SAPO-34 (an acid catalyst) converts methanol to olefins (selectivity higher than 80% to $C_2^=$ and $C_3^=$) and MgO (base catalyst) catalyzes the condensation reactions between olefins and methanol to produce isobutanol [61, 69]. It could then became possible to produce 1-propanol and isobutanol from methanol in one step by using a physical mixture of SAPO-34 and Mg_5CeO_x. To test this possibility, a physical mixture of SAPO-34 (6.7 mg) and Mg_5CeO_x (26.2 mg) was charged into a gradientless batch reactor and pretreated in 10 % H_2 (balance He) at 623 K for 30 min. The feed gas composition was CH_3OH/He = 5.8/90.0 kPa. The reaction was carried out at 623 K and 101.3 kPa in the RRU. The results are summarized in Figure 2.65.

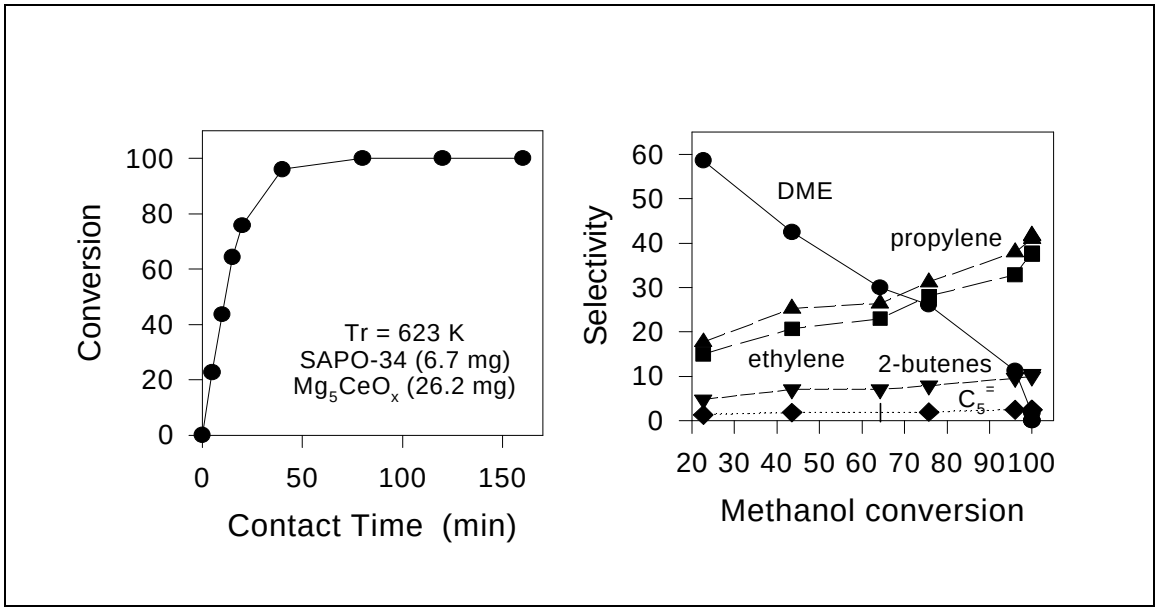

Figure 2.65. Methanol reactions on a physical mixture of SAPO-34/Mg_5CeO_x (6.7/26.2 mg). a) Methanol conversion vs. contact time, b) product selectivity vs. methanol conversion [623 K, 5.8 kPa methanol pressure, 101.3 kPa total pressure].

2.3.9.d. Methanol decomposition on K-Cu-Mg-CeOx catalysts

Methanol was predominantly converted to propylene and ethylene. Other products included DME, CO, CO_2, methane, ethane, propane, butane, pentane, 1-butene, 2-butene, and 1-pentene. The product distribution was similar to that obtained on pure SAPO-34 catalyst charge and no alcohols were detected. Neither isobutanol nor its precursor was observed. Methanol conversion to olefins was much faster than condensation reactions between olefins and C_1 intermediate species and any higher alcohols formed were not detected because their rapid conversion to olefins on the SAPO-34 component within the physical mixture.

Results obtained in CMRU (section 2.2) showed that on 1.0 wt % K-$Cu_{0.5}Mg_5CeO_x$ catalysts the selectivities to DME and hydrocarbon were relatively higher compared to Cs-Cu/ZnO/Al_2O_3 catalysts. These products are formed on acidic sites. Methanol reactions were performed on $Cu_{0.5}Mg_5CeO_x$ samples promoted with 0.1, 1.0 and 3.5 wt % K in order to investigate whether the increased amount of K could decrease the selectivity to DME and hydrocarbons. The catalysts (18 mg) was charged into a gradientless batch reactor and reduced in 10 % H_2 (balance He) at 623 K for 30 min. After the desired reaction temperature was reached, reactants were fed to the reactor. The feed gas composition was CH_3OH /CH_4/He = 7.7/2.5/91.1 kPa. The reaction was carried out at 573 K and 101.3 kPa in the RRU.

Results of methanol decomposition reactions on low Cu loading catalysts with different amount of K (0.1, 1.0 and 3.5 wt %) are summarized as follows:

a) CO and H_2 were the most abundant products on all catalysts. The methanol conversion and the normalized carbon selectivities as a function of contact time are shown in Figures 2.66, 2.67, and 2.68.
b) In addition to CO and H_2, small amounts of methyl formate (from methanol condensation) and CO_2 were produced. CO_2.
c) No DME was detected even on 0.1 wt % K-$Cu_{0.5}Mg_5CeO_x$. These results suggest that the methanol decomposition reactions on this type of materials can not be used to probe the presence of acid sites at the conditions of our experiment.

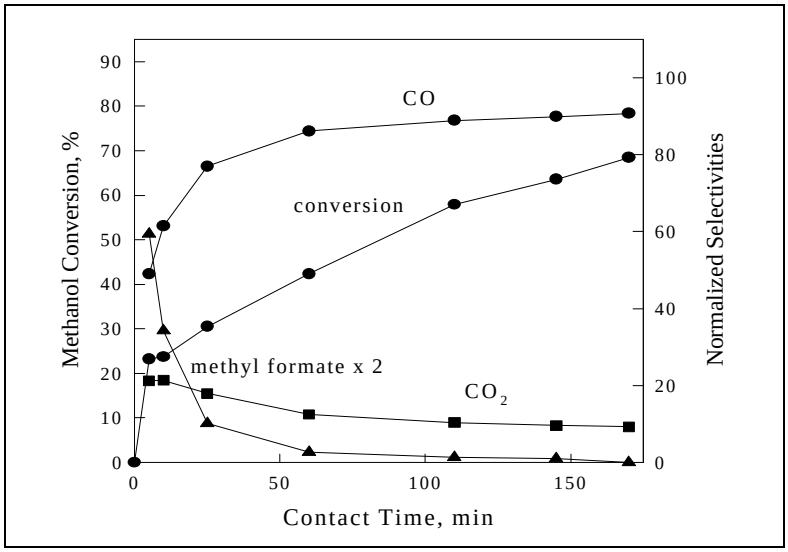

Figure 2.66. Methanol decomposition reactions on 0.1 wt % K-$Cu_{0.5}Mg_5CeO_x$. [573 K, 101.3 kPa total pressure, 7.7 kPa methanol, balance He].

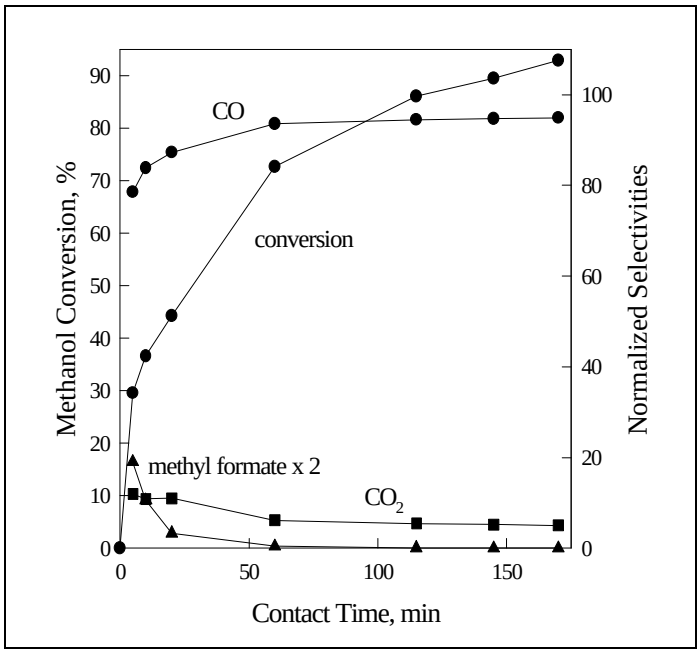

Figure 2.67. Methanol decomposition reactions on 1.0 wt % K-$Cu_{0.5}Mg_5CeO_x$. [573 K, 101.3 kPa total pressure, 7.7 kPa methanol, balance He].

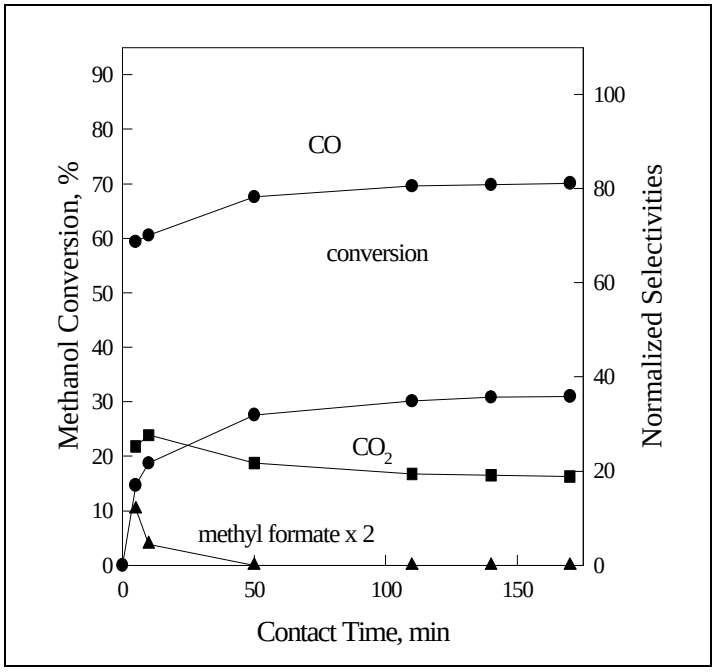

Figure 2.68. Methanol decomposition reactions on 3.5 wt % K-$Cu_{0.5}Mg_5CeO_x$. [573 K, 101.3 kPa total pressure, 7.7 kPa methanol, balance He].

2.3.10. Cross-Coupling Reactions of $^{13}CH_3OH/C_3H_6O$ Mixtures on Mg_yAlO_x

These studies were carried out in collaboration with Professor Carlos Apesteguia's research group. Dr. Carlos Apesteguia is Professor and Chairman of Chemical Engineering Department at Universidad Nacional del Litoral in Santa Fe (Argentina).

Cross-coupling reactions of $^{13}CH_3OH$ (^{13}C: 99 %, ^{18}O: < 1 %; Icon Services Inc.) with 1-propanol (Aldrich, 97%) were carried out in order to probe the reaction pathways on Mg_yAlO_x catalyst. A reactant mixture of $^{12}C_3H_7OH/^{13}CH_3OH/CH_4/He$ = 1.4/2.7/2.4/ 94.8 kPa was used. Catalyst samples (38.0 mg) were pretreated in vacuo (heating up to 723 K at 3.5 K/min) at 723 K for 2.0 h. Reactions were conducted at 573 K and 101.3 kPa in the RRU. Mass spectrometric analysis after chromatographic separation was used to confirm the identity of each reaction product and to determine ^{13}C content, position, and distributions in reactants and products. Five samples have been tested: HT-1 ($MgAlO_x$), HT-5 (Mg_5AlO_x), HT-0.5 ($Mg_{0.5}AlO_x$), HT-9 (Mg_9AlO_x), and MgO. The results obtained on those samples are shown in Tables 2.30 and 2.31.

Reaction pathways involved for the formation of the main products are shown in Figure 2.29. The ^{13}C-contents in 1-propanol and products are shown in Table 2.32. The isotopic tracer studies (Table 2.32) are consistent with the sequence of steps shown in Figure 2.69. DME is only doubly-labeled ($^{13}CH_3O^{13}CH_3$) suggesting that it forms from $^{13}CH_3OH$ via dehydration reactions. 1-propanol contains only 0.2 % of ^{13}C at the end of the reaction (170 min), suggesting that the reverse aldol condensation observed on K-$Cu_yMg_5CeO_x$ catalysts is not important on $MgAlO_x$ catalysts. Propionaldehyde showed no significant ^{13}C-enrichment (Table 2.32) and was formed from 1-propanol dehydrogenation. Also, n-propyl ether showed no ^{13}C, indicating that they are formed exclusively from 1-propanol. Isobutanol and isobutyraldehyde (from isobutanol dehydrogenation) contain predominantly one ^{13}C atom, suggesting that it is formed by condensation of 1-propanol with methanol. The analysis of mass spectra patterns showed that labeled carbon was either at the CH_3 or at the CHO fragment of isobutyraldehyde, suggesting that aldol condensation reactions occur with retention of either one of the two oxygen atoms in aldol-keto species, also found on $MgCeO_x$-based catalysts.

This product distribution is consistent with the presence of both acid and basic functions on these catalysts. Dehydrogenation and aldol condensation take place on basic sites. Both propionaldehyde (dehydrogenation product) and isobutanol (condensation product) selectivities and initial reaction rates decrease with increasing Al content. The origin of the unexpected values obtained on HT-0.5 is not yet clear. Propylene (dehydration), DME (dehydration and coupling), DPE (dehydration and coupling) and MPE (dehydration and coupling) are among the dehydration products produced on acid sites. MPE is selectively produced over the other products. The initial rates (site-time yields per gram of catalyst) for methyl propyl ether (MPE) increase with Al content. Al_2O_3 provides acid sites for the formation of dehydration products.

Table 2.30. Cross-coupling reactions of $^{13}CH_3OH$ with 1-propanol

	MgO	HT-9	HT-5	HT-1	HT-0.5
Al/(Al+Mg)	1	0.1	0.17	0.5	0.67
BET S_g (m^2/g)	191	114	184	230	298
Exchangeable CO_2 (10^{-6} mol/m^2)	0.38	0.17	0.18	0.36	0.17
Contact time, min	5	5	5	6	5
X n-propanol	11.0	8.8	8.5	12.9	24.0
X methanol	9.0	4.9	5.8	8.4	14.5
Selectivities					
Propylene	0	0	0	4.0	3.0
DME	0	0	0	7.2	8.9
MPE	0	2.8	0	29.7	28.9
DPE	0	0	0	7.2	6.1
CO_x	1.5	2.2	0	1.3	.9
Propionaldehyde	77.1	75.6	89.2	27.9	36.4
Isobutyaldehyde	0	0	0	0	0.8
Isobutanol	5.4	8.1	10.8	5.8	9.8
Reaction rates (10^{-8} mol / g_{cat} - s)					
MPE	0	4.2	1.6	32.8	119.6
Propionaldehyde	192.7	148.3	71.2	40.8	200.7
Isobutanol	10.2	12.0	6.5	6.4	40.7

[573 K, 101.3 kPa total pressure, 1.4 kPa 1-propanol, 2.7 kPa methanol, balance He].

Table 2.31. Cross-coupling reactions of $^{13}CH_3OH$ with 1-propanol at similar methanol and 1-propanol conversions.

	MgO	**HT-9**	**HT-5**	**HT-1**	**HT-0.5**
BET S_g (m^2/g)	191	114	184	230	298
Exchangeable CO_2 (10^{-6} mol/m^2)	0.38	0.17	0.18	0.36	0.17
Contact time, min	60	60	60	30	5
X n-propanol	30.2	33.1	29.3	28.5	24.0
X methanol	15.3	13.4	11.5	15.5	14.5
Selectivities					
Propylene	0	0.8	0.5	4.3	3.0
DME	0	0.8	1.2	6.4	8.9
MPE	0	4.3	4.1	25.4	28.9
DPE	0	0	0.9	4.6	6.1
CO_x	3.0	4.0	5.3	1.4	.9
Propionaldehyde	71.8	52.3	54.7	28.1	36.4
Isobutyaldehyde	2.1	3.7	2.9	0.9	0.8
Isobutanol	13.6	21.3	19.5	15.5	9.8
Reaction rates (10^{-8} mol / g_{cat} - s)					
MPE	0	1.6	1.4	15.7	119.6
Propionaldehyde	46.7	25.3	19.3	23.2	200.7
Isobutanol	4.6	9.9	7.0	9.6	40.7

[573 K, 101.3 kPa total pressure, 1.4 kPa 1-propanol, 2.7 kPa methanol, balance He].

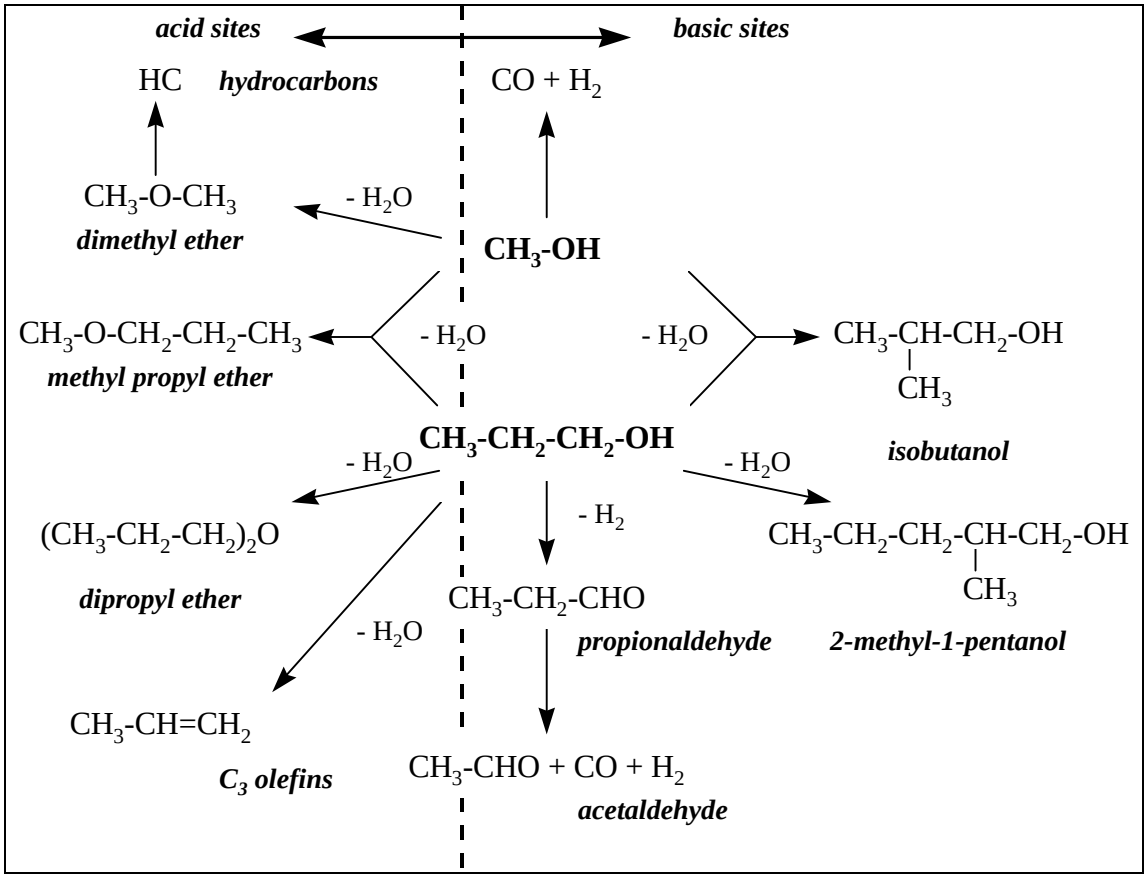

Figure 2.69. Reaction scheme for CH_3OH/CH_3CH_2OH reactions on Mg_yAlO_x catalysts. [573 K, 101.3 kPa total pressure, 1.4 kPa 1-propanol, 2.7 kPa methanol, balance He].

Table 2.32. ^{13}C-Distribution in products of $^{13}CH_3OH$-C_3H_7OH reactions on $MgAlO_x$ (HT-1)

	Number of Carbon-13				
	0 ^{13}C	1 ^{13}C	2 ^{13}C	3 ^{13}C	4 ^{13}C
DME	0	0	100	---	---
n-propanol	98.6	1.6	-0.5	0.3	---
propionaldehyde	99.8	0.2	0	0	---
methyl propyl ether	1.5	98.0	0.4	0	0
isobutanol	4.7	94.6	0.4	0.3	0
isobutyraldehyde	5.9	95.3	-1.2	0	0

[573 K, 101.3 kPa total pressure, 1.4 kPa n-propanol, 2.7 kPa methanol, balance He].

2.3.11. Ethanol Reactions on Mg_yAlO_x

Ethanol dehydrogenation and coupling reactions were carried out on MgO, γ-Al_2O_3 and ex-HT catalysts in order to evaluate the effect the surface basicity has on the catalyst selectivity. These studies were carried out in collaboration with Professor Carlos Apesteguia's research group. Dr. Carlos Apesteguia is Professor and Chairman of Chemical Engineering Department at Universidad Nacional del Litoral in Santa Fe (Argentina).

Catalytic testing was carried out at 573 K in a differential fixed-bed reactor fed with a flow of N_2/ethanol = 10 molar composition. Ethanol conversions were lower than 10%. The initial reaction rates, obtained by extrapolating to zero bed residence time, are shown in Figure 2.70.

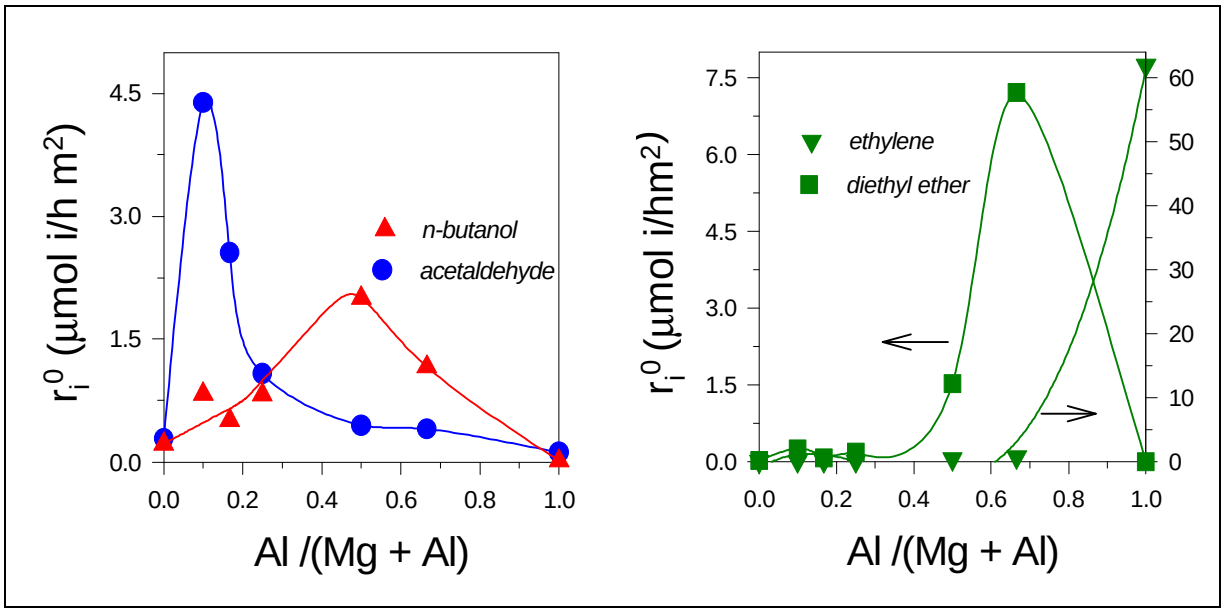

Figure 2.70. Ethanol reactions on Mg_yAlO_x. [573 K, 101.3 kPa, ethanol/N_2=1]

Dehydrogenation to acetaldehyde is favored on catalysts with a low surface oxygen concentration (samples ex-HT9 and ex-HT5) thereby indicating that such a reaction is not highly demanding of catalyst basicity. On the contrary, coupling toward n-butanol requires not only a higher basic site density but also a strong basicity (catalyst ex-HT1). The predominant formation of diethyl ether on samples which contain Al in high concentrations, suggests that this reaction is preferentially catalyzed by a weakly-acidic hydroxylated surface. Ethylene was the exclusive product on the γ-Al_2O_3 strong acid sites. The lack of strong acidity makes the synthesis of ethylene unlikely on ex-HT catalysts. The product distribution in dehydrogenation and coupling of ethanol on ex-HT catalysts depends on the sample composition. The reaction paths leading to the synthesis of each individual product demands a particular combination of basic and acidic sites which results from an adequate balance between Mg^{2+} and Al^{3+} cations.

Task 3. Identification of Reaction Intermediates and Active Sites

3.1. Temperature-Program Reduction (TPR) of MgO-based Cu Catalysts

This study addresses the effects of K and CeO_x on the reducibility of CuO and the generation of required Cu metal sites. The experiment was carried out by first pretreating the samples at 723 K in flowing He (100 cm^3/min) for 0.5 h to remove carbonates, water, and weakly bonded hydroxyl species. Reactor temperature was then lowered to below 313 K and 5 % H_2/He was introduced at a total flow rate of 100 cm^3/min (STP). The temperature was then increased linearly at a rate of 0.17 K/s and the formation of H_2O and the consumption of H_2 were monitored continuously by mass spectroscopy.

The reduction profiles of MgO-based Cu samples are shown in Figure 3.1. The onset and peak maximum temperatures for H_2 consumption and H_2O formation obtained on each sample appeared at the same temperature. The high-temperature tail of the H_2O peak is caused by a strong interaction between H_2O and MgO. This tail was not observed for the H_2 peak, but the signal-to-noise ratio of the H_2 peak was lower than that of H_2O, because of the high H_2 background pressure in the mass spectrometer.

Addition of CeO_x to $Cu_{0.1}MgO_x$ promoted copper reduction and the reduction temperature at peak maximum decreased from 508 K to 436 K. As mentioned earlier, CeO_x addition increases Cu dispersion and decreases Cu particle size due to the strong metal-support interaction between Cu and CeO_x. The large Cu particles in $Cu_{7.5}Mg_5CeO_x$, however, can also be reduced at temperatures lower than those on $Cu_{0.1}MgO_x$. The reduction profiles (Figure 3.1) suggest that the promoting effect of CeO_x on copper oxide reduction increases with increasing Ce/Mg ratios.

CeO_x promotion of metal oxide reduction has also been reported by Schmal *et al.* on $Pd/CeO_2/Al_2O_3$ [70]. The presence of CeO_x shifts the reduction temperature of PdO to lower values. Moreover, the reduction behavior of a $Pd/CeO_2/Al_2O_3$ sample prepared by the coprecipitation of Pd and cerium nitrates differs from that of $Pd/CeO_2/Al_2O_3$ prepared by conventional successive impregnation of CeO_2 and Pd. An appreciable degree of reduction on the sample prepared by the coprecipitation methods occurs at room temperature, as a consequence of an enhanced PdO-CeO_x interaction, probably faciliated by a higher contact area between PdO and CeO_x phases [71]. The coprecipitation method ensures an intimate contact and therefore increases the interaction between CeO_x and Pd. In the case of Cu^{2+}, Lamonier *et al.* [10] – [13] have found that Cu^{2+} insertion into CeO_x occurs during catalyst synthesis by coprecipitation methods. Four different species, present as CuO monomers, dimers, clusters, and small particles have been detected in CuO/CeO_2 mixtures [10] – [13].

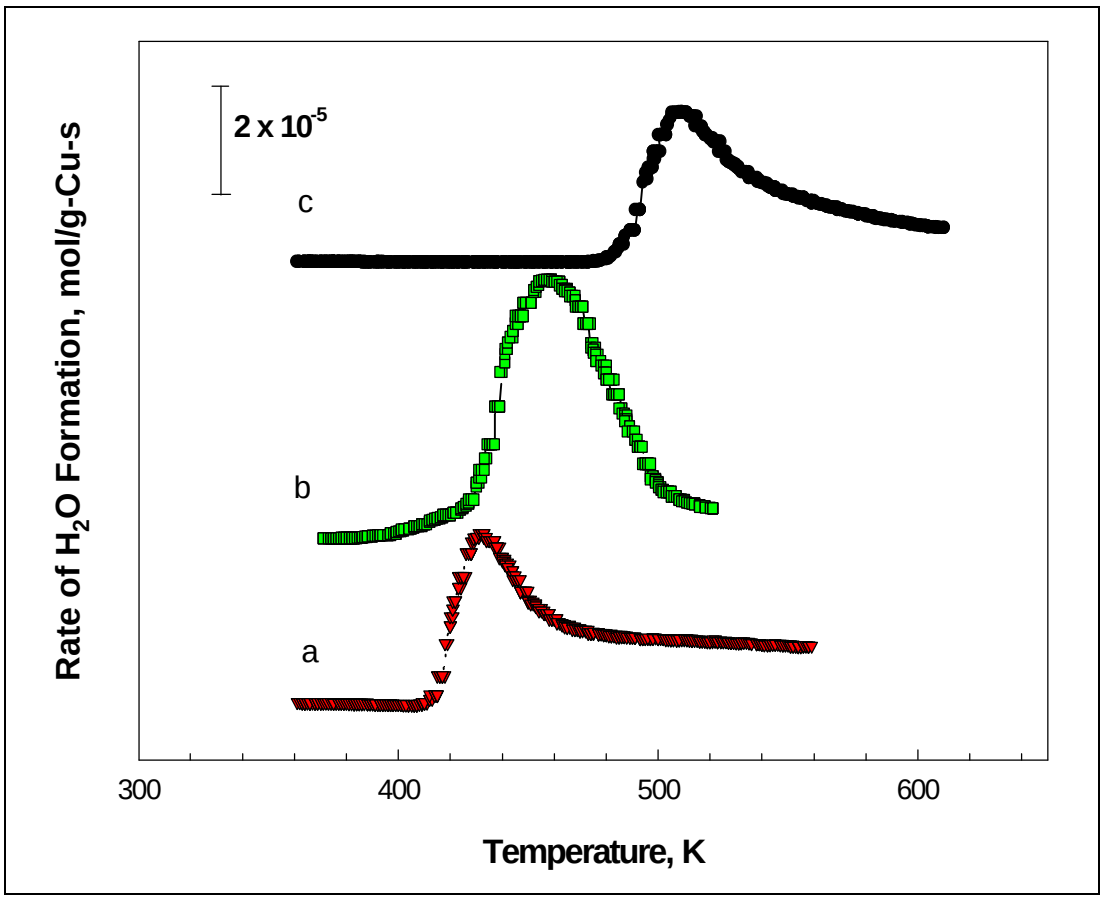

Figure 3.1. Temperature-programmed reduction profiles obtained in 5 % H_2/He of MgO-based Cu catalysts: (a) $Cu_{0.5}Mg_5CeO_x$; (b) $Cu_{7.5}Mg_5CeO_x$; (c) $Cu_{0.1}Mg_5O_x$. [Heating rate: 0.17 K/s; 15-100 mg of sample, 100 cm^3/min 5% H_2/He mixture; pretreatment temperature: 723 K]

ZnO has a similar effect as CeO_x on copper reduction. As reported by Fierro *et al.* [72], [73], the fraction of copper strongly interacting with ZnO increases with increasing Zn/Cu ratio and these copper showed the highest reducibility. Kinetic models of reduction kinetics of CuO/ZnO suggest that the promoting effect of ZnO on copper reduction is mainly caused by enhanced dissociative adsorption of H_2 on ZnO surfaces or CuO in contact with ZnO [74]. The spillover of the activated hydrogen enhances Cu^{2+} reduction. In fact, kinetic analysis showed that the apparent activation energy, E_a, was 84 kJ/mol for the reduction of pure CuO whereas E_a decreased to 77 kJ/mol for the reduction of the CuO-ZnO catalysts [71], in agreement with the promoting effect of ZnO on the reducibility of copper. Similar processes are likely to occur during copper reduction on $CuMgCeO_x$ samples. A better contact between CeO_x and Cu is expected with increasing CeO_x/Cu ratio, resulting in lower copper reduction temperatures.

In contrast to CeO_x, K addition to Cu-containing samples inhibited CuO reduction, as evidenced by the shift of reduction peak maxima to high temperatures (Figure 3.2). The effect of K is more pronounced on low-Cu ($Cu_{0.5}Mg_5CeO_x$) than on high-Cu ($Cu_{7.5}Mg_5CeO_x$) catalysts. The maximum peak temperature increased by 79 K

on the former but only 57 K on the latter. Also, the effect of K was not influenced by the presence of CeO_x because reduction temperatures increased by approximately the same amount on both K-$Cu_{0.5}Mg_5O_x$ and K-$Cu_{0.5}Mg_5CeO_x$. K possibly stabilizes Cu ions and makes them less easily reduced by H_2. Similar phenomena have been observed on Cs-promoted Cu/ZnO/Cr_2O_3 by Klier *et al* [75]; the presence of Cs retarded CuO reduction by about 50 K. This reduction inhibition appears to be caused by stronger interactions between CuO and promoter phases, which inhibit H_2 dissociation.

The inhibition effect of K on copper reduction can also be explained by the formation of stronger Cu-O bonds upon K addition. As reported in the literature [76], [77], the Cu-O bond energy in CuO is about 42 kJ/mol and increases to 63 kJ/mol upon the addition of 10-25 at. % MgO. Addition of MgO is believed to weaken the Cu-Cu interaction accompanied by the enhancement of the Cu-O interaction in the axial position. Similarly, the incorporation of K into CuO during catalyst synthesis may increase the Cu-O bond strength and retard the CuO reduction. K-promoted $CuMgCeO_x$ catalysts reduce at higher temperatures than unpromoted ones, suggesting that Cu metal on K-$CuMgCeO_x$ can be more easily oxidized than on alkali-free catalysts of identical composition.

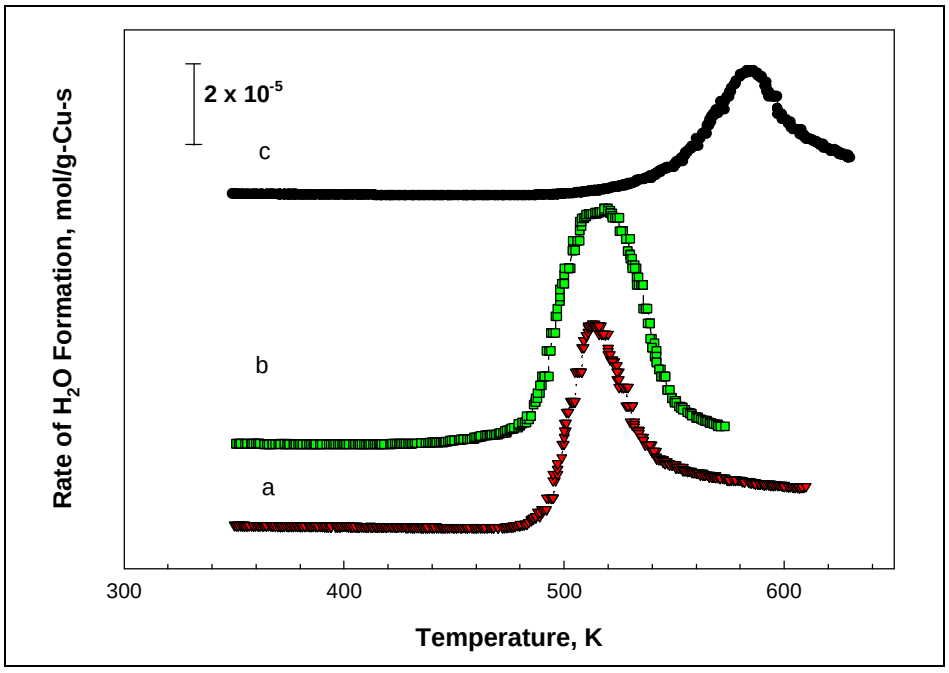

Figure 3.2. Temperature-programmed reduction profiles obtained in 5 % H_2/He of MgO-based Cu catalysts: (a) 1.0 wt % K-$Cu_{0.5}Mg_5CeO_x$; (b) 1.2 wt % K-$Cu_{7.5}Mg_5CeO_x$; (c) 1.1 wt % K-$Cu_{0.1}Mg_5O_x$. [Heating rate: 0.17 K/s; 15-100 mg of sample, 100 cm^3/min 5% H_2/He mixture; pretreatment temperature: 723 K]

3.2. Determination of Copper Surface Area

Exposed Cu surface areas were measured by titrating Cu surface atoms with N_2O (Matheson, ultra high purity) at 363 K. N_2O was introduced as pulses into a He stream. The number of chemisorbed O atoms was obtained from the amount of N_2O consumed and the N_2 produced. A saturation coverage of 0.5:1 O:Cu_s was used to estimate Cu surface area and dispersion [78], [79]. Cu dispersion is defined as the ratio of surface Cu (Cu_s) to the total number of Cu atoms in the catalyst.

In a typical experiment, a 80-140 mesh sample (~33.0 mg) was loaded into a 6 mm-i.d. U-shape quartz reactor and pretreated in flowing helium at 723 K for 20 min to remove carbonates and water before reactor temperature was lowered to below 373 K in He. The sample was then reduced in a hydrogen stream (5 % H_2 in He) as temperature was increased up to 623 K at 10 K/min and stay at 623 K for 30 min. The temperature programmed reduction (TPR) of a Cu/MgO/CeO_2 catalyst indicated that copper reduction took place in the temperature range of 493-553 K. After H_2 reduction, reaction temperature was decreased to 363 K in He and N_2O was introduced by pulse injection through the sample loop. As reported in the literature [78], [79], the optimum titration temperature was 358-368 K, at which the oxidation of copper by N_2O is sufficiently mild that only the surface copper is oxidized to Cu(I). At temperatures > 393 K, bulk oxidation of copper occurs. Lower temperatures may cause the incomplete surface oxidation, because this is an activated process with an apparent activation energy of 2 kcal/mol [80].

For a freshly reduced Cu catalyst, the first few pulses of nitrous oxide titration (5 % N_2O balanced in helium) led to the evolution of gas-phase N_2; the oxygen atoms remained chemisorbed on the surface. Upon further addition of nitrous oxide, a m/e 44 peak of unreacted N_2O was detected in the effluent. Once the mass 44 peak intensity remained constant with subsequent pulses, titration was assumed to be complete. Based on the amount of N_2O consumed or the amount of N_2 formed, the total number of oxygen atoms chemisorbed on the surface can be determined. It should be pointed out that no gas-phase oxygen was observed during pulse injection, indicating all the oxygen atoms from N_2O remained on the surface. As one oxygen atom corresponds to a copper area of 2×10^{-19} m^2 [80], copper surface areas can be calculated from the number of oxygen atoms chemisorbed.

The Cu surface area was 28.5 m^2/g-cat (Cu dispersion: 6.8 %) in $CuZnAlO_x$ and 23.5 m^2/g (Cu dispersion: 5.2 %) in Cs-$CuZnAlO_x$, suggesting that the addition of Cs to $CuZnAlO_x$ decreases the number of surface exposed Cu atoms. The decrease in Cu surface area upon Cs addition can be caused by the total surface area in these samples (from 74 to 62 m^2/g) or by blocking of surface Cu atoms with Cs_2CO_3.

The Cu surface area was found to be 13.1 m^2/g-cat (Cu dispersion: 15.8 %) in 1.0 wt % K-$Cu_{0.5}Mg_5CeO_x$ (MG3-13 O/K). This dispersion value is similar to the value of 14.1 % obtained on MG-11 Ow/K (1.0 wt % K-$Cu_{0.5}Mg_5CeO_x$), suggesting reasonable reproducibility of catalyst preparation methods. MG3-13 O/K and MG3-11 O/K have similar composition, but were prepared as different batches. Cu surface area and dispersion of MgO- and ZnO-based catalysts are shown in Table 3.1.

The copper dispersion in $Cu_{0.5}Mg_5CeO_x$ is 23 %; this value is among the highest reported in the literature for Cu-based methanol and higher alcohol synthesis catalysts. A $Cu_{0.1}MgO_x$ sample with similar Cu content as $Cu_{0.5}Mg_5CeO_x$ has a copper dispersion of only 6 %. Thus, the presence of Ce oxide species appears to stabilize small Cu metal crystallites on MgO supports.

Table 3.1. Composition, surface area, and basic site density of mixed metal oxides

Sample	[a]K content (wt %)	Sg (m^2/g)	[b]Cu dispersion (%)
$Cu/ZnO/Al_2O_3$	0	62	5.0
$Cu_{7.5}Mg_5CeO_x$	1.2	92	4.7
$Cu_{0.1}MgO_x$	0.2	118	6.0
Mg_5CeO_x	0.01	188	---
MgO	0.01	191	---
$Cu_{0.5}Mg_5CeO_x$	0.1	167	23.0
$Cu_{0.5}Mg_5CeO_x$	1.0	147	14.0
$Cu_{0.5}Mg_5CeO_x$	3.5	62	6.2

[a] Bulk composition measured by atomic absorption.

Copper dispersion decreased with increasing K loading (Table 3.1) because of a decrease in the surface area of the Mg_5CeO_x support and also because K species are likely to block surface Cu atoms or inhibit their reduction to Cu metal, resulting in a decrease in the number of exposed surface Cu atoms. CeO_x addition to $Cu_{0.1}MgO_x$ increased both surface area and copper dispersion (Table 1), indicating that it is a structural promoter.

The decomposition of N_2O on reduced ZnO support sites has been found to contribute significantly to the overall Cu surface area on Cu/ZnO catalysts [81]. It is possible that decomposition of N_2O on reduced CeO_x species in pre-reduced $Cu_{0.5}Mg_5CeO_x$ catalysts also corrupts N_2O titration data and leads to overestimates of copper dispersion. N_2O did not decompose on Mg_5CeO_x samples pre-reduced at 623 K, suggesting that any reduced Ce species did not interact with N_2O at 363 K. CeO_2 may only be reduced, however, when Cu metal is available in order to dissociate H_2. In effect, the presence of Cu may promote the reduction of CeO_2.

A reduction-oxidation cycle was carried out in order to rule out any contribution from reduced Ce species to the N_2O titration measurements of Cu surface area. A $Cu_{0.5}Mg_5CeO_x$ sample was reduced at 623 K and N_2O titration data were obtained. The measured Cu surface area was found to be 19.0 m^2/g-cat (0.23 Cu dispersion). This sample was re-reduced at 473 K instead of 623 K after the titration measurements. Surface oxygen atoms on Cu surface can be removed at 473 K in H_2, but reduction of

CeO_2 is likely to occur only at much higher reduction temperatures. Thus, reduction at 473 K is likely to remove oxygen from Cu surface but not from CeO_x. The Cu surface area of the sample reduced at 473 K was 19.3 m^2/g-cat, which is very similar to the value of 19.0 m^2/g-cat obtained on the fresh sample after reduction at 623 K. This demonstrates that CeO_x does not contribute to the measured copper dispersion and that these high dispersion values accurately reflect the presence of small Cu metal crystallites (about 5 nm) on this sample. An additional exposure of this titrated sample to 5 % H_2 at 423 K resulted in a Cu surface area of 17.9 m^2/g-cat, suggesting that oxygen atoms chemisorbed on Cu can be almost completely removed by H_2 at temperatures as low as 423 K.

In a typical CMRU experiment, the catalyst deactivates with time on stream. Cu surface area of the used sample (1.0 wt % K-$Cu_{0.5}Mg_5CeO_x$) was determined in order to address the effect of high-pressure catalytic reactions on Cu surface area. The used sample was first treated in flowing He at 723 K for 20 min followed by H_2 reduction at 623 K for 30 min before N_2O titration commenced at 363 K. The copper dispersions on the used 1.1 wt % K-$Cu_{0.5}Mg_5CeO_x$ taken from the top and middle-bottom of the CMRU catalyst bed were 3.6 % and 1.2 %, respectively; these values are much lower than on the fresh catalyst (14 %). The smaller value in the latter suggests that the front part of the catalyst bed in the CMRU reactor is less severely deactivated. It should be pointed out that the total surface areas of these two used samples are comparable. The Cu dispersion of the used sample, however, was much less than that of the fresh sample (15.8 %). The decrease in Cu during reaction is due to 1) a decrease in the total surface area (150 m^2/g to 80 m^2/g) 2) deposition of hydrogen deficient hydrocarbon species on the catalyst surface, and 3) Cu metal sintering during the reaction.

In another experiment, the used 1.0 wt % K-$Cu_{0.5}Mg_5CeO_x$ removed from the top of CMRU reactor was treated in flowing O_2 (5 % O_2/He) instead of He at 723 K. This treatment leads to a Cu dispersion of 20.6 % that is even greater than the fresh sample even though the total surface area of the used sample is still approximately one-half of the fresh sample, suggesting that oxygen treatment at 723 K is able to remove all carbonaceous deposits covering on Cu metal atoms. Moreover, alcohol (ROH) and water formed during the reaction could react with surface K^+ ions to form RO^-K^+ and KOH. The loss of RO^-K^+ and water from surface to gas phase results in a loss of surface K^+ ions and an increase in the exposed surface Cu atoms.

3.3. Determination of Basic Site Density and Strength

Because of the role of basic sites in chain-growth reactions leading to isobutanol, it is important to determine the basic site density and strength in isobutanol synthesis catalysts. In this study, the density and strength of basic sites have been measured from the exchange capacity and exchange rates obtained using a $^{13}CO_2/^{12}CO_2$ isotopic exchange method developed as part of this project; this method provides a direct measure of the number of basic sites *"kinetically available" at reaction temperatures*. In addition, this technique provides a measure of the distribution of reactivity among available basic sites. In this method, a pre-reduced catalyst (50 mg) is exposed to a 0.1 % $^{13}CO_2$/0.1 % Ar/He stream (100 cm^3/min) and after $^{13}CO_2$ reached a constant level in the effluent, the flow is switched to 0.1 % $^{12}CO_2$/He (100 cm^3/min). The relaxation of the $^{13}CO_2$ displaced from the surface is followed by mass spectrometry. In contrast with CO_2 temperature programmed desorption (TPD), $^{13}CO_2/^{12}CO_2$ exchange methods probe the density and reactivity of reactive basic sites at reaction temperatures and chemical equilibrium, without contributions from unreactive carbonates and without disrupting the steady-state coverage on catalytic solids.

Figure 3.3 shows the transients obtained on a $Cu_{0.5}Mg_5CeO_x$ catalysts when the isotopic composition of CO_2 was switched at 573K. As $^{13}CO_2$ was switched to $^{12}CO_2$ at zero time, without altering the partial pressure or flow rate of CO_2, the concentration of $^{13}CO_2$ decreases as $^{12}CO_2$ concentration increases, but the total gas phase concentration of CO_2 (i.e., $^{12}CO_2$ + $^{13}CO_2$) remains constant. The presence of Ar as an inert tracer permits correction for gas holdup and hydrodynamic delay in the apparatus.

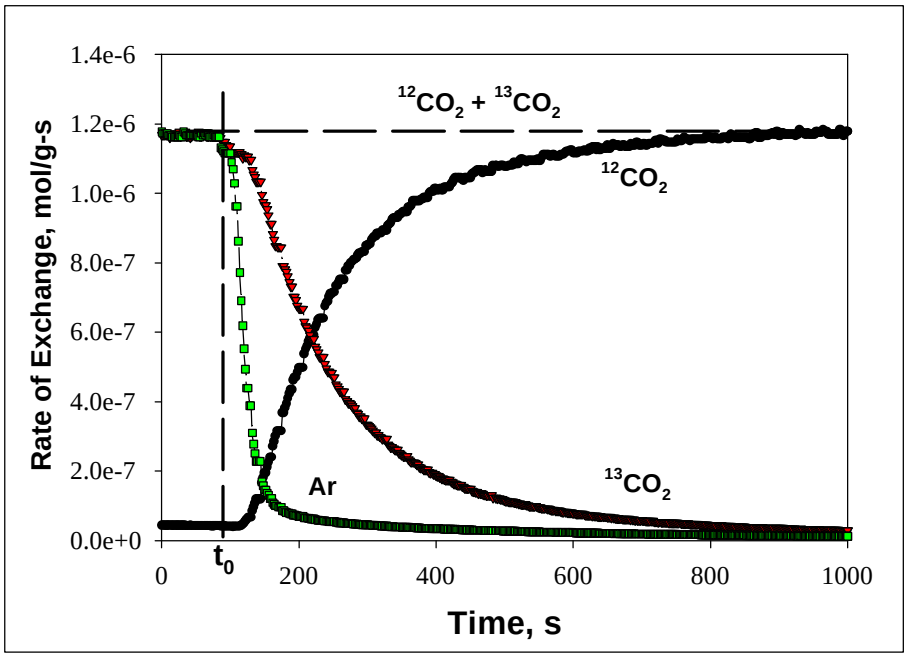

Figure 3.3. Steady-state transients observed for $Cu_{0.5}Mg_5CeO_x$ upon switching from $^{13}CO_2$/He to $^{12}CO_2/H_2$ at 573 K.

The significant delay in the steady-state transient of $^{13}CO_2$, relative to the Ar transient, indicates that the former originates from catalyst-bound $^{13}CO_2$ species that desorb slowly at the temperature of the isotopic exchange experiment. The coverage or number of surface CO_2 species remains constant, i.e.,

$$\theta_{^{13}CO_2\,(t=0)} = \theta_{^{13}CO_2\,(t)} + \theta_{^{12}CO_2\,(t)} = \theta^{total}_{CO_2\,(t)} = \theta_{^{12}CO_2\,(t=\infty)}$$

At the time of the switch (t_0) the surface exchangeable sites are only covered by $^{13}CO_2$ and at long times after the switch, the surface exchangeable sites are predominantly occupied by $^{12}CO_2$. Therefore, the amount of $^{13}CO_2$ displaced from the surface by $^{12}CO_2$ reflects the exchange capacity of the catalyst at the reaction temperature. The exchange capacity is determined from the area under the $^{13}CO_2$ curve (Figure 3.3). This area, properly corrected for the response factor of the mass spectrometer and for gas holdup, corresponds to the number of basic sites that participate in exchange reactions at 573 K and the results obtained on K-CuMgCeOx and individual components are shown in Table 3.2. Weakly interacting sites are mostly unoccupied by CO_2 and strongly interacting sites do not exchange at all in the time scale of the isotopic relaxation experiment. These strongly interacting sites and weakly interacting sites are also unlikely to contribute to catalytic reactions of similar molecules at similar temperatures.

Table 3.2. Composition, surface area, and basic site density of mixed metal oxides

[a]Sample	[b]Sg (m^2/g)	[c]Cu, dispersion (%)	Exchangeable CO_2 at 573 K 10^{-6} mol/m^2	CO_2 desorbed during TPD at T < 573 K 10^{-6} mol/m^2
MgO	191	-	0.38	0.50
CeO_2	80	-	0.92	/
Mg_5CeO_x	188	/	0.95	0.84
$Cu_{0.5}Mg_5O_x$	118	6	0.40	/
0.1 wt% K-$Cu_{0.5}Mg_5CeO_x$	167	23	1.2	0.62
1.1 wt% K-$Cu_{0.5}Mg_5CeO_x$	147	14	2.3	0.64
3.5 wt% K-$Cu_{0.5}Mg_5CeO_x$	62	6.2	5.2	0.65
1.2 wt % K-$Cu_{7.5}Mg_5CeO_x$	92	4.7	3.3	0.91
Cs-Cu/ZnO/Al_2O_3	62	5.0	1.1	0.72

[a] Bulk composition measured by atomic absorption.
[b] Total surface area determined by N_2 BET adsorption at 77 K.
[c] Dispersion calculated from the ratio of surface Cu (determined by N_2O decomposition at 90 ^oC (52,53)) to the total number of Cu atoms in the catalyst.

The basic site densities determined by the conventional temperature-programmed desorption (TPD) of CO_2 are also listed in Table 3.2. In TPD experiments, CO_2 is adsorbed on the pre-reduced catalyst at room temperature. The catalyst surface is subsequently flushed with He to remove gas phase and weakly adsorbed CO_2 before linearly ramping the temperature at 0.5 K/s, and measuring the desorption profile of CO_2 by mass spectrometry (Figure 3.4). This method gives both physically and chemically adsorbed CO_2. Nevertheless, the number of basic sites determined from CO_2 TPD based on the total amount of CO_2 desorbed below 573 K on each catalyst is significantly lower than that the corresponding value obtained from $^{13}CO_2/^{12}CO_2$ switch experiments.

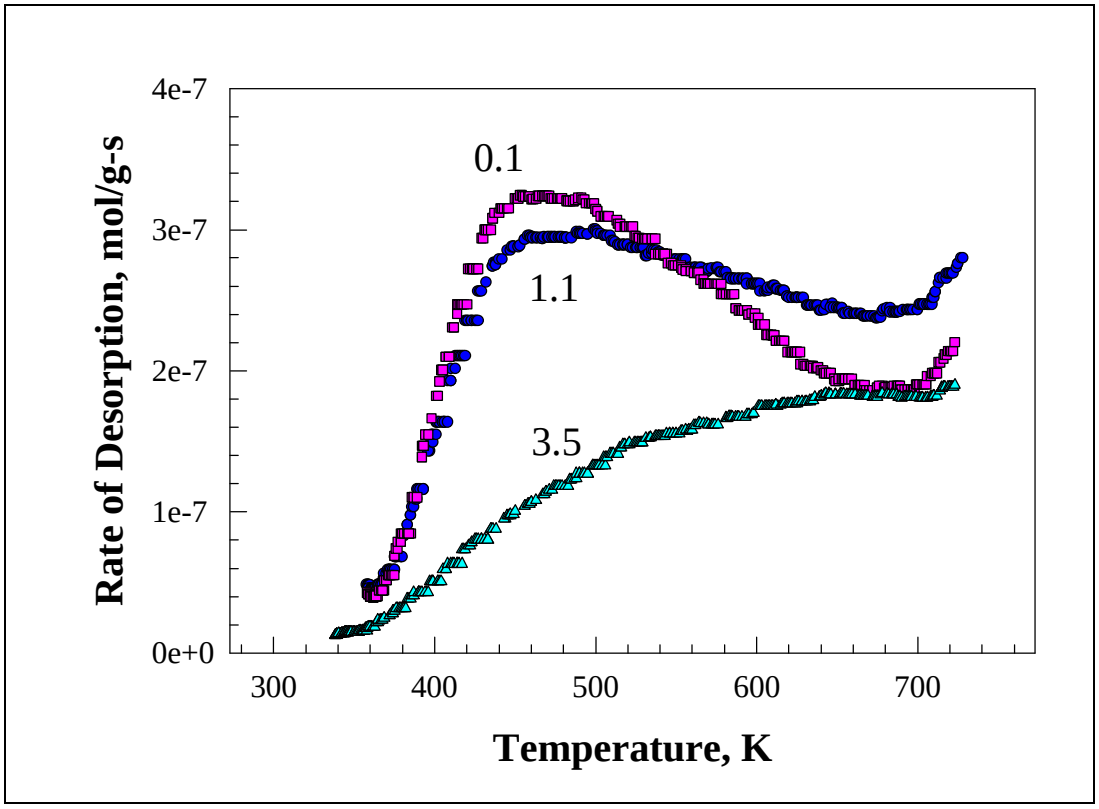

Figure 3.4. CO_2 temperature-programmed desorption spectra in He on K-$Cu_{0.5}Mg_5CeO_x$

In contrast with CO_2 temperature-programmed desorption (TPD), $^{13}CO_2/^{12}CO_2$ exchange methods probe the density and reactivity of basic sites at reaction temperatures, without contributions from unreactive carbonates and without disrupting the steady-state surface composition of the catalytic solid. The competitive adsorption of CO_2 with aldol-coupling precursors on basic sites appears to be one of the hurdles in achieving high isobutanol synthesis rates at low temperatures, making CO_2 a relevant probe of basicity on isobutanol synthesis catalysts.

As shown in Table 3.2, the surface density of available basic sites on MgO at 573 K is 0.38 x 10^{-6} mol/m^2. This site density is much lower than the value of 18.3 x 10^{-6} mol/m^2 reported for MgO surface oxygen density [82], and it corresponds to about 2.1 % of these surface oxygen in MgO acting as basic sites available for $^{13}CO_2/^{12}CO_2$ isotopic

exchange reaction at 573 K. This number (2.1 %) is lower than the values reported by Davis et al. [82] (25 %) and Kurokawa et al. [83] (10 %) using CO_2 TPD. This is not unexpected since the $^{13}CO_2/^{12}CO_2$ isotopic switch method only probes the number of basic sites that participate in the exchange reactions near 573 K. Weakly basic sites are mostly unoccupied by CO_2 and strongly interacting basic sites do not exchange in the time scale of isotopic exchange experiment. The number of basic sites given by Davis and Kurokawa, however, include both weak and strong basic sites that are not detected by the isotopic exchange method. Neither strong nor weak basic sites are likely to contribute to catalytic reactions at temperatures similar to those of the isotopic switch experiments. The CO_2 TPD results shown in Table 3.2 do not reflect the total but the number of basic sites that release CO_2 below 573 K. It should be pointed out that the basicity of MgO depends strongly on the source, purity, preparation procedures, and calcination temperatures of MgO [84 - 85]. All these variables affect the concentrations of surface OH species (weak basic sites) and coordinately unsaturated oxygen (O_{cus}, strong basic sites) sites like steps, corners, and edges.

Basic site densities in CeO_2 determined by either isotopic exchange or CO_2 TPD method are higher than on MgO (Table 3.2). This does not necessarily mean that CeO_2 is a stronger base than MgO, because the stronger basic sites on MgO are not probed by $^{13}CO_2/^{12}CO_2$ exchange experiment at 573 K, they are also not catalytically relevant. $^{13}CO_2/^{12}CO_2$ exchange experiments carried out on a CeO_x sample without 5 % H_2/He reduction at 623 K show a similar density of basic sites and strength compared to the sample subject to H_2 treatment, suggesting that H_2 treatment at 623 K did not affect the properties of available basic sites at 573 K.

The presence of small amounts of CeO_x in MgO (Mg/Ce = 5) increases the density (Table 3.2) of basic sites kinetically accessible for exchange reactions at 573 K. Similar phenomena have been reported by Rane et al. [86] using a CO_2 temperature programmed desorption. These authors observed a marked increase in the number of both weak and strong basic sites per gram of catalyst upon addition of ceria to MgO. The electron density and consequently the basicity of oxygen ions associated with both Ce^{4+} and Mg^{2+} cations are expected to be different from the ones bonded only to Ce^{4+} or Mg^{2+} ions. As mentioned early, MgO surfaces may have a high density of very strong basic sites, but which are not probed by $^{13}CO_2/^{12}CO_2$ exchange or involved in catalytic reactions near 573 K. The presence of Ce^{4+} ions, because of their higher electron affinities compared to Mg^{2+} ions, tend to attract electrons from the oxygen ions associated with Mg^{2+}, resulting in a decrease in *electron* density and basic strength of these oxygen ions and therefore makes them available for exchange (and catalysis) at 573 K.

The presence of Cu in $MgCeO_x$ samples slightly increase the basic site density (Table 3.2). Ikawa and co-workers [83] have reported recently that the distribution of surface basicity on MgO is not modified by the presence of Cu^{2+} ions even though the basic site density increased significantly. They proposed that the larger Cu^{2+} ion is introduced into the MgO lattice, which causes a distortion in the lattice and leads to an increase in the Mg-O bond length and in the localization of electrons near the oxygen ions. The slight increase in basic site density in $Cu_{0.5}Mg_5CeO_x$ compared to Mg_5CeO_x may reflect instead the contribution of adsorption sites associated with Cu^{2+} ions because Cu metal in the pre-reduced sample could be oxidized by CO_2 during the $^{13}CO_2/^{12}CO_2$

exchange experiment at 573 K. In fact, during CO_2 temperature programmed desorption experiments where Cu is likely to remain metallic, the number of basic sites is lower in $Cu_{0.5}Mg_5CeO_x$ than in Mg_5CeO_x.

The addition of K (1.1 wt %) increases not only the density of basic sites on $Cu_{0.5}Mg_5CeO_x$ (Table 3.2) but also the strength of basic sites. An increase in K loading from 1.1 to 3.5 wt % increased basic site density from 2.3 to 5.2 x 10^{-6} m^2/g. Because of the lower electron affinity of K^+ compared to Mg^{2+}, oxygen ions in K_2O have larger negative charge, and therefore are more basic than that those in MgO. Moreover, the oxygen ions connected with both K^+ and Mg^{2+} ions are expected to have higher electron density compared to ones associated with only Mg^{2+}, resulting in the formation of additional basic sites, which are available for exchange in pure MgO.

Calcination of Mg-Al hydrotalcite (magnesium-aluminum hydroxycarbonate) structures results in a mixed-oxide solid solution with high surface area and high thermal and hydrothermal stability. This material is active for base-catalyzed reactions, including aldol-condensation and double bond isomerization reactions [87], [88]. Stork and co-workers [88] used Hammett indicators and the kinetics of double-bond isomerization to suggest that $MgAlO_x$ oxides exhibit strong basic sites similar to those of pure MgO. McKenzie et al. [82] using temperature-programmed desorption of CO_2 and the decomposition of 2-propanol and Dumesic et al. [89] using microcalorimetric measurement of CO_2 heat of adsorption concluded that $MgAlO_x$ mixed-metal oxides are weaker bases than pure MgO. In this study, the basicity of $MgAlO_x$ mixed-metal oxides was measured by using both temperature-programmed desorption of CO_2 and $^{13}CO_2/^{12}CO_2$ isotopic exchange methods and the results are shown in Table 3.3.

Table 3.3. Composition, surface area, basic site density of mixed metal oxides

Sample	K (wt %)	Surface Area (m^2/g)	$^{13}CO_2/^{12}CO_2$ exchange at 573 K ($\mu mol/m^2$)	$^{13}CO_2/^{12}CO_2$ exchange at 473 K ($\mu mol/m^2$)	$^{13}CO_2$ TPD at T < 573 K ($\mu mol/m^2$)	$^{13}CO_2$ TPD at T< 723 K ($\mu mol/m^2$)
$MgAlO_x$	0.08	230	0.21	0.25	0.50	0.66
Mg_3AlO_x	0.02	238	0.17	0.21	0.34	0.50
Mg_5AlO_x	0.02	184	0.10	0.09	0.30	0.41
MgO	/	125	0.35	0.43	1.17	1.50

The basic site density on MgO determined by the $^{13}CO_2/^{12}CO_2$ exchange method is higher than on all $MgAlO_x$ samples (Table 3.3), suggesting that the addition of Al to MgO decreases the number of basic sites kinetically available at 573 K. The basic site density in Mg_5AlO_x is lower than in MgO, suggesting that the presence of AlO_x decreases the basicity of MgO, possibly due to the formation of a Mg-Al-O solid solution. The higher basic density (Table 3.3), though with high Al content, observed on $MgAlO_x$ and Mg_3AlO_x than on Mg_5AlO_x, suggests that the existence of separate domains of MgO and

Al_2O_3 in $MgAlO_x$ and Mg_3AlO_x samples. Only surface MgO contributed to the number of measured basic sites. The basic site density, however, was calculated based on the total surface area (MgO + Al_2O_3). This leads to lower basic site density without any effect on the strength distribution of basic sites related to MgO. Based on the $^{13}CO_2/^{12}CO_2$ isotopic exchange results, one can conclude that MgO and Al_2O_3 exist in separate phase, i.e., no solid solution formed in $MgAlO_x$ and Mg_3AlO_x samples.

The local slope in this semi-logarithmic plot reflects exchange dynamics and thus the kinetic behavior of basic sites. The curvature of the semi-logarithmic curve indicates the heterogeneity of surface basic sites since a linear line would be expected of a uniform surface. Short relaxation times (e.g. 0.1 wt % K) reflect short CO_2 surface lifetimes, high exchange rates, and more weaker basic sites. The distribution of basic site strength was determined using the inverse Laplace transform of the $^{13}CO_2$ transient curve according to the method described by DePontes et al. [90]. For a first-order $^{13}CO_2/^{12}CO_2$ exchange reaction on a uniformed surface, i.e., only one type of reactive site, the intrinsic desorption rate of $^{13}CO_2$ is

$$r(t) = q_0 \cdot k \cdot \exp(-kt) \qquad (1)$$

Where θ_0 is the initial surface coverage of $^{13}CO_2$ and k is the first-order intrinsic desoprtion rate constant. For a nonuniform surface with a distribution of exchange rate constant, the total exchange rate at any time during the transient can then be represented by

$$r(t) = q_0 \int_0^\infty kf(k) \cdot \exp(-kt) \cdot dt \qquad (2)$$

Where f(k)dk is the fraction of the total number of kinetically accessible basic sites with exchange rate constants between k and k+dk. Two approaches can be taken to obtain the distribution function f(k). One approach is based on a constrained, standard Tikhonov regularization of first-kind Fredholm integral equations (e.g., Eq. (3)) [91], [92]. This method, though less subjective and more exact, but computationally more demanding that the inverse Laplace transform method introduced by Bell and coworkers [90]. Bell's approach starts by recognizing that r(t) represents the Laplace transform of $\theta_0 kf(k)$. One could, therefore, determine f(k) by taking the inverse Laplace transform of the experimental values of r(t) and then dividing it by $k\theta_0$. Because this method has been found to provide reasonable relative pool sizes and reactivity-distribution and is computationally less demanding [90], [91], it will be used to determine the distribution of exchange rate constant.

The distribution of exchange rate constants (Figures 3.5b,c) obtained using inverse Laplace transform deconvolution methods is shown in Figure 3.5 b, c [90]. The results suggest that K increases the strength of the available CO_2 adsorption sites. The distribution curves were normalized to give an area of unity. The y-axis represents the distribution function f(k).

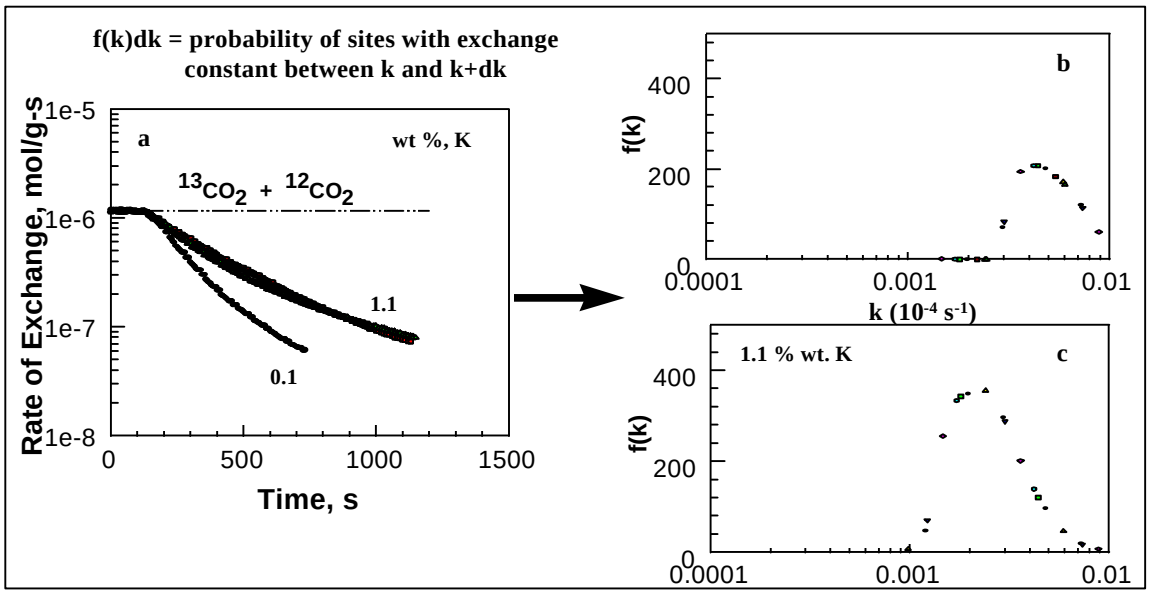

Figure 3.5. Exchange methods probe dynamics on non-uniform surface of K-$Cu_{0.5}Mg_5CeO_x$.

As mentioned earlier, the amount of $^{13}CO_2$ reversibly adsorbed at 573 K, n_e (mol/g), was calculated from the areas under $^{13}CO_2$ and Ar decay curves after correcting mass spectral data for their respective response factors. The amount of $^{13}CO_2$ reversibly adsorbed is not influenced by carrier gas flow rate. This is not surprising since the exchangeable amount is coverage-dependent and the coverage depends on CO_2 gas phase concentration. An isotherm for reversibly adsorbed $^{13}CO_2$ on 3.5 wt% K-$Cu_{0.5}Mg_5CeO_x$ was obtained by relating n_e to C_0, the gas phase concentration of CO_2 ($^{13}CO_2$ + $^{12}CO_2$). The results are shown in Figure 3.8. The amount of CO_2 adsorbed (n_e) increases slightly from 3.8 x 10^{-4} mol/g to 4.7 x 10^{-4} mol/g as the CO_2 gas phase concentration increases by an order of magnitude. This is consistent with a Langmuir-type adsorption isotherm (Equation 1) as the surface approaches saturation coverage.

$$n_e = \frac{K \cdot C_0}{1 + K \cdot C_0} \cdot n_s \,, \qquad (1)$$

where K is the adsorption equilibrium constant and n_s is the amount of $^{13}CO_2$ reversibly adsorbed at saturation coverage.

The number of $^{13}CO_2$ molecules adsorbed at 573 K and a CO_2 gas phase concentration of 2.1 x 10^{-7} mol/cm^3 is 4.7 x 10^{-4} mol/g, corresponding to a surface density of CO_2-binding sites of 7.6 x 10^{-6} mol/m^2 on 3.5 wt % K-$Cu_{0.5}Mg_5CeO_x$. The density of surface oxygen atoms on pure MgO is 18.3 x 10^{-6} mol/m^2 [82] suggesting that about 40 % of the surface oxygen atoms reversibly adsorb $^{13}CO_2$ at 573 K. The actual $^{13}CO_2$ surface coverage may be greater than 0.4 since some of the adsorbed $^{13}CO_2$ desorbs at undetectable rate at 573 K and the surface of 3.5 wt % K-$Cu_{0.5}Mg_5CeO_x$ contains other components contributing to its surface area.

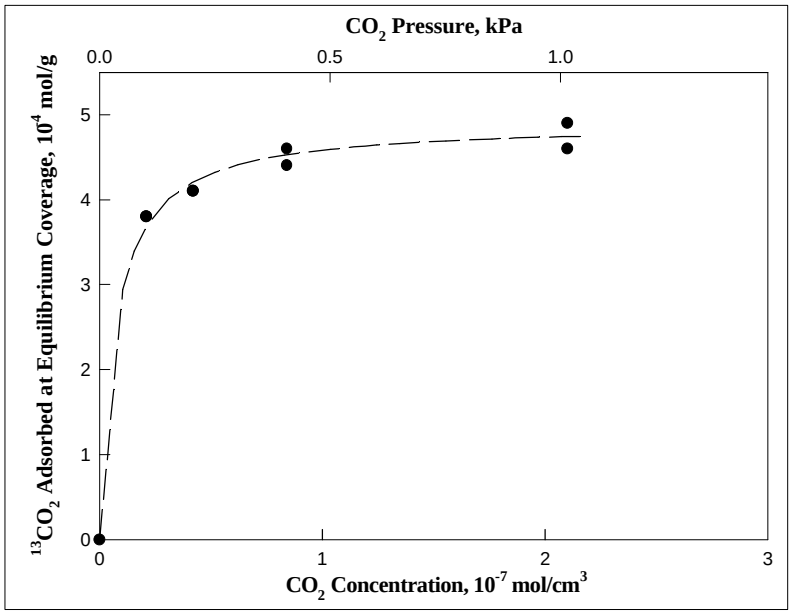

Figure 3.6. Adsorption isotherm of $^{13}CO_2$ on 3.5 wt % K-$Cu_{0.5}Mg_5CeO_x$ at 573 K (1.7 x 10^8 cm^3/mol).

As discussed previously, CO_2 desorption processes are first-order in surface concentration and the local slope of a transient decay curve plotted in a semi-logarithmic scale gives the desorption rate constant. A large value of this slope reflects rapid desorption and a large value of this rate constant. In Figure 3.7a, the slope of the transient decay curve at short times, and therefore the desorption rate constant for sites with the highest desorption rates, increases with increasing concentration of CO_2 in the gas phase. As discussed in the introduction section, the enhancement of desorption rates by gas phase CO_2 could then be attributed to the higher surface coverage of adsorbed CO_2 present at the higher gas phase concentration levels. In such a proposal, repulsive interactions among adsorbed CO_2 would then lead to lower desorption activation energies as CO_2 coverages increase and therefore to faster desorption processes. In this study, the surface coverage by reversibly adsorbed CO_2 increases only from 6.1 x 10^{-6} to 7.6 x 10^{-6} mol/m^2 as CO_2 gas phase concentrations increase from 2.1 x 10^{-8} to 2.1 x 10^{-7} mol/cm^3. The large change in desorption rate constant appears surprising, in view of the limited range of surface densities giving rise to these marked changes in kinetic parameters.

In our experiments, the desorption rate constant for adsorbed $^{13}CO_2$, however, depends not only on the concentration of $^{12}CO_2$ in the gas phase but also on the flow rate of the carrier stream carrying this $^{12}CO_2$ (Figure 3.7b). Desorption rate constants appear to increase with increasing carrier gas flow rate. Clearly, changes in surface coverage alone cannot account for these effects, because in the absence of readsorption, the surface coverage cannot be influenced by the rate at which desorption products are removed by a carrier gas. The surface is always in chemical equilibrium with the gas phase and this equilibrium surface coverage is controlled only by the temperature and the CO_2 concentration in the gas phase, neither of which changes with changes in carrier gas flow rate. Thus, changes in desorption activation energies caused by differences in surface

coverage cannot account for the effects of flow rate on the apparent desorption rate constant (Figure 3.7b). We consider below the proposal that readsorption of desorbed CO_2 accounts for both gas phase concentration and flow rate effects on the rate of $^{13}CO_2$ desorption.

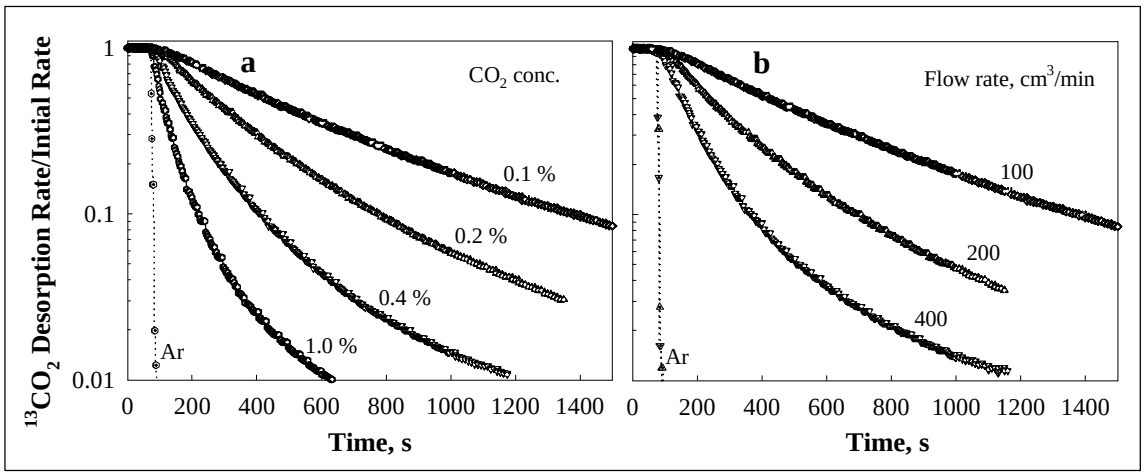

Figure 3.7. Effects of CO_2 concentration and total flow rate on the desorption rate of preadsorbed CO_2 on a 3.5 wt % K-$Cu_{0.5}Mg_5CeO_x$ catalyst. [75 mg catalyst charge, 573 K]

The promoting effect of the gas phase on desorption rates was previously reported for desorption of CO from Group VIII transition metals. Our study shows that such effects appear to be quite general and apply to a different adsorbate on metal oxide surfaces. In a previous study, Herz *et al*. [93] carried out temperature-programmed desorption studies of CO on a thin wafer of a supported Pt catalyst and showed that significant readsorption occurred whether the desorption of CO took place in a flowing carrier gas or in a high vacuum system. In fact, adsorption-desorption equilibrium was approached closely during desorption and the obtained desorption spectra reflected the thermodynamics, rather than the kinetics of desorption. The conditions of these experiments by Herz *et al*. [93] were typical of most experimental studies of CO desorption from catalytic solids. The increase in $^{13}CO_2$ desorption rate with increasing $^{12}CO_2$ gas phase concentration or increasing carrier flow rate can be explained by taking into account the ubiquitous readsorption of the desorbed $^{13}CO_2$ during our experiments. Readsorption effects also explain the similar "adsorption-assisted" phenomena reported previously by others [94], [95].

For a given sample, the number of adsorption sites, n_s (mol/g), occupied by CO_2 when all surface sites are covered (saturation coverage) is independent of flow rate and gas phase composition. At conditions of chemical equilibrium, the number of adsorption sites, n_e, actually occupied by CO_2 increases with gas-phase CO_2 concentration, initially in a linear manner but then only slightly as saturation coverages are approached (Equation 1). The number of unoccupied adsorption sites (n_s-n_e) at equilibrium is small and inversely proportional to the CO_2 gas phase concentration at conditions approaching

saturation coverage, as shown by equation 2 as the KC_o term in the denominator becomes larger than unity:

$$n_s - n_e = \frac{n_s}{1 + K \cdot C_0} \qquad (2)$$

Therefore, the density of unoccupied adsorption sites (n_s-n_e) decreases and the probability that desorbed $^{13}CO_2$ will readsorb also decreases with increasing concentration of $^{12}CO_2$ in the gas phase. In effect, as CO_2 gas phase concentration or carrier gas flow rate increase, we measure a net desorption rate that becomes closer to the intrinsic (unidirectional) rate of desorption, uncorrupted by its reverse step - the readsorption of $^{13}CO_2$. It should be pointed out that we only treat the initial part of the decay, i.e., the compartment on the surface with the fastest desorption rate using Langmuir-type adsorption isotherm.

A rigorous mole balance on $^{13}CO_2$ in a flow system subjected to a $^{13}CO_2$ to $^{12}CO_2$ switch at zero time is given by:

$$-\left[\left(\frac{d}{dt}\theta^{13}\right)\cdot N_s\right] = k_d \cdot \theta^{13} \cdot N_s - k_a \cdot C^{13} \cdot \left(N_s - N_e\right) \qquad (3)$$

and

$$-\left[\left(\frac{d}{dt}\theta^{13}\right)\cdot N_s\right] = F \cdot C^{13} \qquad (4)$$

when the pseudo-steady-state hypothesis is valid. In this hypothesis, $^{13}CO_2$ desorption rate from the surface equals the rate of $^{13}CO_2$ coming out of the reactor. This is valid only when the void volume of the catalyst bed is small and therefore no accumulation of $^{13}CO_2$ in the void volume shortly after CO_2 isotopic switch. In these expressions, θ^{13} is the fraction of adsorption sites occupied by $^{13}CO_2$ at any time after the switch, C^{13} is the gas phase concentration of $^{13}CO_2$ (mol/cm^3), C_0 is the total gas phase concentration of CO_2, irrespective of isotopic label (mol/cm^3), N_s is the number of adsorption sites occupied by CO_2 at saturation coverage (mol), N_e is the number of adsorption sites occupied by CO_2 at thermodynamic equilibrium (mol), F is the volumetric gas flow rate (cm^3/s), and k_a (cm^3/mol-s) and k_d (s^{-1}) are the adsorption and desorption rate constants, respectively. The solution to the above equations describes the decay curve for $^{13}CO_2$ concentration in the effluent:

$$C^{13} = \frac{N_e \cdot k_d}{F + \frac{N_e \cdot k_d}{C_0}} \cdot \exp\left[-\frac{k_d}{1 + \frac{N_e \cdot k_d}{F \cdot C_0}} \cdot t\right] \qquad (5)$$

We note that if we define an apparent desorption rate constant k_d':

$$k'_d = \frac{k_d}{1 + \frac{N_e \cdot k_d}{F \cdot C_0}} \qquad (6)$$

Equation (5) can then be rewritten as:

$$r^{13} = F \cdot C^{13} = N_e \cdot k'_d \cdot \exp\left(-k'_d \cdot t\right) \qquad (7)$$

The desorption rate corresponds to that for a first-order rate expression with a pseudo-kinetic rate constant k_d', which can be obtained from the initial slope of a semi-logarithmic plot. As shown by equation 6, this apparent rate constant carries kinetic information (k_d), but also experimental variables such as carrier gas flow rate and CO_2 gas phase concentration and thermodynamic properties reflected in the value of N_e. The measurement of unidirectional rate of desorption using initial slope is corrupted by the presence of a significant rate of the reverse reaction, i.e., the readsorption of desorbed $^{13}CO_2$.

The apparent rate constant defined by Equation (6) can be re-written as:

$$\frac{1}{k'_d} = \frac{1}{k_d} + \frac{W_g \cdot n_e}{C_0} \cdot \frac{1}{F} \qquad (8)$$

where W_g is the mass of sample used (g) and n_e (N_e/W_g) is the density of sites available for CO_2 adsorption-desorption processes (mol/g-cat) at a given temperature on a given sample. This site density is unaffected by readsorption processes and independent of carrier gas flow rate; it is obtained directly from the area under the $^{13}CO_2$ decay curves. A description of the dynamics of these decay curves, however, requires that we account for readsorption effects that decrease the net rate of desorption of $^{13}CO_2$ from surfaces .

For a given material and mass of sample, we observe that the apparent rate constant k_d' increases with increasing flow rate and gas phase CO_2 concentration (Figures 3.7a and 3.7b). The reciprocal of the value of k_d' (obtained from the initial slope of the semi-logarithmic plot of the data in Figure 3.7) is plotted as a function of the reciprocals of CO_2 concentration and flow rate in Figures 3.8a and 3.8b, respectively. The linear plots in Figures 3.8a and 3.8b are consistent with the form of the apparent desorption rate constant suggested by Equation (8). The slopes in Figure 3.8 depend only on the equilibrium amount of adsorbed CO_2 (n_e) at 573 K. It should be pointed out that n_e does not change with increasing carrier flow rate but increases slightly as CO_2 gas phase concentration increases from 2.1 x 10^{-8} to 2.1 x 10^{-7} mol/cm^3. The increase in the apparent desorption rate constant of $^{13}CO_2$ with increasing carrier gas flow rate and gas phase CO_2 concentration has also been observed on 1.0 wt % K-MgO samples. It should be noticed that $1/k_d'$ goes to zero as the abscissa goes to zero, suggesting that the intrinsic rate of desorption is very large. This is not surprising since we measure the initial slope of the decay curves and therefore probe almost by definition those sites that desorb fastest at the conditions of the experiment.

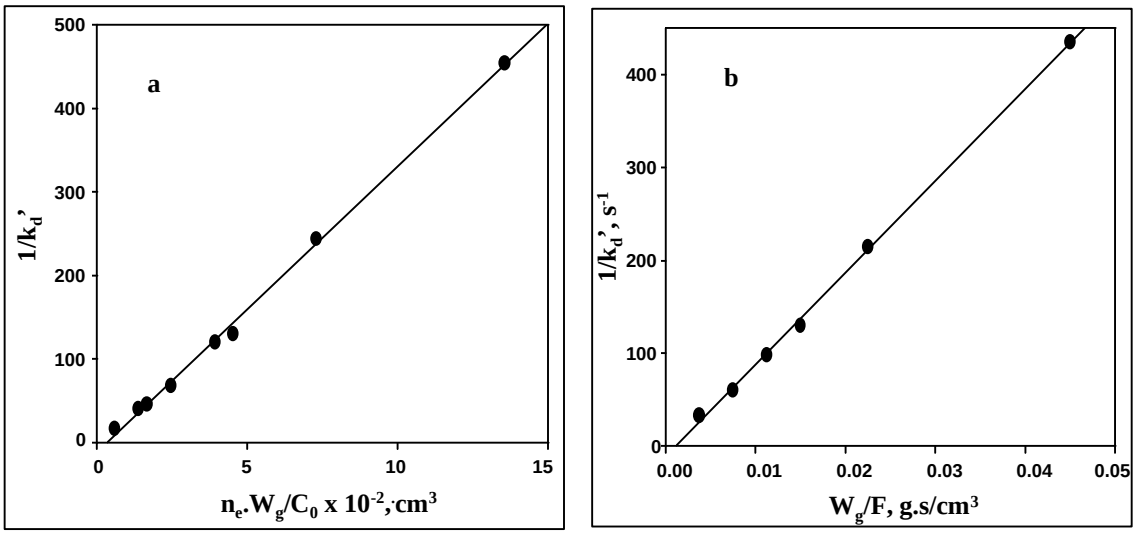

Figure 3.8. Effects of total gas phase CO_2 concentration (C_o), carrier gas flow rate (F), and amount of sample on the apparent desorption rate constant (k_d') for $^{13}CO_2$ desorption from 3.5 wt % K-$Cu_{0.5}Mg_5CeO_x$ at 573 K.

These data show that higher $^{12}CO_2$ gas phase concentrations lead to higher net $^{13}CO_2$ desorption rates because the probability that a desorbed $^{13}CO_2$ molecule will readsorb decreases with increasing surface coverage of CO_2 species and decreasing surface vacant adsorption sites, irrespective of their isotopic label. The desorption rate constant reported by Tamaru *et al*. [95] for CO on Pd polycrystalline surfaces may have also been influenced by readsorption phenomena because the rate of desorption was measured under such conditions that the adsorption was actually proceeding. If unlabeled gas phase CO can adsorb on Pd polycrystalline surfaces during the desorption process of labeled CO, it is reasonable to expect the occurrence of readsorption of the desorbed CO and the relative rates depend exclusively on the abundance of the two isotopes in the gas phase. As reported by Tamaru *et al*. [95] surface concentration of CO increases by < 5 % as gas phase CO pressure increased from 2 x 10^{-6} to 13 x 10^{-6} Pa at 339 K, suggesting the approaches of surface saturation coverage of CO. Although surface CO concentration increases slightly, the desorption rate constant increases by at least a factor of 2. It is surprising that the enhanced intermolecular repulsive interaction due to the slightly increased surface coverage could cause the dramatic increase in CO_2 desorption rate. The kinetic parameter that characterizes the unidirectional desorption rate may be much larger than those measured when readsorption occurs during desorption processes. At higher CO_2 pressure, fewer vacant sites are available for readsorption of the desorbed $^{13}CO_2$ and desorption rates approach their values for the unidirectional desorption process.

Significant readsorption of desorbed $^{13}CO_2$ occurs during isotopic switch experiments with 0.1% $^{12}CO_2$/He as a carrier on K-promoted $Cu_{0.5}Mg_5CeO_x$ even at the highest carrier flow rates (200 cm^3/min) and smallest catalyst samples (25 mg). The corresponding residence times within the sample bed at these conditions are expected to be shorter than those used in typical temperature-programmed desorption studies of CO_2 on basic oxides (typical flow rate is 200 cm^3/min for 50-100 mg of catalyst) [96].

Figure 3.9 shows the temperature-programmed desorption spectrum of $^{13}CO_2$ preadsorbed on 3.5 wt % K-$Cu_{0.5}Mg_5CeO_x$ (25 mg) when the carrier gas is pure He (200 cm^3/min) (curve a). Two distinct peaks with different intensity appear at about 434 K and 656 K. When 0.1 % $^{12}CO_2$/He is used as the carrier gas the $^{13}CO_2$ TPD spectrum shifts to lower desorption temperatures, but retains the two peaks with intensities higher than those observed in a He carrier gas (Figure 3.9, curve b). The high-temperature desorption peak decreases from 656 K to 640 K and the low temperature feature appears to move to even lower temperature when gas phase $^{12}CO_2$ is present. The number of desorbed $^{13}CO_2$ molecules is significantly larger when $^{12}CO_2$ is present in the carrier gas stream. If the desorption temperature kept increasing, the number of $^{13}CO_2$ molecules desorbed in both He and 0.1% $^{12}CO_2$/He stream is expected to be similar because the number of pre-adsorbed $^{13}CO_2$ in these two experiments is identical.

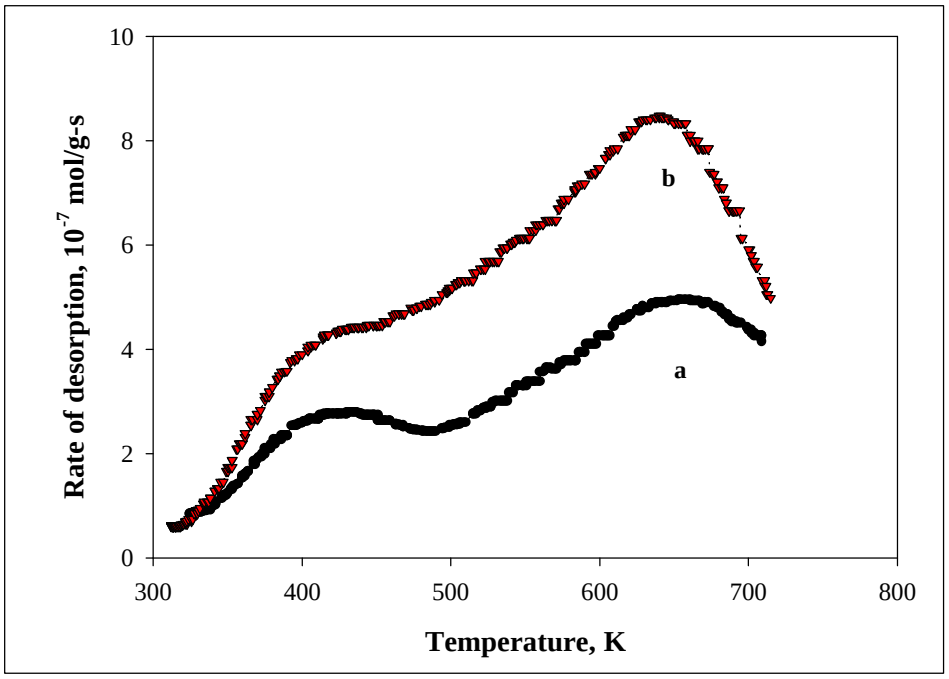

Figure 3.9. $^{13}CO_2$ TPD from 3.5 wt % K-$Cu_{0.5}Mg_5CeO_x$ in He (a) and (b) in 0.1 % $^{12}CO_2$/He [25 mg catalyst charge, 200 cm^3/min]

The promoting effect of gas phase $^{12}CO_2$ on the observed $^{13}CO_2$ desorption rate has also been observed on 1.0 wt % K-MgO, as evidenced by the increased desorption rate in the presence of 0.1 % $^{12}CO_2$ (Figure 3.10). Increasing $^{12}CO_2$ concentration results in further increase in the desorption rate. It should be pointed out that the presence of gas phase $^{12}CO_2$ causes the disappearance of the shoulder peak around 570-580 K observed in He flow (Figure 3.10, curve a). The presence of gas phase $^{12}CO_2$ may shift this peak to lower temperatures because readsorption is inhibited when $^{12}CO_2$ adsorbed on otherwise unoccupied surface sites. Since there are at least four desorption peaks (around 370 K, 425 K, 500 K, and 580 K) in $^{13}CO_2$ TPD spectrum in He flow (Figure 3.10, curve a), it is difficult to establish which peak in curves b and c corresponds to the peak in curve a.

The minimization of readsorption in the presence of gas phase CO_2 will definitely shift the desoprtion peaks to lower temperatures.

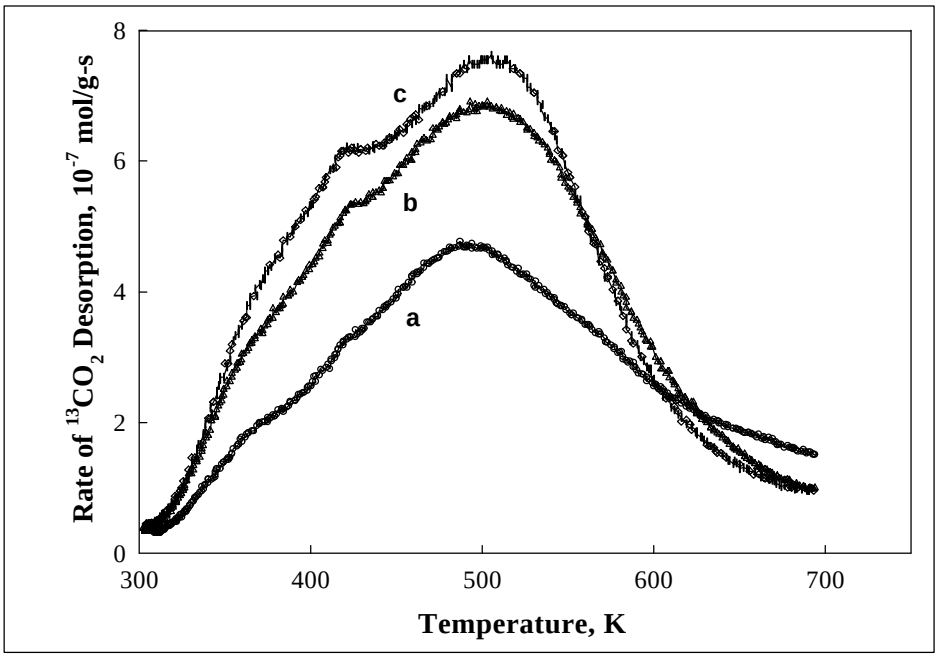

Figure 3.10. $^{13}CO_2$ TPD from 1.0 wt % K-MgO in He (a), (b) in 0.1 % $^{12}CO_2$/He, and (c) in 0.4 % $^{12}CO_2$/He [25 mg catalyst charge, 200 cm^3/min]

The surface coverage of $^{13}CO_2$ for a given sample at the start of the temperature ramp is identical in these types of TPD experiments. In the presence of $^{12}CO_2$, however, the total surface coverage of CO_2 ($^{13}CO_2$ + $^{12}CO_2$) is higher at every temperature than when pure He is used as the carrier gas. Meanwhile, the probability of readsorption increases as $^{13}CO_2$ desorbs from the surface and unoccupied adsorption sites rapidly form, until at higher temperatures the surface is almost bare and the sticking coefficient for colliding CO_2 molecules is very high. In the presence of a constant gas phase concentration of $^{12}CO_2$, the total surface coverage of CO_2 remains higher at every temperature and they depend only on the equilibrium coverage at each temperature. Then, as $^{13}CO_2$ is depleted from the surface, vacant adsorption sites are occupied by the majority $^{12}CO_2$ species in the gas phase; therefore, readsorption of desorbed $^{13}CO_2$ is minimized. It is well known that readsorption will shift the desorption peak to higher temperatures (101). Thus, it is not surprising that higher gas phase $^{12}CO_2$ concentrations, which minimize readsorption, lead to a shift of desorption peaks to lower temperatures. The higher temperature $^{13}CO_2$ peak or at least part of it obtained in He flow (Figures 3.9 and 3.10) is caused by the readsorption of the $^{13}CO_2$ desorbed at lower temperature. In a TPD experiment of preadsorbed $C^{18}O$ on Ni(100) surfaces, Goodman et al. [97] have also reported a higher desorption rate and a shift of the desorption peak to low temperature in the presence of gas phase ^{12}CO. They suggest that the instantaneous high surface CO coverage in the presence of CO flux compared to that of desorption into vacuum during heating program favors desorption because of the lower desorption energy at high

coverages.The adsorption and desorption of CO on solid surfaces has been studied extensively by Tamaru and co-workers using isotopic jump methods [94], [95], [97] - [98]. They reported that the rate of $^{12}C^{18}O$ desorption from Pd and Rh polycrystalline surfaces is enhanced by gas phase $^{12}C^{16}O$. The desorption rate of $^{12}C^{18}O$ is found to be proportional to $^{12}C^{16}O$ gas phase pressure. This phenomenon has been called "adsorption-assisted desorption". Most of the experiments were performed under non-steady state conditions in which surface CO coverages changed with time. Zhdanov [99] claimed that the absolute rate of desorption in the experiments of Tamaru was overestimated by the treatment of their data. A mathematical model reveals that the desorption rate is independent of gas-phase pressure [99]. More recently, Weinberg et al. [Reference] studied the kinetics of adsorption and desorption of CO on Ir(111) surfaces using Fourier transform infrared reflection-adsorption spectroscopy (FT-IRAS). They found that the rates of CO desorption into vacuum and the desorption in the presence of an ambient CO background pressure are similar by taking into account the coverage-dependent rate coefficient of desorption. The "adsorption-assisted desorption" phenomenon for the Ir(111) surface has been excluded. The increased rate of $^{13}CO_2$ desorption from modified MgO with increasing gas phase $^{12}CO_2$ concentration, though in every aspect is similar to that reported by Tamaru and co-worker in CO/metal system, can be simply explained by the decreased probability of readsorption of desorbed $^{13}CO_2$ without using adsorption-assisted desorption theory.

The presence of gas phase $^{12}CO_2$ decreases the probability of readsorption for desorbed $^{13}CO_2$, and therefore also decreases the average surface lifetime of $^{13}CO_2$. The number of $^{13}CO_2$ desorbed from the surface in the absence of gas phase $^{12}CO_2$ is very small (Figure 3.11, region II), which is only about 5×10^{-5} mol/g. This accounts of about 10 % of the total number of $^{13}CO_2$ exchanged at 573 K in the presence of $^{13}CO_2$. The remaining $^{13}CO_2$ has very long surface lifetime (> 700 s). The difficulty in removing these $^{13}CO_2$ from the catalyst surface in He flow is due to 1) the readsorption of the desorbed $^{13}CO_2$ becomes more favorable as more free adsorption sites become available, and/or 2) the decrease in surface $^{13}CO_2$ coverage results in an increase in the desorption activation energy. The remaining 90 % of the exchangeable adsorbed $^{13}CO_2$ was displaced from the surface quickly when $^{12}CO_2$ was added into He stream (Figure 3.11, region III). This again suggests that the presence of gas phase $^{12}CO_2$ decreases the average surface lifetime of $^{13}CO_2$.

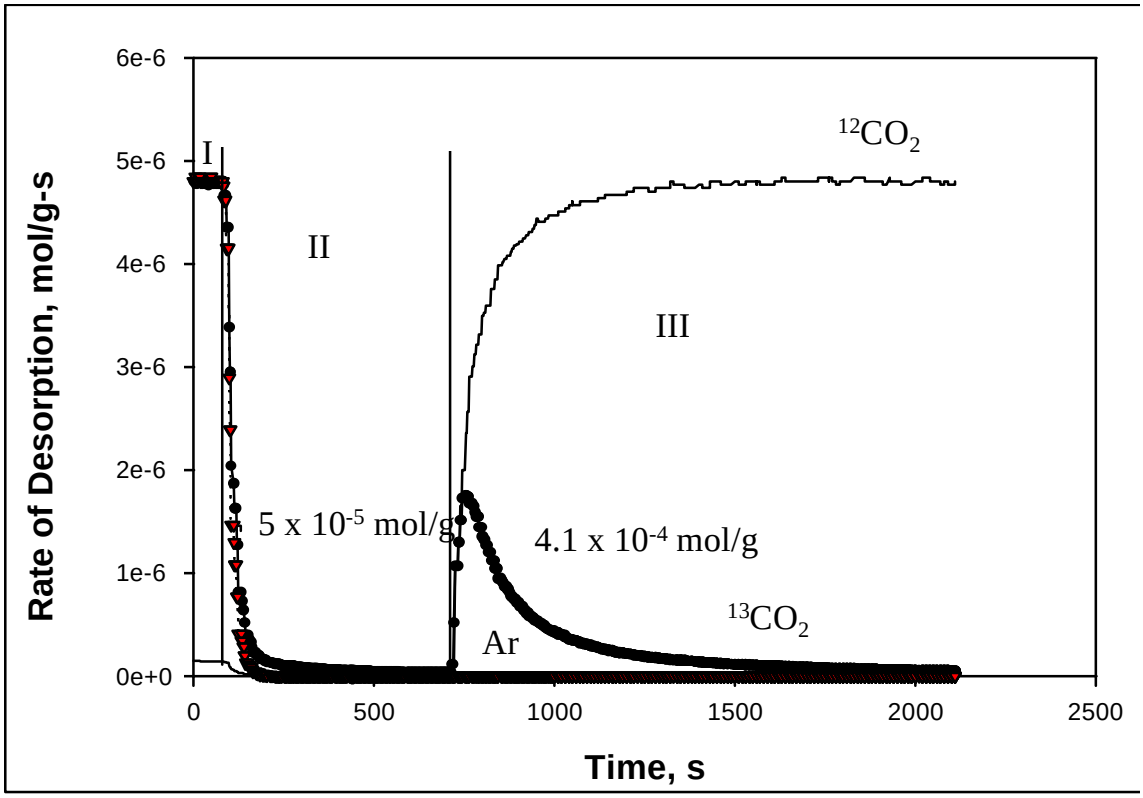

Figure 3.11: Desorption of $^{13}CO_2$ from 3.5 wt % K-$Cu_{0.5}Mg_5CeO_x$ surface in the absence and presence of gas phase $^{12}CO_2$ at 573 K [25 mg, 200 mL/min, I: 0.1 % $^{13}CO_2$/He, II: He, III: 0.1% $^{12}CO_2$/He]

The number of available basic sites determined at 573 K on 1.0 wt % K-$Cu_{0.5}Mg_5CeO_x$ by $^{13}CO_2/^{12}CO_2$ isotopic jump methods is 3.2 x 10^{-4} mol/g. As a comparison, the total number of basic sites has also been determined by temperature programmed desorption of $^{13}CO_2$. The $^{13}CO_2$ TPD experiment was carried out by first pretreating the catalyst in He at 723 K for 20 min, exposing $^{13}CO_2$ to the catalyst at 723 K, and lowering the temperature to 303 K in flowing 0.1 % $^{13}CO_2$/He. After saturation with $^{13}CO_2$, the sample was flushed with He and the temperature was increased to 573 K at 0.5 K/s in flowing He (200 mL/min) and kept at 573 K for 10 min. The amount of $^{13}CO_2$ desorbed between 303-573 K is 1.8 x 10^{-4} mol/g (Figure 3.12, region I). The temperature was further increased to 723 K and stayed at this temperature for another 10 min. The amount of $^{13}CO_2$ desorbed between 573-723 K is 0.7 x 10^{-4} mol/g (Figure 3.12, region II).

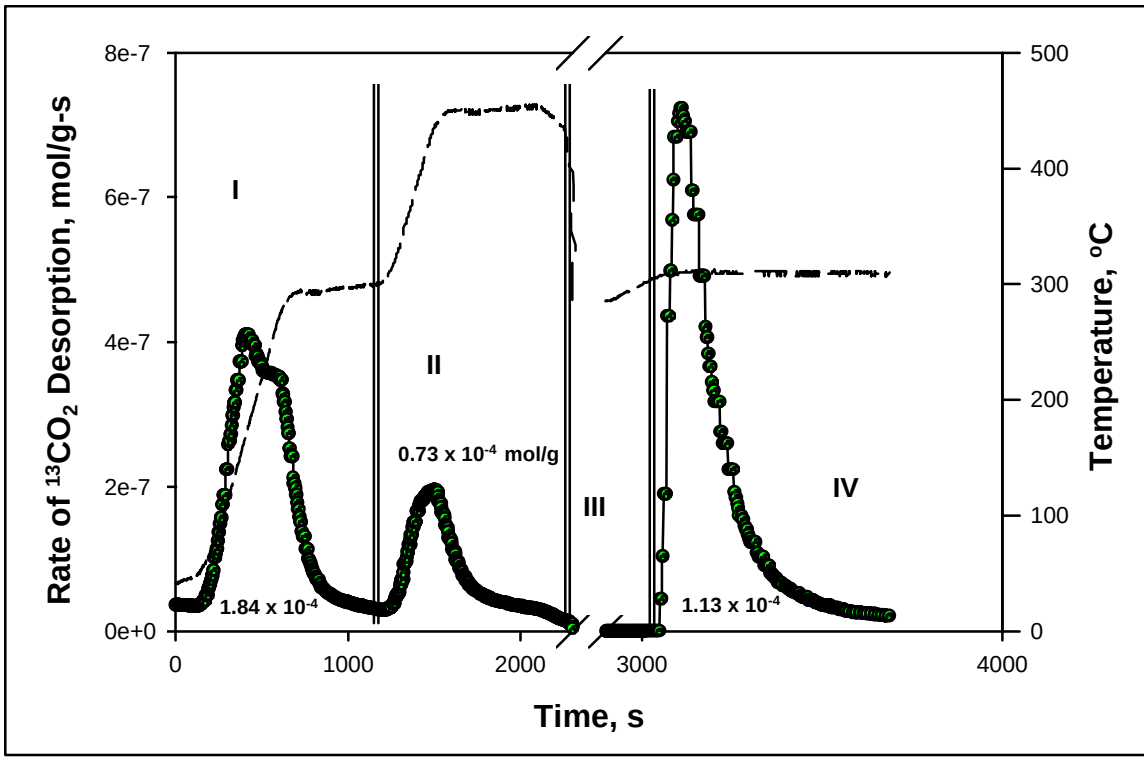

Figure 3.12. Desorption profile of $^{13}CO_2$ and reactor temperature vs. time on stream on 1.0 wt % K-$Cu_{0.5}Mg_5CeO_x$.

If a CO_2 adsorption isotherm experiment was conducted at 573 K on a 1.0 wt% K-$Cu_{0.5}Mg_5CeO_x$ sample pretreated at 723 K, one may expect that the amount of CO_2 irreversibly adsorbed is about 0.7 x 10^{-4} mol/g. The total amount of CO_2 desorbed below 723 K is 2.5 x 10^{-4} mol/g, which is less than the amount determined by $^{13}CO_2/^{12}CO_2$ exchange experiment (3.2 x 10^{-4} mol/g), even though the former contains physisorbed and weakly chemisorbed CO_2. After the TPD experiment at temperatures up to 723 K, the temperature was lowered to 573 K in flowing He and 0.1 % $^{12}CO_2$/He was introduced. *The introduction of $^{12}CO_2$ in the feed displaced more $^{13}CO_2$ from the catalyst surface at 573 K even though the catalyst was subject to He treatment at 723 K for more than 10 min* (Figure 3.12, region IV). The amount of $^{13}CO_2$ displaced by $^{12}CO_2$ is 1.1 x 10^{-4} mol/g. The total amount of $^{13}CO_2$ released from the surface is 3.6 x 10^{-4} mol/g (regions I + II + IV, Figure 3.12), which is larger than 3.2 x 10^{-4} mol/g determined in $^{13}CO_2/^{12}CO_2$ exchange experiment and the difference (0.4 x 10^{-4} mol/g) is the number weakly adsorbed sites that might not participate in the base-catalyzed reactions at 573 K.

As mentioned above, part of $^{13}CO_2$ remained on K-promoted $Cu_{0.5}Mg_5CeO_x$ after He treatment at 723 K can be displaced by gas phase $^{12}CO_2$ at 573 K. The amount displaced increases with increasing K loading. For example, only 0.13 x 10^{-4} mol/g $^{13}CO_2$ was displaced from 0.1 wt% K-$Cu_{0.5}Mg_5CeO_x$ and the amounts were increased to 1.13 x 10^{-4} mol/g and 2.10 x 10^{-4} mol/g for 1.0 wt% and 3.5 wt% K-$Cu_{0.5}Mg_5CeO_x$, respectively. Again, all these data were obtained by first heating the sample preadsorbed with $^{13}CO_2$ to 723 K in flowing He and staying at such temperature for 10 min. The temperature was then lowered to 573 K and the sample was exposed to 0.1 % $^{12}CO_2$/He

(200 mL/min) and $^{13}CO_2$ displaced was monitored by mass spectroscopy. The presence of K in $Cu_{0.5}Mg_5CeO_x$ increases the number of basic sites that bind $^{13}CO_2$ strongly at 723 K and provides a surface pool of $^{13}CO_2$ for exchange at 573 K. The addition of K to $Cu_{0.5}Mg_5CeO_x$ increases the number of stronger basic sites; this is consistent with the TPD results obtained on the samples with different K loadings (Figure 3.4)
A CO_2 TPD spectrum, however, can only provide qualitative information about basic strength. As we reported previously, $^{13}CO_2$ transient curves provide information about exchange dynamics of basic sites. Short relaxation times reflect short CO_2 surface lifetimes, high isotopic exchange rates, and weaker basic sites. The local slope in the semi-logarithmic plots of $^{13}CO_2$ transient curves reflects the dynamics of the first-order CO_2 exchange reaction and thus the exchange rate constant on available basic sites.

Unlike the density of site that reversibly adsorb CO_2, the observed exchange rate constant, i.e., the slope, however, is not a unique function of catalyst surface properties. It also depends on experimental parameters such as carrier gas flow rate (Figure 3.7b, 3.13) and CO_2 gas phase concentration (Figure 3.7a). The initial slope of the transient curve increases with increasing carrier flow rate, suggesting that we are not probing the intrinsic desoption rate constant because it is flow-rate and concentration independent. Applying the inverse Laplace transform to the transient curves obtained on 1.0 wt% K-MgO at different flow, one gets a distribution of kinetic available CO_2-binding sites that varies with carrier gas flow rate (Figure 3.14). The desorption rate constant at peak maximum increases from 0.006 to 0.03 s^{-1} as the carrier gas flow rate increases from 100 cm^3/min to 400 cm^3/min. The exchange capacity, i.e., the number of sites that reversibly adsorb does not change with flow rate at constant temperature and it is a unique property of catalyst surfaces.

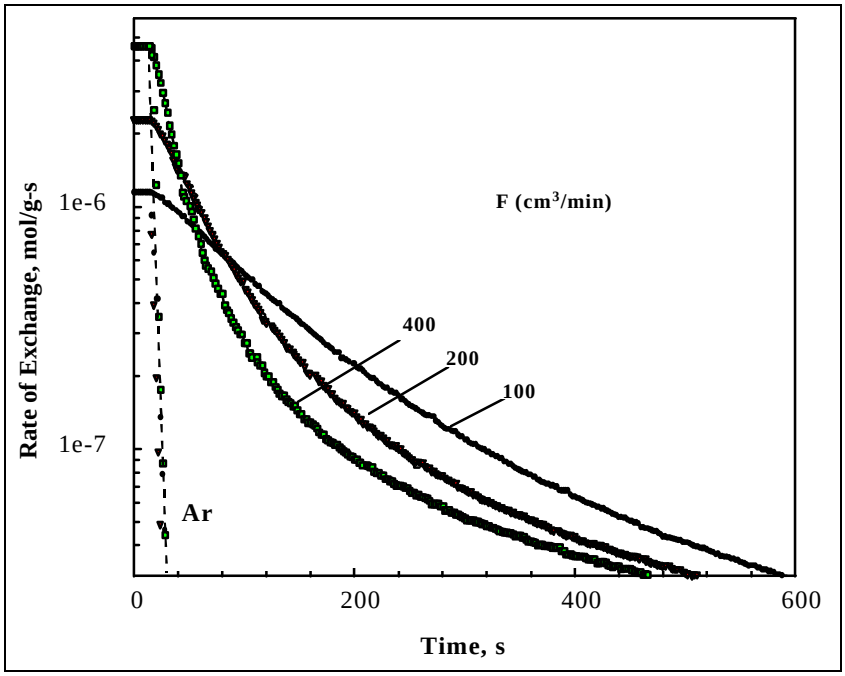

Figure 3.13. Effects of total flow rate on the desorption rate of preadsorbed CO_2 on a 1.0 wt % K-MgO catalyst. [50 mg catalyst charge, 573 K, 0.1 % CO_2/He]

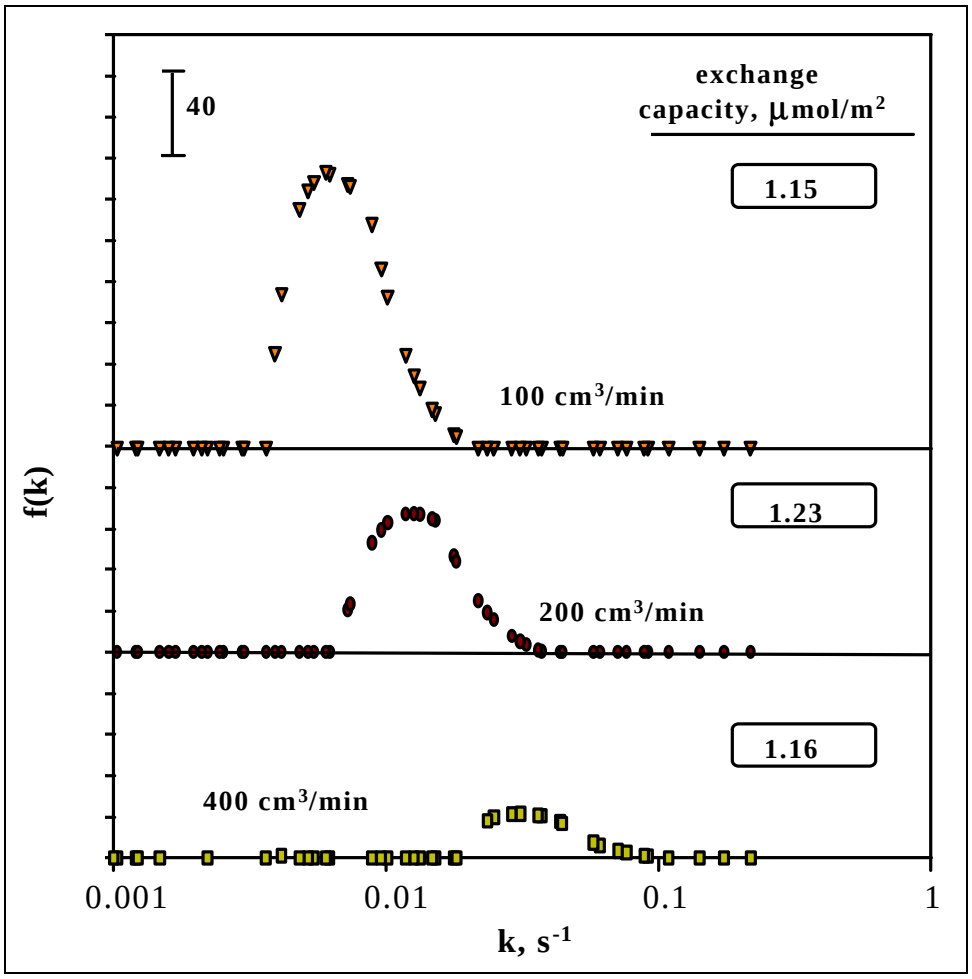

Figure 3.14. Distribution of CO_2 exchange rate constant on 1.0 wt % K-MgO at different flow rate. [75 mg of catalyst charge, 573 K, 0.1% CO_2/He]

The increased $^{13}CO_2$ desorption rates with increasing carrier gas flow rate are caused by a decrease in the probability of $^{13}CO_2$ readsorption [100]. By taking into account of the readsorption of the desorbed $^{13}CO_2$, a rate expression for $^{13}CO_2$ desorption from a uniform surface can be obtained:

$$r^{13} = F \cdot C^{13} = N_e \cdot k'_d \cdot \exp\left(-k'_d \cdot t\right) \qquad (3)$$

where

$$k'_d = \frac{k_d}{1 + \frac{N_e \cdot k_d}{F \cdot C_0}} \qquad (4)$$

and C^{13} is the gas phase concentration of $^{13}CO_2$ (mol/cm^3), C_0 is the total gas phase concentration of CO_2, irrespective of isotopic label (mol/cm^3), N_e is the number of adsorption sites occupied by CO_2 at thermodynamic equilibrium (mol), F is the volumetric gas flow rate (cm^3/s), and k_d (s^{-1}) are the adsorption and desorption rate constants.

It is still a first-order reaction expression (eq. 3), but the slope or rate constant, k_d', is a function of flow rate, gas phase CO_2 concentration, and equilibrium surface CO_2 coverage. Although equations 1 and 7 are similar, one cannot regard the distribution f(k_d) in Figure 3.14 as f(k_d'). In the work of DePontes et al. [90], the overall rate express (equation 2) was obtained by assuming a large number of surface pools that *react independently*. However, one cannot get a similar overall rate expression from equation 7 because each pool *does not* react independently due to readsorption. In the following sections, a four-parameter two-compartment model will be used in order to obtain the intrinsic CO_2 desorption rate constant on MgO.

The two-compartment model begins by assuming there are two types of CO_2 binding sites on MgO. This assumption is based on the infrared results of adsorbed CO_2 on MgO reported by Di Cosimo et al. [101]. Only unidnetate and bidentate species exist on MgO at 573 K. By applying mole balance on $^{13}CO_2$ in gas phase and each surface compartment subjected to a $^{13}CO_2$ to $^{12}CO_2$ switch, one can get:

- for gas phase

$$\tau \frac{dC_{^{13}CO_2}}{dt} = -C_{^{13}CO_2} - \tau \cdot \sum_{i=1}^{2} [k_{ai} \cdot C_{^{13}CO_2} \cdot (1-\theta_0) - k_{di} \cdot {}^{13}\theta_i] \qquad (5)$$

- for surface each compartment

$$\frac{d^{13}\theta_i}{dt} = k_{ai} \cdot C_{^{13}CO_2} \cdot (1-\theta_0) - k_{di}\theta_{^{13}CO_2} \qquad (6)$$

where k_a and k_d are the adsorption and desorption rate constants of CO_2. θ_0 is the total CO_2 surface coverage. The following four parameters in equations 5 and 6 were used to fit $^{13}CO_2$ transient curves obtained on MgO (Figure 3.15):

k_{d1}, k_{d2}, $K_1=k_{a1}(1-\theta_0)/k_{d1}$, and $K_2=k_{a2}(1-\theta_0)/k_{d2}$

K_1 and K_2 are CO_2 adsoprtion-desorption equilibrium constants. The theoretical (dashed lines) and experimental (data points) agrees well with each other if the following parameter values were used:

k_{d1}=0.0954 s^{-1}, k_{d2}=0.00461s^{-1}, K_1=0.991cm^3/mol, and K_2=0.740 cm^3/mol.

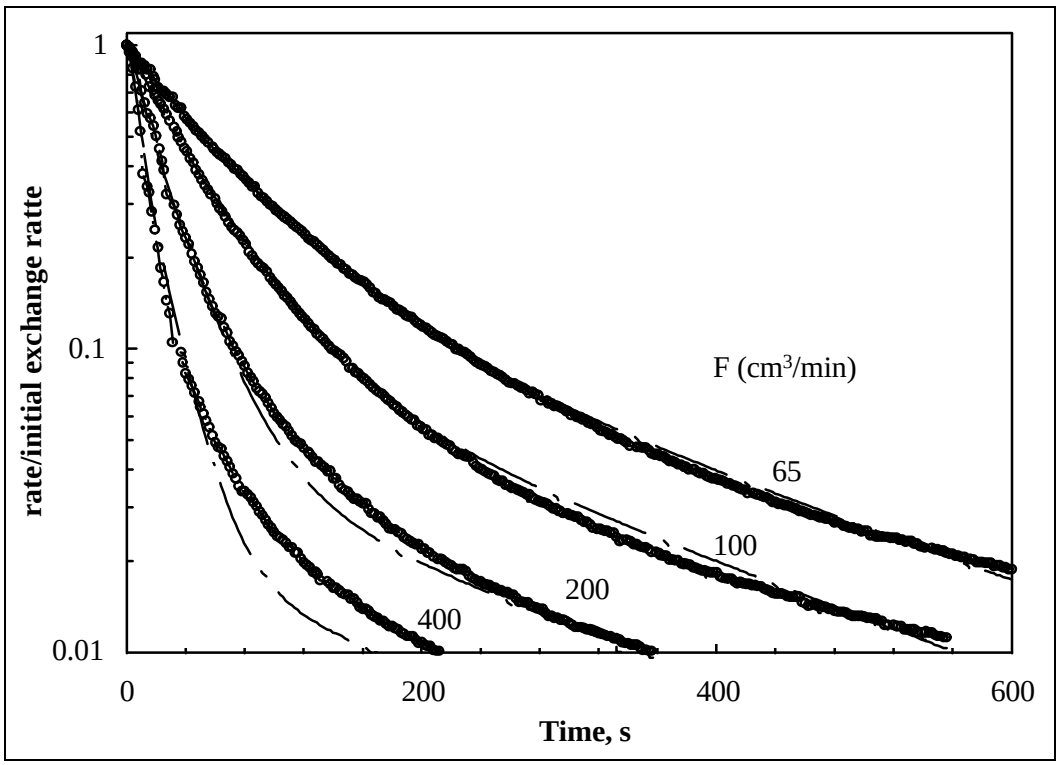

Figure 3.15. Four-parameter, two-compartment model fit $^{13}CO_2$ desorption rate at various flow rates on MgO. [50 mg of catalyst charge, 0.1% CO_2, 573 K]

It can be seen that one type of site on MgO exchanges faster that the other. Readsorption of the desorbed CO_2 prevents the deconvoluting of transient curves getting the distribution of intrinsic rate constant. It however provides thermodynamic information about the adsoption-desorption process. Using the four-parameter, two-compartment model, one can not only get the intrinsic desoprtion rate constant but also adsorption equilibrium constant.

3.4. TPSR of Alcohols and Aldehydes on Isobutanol Synthesis Catalysts

Surface reactions of ethanol and other oxygenated compounds have been studied on several isobutanol synthesis catalysts using a temperature programmed surface reaction (TPSR) technique. Because of the transient nature of TPSR, in which both temperature and surface adsorbate coverage vary with time, information that is unavailable from steady-state measurement can be obtained.

All transfer lines after the thermostated saturator in the TPSR unit were kept at 333-343 K using heating tape in order to minimize the adsorption of reactants and products on the transfer line walls. Ethanol and other oxygenates were introduced by passing helium through the saturator containing the compound of interest at room temperature. Pulse injection of ethanol diluted in He through a 0.93 mL sample loop into the reactor yielded a sharp and reproducible peak containing 2.5 μmol of ethanol. For example, the half peak width of ethanol mass 45 fragment is only about 3 s. The amount of ethanol calculated from the peak area is in excellent agreement with that calculated from the size of the sample loop.

In a typical experiment, 33-100 mg of catalyst (80-140 mesh) was charged into a 1.0 cm-i.d. U-shape reactor. Smaller particle sizes lead to unacceptable pressure drops within the catalyst bed; larger particle sizes can cause intraparticle diffusional restrictions that cause changes in desorption peak temperature or the curve shape. A thermocouple well was located in the middle of a catalyst bed that is supported on a fine quartz frit. The catalyst was first purged with pure He for 10 min at room temperature, followed by the introduction of 5 % H_2 in helium. The reduction was performed at a heating rate of 10 K/min up to 623 K, and the sample kept at this temperature for 0.15 h. A mass spectrometer was used to measure the change of gas composition in the helium stream as a function of sample temperature. After reduction, ethanol was preadsorbed by passing a mixture of ethanol and helium through the catalyst for 10 min at 308 K, followed by pure helium purging for 0.5 h in order to flush out the gas phase and weakly adsorbed ethanol. The sample was then heated up to about 673 K at a rate of 30 K/min in a helium flow of 100 cm^3/min. At higher helium flow rates, concentrations of desorbed components are small and less accurately measured. Also, impurities can be more important at higher flow rates. However, higher carrier gas flows can minimize product readsorption on the catalyst dowmstream and the time lag between desorption and detection. The flow rate must be sufficient so that desorption peak shapes remain unchanged by further increases in flow rate. The low sensitivity at higher flow rates can be compensated by increasing heating rate. But higher heating rates result in the shift of peak maximum to higher temperatures. The desorption products were monitored continuously using a mass spectrometer. At the same time, the products at different temperatures were analyzed by GC-MS through syringe sampling.

3.4.1. Ethanol and Acetic Acid TPSR on Cs-Cu/ZnO/Al_2O_3 and ZrO_2/MnO/ZnO

Initial TPSR studies focused on ethanol reactions on Cs-promoted Cu/ZnO/Al_2O_3 catalysts. This catalyst has been reported to be active and selective for higher alcohol synthesis from CO/H_2 [102].

As shown in Figure 3.16, TPSR measurements of ethanol over the Cs-promoted Cu/ZnO/Al_2O_3 are characterized by two major desorption peaks, with a peak maximum at 373-383 K for ethanol and one at about 573 K for acetone. The additional small peak observed for mass fragments 43 and 44 at *ca*. 443 K might be attributed to acetaldehyde, which is a very reactive intermediate. CO_2 was responsible for mass fragments 44 and 28 at about 320 ^oC. Interestingly, replacement of pure He by 5 % H_2 balanced in helium as a carrier gas enhanced acetone peak intensity. The role of H_2 might be to prevent further condensation reactions of acetone on the catalyst surface.

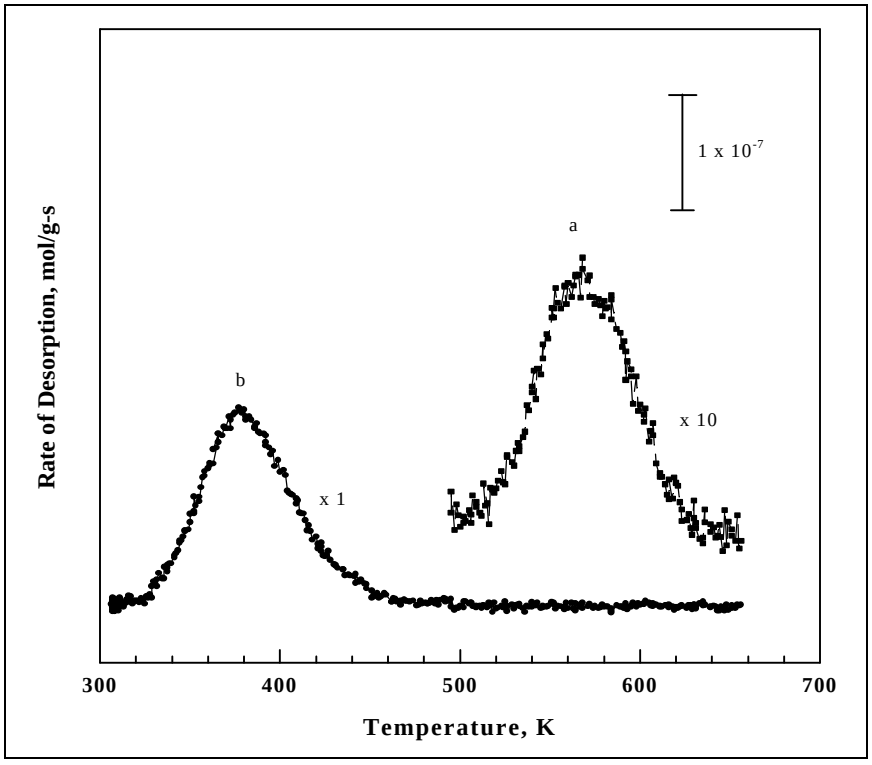

Figure 3.16. Ethanol TPSR on Cs-promoted $CuZnAlO_x$ (a: acetone, b: ethanol)

The formation of acetone can be explained by the decarboxylation of surface acetate ions which result from the oxidation of acetaldehyde by lattice oxygen [103]:

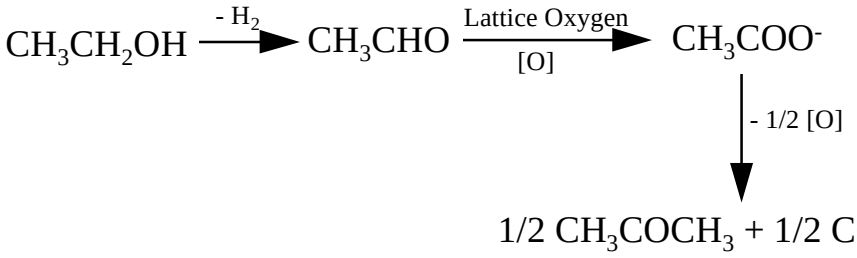

Lattice oxygen may come from a reducible metal oxide in the catalyst. The decomposition of metal acetate leads to the formation of acetone [103]. However, acetone could also result from the aldol condensation of acetaldehyde:

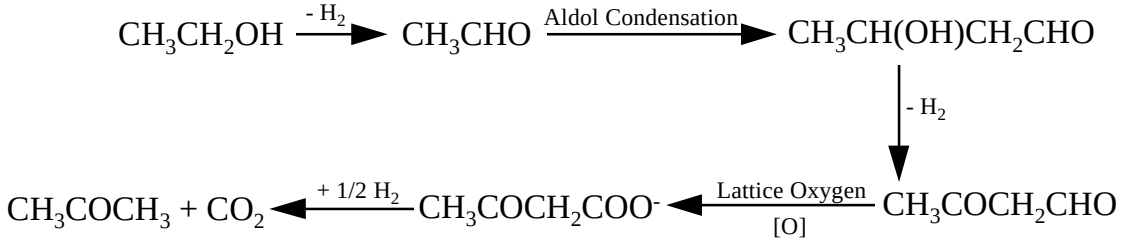

Yet no intermediate species, such as $CH_3CH(OH)CH_2CHO$ or CH_3COCH_2CHO, were observed to support this mechanism. The third pathway can be the reverse-aldol condensation, which is similar to the mechanism proposed on MgO modified catalysts in section 2.3.3. The results of Figure 3.13 show that the amount of acetone produced is about 10 % of ethanol desorbed. This indicates that only a small fraction of adsorbed ethanol can be held strong enough to undergo surface reactions before desorption.

The TPSR results of acetic acid over a Cs-promoted $Cu/ZnO/Al_2O_3$ catalyst, depicted in Figure 3.17, show that there are two acetone peaks with one at *ca.* 543 K and the other at 573 K, indicating that surface acetate ions are the precursors of acetone. These two distinct peaks might be caused by the decomposition of different forms of metal acetates. The acetone formed could undergo secondary reactions on the surface basic sites, resulting in an acetone-to-CO_2 ratio less than unity.

Surprisingly, the TPSR of ethanol over a $ZrO_2/MnO/ZnO$ catalyst yielded only ethanol with peak maximum at about 413 K. However, ethanol desorption peak observed over this catalyst (323 - 553 K) is broader and extends to higher temperatures than on the Cs-promoted $Cu/ZnO/Al_2O_3$ catalyst (323 - 473 K), indicating the presence of stronger adsorption sites on the former catalyst. The lack of acetone in the product stream is surprising because the $ZrO_2/MnO/ZnO$ catalyst could also provide lattice oxygen necessary for the formation of acetate ions from acetaldehyde. This can be explained by the fact that acetaldehyde, *i.e.*, the precursor for acetate ions, was not formed over this catalyst during the reaction. This further address the role of Cu metal plays in the dehydrogenation reactions of ethanol to acetaldehyde.

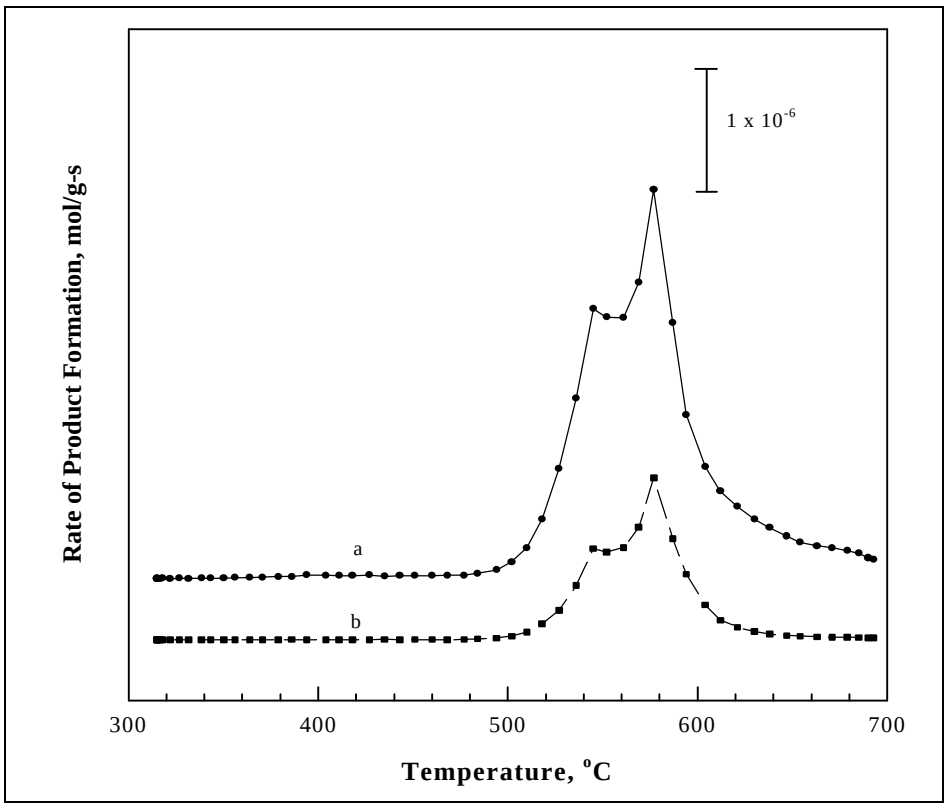

Figure 3.17. Acetic acid TPSR on Cs-promoted $CuZnAlO_x$ (a: CO_2, b: acetone)

3.4.2. Ethanol TPSR Studies on Mg/Al hydrotalcites

Hydrotalcites, or magnesium-aluminum hydroxycarbonates, became attractive basic oxides upon calcination because the high surface area is stable to steam treatment [88]. These materials have also been reported to be active for typical base-catalyzed reactions including aldol condensation [89]. Davis and co-workers have found that the basicity of hydrotalcite is, however, weaker than that of MgO [82], which might prevent further aldol condensation of reaction products to yield coke over the stronger basic sites on MgO.

The TPSR results of ethanol over MgO/Al_2O_3 with Mg/Al ratio ranging from 1.5 to 10 were shown in Figure 3.18, 3.19. Broad ethanol desorption peaks were observed in the temperature range of 330-670 K on all three catalysts, indicating highly non-uniform distributions of adsorption sites. The amount of ethanol desorbed increased in the order of MgAl(5) > MgAl(1.5) > MgAl(10). Here, MgAl(x) represents a MgO/Al_2O_3 catalyst with a magnesium-to-aluminum ratio of x. Ethylene, which resulted from the dehydration of surface ethanol, was formed at 660 K. Less ethylene was produced over MgAl(10) than over MgAl(1.5) or MgAl(5) catalysts, suggesting the role of aluminum ion or acid site plays in the dehydration reaction of ethanol to ethylene.

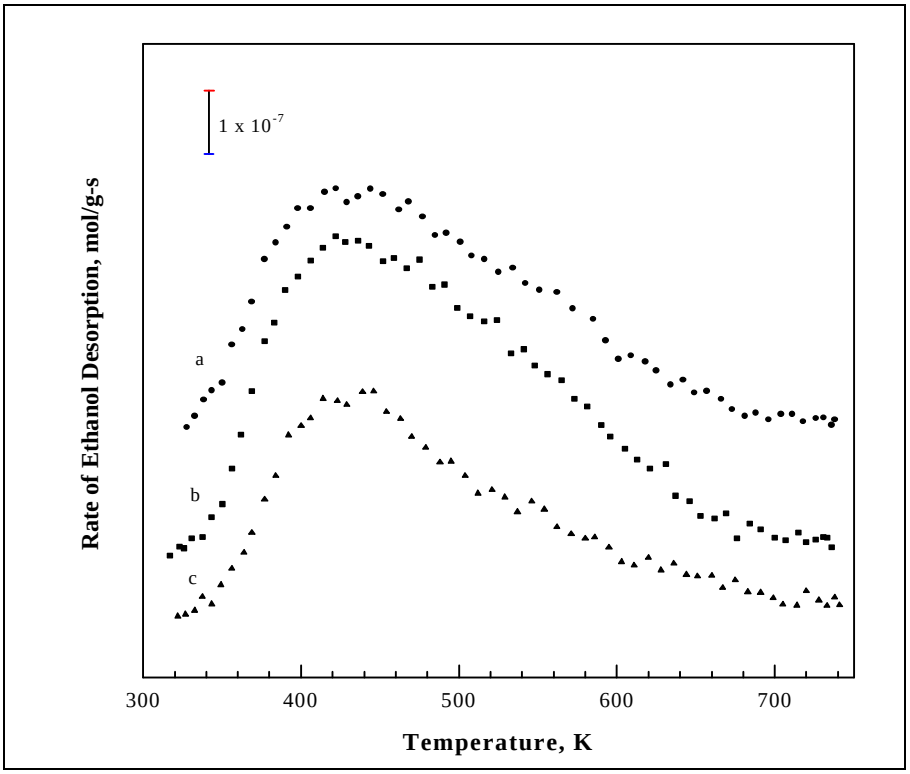

Figure 3.18. Ethanol desorption during ethanol TPSR on Mg/Al (a: Mg/Al=1.5, b: 5, c: 10).

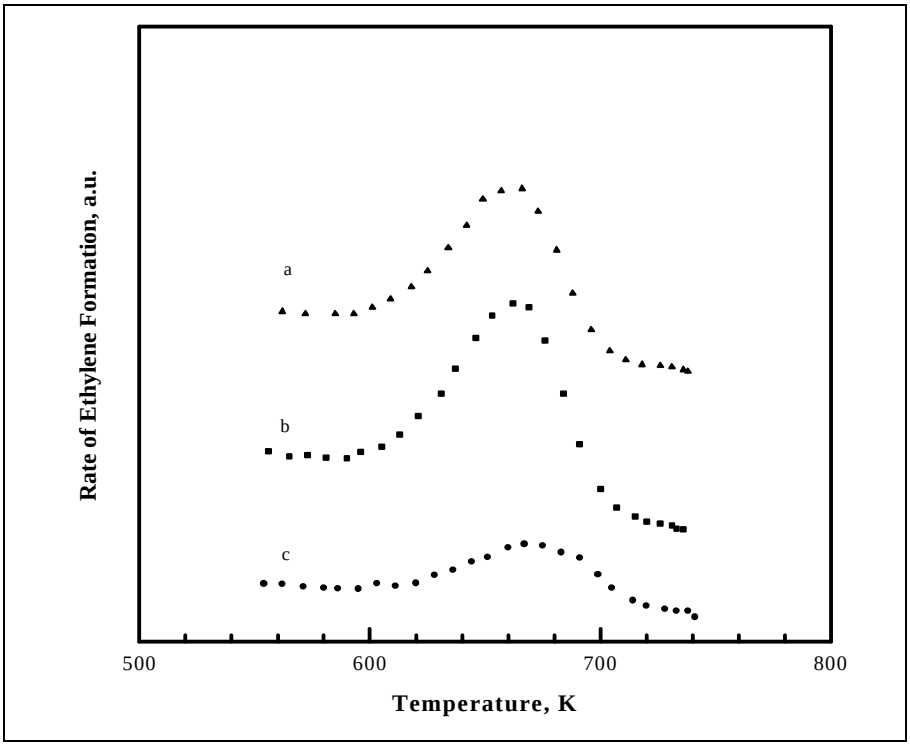

Figure 3.19. Ethylene formaction during ethanol TPSR on Mg/Al (a: 1.5, b: 5, c: 10).

3.4.3. Acetaldehyde and Ethanol TPSR on $CuMgCeO_x$ Catalysts

I. Acetaldehyde TPSR

The desorption products observed on MgO/CeO_2, $Cu/MgO/CeO_2$ and K-$Cu/MgO/CeO_2$ are shown in Figure 3.20, the major desorption features are the evolution of acetaldehyde, crotonaldehyde (m/e 70), and water with peak maxima at about 373 K. Self-condensation of acetaldehyde on basic sites results in the formation of 3-hydroxybutanal, which undergoes subsequent dehydration reaction to form crotonaldehyde and to water.

Water formed from condensation of surface hydroxyl species accounts the tailing water peak at high temperatures. MgO, a strong basic oxide, is inactive in dehydration reactions because of its lack of acid sites. Kita and co-workers [104] have reported that the main product in the self-condensation of n-butyraldehyde on MgO was 2-ethyl-3-hydroxyhexanal, and the selectivity to 2-ethyl-2-hexanal, the dehydration product, was less than 2 %. Addition of γ-Al_2O_3, an acidic oxide, increased 2-ethyl-2-hexenal yield at the expense of 2-ethyl-3-hydroxyhexanal [104]. Since crotonaldehyde is formed on both MgO/CeO_2 and (K)$Cu/MgO/CeO_2$ but not on MgO, sites associated with CeO_x might be responsible for its formation. Cerium oxide pretreated in a reducing atmosphere may contain oxygen vacancies and coordinately unsaturated cerium ions exhibiting Lewis acidity [105]. The insertion of lower-valance cations such as Cu^{2+} and Mg^{2+} into ceria lattice may also lead to the creation of anionic vacancies. These anionic vacancies can be titrated by surface hydroxyl species formed in dehydration reactions.

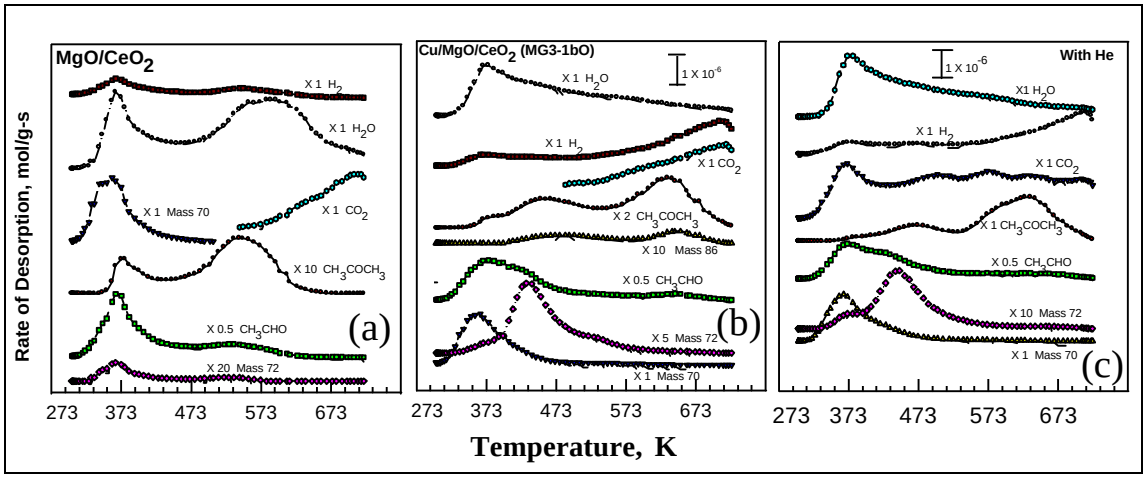

Figure 3.20. Acetaldehyde TPSR on a) Mg_5CeO_x, b) $Cu_{0.5}Mg_5CeO_x$, and c) K-$Cu_{0.5}Mg_5CeO_x$.

A major difference between MgO/CeO_2 and (K)$Cu/MgO/CeO_2$ is that the latter desorbs of methyl ethyl ketone (MEK) at ~ 443 K, as shown by the evolution of species with m/e 72, 43 and 29 in this temperature range. MEK was not observed on MgO/CeO_2. Its formation has been further confirmed by GC-MS analysis of the desorption products.

Another significant feature of (K)Cu/MgO/CeO_2 is the formation of acetone at both 453 and 633 K. The amount of acetone produced on MgO/CeO_2 is an order of magnitude less than that on (K)Cu/MgO/CeO_2, indicating a critical role of copper in MEK and acetone formation. The precursor of methyl ethyl ketone and low-temperature acetone might be 3-hydroxybutanal formed via self-condensation of surface acetaldehyde species. As will be discussed in the case of ethanol, alcohol dehydrogenation takes place readily at 443-453 K over copper metal. Thus, at these temperatures 3-hydroxybutanal could undergo either dehydration, as evidenced by the continuous production of crotonaldehyde up to 473 K (Figure 3.20), or dehydrogenation on copper metal to form 3-oxobutyraldehyde as shown by reaction 2:

$$CH_3\text{-}\underset{\displaystyle OH}{\underset{|}{CH}}\text{-}CH_2CHO_{(a)} \xrightarrow{Cu} CH_3\text{-}CO\text{-}CH_2\text{-}CHO + 1/2H_2 \qquad (2)$$

The formation of 3-oxobutyraldehyde on Cu/MgO/CeO_2 catalysts, though in small quantity, has been confirmed by GC-MS. 3-oxobutyraldehyde can either react with lattice oxygen from the reducible oxide to form acetoacetate, or produce methyl ethyl ketone and an oxygen atom. Oxygen species can then migrate and heal a surface anionic vacancy. Since acetoacetic acid is not stable and undergoes decarboxylation readily at temperatures of 373-423 K [106], it is expected that acetoacetate, once formed, will decompose to acetone. The reaction pathways of 3-oxobutyraldehyde are illustrated as follow:

$$CH_3\text{-}CO\text{-}CH_2\text{-}CHO_{(a)} + O_s \longrightarrow CH_3\text{-}CO\text{-}CH_2\text{-}COO_{(a)} + H_{(a)} \longrightarrow CH_3COCH_3 + CO_2 \qquad (3)$$

$$CH_3\text{-}CO\text{-}CH_2\text{-}CHO_{(a)} + 2\,H_{(a)} \longrightarrow CH_3\text{-}CO\text{-}CH_2\text{-}CH_3O_s \qquad (4)$$

A similar mechanism for MEK formation on Cu/ZnO/Al_2O_3 has been proposed by Pennella et al. [46].

The acetone formed at 653 K, however, requires a different pathway because none of the intermediates in the above mechanism are likely to survive at these high temperatures. Surface acetate species, formed by the nucleophilic attack of the carbonyl group of acetaldehyde by electronegative O^{2-} from reducible metal oxides, is likely to be responsible for the formation of these high-temperature species. The formation of acetone at T > 573 K has also been reported by Prieto and co-workers in TPSR studies of acetic acid on TiO_2 [107]. They proposed that a bimolecular reaction involving ketene and molecularly adsorbed acetic acid in equilibrium with the gas phase leads to the formation of acetone:

$$CH_2{=}C{=}O + CH_3COOH_{(a)} \longrightarrow CH_3COCH_3 + CO_2 \qquad (5)$$

No gas-phase ketene was observed on this catalyst. They believed that ketene, once formed, remains strongly adsorbed on coordinately unsaturated Ti^{4+} sites. It should be

pointed out that the presence of gas-phase ketene has been observed during the temperature-programmed surface reactions of acetic acid and acetaldehyde on both Cu [108] and ZnO [109].

In the TPSR of preadsorbed acetaldehyde on (K)Cu/MgO/CeO_2 and MgO/CeO_2, however, no gas-phase ketene was observed. In analogy with Ti^{4+}, the ketene formed can be strongly adsorbed on coordinately unsaturated Ce^{4+} sites. A mechanism similar to that proposed by Prieto et al. [107] may account for the formation of high-temperature acetone on (K)Cu/MgO/CeO_2. Yet, molecularly adsorbed acetic acid is less likely to exist in our study because of the basic properties of our catalyst and because of gas-phase acetic acid was not detected in our study. Therefore, ketene and surface acetate species instead of acetic acid might be the precursors of the acetone formed at high temperatures. The presence of basic site increased the amount of acetone formed; therefore, it is possible that $^{-}CH_2COO_{(a)}$ species, formed via α-H abstraction of acetate by a strong basic site, attacks the carbonyl group of ketene, leading to the formation of acetone:

$$CH_2=C=O + {}^{-}CH_2COO_{(a)} + 2H_{(a)} \longrightarrow CH_3COCH_3 + CO_2 \qquad (6)$$

Since the acidity of the α-hydrogen in acetate ions is weaker than that of α-hydrogen in acetaldehyde, only strong basic sites such as alkali metal oxides may be able to break the C-H bond in acetate species. The formation of very small amounts of acetone over Cu, ZnO and MgO/CeO_2 is not surprising, because they lack strong basic sites. Cu promotes ketene production, whereas alkali metal oxides favor $^{-}CH_2COO_{ad}$ formation. The co-existence of Cu and strong basic sites increases the rate of acetone production. The hydrogenation of acetone leads to the formation of 2-propanol observed in high-pressure reactions of H_2/CO mixtures. As shown in Figure 3.17, the amount of high-temperature acetone produced on K-promoted Cu/MgO/CeO_2 (1 wt % K) is twice as much as that on Cu/MgO/CeO_2 (with no K addition); whereas, the low-temperature acetone, whose formation did not require the strong basic sites, was comparable on these two catalysts. The potassium content in K-Cu/MgO/CeO_2, determined by atomic absorption, is 1.5 wt % in comparison to 0.4 wt % in Cu/MgO/CeO_2. Although potassium is necessary for acetone formation, excess potassium can block CeO_x species, and therefore decrease the concentration of surface $CH_3COO_{(ad)}$ species, whose formation requires the presence of lattice oxygen from a reducible metal oxide. Moreover, the presence of potassium appears to reduce the dispersion of copper and thus decrease the rate of ketene formation. Thus, it is necessary to optimize potassium loading in order to achieve a high yield of higher oxygenates.

The high-temperature evolution of H_2, H_2O and CO_x may arise from decarboxylation of residual acetate:

$$CH_3COO_{(a)} \longrightarrow CH_{3(a)} + CO_2 \qquad (7)$$

This reaction has been reported to take place on Cu [108] and ZnO [109]. Reactions of ketene with surface oxygen species can lead to the formation of surface hydrocarbon species [110].

$$CH_2=C=O_{(a)} + O_s \longrightarrow CH_{2(a)} + CO_2 \quad (8)$$

Further reactions of these surface hydrocarbon residues at high temperatures then form H_2, H_2O and CO_x.

Since both H_2 and CO are the reactants in the catalytic conversion of syngas to isobutanol, it is of interest to study their effects on aldol-condensation reactions. TPSR studies of preadsorbed acetaldehyde with H_2 or CO in the He carrier gas were carried out on (K)Cu/MgO/CeO_2 catalysts. As shown in Figure 3.21, the addition of H_2 during acetaldehyde TPSR produced an acetaldehyde peak at about 663 K in addition to the one previously observed at 363 K in He carrier gas to form acetaldehyde in a reactive desorption step. This might be attributed to the reduction of surface ketene species by H_2:

$$CH_2=C=O_{(a)} + H_2 \longrightarrow CH_3CHO \quad (9)$$

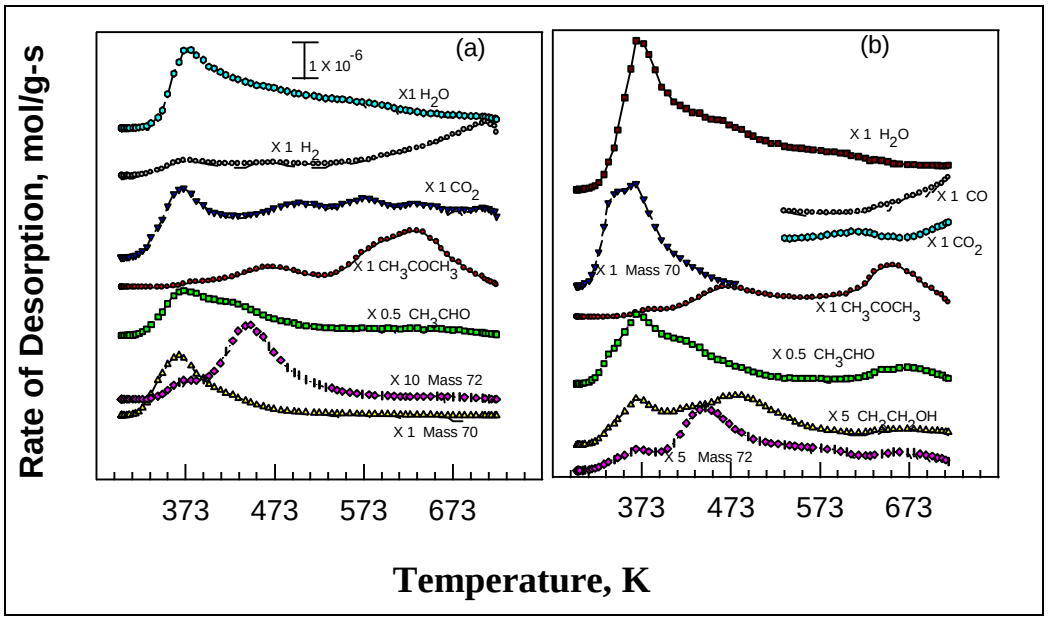

Figure 3.21. H_2 Effect on acetaldehyde TPSR on K-$Cu_{0.5}Mg_5CeO_x$: a) in He, b) in 5 % H_2/He.

The formation of CO is a result of water-gas shift reaction:

$$CO + H_2O \rightleftharpoons CO_2 + H_2 \quad (10)$$

This accounts for the observed decrease in CO_2 production when CO was added to the carrier gas (Figure 3.22). Water was formed via dehydroxylation of surface hydroxyl species. Another interesting feature is the appearance of ethanol at 373-473 K when H_2 is

added; this ethanol evolution arises from the hydrogenation of acetaldehyde by gas phase H_2.

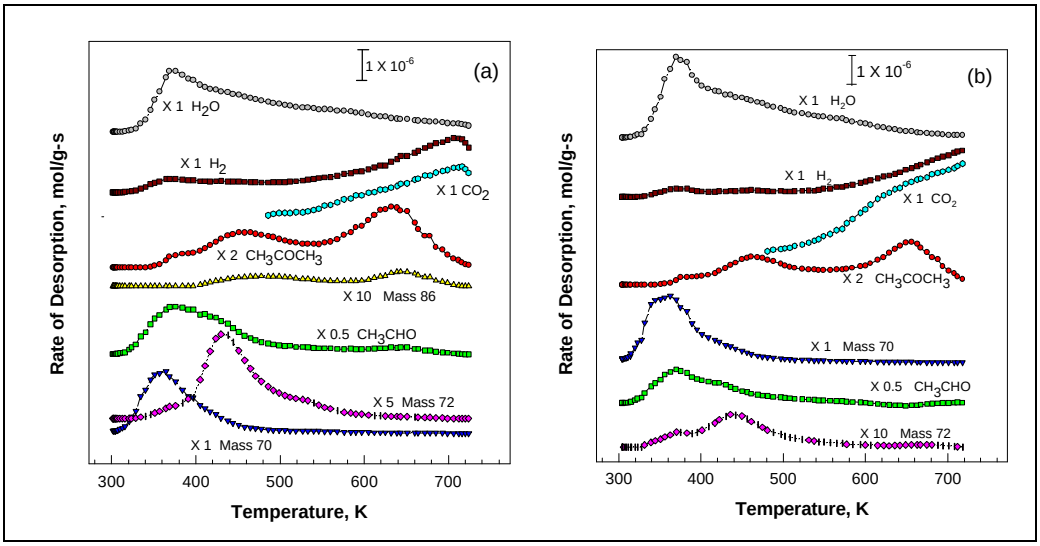

Figure 3.19. Effect of CO on acetaldehyde TPSR on K-$Cu_{0.5}Mg_5CeO_x$: a) in He, b) in 5 % CO/He.

The presence of CO during acetaldehyde TPSR inhibits acetone formation because of the formation of CO_2 via water-gas shift reaction. CO_2 adsorbs on the strong basic sites necessary for aldol condensation reactions.

II. Ethanol TPSR

Ethanol adsorbs dissociatively on the surface to form surface ethoxide species over Cu [111] and metal oxides [55], [48], [58]. Based on literature results and our current observation, a schematic diagram for ethanol adsorption and reactions on metal-oxide and copper-containing catalyst surfaces is Figure 3.23.

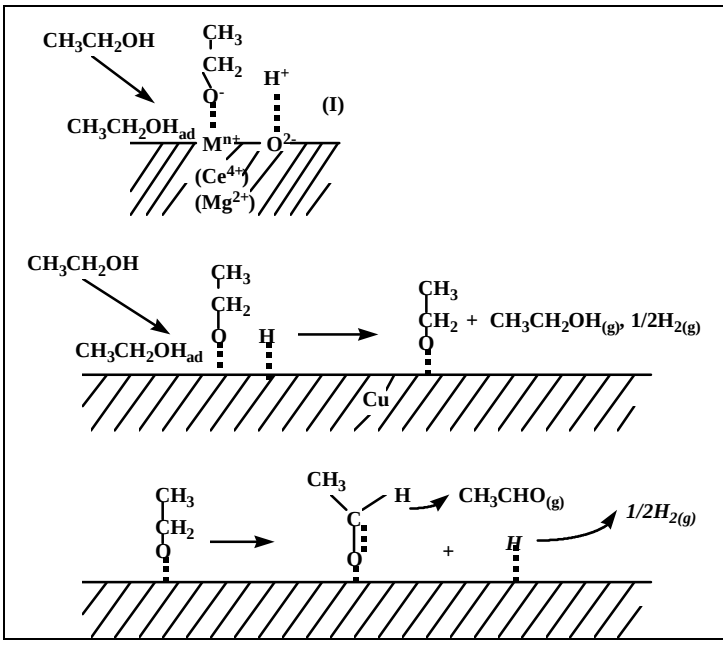

Figure 3.23. Schematic diagram of ethanol adsorption and reactions on catalyst surface.

On metal oxides such as CeO_2 and MgO, the abstracted protons react with lattice oxygen to form water. Hydrogen atoms formed during dissociative adsorption of ethanol on copper can either recombine with ethoxide to form ethanol, or react with another H atom to produce H_2. Upon heating, most of the ethoxide species desorb as ethanol via recombination with surface hydrogen. The remaining ethoxide may either react with lattice oxygen on metal oxides to form surface carboxylic species or undergo α-H scission with the help of Cu to form acetaldehyde. The resulting surface hydrogen recombines to produce more H_2. As shown in Figure 3.24, acetaldehyde and H_2 were produced in large quantities on Cu-containing catalysts, and acetaldehyde production reached a maximum at 453 K. However, below 453 K the rate of H_2 production is higher than that of acetaldehyde. As illustrated in the above schematic diagram, there are two hydrogen sources with one from O-H bond breaking and the other from C-H bond cleavage. This may explain the appearance of two hydrogen peaks in the temperature range of 373-473 K. The first H_2 peak, which appears at a temperature similar to that of the ethanol evolution peak reflects the recombination of surface H atoms produced via O-H rupture. The second H_2 peak, evolved at approximately the same temperature range as acetaldehyde, is attributed to C-H bond cleavage. These results suggest that the formation of H_2 and acetaldehyde from surface ethoxide species is reaction-limited. It is noteworthy that in the TPSR of ethanol over Cu(110) single crystal carried out by Madix

et al. [111], the desorption temperature of H_2 was about 298 K higher than that of aldehyde. Thus, they concluded that the formation of H_2 is desorption-limited and not limited by its formation in C-H activation steps.

TPSR of preadsorbed ethanol on MgO/CeO_2 yielded small amounts of H_2, indicating the importance of Cu in ethanol dehydrogenation steps. The amount of H_2 produced on K-promoted $Cu/MgO/CeO_2$ is lower than that on unpromoted $Cu/MgO/CeO_2$. This is in agreement with the lower copper surface area observed on K-$Cu/MgO/CeO_2$. Potassium compounds can block Cu surface atoms, resulting in fewer copper surface atoms available for dehydrogenation reactions. Once acetaldehyde is formed, it will react with lattice oxygen from reducible metal oxides to form surface acetate species, which undergo subsequent reactions leading to the formation of acetone as discussed in the case of acetaldehyde TPSR studies. It is noteworthy that the amount of acetone produced, however, is less than that in acetaldehyde TPSR. The peak temperature shifted to 653 K and 673 K over Cu-MgO/CeO_2 and K-$Cu/MgO/CeO_2$, respectively. Moreover, acetone formed on K-$Cu/MgO/CeO_2$ is less than that on $Cu/MgO/CeO_2$. These effects are attributed to the lower acetaldehyde production on the lower copper surface area catalyst, which results in a decrease in the concentration of adsorbed acetone precursors. In contrast to acetaldehyde TPSR, only very small amounts of crotonaldehyde and acetoacetaldehyde were produced (Figure 3.24).

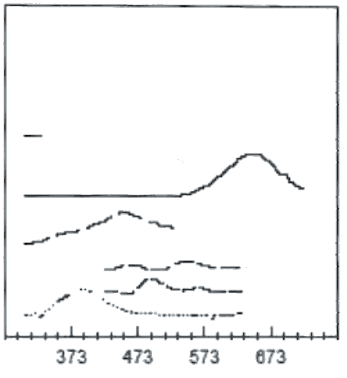

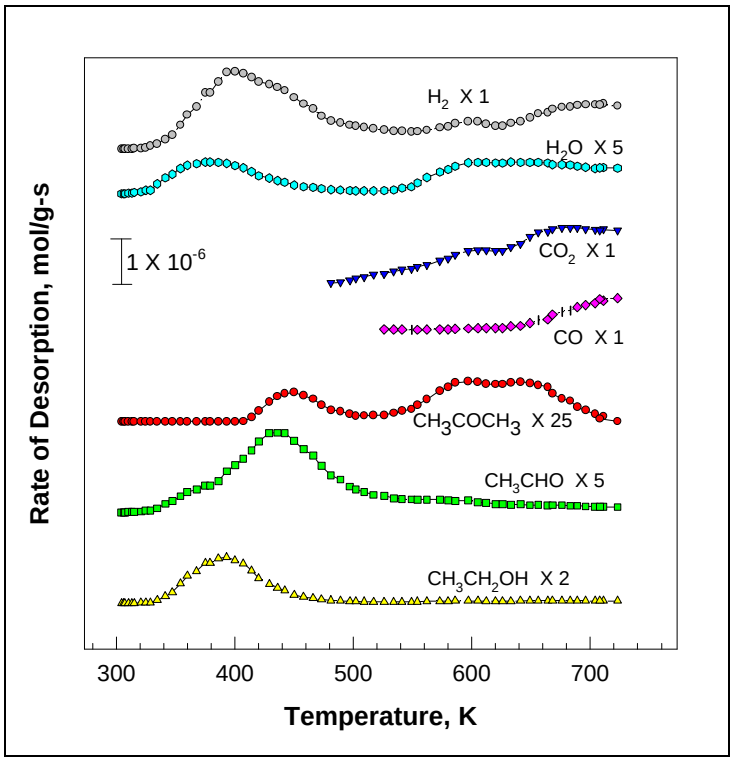

Figure 3.25. Ethanol TPSR on $Cu_{0.1}MgO_x$ (MG3-5 O).

The effects of H_2 and CO on acetone production have also been studied during ethanol TPSR and the results are shown in Figure 3.26. The addition of H_2 to the carrier gas stream increased CO and H_2O production and decreased CO_2 formation because of water-gas shift reaction. The presence of H_2 shifted the equilibrium of reaction 10 to the left, thus favoring CO and H_2O formation. In addition to the peak at 373-473 K, an acetaldehyde peak at 653 K was also observed. Its appears to form via ketene reduction by H_2. Interestingly, no crotonaldehyde or methyl ethyl ketone was formed in the temperature range of 423-523 K on K-Cu/MgO/CeO_2. Instead, they evolved at about 663 K. Aldol condensation of acetaldehyde species formed at 653 K are responsible for crotonaldehyde and methyl-ethyl ketone formation. The presence of H_2 also increased acetone production. This reflects two effects. First, H_2 decreased CO_2 production via water-gas shift reaction; therefore, strong basic sites remain available for aldol condensation reactions leading to acetone. Apparently, CO_2 will block the strong basic sites due to its acidic character.

The addition of CO to the carrier 1) increased H_2 and CO_2 at T > 473 K because of water-gas shift reactions, 2) caused a marked decrease in acetone production and 3) decreased H_2 production at temperatures below 473 K. As illustrated in the ethanol adsorption diagram (Figure 3.20), at room temperature, some ethanol adsorbs molecularly, while the rest adsorbs dissociatively. Upon heating, some of the molecularly adsorbed ethanol may dissociate via O-H bond cleavage on the surface. The dissociation of ethanol and the decomposition of surface ethoxide species require the presence of unoccupied surface sites to accommodate H species. During ethanol TPSR in

the presence of CO, however, all sites not occupied by ethanol will be taken up by CO. Then, dissociation reactions leading to ethoxide, H and acetaldehyde became unfavorable, because sites are unavailable to accommodate H atoms. This results in fewer gas phase H_2 molecules and fewer surface intermediates for acetone formation. The amount of ethanol produced is slightly higher when CO is added than in the presence of either H_2 or pure He. Since CO_2 was produced via water-gas shift reaction in the presence of CO, more strong basic sites were blocked. Thus, the rate of aldol condensation reactions leading to acetone was decreased. Because acetone production was decreased by only 50 % in acetaldehyde TPSR with the addition of CO, the combined effect of low surface intermediate concentrations and less basic sites appear to be responsible for the marked decrease in acetone production during ethanol TPSR when CO (5 %) is present in the He carrier stream.

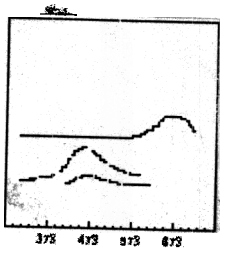

product of CH_3OH TPSR on Cu/MgO. Small amounts of H_2, H_2O and carbon oxides were also observed on MgO/CeO_2. H_2 production was higher on K-Cu/MgO/CeO_2 and Cu/MgO than on MgO/CeO_2, suggesting that copper is involved in methanol dehydrogenation and H_2 desorption. Interestingly, a hydrogen peak appeared at 533 K, which was absent during ethanol TPSR. The only difference between ethanol and methanol is that the dehydrogenation product (acetaldehyde) of the former does not undergo subsequent dehydrogenation to form additional H_2, while the formaldehyde formed by methanol dehydrogenation reacts further on the surface to generate H_2 and CO On Cu/MgO, large amounts of CO were also formed, but it evolved at temperatures about 10 K higher than H_2. On K-Cu/MgO/CeO_2, CO production was lower, but CO_2 was higher on Cu/MgO. Some high-temperature CO_2 products may form by CO oxidation using lattice oxygen in CeO_2. The presence of formate on K-Cu/MgO/CeO_2 may also lead to the formation of CO_2 and H_2. Gas phase formaldehyde was not detected on these catalysts. Formaldehyde, once formed, is likely to decompose immediately to H_2 and CO_x before detection.

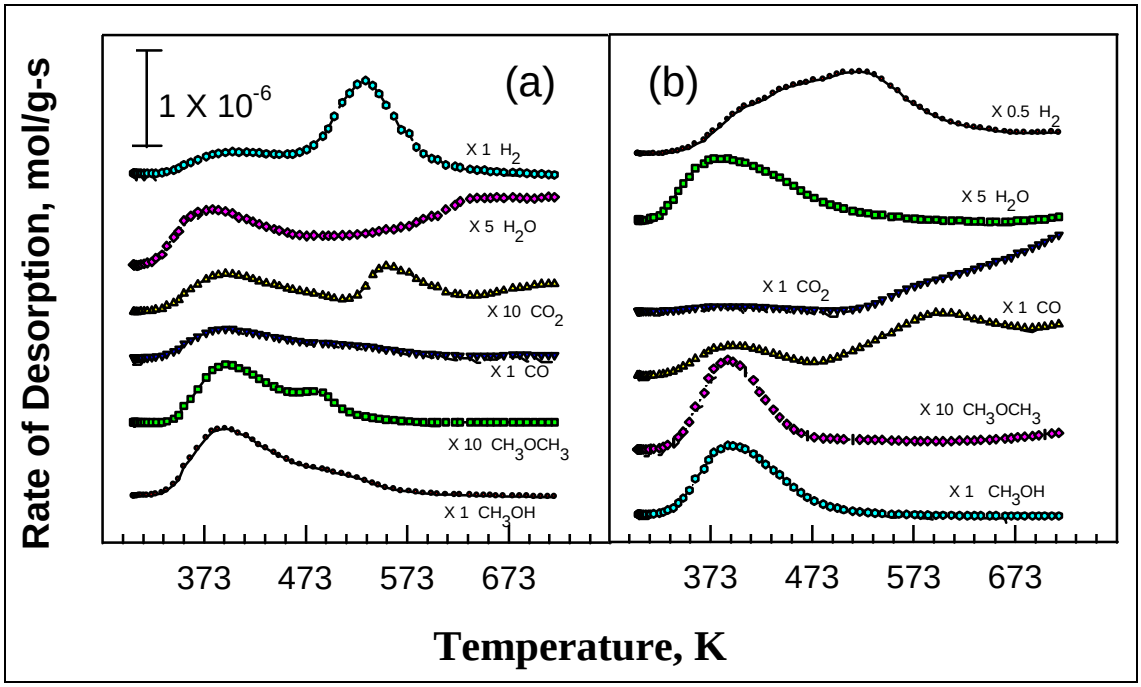

Figure 3.27. Methanol TPSR on a) Mg_5CeO_x and b) K-$Cu_{0.5}Mg_5CeO_x$ (MG3-1 bO/K).

3.5. In-situ IR Studies on Surface Intermediate Species during Ethanol Surface Reactions

The temperature-programmed surface reactions of ethanol on $Cu_{0.5}Mg_5CeO_x$ catalysts reveal the formation of acetone and crotonaldehyde. Surface acetate species are believed to be the precursor to acetone. By monitoring surface species and the change in the intensity of their vibrational IR bands as temperatures increases using in-situ infrared spectroscopy, it is possible to address the role of each individual surface species in chain-growth reactions. Ethanol and d_6-ethanol reactions on $Cu_{0.5}Mg_5CeO_x$ and its component oxides (MgO, CeO_2, Mg_5CeO_x and $Cu_{0.5}Mg_5CeO_x$) were carried out in a high-pressure and high-temperature in-situ IR reactor (Figure 3.28). The results obtained on MgO at different temperatures are shown in Figure 3.29.

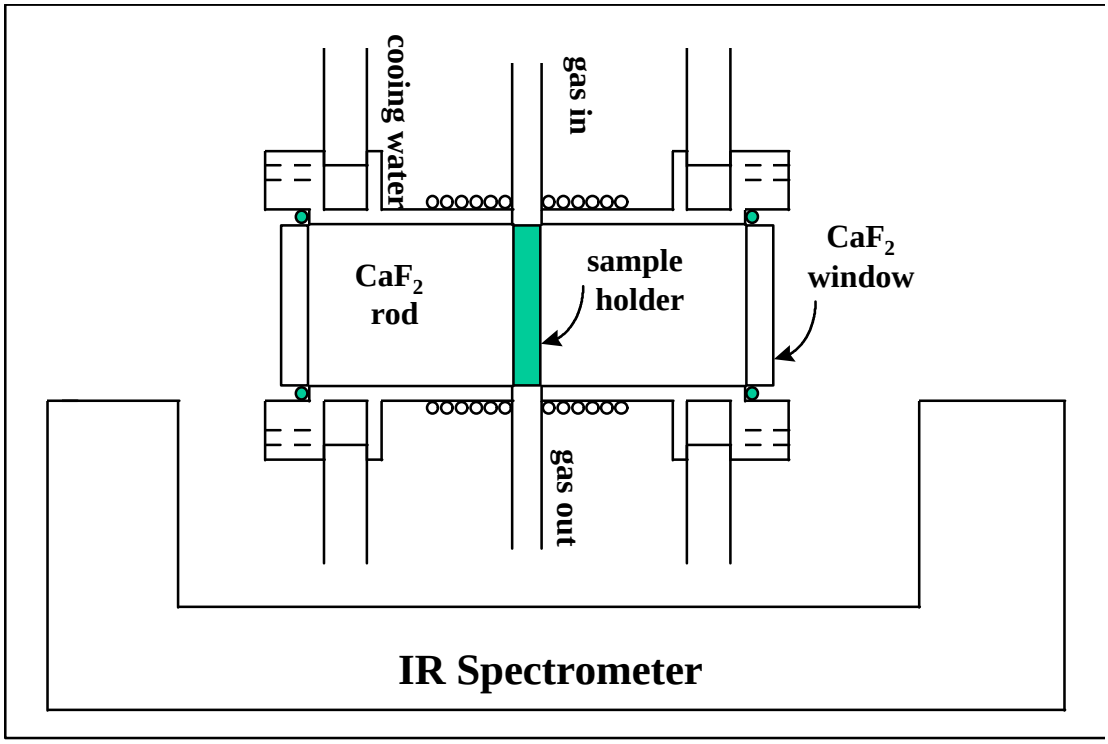

Figure 3.28. High-pressure and high-temperature in-situ IR cell/reactor

The sample wafer (10 mg/cm^2) was pretreated at 723 K in flowing He for 30 min followed by H_2 treatment at 623 K for another 30 min. The temperature was raised to 673 K upon H_2 removal in order to obtain the background spectra. The disk was cooled to room temperature in a stepwise manner and background spectra were recorded from 673 K00 at intervals of 100 K. Ethanol vapor was introduced into the IR cell at room temperature (298 K). After adsorption for 10 min, physically adsorbed and gas phase ethanol were removed by He purging at the same temperature. Decomposition of the adsorbed species was investigated at elevated temperatures in a stepwise manner from

298 to 673 K and *in-situ* IR spectra were taken 5 min after the desired temperature was reached.

Figure 3.29a shows the spectrum recorded after purging the sample with helium at 298 K for 30 min. Bands observed in the frequency region 3000-2800 cm^{-1} are attributed to (CH_3) and (CH_2) of adsorbed undissociated ethanol and ethoxide species, respectively. The bands near 1100 cm^{-1} are due to C-O in surface ethoxide species. The three distinct bands at 1060, 1108 and 1144 cm^{-1} suggest that three types species are formed by adsorption of ethanol at room temperature [10 - 14]. At 473 K, the band at 1108 cm^{-1} disappeared, and the other two bands were weakened. The former might be due to the weakly bonded ethoxide or undissociated adsorbed ethanol species. The deformation modes of methyl and methylene groups are characterized by the bands in the region of 1300-1500 cm^{-1}. The broad band centered at 3600 cm^{-1} shows the formation of surface OH groups from the dissociative adsorption of ethanol. At 373 K (Figure 3.26b), all the bands decrease owing to the desorption of surface ethoxide in the form of C_2H_5OH. Interestingly, the ratio of the intensity of the band near 3730 cm^{-1} to that of the broad band centered around 3600 cm^{-1} increased with increasing temperature (Figures 3.26a-c), suggesting that the dehydroxylation of MgO leads to isolated hydroxyl species.

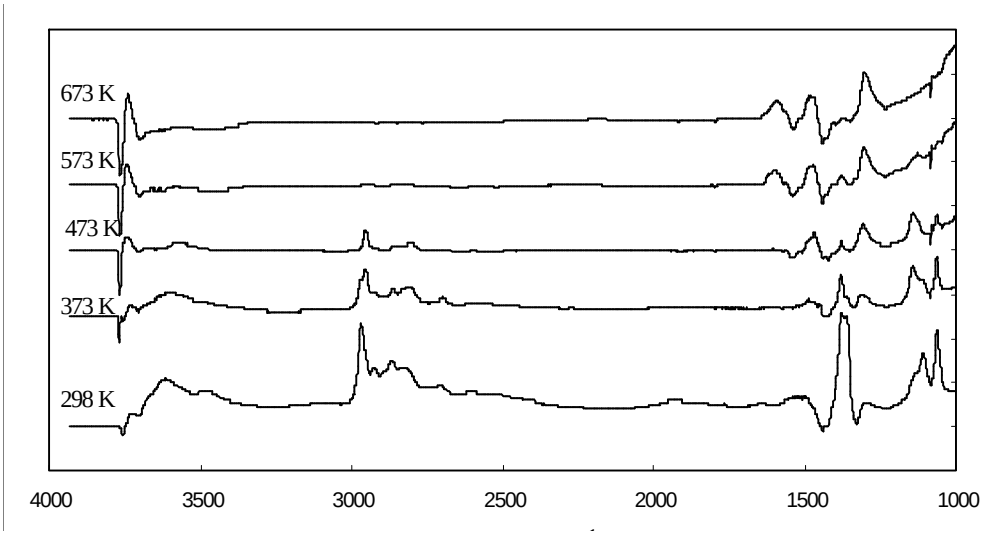

Figure 3.29. IR spectra vs. catalyst temperature for ethanol reaction on MgO.

Both the band at 1380 cm^{-1} and the ones at 2800-3000 cm^{-1} decreased with increasing temperatures (Figures 19a-c), and disappeared at 573 K, which again indicates that these bands arise from (CH_3) and (CH_2) species. The decrease in the intensity ratio of the 2925 cm^{-1} band to the 2967 cm^{-1} band (Figures 3.29a-c) indicates that methylene species disappear at a faster rate than the methyl groups. This may be attributed to the dehydrogenation of ethoxide species on MgO surface as illustrated by the following reaction:

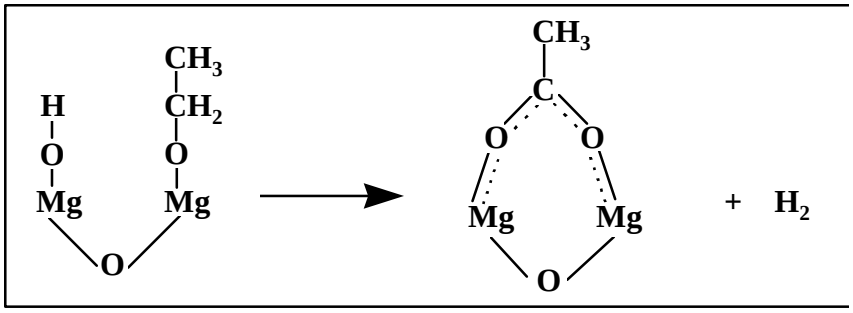

A similar mechanism has been proposed on the oxidation of surface methoxide species on MgO [112]. The evolution of H_2 has been confirmed by temperature-programmed surface reactions of ethanol on MgO. As temperature increased to 573 K, C-C cleavage occurred, resulting in the disappearance of C-H bands (2800-3000 cm^{-1}) and leaving the carbonate species on MgO surface (Figures 3.29d, e).

3.6. Probing initial C-C formation from CO/H_2 by isotopic tracer studies in CMRU-II

A high-pressure catalytic microreactor has been built and attached to the temperature-programmed surface reaction unit for the study of higher alcohol synthesis from CO/H_2. This experiment will focus on the reaction mechanisms for higher alcohol formation especially the chain-growth pathways from C_1 to C_2 alcohols. To fulfill this objective, a mixture of $^{13}CO/H_2$ and CH_3OH will be used as reactants. ^{13}CO contained in a lecture bottle (2.0 MPa) was pressurized using H_2 to make a 1/1 $^{13}CO/H_2$ mixture. A mixture of $^{13}CO/H_2$ (1/1) and $^{12}CH_3OH$ was used in these experiments which were carried out at 2.0 MPa with a small amount of catalyst (0.10 ~ 0.25 g) in order to operate at high space velocities and minimize ^{13}CO usage.CH_3OH will be introduced by passing $^{13}CO/H_2$ mixtures through a saturator containing CH_3OH at a desired temperature. All the gas feeding lines after the saturator will be wrapped up with heating tapes to ensure no readsorption and condensation of reactants and products. A part of effluent will be analyzed in-situ by mass spectrometry and the remainder will be trapped and analyzed using GC-MS and liquid-phase NMR.

CMRU-II was first certified using a 1.0 wt % K-$Cu_{0.5}Mg_5CeO_x$ (MG3-13 O/K) and a mixture of $CO/H_2/Ar$ = 0.45/0.45/0.10. The catalyst (150 mg) was exposed to flowing H_2 (30 mL/min) while the temperature was raised to 593 K at a rate of 0.45 K/min and kept at this temperature for 4 h. After the temperature was lowered to 573 K, H_2 was stopped and the reaction mixture ($CO/H_2/Ar$ = 0.45/0.45/0.10) was introduced. The reaction pressure was raised to 2.0 MPa in less than a minute. The effect of space velocity on methanol and higher alcohol formation was first investigated. In each experiment the first activity measurement was made 15 min after adjusting the flow rate for the desired space velocity, others were made after 20 min. Samples of the reactor effluents were taken at atmospheric pressure by syringe extraction and analyzed by GC-MS.

Methanol and CO_2 were the main products (Figure 3.30). The methanol synthesis rate does not increase linearly with increasing bed residence time, suggesting that methanol undergoes further reactions and/or methanol synthesis step is reaching thermodynamic equilibrium at longer bed residence times. It should be pointed out that the GHSV employed in this study varies from 4200 to 34000 cm^3/g-cat-h, values much higher than in the higher-pressure (4.5-5.0 MPa) studies (CMRU-I).

The non-linear increases of ethanol and 1-propanol production rates with increasing bed residence time suggests that both are reaction intermediates and precursors to higher alcohols. Isobutanol synthesis rate increases linearly with increasing residence time, suggesting that isobutanol is a final product which does not undergo further reactions. Moreover, isobutanol production is not inhibited by CO_2 produced during the reaction possibly due to the much lower CO_2 content at the higher space velocities and lower CO conversions of this study.

The effect of CO_2 on methanol and isobutanol production was further investigated on 1.0 wt % K-$Cu_{0.5}Mg_5CeO_x$ by systematically adding CO_2 (0.02 MPa) into the CO/H_2 stream. The reaction was carried out at 573 K and 2.0 MPa with a GHSV of 23000

cm^3/g-cat-h. The addition of 0.02 MPa (1 %) CO_2 decreased methanol productivity by 50 % (Figure 3.31). An even stronger inhibition effect of CO_2 on isobutanol production was observed. Removal of CO_2 from the stream recovers methanol but does not fully recover isobutanol production. The introduction of CO_2 into the reactor increases the ratio of CO_2-to-($CO+H_2$) and decreases the number of surface Cu sites due to the oxidation of surface Cu atoms by CO_2, resulting in a decrease in methanol synthesis rate. CO_2 could also occupy surface basic sites. The dramatic decrease in isobutanol synthesis rate upon CO_2 addition is due to the decrease in 1) both Cu and basic sites required for chain-growth aldol-condensation reactions and 2) the concentration of methanol.

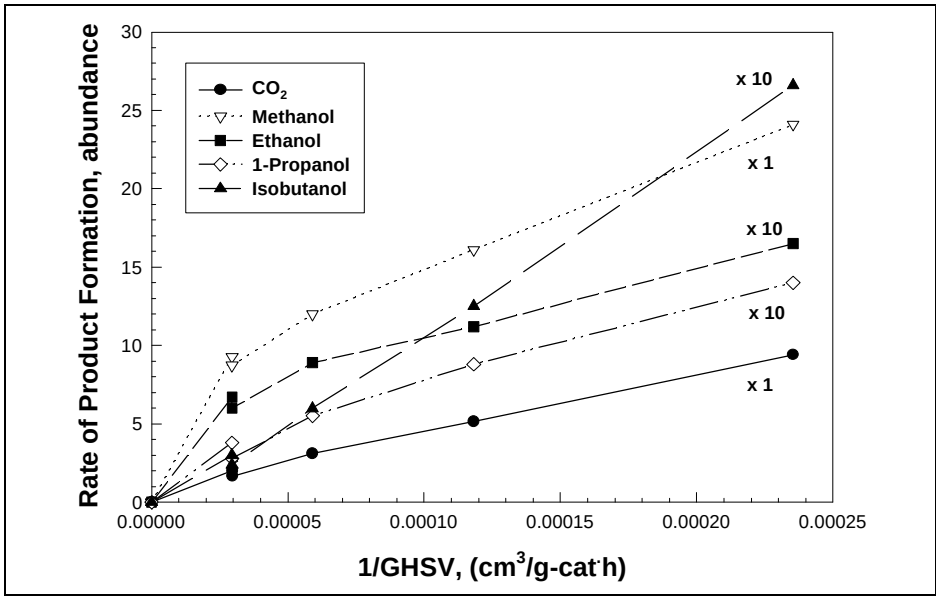

Figure 3.30. Effect of GHSV on alcohol production on 1.0 wt % K-$Cu_{0.5}Mg_5CeO_x$. [$CO/H_2/Ar$ = 0.45/0.45/0.10, 573 K, 2.0 MPa, 150 mg catalyst charge].

The effect of temperature on alcohol formation was studied at 2.0 MPa with a GHSV of 17000 cm^3/g-cat-h. The Arhenius plots of alcohol formation rates versus the reciprocal of temperature are shown in Figure 3.32. Alcohol production rates increases with increasing temperature. The apparent activation energy is greater for isobutanol formation than for other alcohols. The lower apparent activation energies observed for ethanol and 1-propanol formation are due to the fact that they are reaction intermediates. More ethanol and 1-propanol react once they form at higher temperatures. Higher temperature favors isobutanol over methanol, because the latter is thermodynamically-limited and also undergoes secondary reactions at high temperatures.

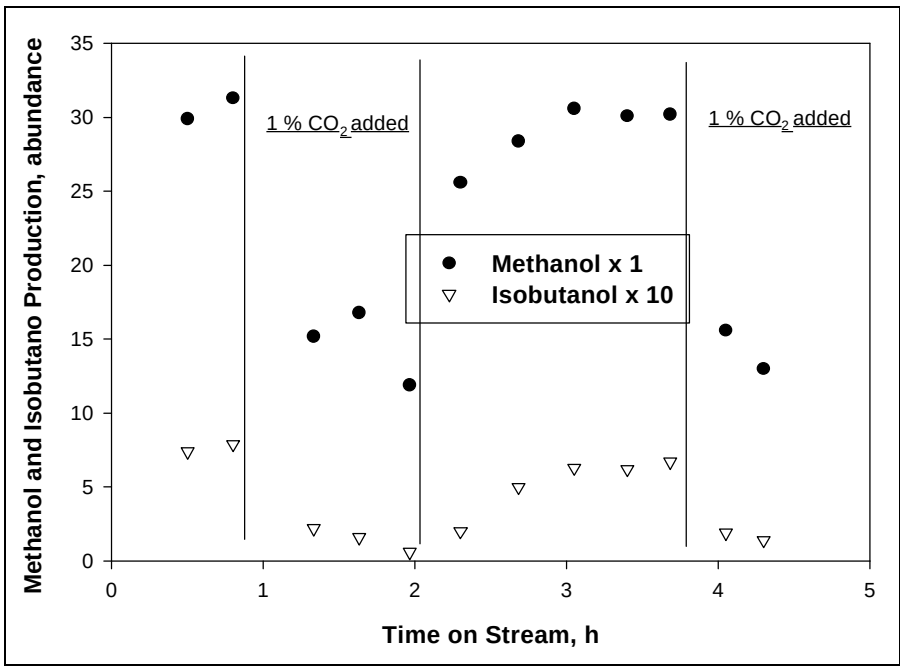

Figure 3.31. Effect of CO_2 on methanol and isobutanol production on 1.0 wt % K-$Cu_{0.5}Mg_5CeO_x$. [$CO/H_2/Ar/CO_2$ = 0.45/0.45/0.10/0.01, 573 K, 2.0 MPa, GHSV = 23000 cm^3/g-cat-h].

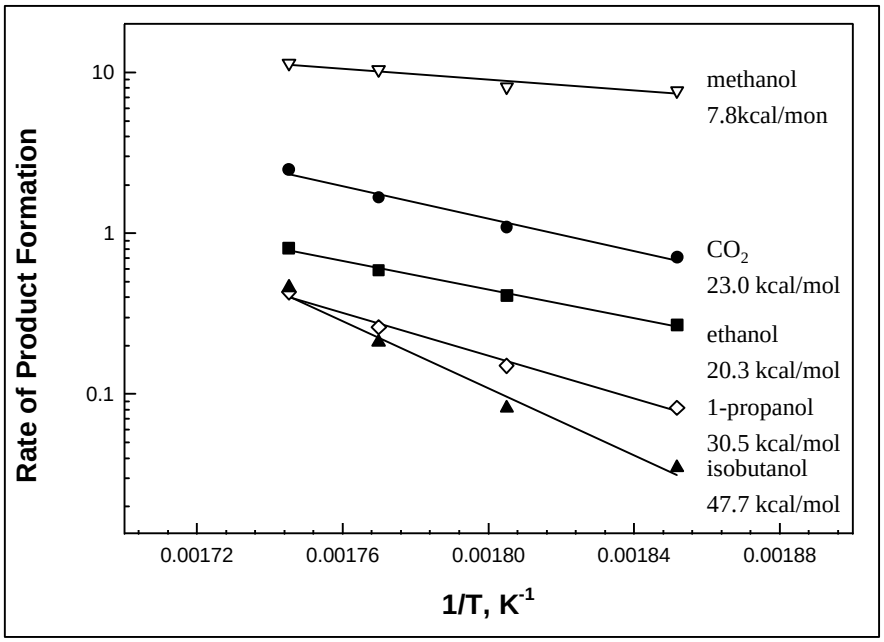

Figure 3.32. Arrhenius plot of the rate of product formation vs. temperature on 1.0 wt % K- $Cu_{0.5}Mg_5CeO_x$. [$CO/H_2/Ar$ = 0.45/0.45/0.10, 2.0 MPa, GHSV = 17000 cm^3/g-cat-h].

The formation of higher alcohols from synthesis gas (CO/H_2) has been widely studied, predominantly on alkali-modified methanol synthesis catalysts, but significant details about the reaction pathways involved in the formation of initial carbon-carbon bonds remain unresolved. Elliot and Pennella [100] and Nunan et al. [27] used isotopic tracer methods in order to identify the intermediate species involved in the formation of ethanol from CO/H_2 on $Cu/ZnO/Al_2O_3$ and Cs-promoted Cu/ZnO catalysts.

The addition of ^{13}C-labeled methanol to CO/H_2 feeds on Cs-promoted Cu/ZnO led to ethanol with substantial ^{13}C content [27]. The concentration of injected methanol was much lower than the equilibrium methanol concentration at their reaction conditions. ^{13}C NMR analysis of reaction products confirmed the presence of a large fraction of doubly-labeled ethanol and showed that the ^{13}C-atom in singly-labeled ethanol molecules was distributed with equal probability among the two carbon positions. These data led to the conclusion that secondary reactions of primary methanol products were the predominant and possibly exclusive pathways for the formation of ethanol. Klier et al. [27] proposed that the initial C-C formation occurs by the nucleophilic attack of formaldehyde by an adsorbed formyl species on Cs^+. Both formyl and formaldehyde species are believed to be formed from methanol.

A similar study on $Cu/ZnO/Al_2O_3$ was reported by Elliot and Pennela [100] at reaction conditions leading to very low conversions of CO and H_2. The experiments were carried out at conditions far removed from methanol synthesis equilibrium in order to minimize isotopic contamination of ^{12}CO by decomposition of $^{13}CH_3OH$. Both unlabeled and labeled ethanol were detected, even at very low conversions, suggesting that both ^{12}CO and $^{13}CH_3OH$ participate in the synthesis of ethanol. Smith et al. [101] also reported that both methanol and CO are direct precursors to the C_1 species that lead to ethanol formation on these catalysts. Our studies extend these previous studies by exploring reaction pathways for the formation of initial C-C bonds during synthesis gas conversion to higher alcohols on $K\text{-}Cu\text{-}Mg_5CeO_x$ catalysts.

Isotopic tracer studies of alcohol synthesis pathways were carried out on 1.0 wt % $K\text{-}Cu_{0.5}Mg_5CeO_x$ catalysts using a mixture of $^{13}CO/H_2$ and $^{12}CH_3OH$ in order to probe the roles of CO and methanol in chain growth pathways. $K\text{-}Cu_{0.5}Mg_5CeO_x$ is among the most active and selective catalysts for the synthesis of higher alcohols at low temperatures [7], [8], [30]. These catalysts were prepared by synthesis procedures described in the literature [8], [30]. ^{13}CO (^{13}C: 99%, ^{18}O < 1%, Cambridge Isotope) was used as the labeled reactants because an ^{18}O impurity typically present in ^{13}C-labeled methanol severely compromises the accuracy of isotopic analyses of reaction products.

Isotopic tracer experiments were carried out at low temperatures (538 K) in order to maintain low conversions and to keep the reaction far removed from methanol synthesis equilibrium. Reaction rates were first measured at 2.0 MPa and a gas hourly space velocity of 6000 $cm^3(CO+H_2)$/g-cat-h using an equimolar mixture of ^{13}CO and H_2 and a 100 mg catalyst sample. After steady-state rate measurements, the equimolar $H_2/^{13}CO$ mixture was routed through a saturator containing liquid $^{12}CH_3OH$ at room temperature and isotopic tracer experiments were carried out at several space velocity and CO conversion levels. All inlets and effluent lines were heated to 363 K in order to prevent condensation of reactants and products. The effluent stream was analyzed by extracting a sample using a syringe and injecting it into a gas chromatograph-mass spectrometer system (Hewlett-Packard, Model 5890 II Plus GC; Hewlett-Packard, Model

5972 Mass Selective Detector). Reaction products were also trapped after the reactor using a tube cooled by liquid nitrogen. This method allowed the accumulation of larger amounts of products for multiple GC-MS analyses required to increase the accuracy of isotopic content measurements. The ^{13}C-content in reactants and products was calculated from mass spectra using a matrix deconvolution method that accounts for natural abundant isotopic impurities and for mass fragmentation [65].

At the conditions of our study (538 K, 2.0 MPa, and $H_2/^{13}CO = 1$) the equilibrium partial pressure of methanol is 86.6 kPa (118)[8]. The partial pressure of $^{12}CH_3OH$ in the feed was 13.3 kPa; and the ratio of $^{12}CH_3OH$ to ^{13}CO was 1:75. All experiments were carried out at CO conversions below 1 %. The most abundant reaction products were $^{13}CH_3OH$ and $^{13}CO_2$. Ethanol, 1-propanol, isobutanol, methyl formate, and methyl acetate were also detected and their concentrations in the effluent stream and their formation rates as a function of bed residence time are shown in figures 3.33 and 3.34. Bed residence time is calculated from the gas volumetric flow rate at reaction temperature and pressure and the catalyst bed volume.

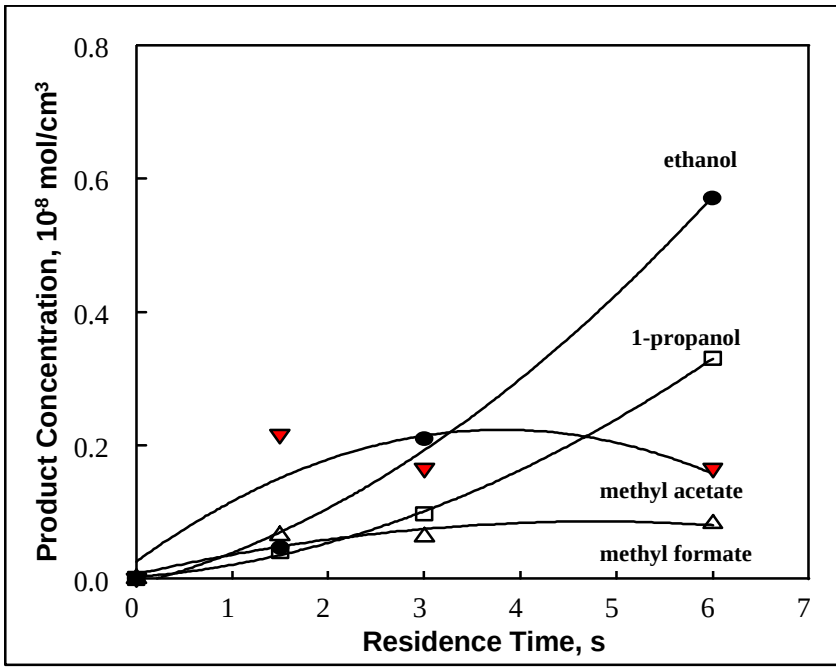

Figure 3.33. Effect of bed residence time on product concentration for 1.0 wt % K-$Cu_{0.5}Mg_5CeO_x$. [538 K, 2.0 MPa, $^{13}CO/H_2/CH_3OH = 100/100/1.3$].

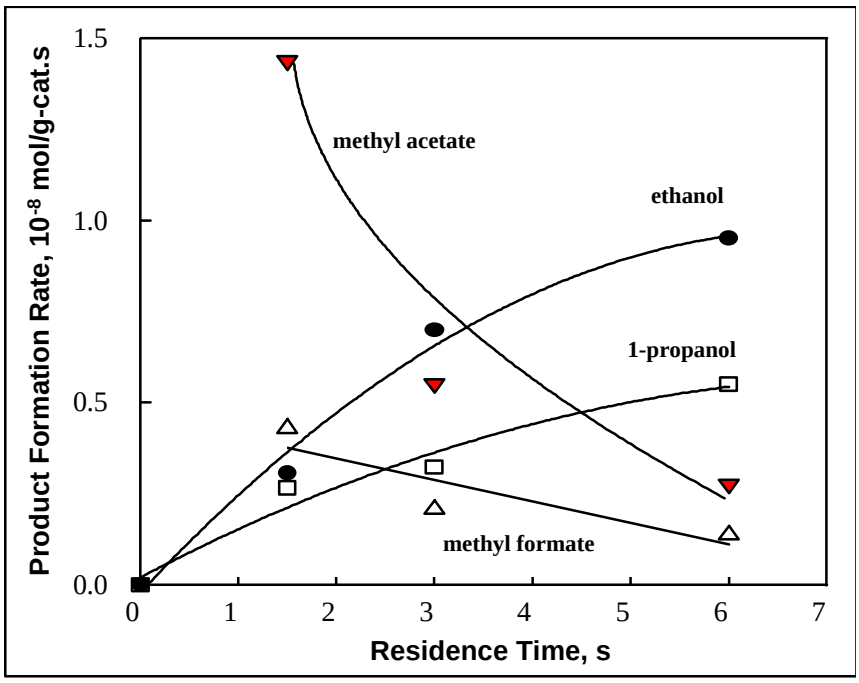

Figure 3.34. Effect of bed residence time on product formation rate for 1.0 wt % K-$Cu_{0.5}Mg_5CeO_x$. [538 K, 2.0 MPa, $^{13}CO/H_2/CH_3OH$ = 100/100/1.3].

Ethanol and 1-propanol concentrations increased with increasing bed residence time (figure 3.33), suggesting that neither reaction product approaches thermodynamic equilibrium. The increased formation rates of ethanol and 1-propanol with increasing residence time suggest that they are secondary reaction products (figure 3.34). Both methyl formate and methyl acetate concentrations, however, leveled off with increasing residence time (figure 3.33), suggesting that they are reaction intermediates or approach thermodynamic equilibrium, consistent with the decreased formation rates of methyl formate and methyl acetate as residence time increases (figure 3.34).

^{13}C contents as a function of bed residence time are shown in figure 3.35 for each alcohol product detected. The ^{13}C content in methanol increases with increasing bed residence time because ^{13}CO hydrogenation leads to the formation of labeled methanol. The ^{13}C content in ethanol decreases with increasing bed residence; extrapolation of the ethanol isotopic content to zero residence time shows that the initial ethanol product is predominantly labeled (94 %). Thus, ethanol is formed predominantly by direct reactions of ^{13}CO without significant involvement of the $^{12}CH_3OH$ present in the feed, at least under our experimental conditions using a $^{13}CO/^{12}CH_3OH$ ratio of 75 in the feed.

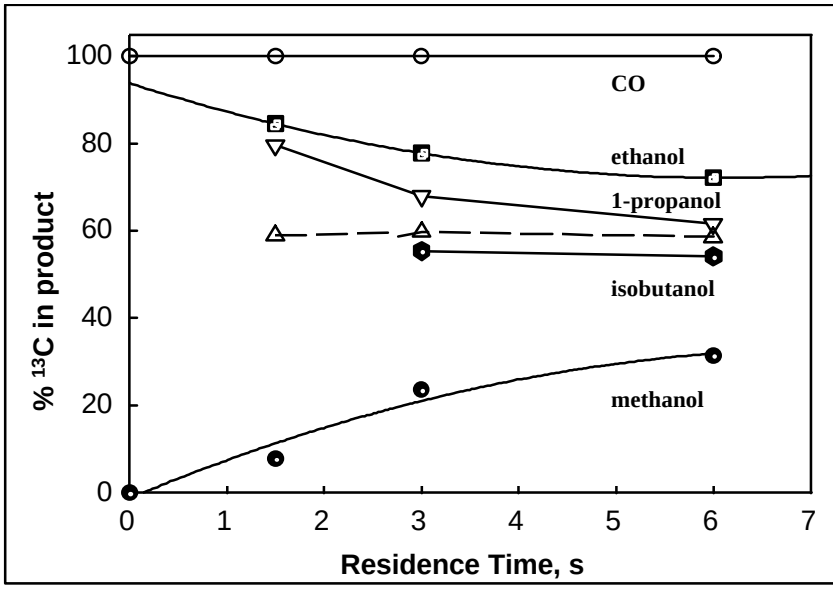

Figure 3.35. Effect of bed residence time on product carbon-13 distribution for 1.0 wt % K-$Cu_{0.5}Mg_5CeO_x$. [538 K, 2.0 MPa, $^{13}CO/H_2/CH_3OH$ = 100/100/1.3]

At longer residence times, ethanol is also formed by reverse aldol reactions of higher alcohols, which contain lower ^{13}C contents because of the significant involvement of $^{12}CH_3OH$ in their formation. This reverse reaction leads to the observed decrease in ^{13}C content in ethanol with increasing residence time. Indeed, ^{13}C contents in 1-propanol and 2-methyl-1-propanol (isobutanol) are significantly lower than in ethanol. This is consistent with synthesis pathways involving condensation reactions of ethanol and methanol, leading to the formation of 1-propanol and 2-methyl-1-propanol [30]. The detailed mechanism for the reversed aldol-condensation reactions, which lead to the decreased ^{13}C content in ethanol, can be described as follow:

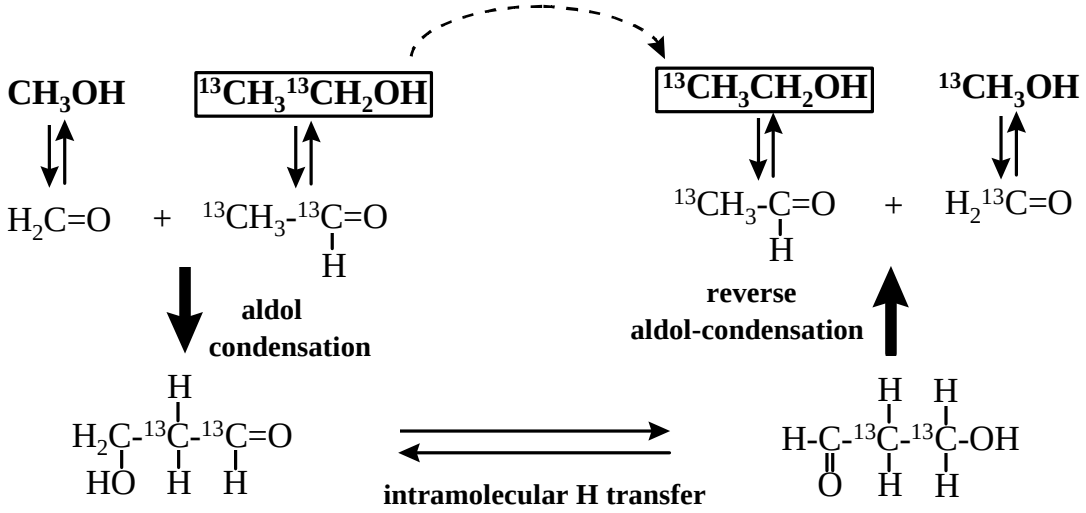

The ^{13}C contents in 1-propanol calculated by assuming 1-propanol formed exclusively from methanol addition to ethanol via aldol-condensation reactions (dashed line in figure 3.32) is, however, lower than experimental values. This indicates that one pathway for ethanol to 1-propanol chain growth involves carbonylation of C_2H_5OH by ^{13}CO. This is consistent with linear chain growth pathways that lead to the formation of some 1-butanol during CO hydrogenation on K-$Cu_{0.5}Mg_5CeO_x$ [59].

In addition to labeled higher alcohols, methyl formate and methyl acetate with significant ^{13}C enrichment were also formed. The ^{13}C content and isotopic distribution in methyl formate are reported in table 1 at several values of residence time. The methyl formate products at short residence time (1.5 s) are mainly singly-labeled (90%), with about 95 % ^{13}C at the carbonyl carbon atom for the singly-labeled methyl formate. Methyl formate has been shown to form by reactions of methanol with CO on basic catalysts (36). Our results are consistent with the nucleophilic attack on ^{13}CO by the oxygen atom in $^{12}CH_3OH$, leading to the predominant presence of ^{12}C in the methyl group of methyl formate. The ^{13}C content in the methyl group of methyl formate increases with increasing bed residence time, because the required methanol reactant acquires increasing amounts of ^{13}C via ^{13}CO hydrogenation. The ^{13}C content in the carbonyl group remains high because CO retains its high isotopic purity throughout the entire range of residence time. As discussed below, reactions involving methyl formate or related surface precursors, such as $CH_3O^*CO^-$, may lead to the initial C-C bond formation during the synthesis of ethanol from H_2-CO mixtures.

Table 3.4. Isotopic composition of methyl formate formed from $^{13}CO/^{12}CH_3OH/H_2$ reactants on 1.0 wt % K-$Cu_{0.5}Mg_5CeO_x$ at several bed residence times [538 K, 2.0 MPa, $^{13}CO/H_2/CH_3OH$ = 100/100/1.3]

Contact time, s	1.5	3.0	6.0
		^{13}C, %	
H-^{13}CO-O-$^{13}CH_3$	7.8	21.7	29.5
H-^{13}CO-O-$^{12}CH_3$	88.9	68.3	60.7
H-^{12}CO-O-$^{13}CH_3$	3.3	4.8	4.4
H-^{12}CO-O-$^{12}CH_3$	0	5.2	5.4
total ^{13}C content	52.3	55.9	59.9

At short residence time and low CO conversion levels, gas phase methanol and any surface intermediates derived from methanol are predominantly unlabeled. CO insertion into surface methoxide species leads to an intermediate species ($CH_3O^*CO^-$) stabilized by alkali cations present in alkali-modified basic oxides [41]. Theoretical studies carried out by Klier et al. [113] show that the nucleophilic attack of CO by surface methoxide species is an exothermic reaction and no activation barrier exists for such a reaction. These intermediates ($CH_3O^*CO^-$) lead to either methanol via hydrogenation reactions, as suggested for surface formate species [114]- [115] or to methyl formate with labeled ^{13}C predominantly in the carbonyl group via the following hydrolysis reactions [41]:

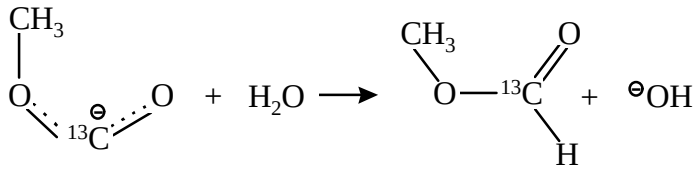

In addition to hydrogenation and hydrolysis reactions, surface $CH_3O^*CO^-$ species can also undergo isomerization reactions leading to acetate species that contain the initial carbon-carbon bond. Hydrolysis of these surface acetate species followed by esterification reaction with methanol can lead to methyl acetate. As mentioned earlier, methyl acetate production goes through a maximum with increasing bed residence time, suggesting that it is a reaction intermediate and the hydrogenolysis of which could form ethanol. Unlike the hydrolysis reactions of $CH_3O^*CO^-$, which are exothermic and require no activation energy, theoretical calculations show that isomerization of surface $CH_3O^*CO^-$ (via methyl shift) to $CH_3{}^*COO^-$ (acetate) on alkali cations, however, requires a very high activation energy [27]. Therefore, the formation of surface acetate species and thus the hydrogenolysis of such species to form ethanol is not expected. Also, such pathways would predict the initial formation of ethanol molecules with a single ^{13}C-atom at the 1-position. Our data show that the initial ethanol products are doubly-labeled (figure 3.35). At short residence times, doubly-labeled methyl acetate is also the predominant species and ^{13}C atoms are located in the CH_3-CO group (table 3.5). Therefore, isomerization of surface methyl formate species cannot account for the formation of carbon-carbon bonds in either methyl acetate (table 3.5) or ethanol (table 3.6).

Table 3.5. Isotopic composition of methyl acetate formed from $^{13}CO/^{12}CH_3OH/H_2$ reactants on 1.0 wt % K-$Cu_{0.5}Mg_5CeO_x$ at several bed residence times [538 K, 2.0 MPa, $^{13}CO/H_2/CH_3OH$ = 100/100/1.3]

Contact time, s	1.5	3.0	6.0
		^{13}C, %	
$^{13}CH_3$-^{13}CO-O-$^{13}CH_3$	5.5	15.8	26.8
$^{13}CH_3$-^{12}CO-O-$^{13}CH_3$ $^{12}CH_3$-^{13}CO-O-$^{13}CH_3$	0.5	6.4	11.6
$^{13}CH_3$-^{13}CO-O-$^{12}CH_3$	63.1	51.5	42.8
$^{13}CH_3$-^{12}CO-O-$^{12}CH_3$ $^{12}CH_3$-^{13}CO-O-$^{12}CH_3$	23.1	17.8	11.1
$^{12}CH_3$-^{12}CO-O-$^{13}CH_3$	1.4	2.8	7.7
$^{12}CH_3$-^{12}CO-O-$^{12}CH_3$	6.6	5.6	0
total ^{13}C content	56.2	60.6	69.3

Table 3.6. Isotopic composition of ethanol formed from $^{13}CO/^{12}CH_3OH/H_2$ reactants on 1.0 wt % K-$Cu_{0.5}Mg_5CeO_x$ at several bed residence times [538 K, 2.0 MPa, $^{13}CO/H_2/CH_3OH$ = 100/100/1.3]

Contact time, s	1.5		3.0		6.0	
	^{13}C, %					
	expt.	[a]predicted	expt.	[a]predicted	expt.	[a]predicted
$^{13}CH_3$-$^{13}CH_2OH$	77.0	68.6	63.1	67.3	57.0	69.6
$^{13}CH_3$-$^{12}CH_2OH$	4.6	[b]23.6	9.8	[b]24.2	11.8	[b]22.7
$^{12}CH_3$-$^{13}CH_2OH$	10.4		16.5		19.2	
$^{12}CH_3$-$^{12}CH_2OH$	8.0	8.0	10.6	8.4	12.0	7.7
total ^{13}C content	84.5		76.3		72.5	

[a] Predicted values if ethanol formed from methyl acetate.

[b] Percentage of singly-labeled ethanol with ^{13}C in either carbon group.

The isotopic composition of methyl acetate is consistent with the pathways shown in figure 4, where M^+ represents cations such as K^+ and Mg^{2+}. The nucleophilic attack of surface methyl formate (or formate) species containing ^{13}C in the carbonyl group by surface CH_3O*CO^- (or formate) species leads to the formation of the initial C-C bond (steps I and II, figure 3.36). Methyl formate ions could also react with surface formaldehyde species derived from methanol to form a singly-labeled carbon-carbon moiety (step III). Aldol self-condensation reactions of formaldehyde derived from methanol, as suggested by Klier et al. [27], lead only to an unlabeled carbon-carbon moiety. Since most carbon-carbon moieties in ethanol and methyl acetate are doubly-labeled, reaction pathways I and II are most likely to occur. Hydrogenation of these surface oxygenated species leads to the formation of methyl acetate species that can desorb from the surface or undergo hydrogenolysis to form ethanol and methanol at the high hydrogen pressures typical of higher alcohol synthesis.

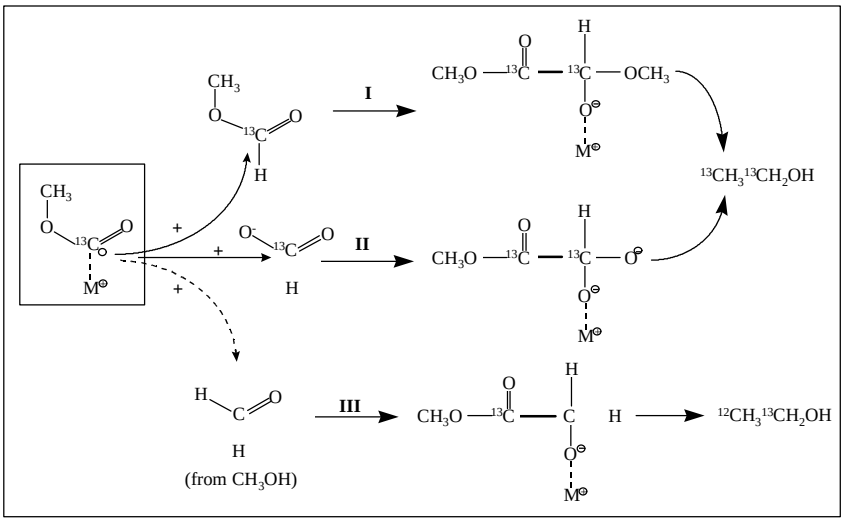

Figure 3.36. Pathways for carbon-carbon bond formation in methyl acetate.

The hydrogenolysis of surface formate leads to the formation of methanol on methanol synthesis catalysts [113 - 116]. A similar type of reaction would lead to ethanol and methanol via hydrogenolysis of methyl acetate. This is consistent with the observed similarity between the ^{13}C content and distribution in the CH_3CO group within methyl acetate (table 3.5) and in the ethanol product of $^{13}CO/^{12}CH_3OH/H_2$ reactions (table 3.6). At short bed residence time, both carbon atoms in the C-C group of methyl acetate and ethanol are predominantly labeled (tables 3.5 and 3.6). The effects of residence time on the rate and selectivity for the formation of ethanol, methyl formate, and methyl acetate are consistent with the intermediate role of methyl formate in the formation of methyl acetate and with a subsequent role of the methyl acetate in the formation of ethanol during CO hydrogenation. Ethanol formation rates increase with increasing residence time, while formation rates for methyl acetate and methyl formate are only weakly affected. If ethanol were a precursor to methyl acetate, methyl acetate formation rates would increase as ethanol formation rate increases. Our experimental results, however, suggest that methyl acetate might be a precursor to ethanol. It is also possible that ethanol and methyl acetate are formed from a similar precursor, the concentration of which increases with increasing residence time. The rate of formation of methyl acetate goes through a maximum with increasing residence time, suggesting that, in contrast with ethanol, methyl acetate is a reactive intermediate.

Reaction pathways for the formation of higher alcohols from CO/H_2, especially the chain-growth pathways from C_1 to C_2 alcohols, were investigated on Cs-promoted $CuZnAlO_x$ catalysts. The experiments described attempts to resolve the wide range of conclusions reached on $Cu/ZnO/Al_2O_3$, Cs-promoted Cu/ZnO, and K-Cu-Mg_5CeO_x by a more detailed analysis of the chemical and isotopic composition of reaction products. At the conditions of our study (538 K, 2.0 MPa, and $H_2/^{13}CO$ = 1) the equilibrium partial pressure of methanol is 86.6 kPa (118). The partial pressure of $^{12}CH_3OH$ in the feed was 13.3 kPa; and the ratio of $^{12}CH_3OH$ to ^{13}CO was 1:75. All experiments were carried out at less than 1 % CO conversion. Methanol, ethanol, 1-propanol, isobutanol, methyl formate, methyl acetate, and CO_2 were detected. The ratio of alcohols to methyl formate and methyl acetate was larger for Cs-$CuZnAlO_x$ than for K-Cu-Mg_5CeO_x. Alcohol concentrations in the effluent are shown in figure 3.37 as a function of bed residence time. Bed residence time is calculated from the gas volumetric flow rate at reaction temperature and pressure and the catalyst bed volume.

Methanol concentration in the effluent increases with increasing bed residence time, suggesting that the methanol synthesis step is not totally controlled by thermodynamic equilibrium at conditions of these experiments. The nonlinear increases of ethanol and 1-propanol production rates with increasing bed residence time suggest that both species are intermediate products that undergo further reaction. Isobutanol formation increases with increasing bed residence time, suggesting that isobutanol is a final product which does not undergo further reactions. Moreover, isobutanol production is not inhibited by CO_2 produced during the reaction possibly due to the much lower CO_2 content at the higher space velocities and lower CO conversions of this study compared to that at lower space velocity and high CO conversions [30].

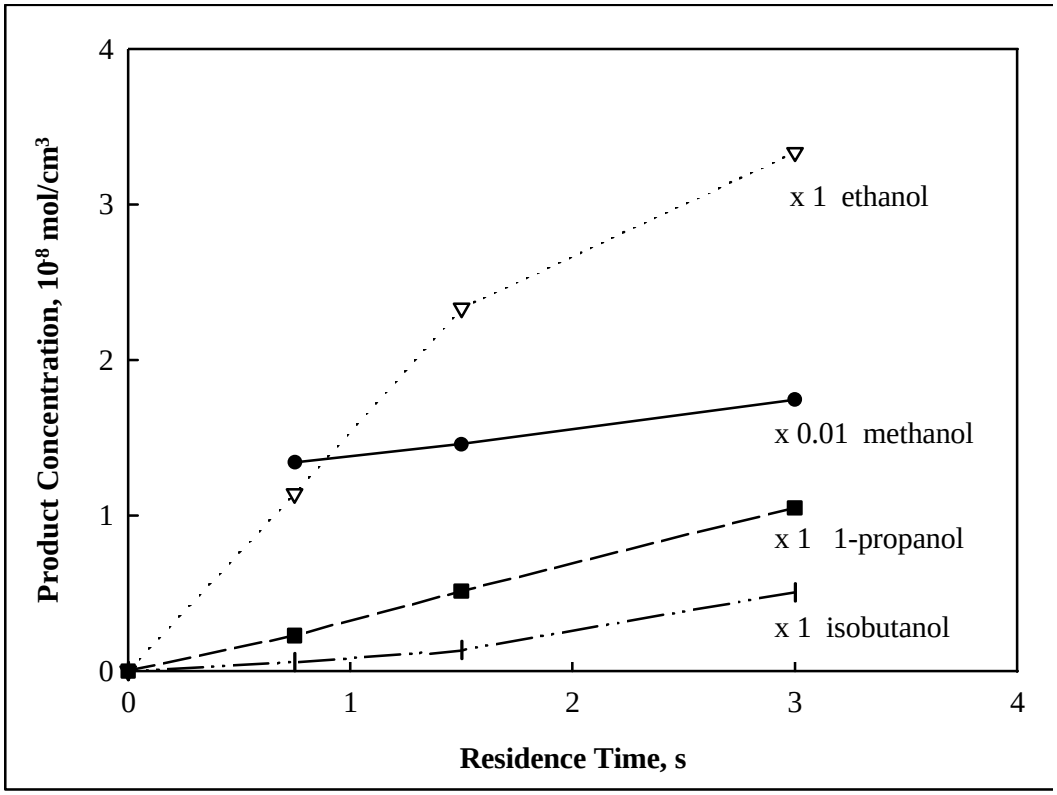

Figure 3.37. Effect of bed residence time on production concentration for Cs-$CuZnAlO_x$. [538 K, 2.0 MPa, $^{13}CO/H_2/^{12}CH_3OH$ = 100/100/1.3]

^{13}C contents as a function of bed residence time are shown in figure 3.38 and table 3.7 for methanol, ethanol, and 1-propanol. The ^{13}C content in methanol increases with increasing bed residence time because ^{13}CO hydrogenation leads to the formation of labeled methanol. The ^{13}C content in ethanol also increases with increasing bed residence; extrapolation of the ethanol isotopic content to zero residence time shows that the initial ethanol is predominantly unlabeled (86%) . This behavior differs from that observed on K-$Cu_{0.5}Mg_5CeO_x$, but it is similar to the results of Pennela and Elliot [1] on $Cu/ZnO/Al_2O_3$ and of Nunan et al. [27] on Cs-promoted Cu/ZnO. The ^{13}C content in ethanol formed on K-$Cu_{0.5}Mg_5CeO_x$ increases with decreasing bed space velocity [30]; extrapolation of the ethanol isotopic content to zero residence time shows that the initial ethanol product is predominantly unlabeled (> 90%). On 1.0 wt% K-$Cu_{0.5}Mg_5CeO_x$ we then concluded that ethanol is formed mainly by direct reactions of ^{13}CO, without significant involvement of the $^{12}CH_3OH$ present in the feed. On Cs-promoted $CuZnAlO_x$ catalysts, however, ethanol appears to be formed by the coupling reactions of methanol as suggested by Klier and co-workers [41], or ethanol and methanol formed from the same precursor, as proposed by Pennela [27], since ^{13}C contents in both methanol and ethanol increase with increasing bed residence time.

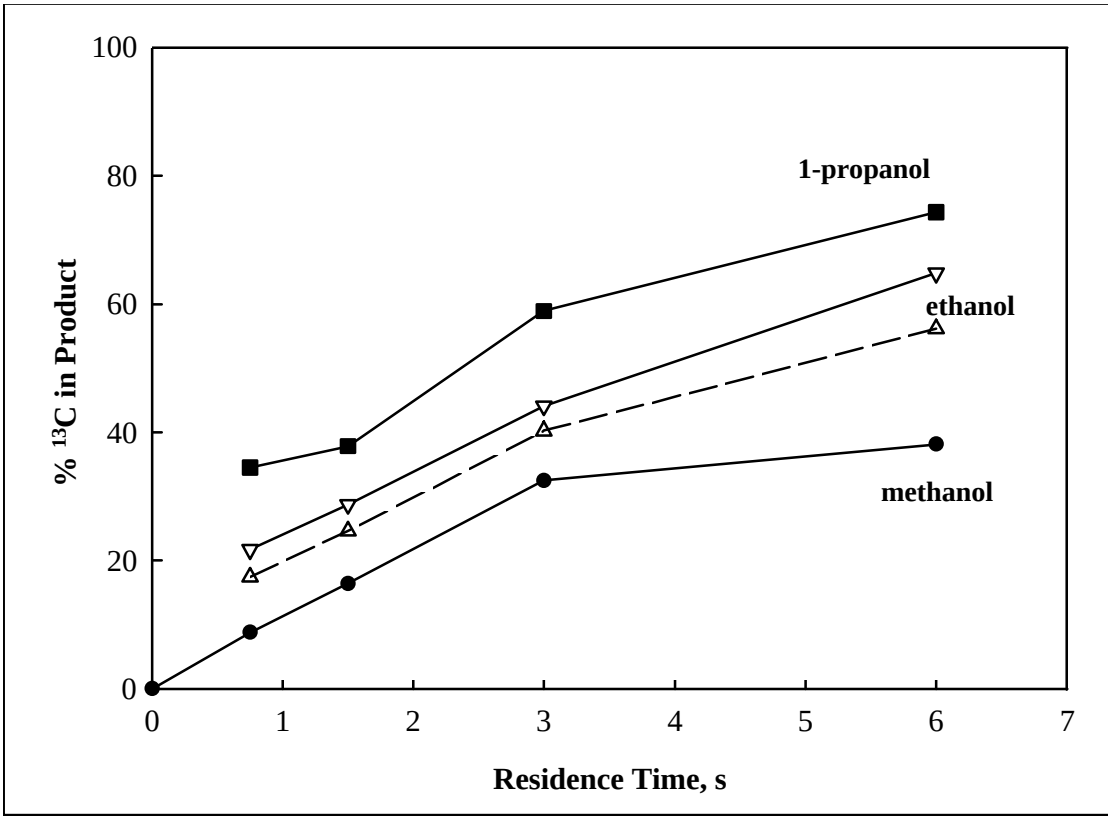

Figure 3.38. Effect of bed residence time on product carbon-13 distribution for Cs-$CuZnAlO_x$. [538 K, 2.0 MPa, $^{13}CO/H_2/^{12}CH_3OH$ = 100/100/1.3]

Table 3.7. Isotopic composition of ethanol formed from $^{13}CO/^{12}CH_3OH/H_2$ reactants on Cs-$CuZnAlO_x$ at several bed residence times. [538 K, 2.0 MPa, $^{13}CO/H_2/CH_3OH$ = 100/100/1.3].

Contact time, s	0.75	1.5	3.0	6.0
		Isotopomer Distribution, mol%		
$^{13}CH_3$-$^{13}CH_2OH$	7.6	11.0	22.6	48.0
$^{13}CH_3$-$^{12}CH_2OH$	9.6	12.8	15.9	12.0
$^{12}CH_3$-$^{13}CH_2OH$	18.8	22.6	27.2	21.5
$^{12}CH_3$-$^{12}CH_2OH$	64.0	53.6	34.2	18.5
total ^{13}C content	21.8	28.7	44.1	64.7

Ethanol is predominantly unlabeled (86% ^{12}C) at short bed residence times and low conversions on for Cs-$CuZnAlO_x$ (figure 3.38), suggesting that it forms by the direct coupling reactions of methanol or its derivatives. However, ^{13}C content in ethanol about 14% for Cs-promoted $CuZnAlO_x$ catalysts at zero bed residence time. This labeled ethanol at zero residence time may form directly from ^{13}CO following the pathways described for K-$Cu_{0.5}Mg_5CeO_x$. But the predominant pathway for the formation of ethanol on Cs-promoted $CuZnAlO_x$ is the coupling of methanol. It should be pointed out that predominant pathway for the formation of ethanol on K-$Cu_{0.5}Mg_5CeO_x$ is the direct reactions of ^{13}CO because about 94 % ethanol is labeled at zero bed residence time.

The two different major pathways for the initial C-C formation on Cs-promoted $CuZnAlO_x$ and K-$Cu_{0.5}Mg_5CeO_x$ might be attributed to different properties of alkali promoters. Cs^+-O^{2-} cation-anion pair is able to break the C-H bond of formaldehyde to form surface $Cs^+(CHO^-)$ species (37), which undergoes subsequently neucleophilic attack of formaldehyde species to form initial C-C bond. K^+-O^{2-}, however, may not be able to break C-H bond of formaldehyde or K^+ cannot stabilize the CHO- intermediates because K^+ is less acidic than Cs^+ and the oxygen ion related to K^+ is less basic than that related to Cs^+. The other possibility is that the larger Cu surface area of Cs-$CuZnAlO_x$ (23.5 m^2/g) compared to K-$Cu_{0.5}Mg_5CeO_x$ (11.4 m^2/g) enhances methanol dehydrogenation rate and therefore increases the local concentration of very reactive formaldehyde intermediates may favor direct coupling of methanol-derived C_1 species.

The rate of ethanol formation directly from ^{13}CO is expected to be similar on Cs-promoted $CuZnAlO_x$ and K-$Cu_{0.5}Mg_5CeO_x$ because this pathway is likely to proceed on both K-$Cu_{0.5}Mg_5CeO_x$ [30] and Cs^+-O^{2-} cation-anion pairs. The other pathway, i.e., methanol coupling to form unlabeled ethanol, proceeds faster on Cs- $CuZnAlO_x$ than on K-$Cu_{0.5}Mg_5CeO_x$ because of the lower ethanol isotopic content observed on the former. The overall rate of ethanol formation, therefore, is expected to be larger on Cs-promoted $CuZnAlO_x$ than on K-$Cu_{0.5}Mg_5CeO_x$. Indeed, the rate of ethanol formation is about an order of magnitude greater on $CuZnAlO_x$ (1.1×10^{-8} mol/s) than on K-$Cu_{0.5}Mg_5CeO_x$ (7.0×10^{-10} mol/s).

The ^{13}C content in 1-propanol increases with increasing bed residence time in a similar manner as methanol and ethanol (figure 3.38 and table 3.8), suggesting the involvement of methanol and ethanol via condensation reactions in the formation of 1-propanol. The ^{13}C contents in 1-propanol calculated by assuming 1-propanol formed exclusively from methanol addition to ethanol via aldol-condensation reactions (dashed line in figure 2) is, however, lower than experimental values. This indicates that one pathway for ethanol to 1-propanol chain growth involves carbonylation of C_2H_5OH by ^{13}CO. This is consistent with linear chain growth pathways that lead to the formation of some 1-butanol during CO hydrogenation on Cs-$CuZnAlO_x$ [56].

These isotopic tracer studies have shown that ethanol is formed by both direct reactions of CO and direct coupling of methanol on higher alcohol synthesis catalysts. Although direct reaction of CO is the predominant pathway on K-$Cu_{0.5}Mg_5CeO_x$ at short residence time, the main pathway on Cs-promoted $CuZnAlO_x$ involves the direct coupling reactions of methanol. The different properties of alkali promotes and different Cu surface area may be responsible the two different pathways on these catalysts.

Table 3.8. Isotopic composition of 1-propanol formed from $^{13}CO/^{12}CH_3OH/H_2$ reactants on Cs-$CuZnAlO_x$ at several bed residence times. [538 K, 2.0 MPa, $^{13}CO/H_2/CH_3OH$ = 100/100/1.3]

Contact time, s	0.75	1.5	3.0	6.0
Number of ^{13}C		^{13}C, %		
0	37.5	30.6	10.8	4.9
1	35.5	37.1	30.9	18.3
2	12.9	21.0	29.2	25.9
3	14.1	11.4	29.1	50.9
total ^{13}C content, experimental	34.5	37.8	58.9	74.3
total ^{13}C content, predicted[a]	17.4	24.6	40.2	56.1

[a] Predicted values if 1-propanol formed from methanol and ethanol.

Task 5: Bench Scale Testing at Air Products and Chemicals

Cs-Modified Catalyst Testing

A sample of the Cs-promoted BASF catalyst (sample number 13465-26), previously used as the catalyst for the isobutanol plant trial and sent to UC-Berkeley for testing was evaluated in APCI fixed-bed reactor. The series of data measured in the standard CSTR unit was to be used as the baseline for the performance of this catalyst in the reactor setup at Berkeley. Since the reactor at Berkeley is a PFR (plug flow reactor), it was decided to run some baseline tests in the PFR which had been previously set up at ACPI.

The PFR is described in a recent topic report sent to the DOE for approval. It consists of a copper-lined reactor heated by an aluminum heating block. (The reactor is in series with the 50 ml. CSTR which was not used for this set of experiments and shares the same analytical system which has been described previously.) This reactor is quasi-isothermal. In order to limit the heat generation, the catalyst was diluted with quartz chips in the ratio of 1:5 by weight. All data are reported relative to the active catalyst only. Only one thermocouple at the outlet of bed exists. Therefore, the degree of isothermality was not established for these preliminary experiments.

Data for the initial runs are summarized in Table 5.1. The initial three runs (14047-49 to 53) were characterized by initially reasonable values for methanol and isobutanol productivity judging from the ratio of isobutanol to methanol from the CSTR runs. This was followed by a rapid decrease in the isobutanol productivity within the first 24 h. The level of isobutanol was in fact lower than that expected for an unpromoted methanol catalyst (See 14047-56, for example.) The methanol productivity also showed a decrease in productivity, although the methanol reaction is at very near equilibrium so that decreases in productivity of the catalyst may not be apparent.

Catalyst poisoning was suspected. The apparatus was taken apart and cleaned. Carbon traps were replaced. The quartz powder and glass wool used in the apparatus were washed with acid to remove any possible trace contaminants. A standard methanol run is now being done to establish a baseline and to show that poisons are not present. The catalyst (S3-86) pellets were grounded and screened before use. The results of this run are in Table 5.1. The run appears normal. Catalyst activity is high after 117 h. The isobutanol productivity, although low, shows little fall-off with time. We conclude that the apparatus is now free of poisons.

Table 5.1. Initial Results of Isobutanol Experiments

Run	Catalyst	T (K)	P (psig)	GHSV (h^{-1})	Time on Stream (h)	MeOH Productivity (gm/kg-h)	Isobutanol Productivity (gm/kg-h)	Ratio MeOH to IBuOH
1404749	Cs-promoted S3-68/quartz	573	768	5040	66.7	*	*	0.11
1404749	"	573	761	5040	77	93	0.19	0.002
1404751	"	573	869	5004	4.65*	*	*	0.015
1404751	"	573	927	5004	23.3	246	2.92	0.012
1404753	"	573	872	5008	4.28	*	*	0.08
1404753	"	573	853	5008	23.4	128	1.05	0.008
1404756	S3-86/quartz acid-washed	523	763	5008	17.7	339	6.55	---
1404756	"	523	770	5008	117	361	5.15	---

* Short time sample-material balance could not be checked because of the large flow of N_2 in the system from changeover after reduction. The partial pressure of the syngas components is also suspected at this time. Ratio of isobutanol to methanol (IBuOH/MeOH) is correct. Procedures have been changed so that this should not be a problem any longer.

Other activities

- *Meetings with Air Products and Chemicals Inc. personnel*

1. Two meetings with APCI personnel to discuss project management and technical details, during the period from 1 October to 31 December 1994.
2. Consulting contacts with Dr. Bernard Toseland regarding operational and design details of CMRU during the period from 1 April to 30 June 1995.
3. Meetings between the UCB program manager and Drs. Richard Underwood and Bernard Toseland at Berkeley, at the DOE Contractor's Meeting in Pittsburgh, and during the Fall Meeting of the American Chemical Society in Chicago during the period from 1 July to 30 September 1995.
4. Meetings between the UCB program manager and Dr. Bernard Toseland at Berkeley during the period from 1 January to 31 March 1996.
5. Meeting with Dr. Bernard Toseland at Berkeley during the period from 1 October to 30 December 1996.
6. Meeting with Dr. Bernard Toseland and Peter T. WWW at Berkeley during the period from 1 October to 30 December 1996.

- *List of publications*

1. Iglesia, E., Barton, D.G., Biscardi, J.A., Gines, M.J.L., and Soled, S.L., "Bifunctional Pathways in Catalysis by Acids and Bases," *Catalysis Today*, **38**, 339 (1997).
2. Xu, M., Gines, M.L., Stephens, B.L., Hilmen, A.-M., and Iglesia, E.,"Isobutanol and Methanol Synthesis on Copper Supported on Magnesium Oxide, " *J. Catal.*, **171**, 130 (1997).
3. Xu, M., Stephens, B.L., Gines, M.L., and Iglesia, E., "Reaction Pathways and Structural Requirements in the Synthesis of Isobutanol from CO and Hydrogen," *Proc. 13th Intern. Coal Conference*, S.H. Chiang, Ed., 1996, pp. 1238-1246.
4. Xu, M. and Iglesia,E., "Initial Carbon-Carbon Bond Formation during Synthesis Gas Conversion to Higher Alcohols on K-Cu-Mg_5CeO_x," *Catal. Lett*. **51**, 47 (1998).
5. Xu, M. and Iglesia, E., "Readsorption and Adsorption-Assisted Desorption of Carbon Dioxide on Basic Solids," *J. Phys. Chem. B*, **102**, 961 (1998).
6. Di Cosimo, J.L., Diez, V.K., Apesteguia, C.R., Xu, M., and Iglesia, E., "Properties of Mg-Al Basic Oxides Obtained from Layered Double Hydroxide Precursors," *J. Catal.*, in press.
7. Hilmen, A.-M., Gines, M.J.L., Xu, M., and Iglesia, E., "Synthesis of Higher Alcohols on Copper Catalysts Supported on Alkali-Promoted Basic Oxides," *Appl. Catal.*, **169**, 355 (1998).
8. Gines, M.J.L. and Iglesia, E., "Bifunctional Condensation Reactions of Alcohols on Basic Oxides Modified by Copper," *J. Catal.*, **176**, 155 (1998).

9. Gines, M.J.L., Oh, H.-S., Xu, M., Hilmen, A.-M., and Iglesia, E., “Isobutanol and Methanol Synthesis on Copper Supported on Alkali-Modified MgO and ZnO Supports,” *Stud. Surf. Sci. Catal.*, in press.
10. Xu, M., Li, W., Reyes, S.C., and Iglesia, E., "$^{13}CO_2/^{12}CO_2$ Isotopic Switch Methods for the Characterization of Basic Sites in Modified MgO Catalysts," *J. Catal.*, to be submitted for publication.
11. Xu, M. and Iglesia, E., "Carbon-Carbon Bond Formation in Higher Alcohol Synthesis on Cs-promoted Cu/ZnO-Al_2O_3 Catalysts," *Catal. Lett.*, to be submitted for publication.

- *List of presentations*

1. Xu, M., Stephens, B.L., Gines, M., and Iglesia, E., “Structural Requirements and Reaction Pathways in the Synthesis of Isobutanol from CO-H_2 Mixtures,” *1996 International Coal Conference*, Pittsburgh, PA, September 1996.
2. Iglesia, E., Xu, M., Stephens, B.L., and Gines, M., “Reaction Pathways and Site Requirements for the Synthesis of Isobutanol from H_2/CO,” *1996 Coal Liquefaction and Gas Conversion Contractors Review Conference*, Pittsburgh, PA. July 9-11, 1996.
3. Xu, M., Stephens, B.L., Gines, M., and Iglesia, E., “Structural Requirements and Reaction Pathways in the Synthesis of Isobutanol from CO and H_2,” *1996 California Catalysis Society Meeting*, Berkeley, CA, June 3-4, 1996.
4. Iglesia, E., "Kinetic Coupling and Bifunctional Pathways in Catalysis by Solid Acids and Bases," *15th North American Meeting of the Catalysis Society*, Chicago, May, 1997 (Emmett Award Lecture)
5. Iglesia, E., "Kinetic Coupling and Bifunctional Pathways in Catalysis by Solid Acids and Bases," *University of Cape Town*, Johannesburg, Republic of South Africa, August 18, 1997 (Eminent Visitor Award Lecture).
6. Iglesia, E., "Kinetic Coupling and Bifunctional Pathways in Catalysis by Solid Acids and Bases," *University of Wittswatersrand*, Johannesburg, Republic of South Africa, August 20, 1997 (Eminent Visitor Award Lecture).
7. Iglesia, E., "Catalysis on Solid Acids and Bases," *Asia-Pacific Congress on Catalysis* (*APCAT'97*), Seoul, Korea, November 1997 (Plenary Lecture).
8. Iglesia, E., "Synthesis of Higher Alcohols on Metal-Base Bifunctional Catalysts," *5th Chemical Congress of North America*, Cancun, Mexico, November 11-15, 1997.
9. Xu, M., Gines, M.L., Stephens, B.L., and Iglesia, E., "Isobutanol and Methanol Synthesis on Copper Supported on Modified Magnesium Oxide," *1997 Annual Meeting of the American Institute of Chemical Engineers*, Houston, TX, March 9-13, 1997.
10. Iglesia, E., Xu, M., Gines, M.J., and Hilmen, A.M., "Synthesis of Branched Alcohols on Metal-Base Bifunctional Catalysts," *1997 Fall Meeting of the American Chemical Society, Symposium in Honor of John Sinfelt*, Las Vegas, NV, September, 1997.
11. Iglesia, E., "Kinetic Coupling and Bifunctional Pathways in Catalysis by Acids and Bases," *Catalytica*, Mountain View, CA, 1997.

12. Iglesia, E., "Kinetic Coupling and Bifunctional Pathways in Catalysis by Solid Acids and Bases," *Universita degli Studi di Torino, Dipartimento di Chimica*, Turin, Italy, 1997.
13. Iglesia, E., "Kinetic Coupling and Bifunctional Pathways in Catalysis by Solid Acids and Bases," *Snamprogetti Research Laboratories*, San Donato Milanese, Italy, 1997.
14. Iglesia, E., "Kinetic Coupling and Bifunctional Pathways in Catalysis by Solid Acids and Bases," *Enirecerche, ENI, Corporate Research Laboratory*, 1997.
15. Iglesia, E., "Kinetic Coupling and Bifunctional Pathways in Catalysis by Solid Acids and Bases," *Universita di Venezia, Dipartimento di Chimica*, Venice, Italy, 1997.
16. Iglesia, E., "Isotopic and in-Situ Spectroscopic Studies of Heterogeneous Catalysts," *University of Cape Town*, Cape Town, Republic of South Africa, 1997.
17. Iglesia, E., "Kinetic Coupling and Bifunctional Pathways in Reactions by Solid Acids," *SASTECH*, Sasolburg, Republic of South Africa, 1997.
18. Iglesia, E., "Kinetic Coupling and Bifunctional Pathways in Reactions by Solid Acids," *Brigham Young University*, Salt Lake City, Utah, 1997.
19. Iglesia, E., "Synthesis of Higher Alcohols on Metal-Base Bifunctional Catalysts," *Mobil Technology Company*, Dallas, TX, 1997.
20. Xu, M., Hu, Z, and Iglesia, E., "An Isotopic Switch Method for the Characterization of Basic Sites in Solids," *15th North American Meeting of the Catalysis Society*, Chicago, May, 1997.
21. Gines, M.J.L., Xu, M., Hilmen, A., Stephens, B.L., and Iglesia, E., "Synthesis of Branched Alcohols on Bifunctional (Metal-Base) Catalysts Based on MgO Modified by Cu, CeO_x, and Alkali," *15th North American Meeting of the Catalysis Society*, Chicago, May, 1997.
22. Xu, M., Gines, M.J.L., Hilmen, A.-M., and Iglesia, E., "Mechanistic Studies of Alcohol Coupling Reactions on Metal-Base Bifunctional Catalysts," *1997 Annual AIChE Meeting*, Los Angeles, CA, November, 1997.
23. Gines, M.J.L., Xu, M., DiCosimo, J.I., Apesteguia, C.R., and Iglesia, E., "Chain Growth Reactions of Alcohols on Modified Magnesium Oxide," *1998 Spring Meeting of the American Chemical Society*, Dallas, Texas, March 1998.
24. Gines, M.J.L., Oh, H.-S. Xu, M., Hilmen, A.-M., and Iglesia, E., "Isobutanol and Methanol Synthesis on Copper Supported on Modified Magnesium Oxide," *5th Natural Gas Conversion Symposium*, Sicily, Italy, September 1998.
25. Iglesia, E., "Bifunctional Reaction Pathways in Acid and Base Catalysis," *TOCAT-3*, Tokyo, Japan, July 1998 (Keynote Lecture).
26. Iglesia, E., "The Design of Bifunctional Catalysts for the Activation of C-H Bonds," *1998 Fall Meeting of the Materials Research Society, Symposium on Advances in Catalytic Materials*, Boston, MS, December 1998 (Keynote Lecture).
27. Iglesia, E., "Isotopic Tracers and Transients in Heterogeneous Catalysis," *1998 Spring Meeting of the American Chemical Society*, Dallas, TX, March 1998.
28. Iglesia, E., "Kinetic Coupling and Bifunctional Pathways in Catalysis by Solid Acids," Los Alamos National Laboratory, Los Alamos, NM, 1998.

Acknowledgments

The participating project personnel thanks to:

- Dr. B. Toseland and R. Underwood from Air Products.
- Prof. Michel Boudart.
- Dr. Carlos Apesteguia and his research group from Universidad Nacional del Litoral (Argentina).
- Universidad Nacional del Litoral for the partial support of Dr. Marcelo Gines.
- Norwegian Research Council for the support of Dr. Anne-Mette Hilmen.
- Korea Research Foundation for the support of Dr. Hyung-Seuk Oh.
- The project managers: Richard Tischer, Gary Steigel, and Diane Revay-Maden.

References

1. J.G. Nunan, C.E. Bogdan, R.G. Herman, and K. Klier, *Catal. Lett.* **2** 49, 1989.
2. J.G. Nunan, P.B. Himelfarb, R.G. Herman, K. Klier, C.E. Bogdan, and G.W. Simmons, *Inorg. Chem.* **28** 3868, 1989.
3. W. Ueda, T. Kuwabara, T. Ohshida, and Y. Morizawa, *Catal. Lett.* **12** 97, 1992.
4. F. Cavani, F. Trifiro, and A. Vaccari, *Catal. Today* **11** 97, 1991.
5. A.L. McKenzie, C.T. Fisherl, and R.J. Davis, *J. Catal.* **138** 547, 1992.
6. H. Schaper, J.J. Berg-Slot, and W.H.J. Stork, *Appl. Catal.* **54** 79, 1989.
7. C.R. Apesteguia, S.L. Soled, and S. Miseo, *U.S. Patent:assigned to Exxon Research and Engineering Co.* 1995.
8. C.R. Apesteguia, B. DeRites, S. Miseo, and S.L. Soled, *Catal. Lett.* **44** 1, 1997.
9. M. Ueshima and Y. Shimasaki, *Catal. Lett.* **15** 405, 1992.
10. C. Lamonier, A. Bennani, A. Duysser, and G. Wrobel, *J. Chem. Soc., Faraday Trans.* **92** 131, 1996.
11. J. Soria, *Solid State Ionics* **63-65** 755, 1993.
12. C. Lamonier, A. Bennani, A. Duysser, and G. Wrobel, *J. Chem. Soc., Faraday Trans.* **92** 131, 1996.
13. J. Soria, *Solid State Ionics* **63-65** 755, 1993.
14. L. Volpe and M. Boudart, *Catal. Rev.-Sci. Eng.* **27** 515, 1985.
15. T.E. Holt, A.D. Logan, S. Chakraborti, and A.K. Dayte, *Appl. Catal.* **34** 199, 1987.
16. W. Keim and W. Falter, *Catal. Lett.* **3** 9, 1989.
17. B.D. Dombeck, "Heterogenous Catalytic Process for Alcohol Fuels from Syngas", 1996.
18. P. Forzatti, E. Tronconi, and I. Pasquon, *Cat. Rev.-Sci. Eng.* **33** 109, 1991.
19. G. Natta, U. Colombo, and I. Pasquon, *Catalysis, Vol. V.*, Reinhold, New York, 1957, p.131.
20. K.J. Smith and R.B. Anderson, *Can. J. Chem. Eng.* **61** 40, 1983.
21. G.A. Vedage, P.B. Himmelfarb, G.W. Simmons, and K. Klier, *ACS Symp. Ser.* **279** 295, 1985.
22. A. Beretta, Q. Sun, R.G. Herman, and K. Klier, *Ind. Eng. Chem. Res.* **35** 1534, 1996.
23. K.J. Smith and R.B. Anderson, *J. Catal.* **85** 428, 1984.
24. E. Tronconi, P. Forzatti, and I. Pasquon, *J. Catal.* **124** 376, 1990.
25. J.L. Robbins, E. Iglesia, C.P. Kelkar, and B. DeRites, *Catal. Lett.* **10** 1, 1991.
26. G.C. Chinchen, K.C. Waugh, and D.A. Whan, *Appl. Catal.* **25** 101, 1986.
27. J.G. Nunan, C.E. Bogdan, K. Klier, K.J. Smith, C.-W. Young, and R.G. Herman, *J. Catal.* **113** 410, 1988.
28. Xu, M. and E. Iglesia, *Catal. Lett.*, to be submitted for publication.
29. M.J.L. Gines and E. Iglesia, *J. Catal.* **176** 155, 1998.
30. M. Xu, M.J.L. Gines, A.-M. Hilmen, B.L. Stephens, and E. Iglesia, *J. Catal.* **171** 130, 1997.

31. K. Klier, V. Chatikavanij, R.G. Herman, and G.W. Simmons, *J. Catal.* **74** 343, 1982.
32. G.C. Chinchen, P.J. Denny, R.J. Jennings, M.S. Spencer, and K.C. Waugh, *Appl. Catal.* **36** 1, 1988.
33. E.M. Calverley and K.J. Smith, *J. Catal.* **130** 616, 1991.
34. D.J. Driscoll, W. Martin, J-X. Wang, and J.H. Lunsford, *J. Am. Chem. Soc.* **107** 58, 1985.
35. E. Tronconi, N. Felazzo, P. Forzatti, and I. Pasquon, *Ind. Eng. Chem. Res.* **26** 2122, 1987.
36. J.C. Slaa, J.G. van Ommen, and J.R.H. Ross, *Catalysis Today* **15** 129, 1992.
37. D.J. Elliott, *J. Catal.* **111** 445, 1988.
38. A. Corma, V. Fornes, and F. Rey, *J. Catal.* **148** 205, 1994.
39. N.W. Hurst, S.J. Gentry, A. Jones, and B. McNicol, *Catal. Rev.-Sci. Eng.* **24** 233, 1982.
40. J.C. Nunan, C.E. Bogdan, K. Klier, K.J. Smith, C.-W. Young, and R.G. Herman, *J. Catal.* **116** 195, 1989.
41. J.G. Nunan, R.G. Herman, and K. Klier, *J. Catal.* **116** 222, 1989.
42. K.J. Smith, C.-W. Young, R.G. Herman, and K. Klier, *Ind. Eng. Chem. Res.* **30** 61, 1991.
43. B.B. Breman, A.C.C.M. Beenackers, and E. Oesterholt, *J. Catal.* **49** 4409, 1994.
44. B.B. Berman, A.C.C.M. Beenackers, and E. Oesterholt, *Catalysis Today* **24** 5, 1995.
45. I.E. Wachs and R.J. Madix, *Appl. Surf. Sci.* **1** 303, 1978.
46. D.J. Elliott and F. Pennella, *J. Catal.* **119** 359, 1989.
47. K. Klier, R.G. Herman, P.B. Himelfarb, C.-W. Young, S. Hou, and J.A. Marcos, *Proc. 10th Intern. Catal. Congress*, Budapest, 1992.
48. J.M. Vohs and M.A. Barteau, *Surf. Sci.* **221** 590, 1989.
49. W. Kotowski, J. Kliemiec, J. Lach, R. Gorski, W. Adamus, B. Groschwski, and I. Zalewski, *Polish Patent*, 1986.
50. A. Sofianos, *Catal. Today* **15** 149, 1992.
51. K.J. Smith, P.B. Himmelfarb, G.W. Simmons, and K. Klier, *Ind. Eng. Chem. Res.* **30** 61, 1991.
52. K. Kawamoto and Y. Nishimura, *Bull. Chem. Soc. Japan* **44** 819, 1971.
53. K. Takeshita, S. Nakamura, and K. Kawamoto, *Bull. Chem. Soc. Japan* **59** 2622, 1978.
54. M.J. Chung, S.H. Han, H.Y. Park, and S.K. Ihm, *J. Molec. Catal.* **79** 335, 1993.
55. M. Bowker, H. Houghton, and K.C. Waugh, *J. Chem. Soc., Faraday Trans. 1* **78** 2573, 1982.
56. Hilmen, A.-M., Gines, M.J.L., Xu, M., and Iglesia, E., *Appl. Catal.*, **169** 355, 1998.
57. N. Takezawa, C. Hanamaki, and H. Kobayashi, *J. Catal.* **38** 101, 1975.
58. S.L. Parrott, W. Roger, and J.M. White, *Applications of Surf. Sci.* **1** 443, 1978.
59. T. Mole, J.R. Anderson, and G. Creer, *Appl. Catal.* **17** 141, 1985.
60. E. Iglesia, D.G. Barton, J.A. Biscardi, M.J. Gines, and S.L. Soled, *Catal. Today* **38** 339, 1997.

61. C.A. Radlowski and G.P. Hagen, *U.S. Patent: 5,159,125* Assigned to Amoco Corporation, Chicago, I11.
62. L. Lietti, E. Tronconi, P. Forzatti, *J. Catal.* Jun, **135** 400, 1992.
63. R. Norman and J.M. Coxon, Principles of Organic Synthesis, Blackie Acedemic & Professional) 1993.
64. J.I. Di Cosimo and C.R. Apesteguia, *J. Molecular Catalysis A: Chemical* **130** 177, 1998.
65. G.L. Price and E. Iglesia, *Ind. Eng. Chem.* **28** 839, 1989.
66. M.J. Chung, D.J. Moon, H.S. Kim, K.Y. Park, and S.K. Ihm, *J. Molec. Catal. A: Chemical* **113** 507, 1996.
67. M. Ai, *Bull. Chem. Japan* **64** 1342, 1991.
68. M. Ai, *J. Catal.* **50** 291, 1977.
69. C.A. Radlowski and G.P. Hagen, *U.S. Patent: 5,095,156* Assigned to Amoco Corporation, Chicago, I11.
70. R.S. Monteiro, F.B. Noronha, L.C. Dieguez, and M. Schmal, *Appl. Catal.* **131** 89, 1995.
71. G. Fierro, M.L. Jacono, M. Inversi, P. Porta, F. Cioci, and R. Lavecchia, *Appl. Catal.* **137** 327, 1996.
72. A. Trovarelli, *Catal. Rev.* **38** 439, 1996.
73. G. Fierro, M.L. Jacono, M. Inversi, P. Porta, R. Lavecchia, and F. Cioci, *J. Catal.* **148** 709, 1994.
74. M.C. Annesini, R. Lavecchia, L. Marrelli, M.L. Jacono, M.C. Campa, G. Fierro, G. Moretti, and P. Porta, *Solid State Ionics.* **63-65** 281, 1993.
75. J.M. Campos-Mart, J.L.G. Fierro, A. Guerrero-Ruiz, R.G. Herman, and K. Klier, *J. Catal.* **163** 418, 1996.
76. L.P. Davydova, G.K. Boreskov, V.V. Popovskii, T.M. Yurieva, and V. Yu. Anufrienko, *React. Kinet. Catal. Lett.* **18** 203, 1981.
77. V.Yu, A leksandrov V.V. Popovskii, and N.N. Bulgakov, *React. kinet. Catal. Lett.* **8** 65, 1978.
78. E. Iglesia and M. Boudart, *J. Catal.* **81** 204, 1983.
79. K. Narita, N. Takezawa, and I. Toyoshima, *Reac. kinet. Catal. Lett.* **19** 1982.
80. J.J.F. Scholten and Konvalinka, *Trans. Faraday Soc.* **65** 2465, 1969.
81. D.S. King and R.M. Nix, *J. Catal.* **160** 76, 1996.
82. A.L. Mckenzie, C.T. Fishel, and R.J. Davis, *J. Catal.* **138** 547, 1992.
83. H. Kurokawa, K. Kato, T. Kuwabara, W. Ueda, Y. Morikakawa, Y. Moro-Oka, and T. Ikawa, *J. Catal.* **126** 208-218, 1990.
84. G. Pacchioni, J.M. Ricart, and F. Illas, *J. Am. Chem. Soc.* **116** 10152-10158, 1994.
85. S. Malinowsky, S. Szczepanska, and J. Sloczynski, *J. Catal.* **7** 67, 1967.
86. V.R. Choudhary and V.H. Rane, *Catal. Lett.* **4** 101-106, 1990.
87. W.T. Reichle, *J. Catal.* **94** 547, 1985.
88. H. Schaper, J.J. Berg-Slot, and W.H.J. Stork, *Appl. Catal.* **54** 79-90, 1989.
89. J. Shen, R.D. Cortright, Y. Chen, and J.A. Dumesic, *J. Phys. Chem.* **98** 8067, 1994.
90. M. DePontes, G.H. Yokomizo, and A.T. Bell, *J. Catal.* **104** 147, 1987.
91. T.E. Hoost and J.G. Goodwin Jr., *J. Catal.* **134** 678, 1992.
92. S.L. Shannon and J.G. Goodwin Jr., *Chem. Rev.* **95** 677, 1995.

93. R.K. Herz, J.B. Kiela, and S.P. Marin, *J. Catal.* **73** 66, 1982.
94. T. Yamada and K. Tamaru, *Surface Science* **138** L155, 1984.
95. T. Yamada, T. Onishi, and k. Tamaru, *Surface Science* **133** 533, 1984.
96. J.L. Falconer and J.A. Schwarz, *Catal. Rev.-Sci. Eng.* **25** 141, 1983.
97. J.T. Yates Jr. and D.W. Goodman, *J. Chem. Phys.* **73** 5371, 1980.
98. K. Tamaru, *Bull. Chem. Soc. Japan* **69** 961, 1996.
99. V.P. Zhdanov, *Surface Science* **157** L384, 1985.
100. D.J. Elliott and F. Pennella, *J. Catal.* **114** 90, 1988.
101. J.I. Di Cosimo, V.K. Diez, and C.R. Apestegu, *Appl. Catal.* **137** 149, 1996.
102. K. Klier, R.G. Herman, J.G. Nunan, K.J. Smith, C.E. Bogdan, C.-W. Young, and J.G. Santiesteban, (Amsterdam:Elsevier) 1988.
103. L.F. Fieser and M. Fieser, Organic Chemistry, 1973.
104. H. Tsuji, F. Yagi, H. Hattori, and H. Kita, *J. Catal.* **148** 759, 1994.
105. C. Li, K. Domen, K. Maruya, and T. Onishi, *J. Catal.* **125** 445, 1990.
106. J.D. Roberts and M.C. Caserio, Modern Organic Chemistry, 1965.
107. F. Gonzalez, G. Munuera, and J.A. Prieto, *J. Chem. Soc., Faraday Trans. I* **74** 1517, 1978.
108. M. Bowker, and R.J. Madix, *Appl. Surf. Sci.* **8** 299, 1981.
109. M. Bowker, H. Houghton, and K.C. Waugh, *J. Catal.* **79** 431, 1983.
110. J.G. Nunan, K. Klier, C.-W. Young, P.B. Himelfarb, and R.G. Herman, *J. Chem. Soc. Chem. Commun.* 193, 1986.
111. M. Bowker and R.J. Madix, *Surf. Sci.* **116** 549, 1982.
112. R.O. Kagel and R.G. Greenler, *J. Chem. Phys.* **49** 1638-1647, 1967.
113. K. Klier, D. Zeroka, and D. Bybell, *189th National Meeting of the American Chemical Society*, Miami Beach, FL, April 1985.
114. G.C. Chinchen, M.S. Spencer, K.C. Waugh, and D.A. Whan, *J. Chem. Soc., Faraday Trans.* **83** 2193, 1987.
115. D.B. Clarke and A.T. Bell, *J. Catal.* **154** 314, 1995.
116. R.L. Robbins, E. Iglesia, C.P. Kelkar, and B. DeRites, *Catal. Lett.* **10** 1, 1991.